Damien Brayshaw

The use of numerical optimisation to determine on-limit handling behaviour of race cars

School of Engineering

PhD Thesis

CRANFIELD UNIVERSITY

Damien Brayshaw

The use of numerical optimisation to determine on-limit handling behaviour of race cars

School of Engineering

PhD Thesis

CRANFIELD UNIVERSITY

School of Engineering
Department of Automotive, Mechanical and Structural Engineering

PhD Thesis

2004

Damien Brayshaw

The use of numerical optimisation to determine on-limit handling behaviour of race cars

Supervisor: M. F. Harrison

August 2004

This thesis is submitted in fulfilment of the requirements for the Degree of Doctor of Philosophy.

Abstract

The aim of this research is to use numerical optimisation to investigate the on-limit behaviour of an open wheel downforce type race car using the best compromise of modelling accuracy and computational effort.

The current state of lap simulation methods are identified, and the GG speed diagram is described. The use of constrained optimisation, which is a form of optimal control, is used to develop the methods described in this thesis. A seven degree of freedom vehicle model validated by other researchers is used for method validation purposes, and is extended, where possible, to make the modelling of vehicle components more physically significant, without adversely affecting the computational time.

This research suggests a quasi steady state approach that produces a GG speed diagram and circuit simulation tool that is capable of optimising vehicle parameters and subsystems in addition to the prevailing control vector of steer and throttle response.

The use of numerical optimisation to optimise the rear differential hydraulic pressure and the roll stiffness distribution to maximise vehicle performance is demonstrated. The optimisation of the rear differential hydraulic pressure showed a very small improvement in vehicle performance in combined high speed braking and cornering, but highlighted the ability of the differential to affect the cornering behaviour of the vehicle. The optimisation of the roll stiffness distribution research showed that a significant improvement in the lateral acceleration capability of the vehicle could be achieved at all vehicle speeds between 20 and 80m/s, especially in combined braking and cornering.

In addition, a parameter sensitivity study around a realistic Formula One vehicle setup was conducted, looking at the sensitivity of vehicle mass, yaw inertia, tyres, centre of gravity location and engine torque to vehicle performance. An investigation into the importance of the path finding calculation is also reported.

The author would like to acknowledge the help and support of the following people and groups, without whom this thesis could not have been completed:

Dr. Matthew Harrison, who has been an unwavering supporter of this research in every way. I owe a heavy debt of gratitude that I hope to repay in friendship over time. I can't pay the bursary back though, I hope you can understand.

Dr Karen Young, for all her patience and support during this process, she has been a great source of strength, especially during the writing up process.

My family, whose understanding gave me the final push to pursue this change in career, and for providing the voice of reason when the chips were down in my first year.

Universities UK, for their financial support by providing me with an ORS scholarship. The cost of tuition fees would have crippled my dream, and although they are not my sole supporter, this scholarship enabled me to get on the plane to England in the first place.

Shaun Forth and his colleagues at Cranfield University, Shrivenham, for allowing me to use their MATLAB based automatic differentiation toolbox. Their programs have played a large part in the development of the methods described in this thesis.

Adam Carroll, Andrew Thompson, Michael Keohane and Antonio Pizzonia who provided me with their time, and expertise with the racing line study.

The 'Harrison motorsport group', for all the help they have provided during this period of research, as well as Antonio De Lauretis and Martin Bayliss for their help with the proof reading of this thesis, and the many others for their professional and moral support.

Damien Brayshaw
Cranfield University
November 2004

Contents

Abstract i

Acknowledgements ii

List of Figures vii

List of Tables xii

Nomenclature xiii

List of Abbreviations xvii

1 Introduction 1
- 1.1 Aims and objectives 1
- 1.2 Context 2
- 1.3 Structure of thesis 4

2 Literature survey 7
- 2.1 Lap simulation techniques 7
  - 2.1.1 Quasi Steady State Models (QSS) 8
  - 2.1.2 The GG diagram 9
  - 2.1.3 Shape of the GG speed diagram 10
  - 2.1.4 Transient-optimal control (TO) 13
- 2.2 Constrained optimisation 16
- 2.3 Derivative evaluation 19
  - 2.3.1 Finite differencing 20
  - 2.3.2 Symbolic differentiation 21
  - 2.3.3 Automatic differentiation 22
- 2.4 Vehicle on-limit behaviour 24

2.4.1 Minimum time programs 24
2.4.2 Steady state cornering behaviour 25
2.4.3 Passive systems 26
2.4.4 Active systems 27
2.4.5 Roll stiffness distribution 28
2.4.6 Differentials 32
2.4.7 Vehicle stability 35
2.4.8 Vehicle stability control 36
2.5 The optimal path (racing line) 42
2.6 Driver Modelling for transient vehicle dynamics 43

3 The QSS method 45
3.1 The published vehicle model 45
3.2 GG speed diagram generation 46
3.3 QSS simulation 51
3.4 Results 56
3.4.1 Validation using the published vehicle model 56
3.5 QSS method improvements 59
3.5.1 Derivative evaluation 59
3.6 Extensions to the vehicle model 60
3.6.1 Rear differential model 60
3.6.2 Gear change strategy 62
3.6.3 Ride height sensitivity 62
3.6.4 4DOF suspension analysis 63
3.6.5 Coupled pitch and roll suspension model 68
3.6.6 14DOF vehicle model validation - The double lane change . . 70

4 The optimal path (racing line) 79
4.1 Accuracy of optimal racing line calculation 79
4.2 Vehicle parameter changes 80
4.2.1 GG speed diagram 81
4.2.2 New optimal line 82
4.2.3 Vehicle change or line change? 86
4.3 Practical racing line experiment 90

5 Parametric study 93
5.1 Introduction 93
5.2 Vehicle mass 95
5.3 Yaw inertia 99
5.4 Tyres 101
5.5 Engine torque 106
5.6 Longitudinal location of the centre of gravity (CG) 108
5.7 Aerodynamic downforce 112
5.8 Summary 114

6 Roll stiffness distribution 118
6.1 Optimisation of the roll stiffness distribution 119
6.2 Practical implications 123
6.2.1 Practical calculation example 127
6.3 Summary 129

7 Differentials 134
7.1 Introduction 134
7.2 Open versus locked differentials 135
7.3 Rear differential control 141
7.3.1 Active differential control 144
7.3.2 Practical control 147
7.4 All wheel drive (AWD) 152
7.5 Summary 156

8 Discussion and conclusions 159
8.1 Research objective 1 159
8.2 Research objective 2 160
8.3 Research objective 3 162
8.4 Research objective 4 163
8.5 Conclusions 164
8.6 Further work 165

References 166

Appendix 178

A 7DOF Vehicle Model 179
A.1 Seven Degree of Freedom Model Derivation 179
A.1.1 Assumptions 179
A.2 The Special Equations of Motion - Derivation 179
A.3 Applying the Equations of Motion 186

B 4DOF Suspension Model 195
B.1 Suspension model derivation 195

C 7DOF model stability 200
C.1 Straight line stability 200
C.2 Steady state cornering 203

D Transient path following 206
D.1 The need for transient information 206
D.2 Path following methodology 207
D.2.1 Preview steer control 208
D.2.2 Optimisation implementation 210
D.3 Results 214
D.3.1 Transient optimisation 218
D.4 Nonlinear preview Proportional-Integral (PI) control 225
D.4.1 Throttle control 227
D.4.2 Results 229

E PI method case study: stability control 237
E.1 Forms of β control 237
E.2 β limit VSC via engine torque control 238
E.3 Vehicle on-limit manoeuvring using β limit and $\dot{\beta}$ VSC 242
E.3.1 VSC control methodology 242
E.3.2 Double lane change results 243
E.4 Summary 249

List of Figures

1.1 Vehicle simulation methods. 3
1.2 Analysis of parameter optimisation literature. 6

2.1 GG diagram sketched for a downforce rear wheel driven race car. . . . 11
2.2 Aerodynamic dependency with vehicle speed. 12
2.3 Friction circle/ellipse - A generalised F1 tyre. 13
2.4 GG speed diagram - Using the generalised tyre. 14
2.5 Two dimensional sets. 17
2.6 Three DOF vehicle model. [1, 2] 26
2.7 Roll centre analysis - one axle. 30
2.8 Open differential power balance. 33
2.9 General Limited Slip Differential power balance. 34
2.10 General relationship between longitudinal tyre force and slip ratio, κ. 37
2.11 Sideslip angle β and yaw rate $\dot{\phi}$ 40

3.1 Vehicle Model - 7DOF. 47
3.2 The optimisation routine. 50
3.3 GG speed diagram - base setup. 52
3.4 QSS simulation principle. 54
3.5 Trajectory coordinate relationships. 55
3.6 QSS method validation. 56
3.7 Comparison of QSS and TO methods (arrows show corner locations [see Figure 3.8]). The TO method is from [3]. 57
3.8 Racing line, Barcelona Grand Prix circuit. 58
3.9 Forces and torques on a friction clutch. 61
3.10 GG speed diagram - 7DOF suspension vehicle model. 68
3.11 Acceleration comparison - Base published vehicle model and Base 7DOF suspension vehicle model. Barcelona Grand Prix Circuit. . . . 69

3.12 Speed comparison - Base published vehicle model and Base 7DOF suspension vehicle model. Barcelona Grand Prix Circuit. 70
3.13 7DOF suspension analysis. 71
3.14 Double lane change trajectory. 73
3.15 Tyre loads - published vehicle model and the 14DOF vehicle model. . 74
3.16 Aerodynamic loads, K_{us} - published vehicle model and the 14DOF vehicle model. 75
3.17 K_{us} - Published vehicle model and the 14DOF vehicle model. 76
3.18 K_{us} - Published vehicle model and 7DOF suspension vehicle model. . 77
3.19 GG speed diagram 14DOF vehicle Model and published vehicle model. 78

4.1 Difference in optimal racing lines calculated by the TO method. . . . 80
4.2 GG speed diagram - Base setup vs CG setup 81
4.3 Differences in optimal line due to a 6% CG set up change 83
4.4 Accelerations comparison - base setup and CG set up 84
4.5 Distance from base optimal vehicle to CG optimal vehicle 85
4.6 Accelerations comparison - CG vehicle on base optimal and CG optimal racing lines 87
4.7 Distance from base optimal, CG vehicle to CG optimal, CG vehicle . 88
4.8 Base optimal and CG optimal racing lines, speed history 89
4.9 Racing Line experiment - Experienced racing drivers 91

5.1 Vehicle mass sensitivity analysis - GG speed diagram. 95
5.2 GG speed diagram - area evaluation. 96
5.3 Vehicle mass sensitivity analysis - Percentage Improvements. 97
5.4 Vehicle Yaw sensitivity analysis - Percentage Improvements. 100
5.5 $\dot{\beta}$ QSS simulation - Barcelona GP circuit. 102
5.6 Friction circle/ellipse - Representative tyre. 103
5.7 90% and 110% GG speed diagram results. 104
5.8 Vehicle tyre sensitivity analysis - Percentage Improvements. 105
5.9 Vehicle Engine torque sensitivity analysis - Percentage Improvements. 107
5.10 Vehicle Engine torque - Positive acceleration only, GG Diagram. . . 107
5.11 Vehicle C of G sensitivity analysis - Percentage Improvements. . . . 109
5.12 Vehicle C of G sensitivity - GG diagrams. 110
5.13 Aerodynamic downforce sensitivity analysis - Percentage Improvements. 112

5.14 Aerodynamic downforce sensitivity - GG speed diagram. 114
5.15 Vehicle sensitivity - Positive improvements. 116
5.16 Vehicle sensitivity - Loss of performance. 117

6.1 Roll axis implementation - 7DOF model. 119
6.2 GG speed diagram - Active roll. 120
6.3 Active roll stiffness GG speed diagram - Roll stiffness distribution. . . 122
6.4 Tyre saturation calculation. 123
6.5 Tyre saturation plots Active and Base vehicle 70 m/s - Braking. 124
6.6 Active roll Barcelona GP circuit - Roll stiffness distribution. 126
6.7 Circuit history GG speed diagram - Active roll - Barcelona. 127
6.8 GG speed diagram - R_{sf} set to 0.526. 129
6.9 New static roll ($R_{sf} = 0.526$), Active roll and the base vehicle - speed history. 130

7.1 Open differential GG speed diagram. 137
7.2 Locked differential (spool) GG speed diagram. 138
7.3 Path taken, for three cases of differential operation. 139
7.4 Yaw rate, $\dot{\phi}$, for the three cases of differential operation. 140
7.5 Lateral acceleration, for the three cases of differential operation. . . . 140
7.6 Active Differential 14DOF model - GG speed diagram. 142
7.7 Box plot of rear limited slip differential control. 143
7.8 Double lane change manoeuvre. 143
7.9 Lateral tyre force utilisations. 145
7.10 Longitudinal tyre force utilisation. 146
7.11 Rear differential hydraulic pressure. 147
7.12 Rear differential hydraulic pressure - Control law and Active differential (Corner 1= 136m, Corner 2= 204m, Corner 3= 271m). 149
7.13 Double lane change comparison - Control law and Active differential (Corner 1= 136m, Corner 2= 204m, Corner 3= 271m). 150
7.14 Box plot of differential control. 153
7.15 Rear differential hydraulic pressure - AWD. 154
7.16 Longitudinal tyre force utilisations - AWD. 155
7.17 Double lane change manoeuvre - AWD. 156
7.18 Centre differential control - double lane change manoeuvre. 157

7.19 Lateral tyre force utilisations - AWD. 158

A.1 Vehicle and earth centred axes. 180
A.2 External Forces acting on the Vehicle. 189
A.3 Left Front Wheel. 190
A.4 Right Front Wheel. 190
A.5 Left Rear Wheel. 191
A.6 Right Rear Wheel. 191

B.1 Four degree of freedom pitch model 195

C.1 Root Locus plot - Linear 7DOF model 201
C.2 Root Locus plot - Eigenvalues 7DOF Model CG split 37/63% (Front/Rear) 202
C.3 Root Locus plot - Steady state cornering, Base setup 204
C.4 Root Locus plot - Steady state cornering, CG 37/63% setup 205

D.1 Transient path following optimisation. 208
D.2 Linear driver model structure. 209
D.3 Nonlinear driver model structure. 210
D.4 Inequality constraint implementation methods. 212
D.5 Inequality constraint for path following. 213
D.6 Double lane change - path following result. 214
D.7 Double lane change - path following errors. 215
D.8 Double lane change - steer angle. 216
D.9 Double lane change - Throttle position. 216
D.10 Double lane change - vehicle speed. 217
D.11 Double lane change - vehicle speed - QSS check. 218
D.12 Double lane change comparison - Path taken. 219
D.13 Double lane change comparison - vehicle speed. 220
D.14 Double lane change comparison - Steer angle. 220
D.15 Double lane change comparison - Path taken AD version. 221
D.16 Double lane change comparison - vehicle speed AD version. 221
D.17 Double lane change comparison - Steer angle AD version. 222
D.18 Double lane change comparison - Vehicle speeds. 224
D.19 Transient path following with PI throttle control. 227
D.20 Double lane change comparison - Vehicle speed PI method. 230

D.21 Double lane change comparison - Path PI method. 231
D.22 Double lane change comparison - Steer angle PI method. 232
D.23 Double lane change comparison - Throttle position PI method. 232
D.24 Double lane change comparison - Vehicle speed PI method (Zoom). . 233
D.25 PI method using Transient speed history - Speed comparison (PI controller performance). 234
D.26 Path taken by PI method using QSS and TO speed histories. 235
D.27 Throttle history derived by PI controller using TO method speed history. 236
D.28 Steer angle history comparison using the PI method, compared to the TO method steer history. 236

E.1 Path taken with sideslip angle limit $\beta = 1.5°$, for three steer angles. . . 239
E.2 Vehicle speed with sideslip angle limit $\beta = 1.5°$, for three steer angles. 240
E.3 Sideslip angle with limit $\beta = 1.5°$, for three steer angles. 240
E.4 Yaw rate with sideslip angle limit $\beta = 1.5°$, for three steer angles. . . 241
E.5 Path taken, with four sideslip angle limits, and $\dot{\beta}$ minimisation. 244
E.6 Vehicle longitudinal velocity, with four sideslip angle limits, and $\dot{\beta}$ minimisation. 245
E.7 Steer angle, with four sideslip angle limits, and $\dot{\beta}$ minimisation. 246
E.8 Sideslip angle, with four sideslip angle limits, and $\dot{\beta}$ minimisation. . . 247
E.9 Sideslip angular velocity, with four sideslip angle limits, and $\dot{\beta}$ minimisation. 248
E.10 Yaw rate, with four sideslip angle limits, and $\dot{\beta}$ minimisation. 248

List of Tables

3.1 GG speed optimisation output. 51
3.2 Lap time at Barcelona Grand Prix circuit for QSS and TO methods. . 58
3.3 Simulated lap time using the published model and the 7DOF suspension vehicle model. 71

4.1 Simulated lap time at Barcelona Grand Prix circuit 84
4.2 Simulated lap time using the CG vehicle at Barcelona Grand Prix circuit 86

5.1 Area of constant velocity contours - GG speed diagram for vehicle mass = 600kg (Figure 5.1). 97

6.1 Area of constant velocity contours - GG speed diagram. 121
6.2 Active roll population statistics. 121
6.3 Active roll vehicle state vector 70 m/s - Braking. 131
6.4 Base vehicle state vector 70 m/s - Braking. 132
6.5 Lap times - Barcelona Grand Prix circuit. 132
6.6 Hypothetical suspension and roll settings - open wheel race car. 133

7.1 Steady state values for the on-limit vehicle operation at constant speed. 139
7.2 Manoeuvre time, double lane change. 144
7.3 Polynomial coefficients - Active differential control law. 148
7.4 Manoeuvre time, double lane change. 154

C.1 Damping Ratio found from Root Locus plots 205

E.1 Double lane change manoeuvre segment times. 246

Nomenclature

a, A, b, c	=	Constant term coefficients	
a_y	=	Lateral Acceleration	m/s^2
α_f	=	Front wheel slip angle, averaged across the front axle	deg
α_r	=	Rear wheel slip angle, averaged across the rear axle	deg
β	=	Sideslip angle of the vehicle	deg
$\dot{\beta}$	=	Time derivative of the sideslip angle of the vehicle	deg/s
cp	=	Longitudinal location of the centre of pressure of the aerodynamic forces	
$C_{\alpha f}, C_f$	=	Cornering stiffness, front axle	N/deg
$C_{\alpha r}, C_r$	=	Cornering stiffness, rear axle	N/deg
C_z	=	Negative lift coefficient	
δ	=	Steer Angle	rad
ΔF_{fz_lat}	=	Lateral load transfer, front axle	Nm
ΔF_{rz_lat}	=	Lateral load transfer, rear axle	Nm
ΔT_{LSD}	=	Transferred Torque by the limited slip differential	Nm
e_d	=	fractional accuracy that the derivative of a function can be evaluated with	
e_f	=	fractional accuracy that a function can be evaluated with	
e_m	=	Numerical computer machine accuracy	
e_r	=	Roundoff error	
e_t	=	Truncation error	
f	=	Objective Function	
F_{az}	=	Aerodynamic Downforce force	N
F_{xf}	=	Longitudinal tyre force, front axle	N
F_{xr}	=	Longitudinal tyre force, rear axle	N
F_{yf}	=	Lateral tyre force, front axle	N
F_{yr}	=	Lateral tyre force, rear axle	N
g	=	Gravity	m/s^2
G	=	Constraint Matrix	
h	=	Integration step parameter	
h_g	=	Vertical height of the Centre of Gravity of the vehicle	m

h_{rc}	=	Vertical height of roll axis at the centre of gravity of the vehicle	m
h_{rf}	=	Vertical height of roll axis at the front axle	m
h_{rr}	=	Vertical height of roll axis at the rear axle	m
I_{ZZ}	=	Yaw inertia of the vehicle	kgm^2
κ	=	Slip ratio	
$k_{1..4}$	=	Spring coefficient	N/m
k_f	=	Amalgamated Spring coefficient for the front axle	N/m
k_{f-roll}	=	Anti roll bar rate of the front axle	N/m
k_r	=	Amalgamated Spring coefficient for the rear axle	N/m
k_{r-roll}	=	Anti roll bar rate of the rear axle	N/m
$K_{\phi f}$	=	Roll rate of the front axle	N/m
$K_{\phi r}$	=	Roll rate of the front axle	N/m
λ_i	=	Lagrange multipliers	
l_f	=	The longitudinal location of the centre of gravity from the front axle	m
l_r	=	The longitudinal location of the centre of gravity from the rear axle	m
K_{us}	=	Understeer coefficient	deg/g
mf	=	Unsprung mass, front wheel assembly	kg
mr	=	Unsprung mass, rear wheel assembly	kg
m	=	Slope of friction-velocity characteristic curve	s/m
μ	=	Effective coefficient of friction	
μ_0	=	Coefficient of friction, dynamic	
M	=	Weight of the sprung mass of the vehicle	kg
n	=	Number of clutch friction surface pairs	
ω_i	=	Angular velocity, inside wheel	rad/s
ω_l	=	Angular velocity, left wheel	rad/s
ω_r	=	Angular velocity, right wheel	rad/s
ω_o	=	Angular velocity, outside wheel	rad/s
ω_w	=	Angular velocity, generic wheel	rad/s
P	=	Optimisation Vector	
ϕ	=	Roll angle of the vehicle via a roll axis implementation	rad
p	=	number of constraints in a optimisation problem	
p_e	=	number of equality constraints in a optimisation problem	
P_H	=	Pressure at contacting surfaces	Bar
Q_i	=	Generalised coordinates (DOF) as defined by AutoSIM [4]	
φ	=	Yaw angle about the centre of gravity of the vehicle	rad
$\dot{\varphi}$	=	Yaw rate about the centre of gravity of the vehicle	rad/s
$\ddot{\varphi}$	=	Yaw Acceleration about the centre of gravity of the vehicle	rad/s^2

ρ	=	Density of the surrounding air	kg/m^3
r_1	=	Clutch face radius, inside	m
r_2	=	Clutch face radius, outside	m
R	=	Radius of turn	m
R_w	=	Radius of a generic wheel	m
$\Re$	=	A real number	
R_{sf}	=	Proportion of the roll stiffness carried by the front axle	
R_{sr}	=	Proportion of the roll stiffness carried by the rear axle	
σ	=	Standard deviation term for the normal distribution function	m
S	=	Frontal area of the vehicle	m^2
s	=	Distance	m
T_p	=	Throttle Position	
T_{in}	=	Input torque to the differential cage	Nm
T_L	=	Torque to the left driveshaft	Nm
T_R	=	Torque to the right driveshaft	Nm
t_f	=	Length of the front axle track	m
t_F	=	Manoeuvre time	s
t_r	=	Length of the rear axle track	m
$\dot{\theta}_F$	=	Front Wheel Angular Speed	rad/s
$\dot{\theta}_{LF}$	=	Left Front Wheel Angular Speed	rad/s
$\ddot{\theta}_{LF}$	=	Left Front Wheel Angular Acceleration	rad/s^2
$\dot{\theta}_{LR}$	=	Left Rear Wheel Angular Speed	rad/s
$\ddot{\theta}_{LR}$	=	Left Rear Wheel Angular Acceleration	rad/s^2
$\dot{\theta}_R$	=	Rear Wheel Angular Speed	rad/s
$\dot{\theta}_{RF}$	=	Right Front Wheel Angular Speed	rad/s
$\ddot{\theta}_{RF}$	=	Right Front Wheel Angular Acceleration	rad/s^2
$\dot{\theta}_{RR}$	=	Right Rear Wheel Angular Speed	rad/s
$\ddot{\theta}_{RR}$	=	Right Rear Wheel Angular Acceleration	rad/s^2
$\dot{\theta}_W$	=	Wheel Angular Speed	rad/s
W	=	Total axial force on the rubbing surface	N
W_f	=	Weight on front axle	N
W_r	=	Weight on rear axle	N
W_b	=	Wheelbase of vehicle	m
x	=	Position of the centre of gravity of the vehicle in the longitudinal direction	m
$\dot{x}, u$	=	Longitudinal Speed	m/s
$\ddot{x}$	=	Longitudinal Acceleration	m/s^2
$\bar{x}$	=	Mean position of the longitudinal coordinate	m

y	=	Position of the centre of gravity of the vehicle in the lateral direction	m
v	=	Sliding velocity of two adjacent friction surfaces	m/s
$\dot{y}, v$	=	Lateral Speed	m/s
$\ddot{y}$	=	Sideways Acceleration	m/s^2

List of Abbreviations

Abbreviation	Full description
ABS	Anti-lock braking system
AD	Automatic differentiation
AWD	All wheel drive
CG	Centre of gravity
DOF	Degrees of freedom
ECU	Electronic control unit
F1	Formula one
FD	Finite difference
GP	General problem
KT	Kuhn-Tucker
LF	Left front
LP	Linear programming
LR	Left rear
LSD	Limited slip differential
MAD	MATLAB automatic differentiation
NP	Nonlinear programming
PC	Personal computer
PF	Path following optimisation
PI	Proportional - integral
PID	Proportional - integral - derivative
QP	Quadratic programming
QSS	Quasi steady state
RF	Right front
RR	Right rear
SQP	Sequential quadratic programming
SS	Steady state
TC	Traction control
TO	Transient optimal
WRC	World Rally Car
VSC	Vehicle stability control

Chapter 1

Introduction

1.1 Aims and objectives

The aim of this research is to use numerical optimisation to investigate the on-limit behaviour of an open wheel downforce type race car using the best compromise of modelling accuracy and computational effort. The objectives of this research are:

1. To design, build, and validate fast numerical optimisation race car simulation programs for the purposes of defining vehicle setup parameters, as well as the minimum laptime, using appropriate vehicle models.

2. To explore race car vehicle on-limit behaviour using the vehicle optimisation programs, by analysing the sensitivity of specific vehicle parameters and/or systems on vehicle performance. The following vehicle parameters will be analysed over a wide range of values:

    - Vehicle mass.
    - Yaw inertia.
    - Tyre properties.
    - Engine torque.
    - Longitudinal centre of gravity location.
    - Aerodynamic downforce.

3. To investigate an aspect of vehicle on-limit *control* using a case study on the importance of the optimal path (path finding) to lap simulation studies.

4. To determine the usefulness of certain active control technologies. These are:
    - Active control of the roll stiffness distribution.
    - Active control of electronically controlled limited slip differentials.

1.2 Context

The field of vehicle lap time simulation while significant, is largely under reported in the literature, generally for commercial reasons. These can vary from maintaining a competitive advantage for a race team, to a developers desire to maintain a marketable and unique vehicle dynamics software product for sale to the automotive and motor sport industries.

A car that accelerates, brakes and corners in a smooth fashion can be modelled approximately by joining together a series of static equilibrium or steady state manoeuvres. This is the quasi steady state approach to vehicle-circuit simulation. Conversely transient-optimal methods generally aim to maximise or minimise an objective, by manipulating the vehicle control inputs, in a transient simulation. The most common objective is to minimise the laptime. Transient-optimal methods are a subset of transient simulation methods, which can be characterised as the result of numerical integration of the vehicle equations of motion with respect to time.

To make a contribution to the understanding of vehicle on-limit behaviour via vehicle dynamics simulation, a sensible balance between model accuracy and computational effort is required. From the literature it is clear that quasi steady state methods are significantly faster than transient-optimal methods but their use entails a fundamental loss of knowledge of the transient vehicle dynamics, and may make assumptions that are over simplified for lap time simulation.

The research of Hendrikx et al. [5] and Casanova [3] shows that transient optimal methods that find the optimal path are achievable for minimum time simulations. However, much effort by those researchers was expended in making the programs run as fast as possible. Therefore it is not believed that further research into minimum time optimisation with path finding will significantly improve computational times from hours to minutes unless faster computations can be achieved with parallel processing

techniques or faster computers. This is not a vehicle dynamics issue, but an information technology one.

As open wheel race cars are much simpler to model dynamically, due to their limited suspension movement, it is believed that the use of a quasi steady state method could be developed for minimum time lap simulation, with an acceptable loss of accuracy for the improvement in computational time. The assumptions of the quasi steady state model will be investigated in this thesis, as part of the validation process.

If the transient optimal calculation could be made simpler, by making the simulation path following based rather than path finding based, then the computational 'price' of keeping the transient information may be more palatable. This requires investigation (Figure 1.1).

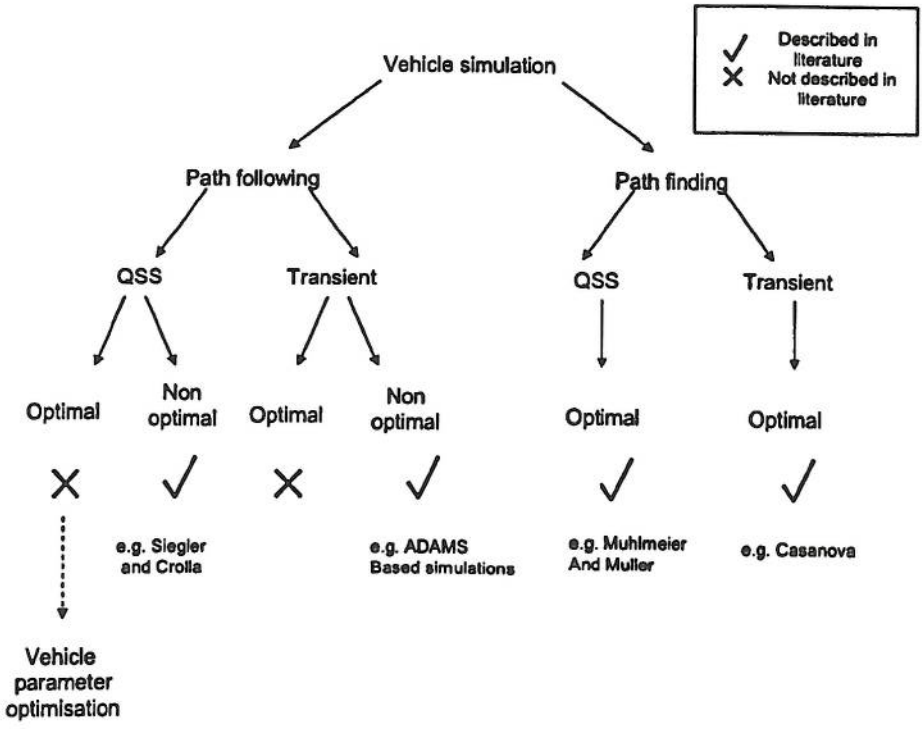

Figure 1.1: Vehicle simulation methods.

The field of characterising and understanding vehicle on-limit behaviour is a subset of general vehicle behaviour research, and many of the standard methods of steady state cornering and stability can be applied. Unfortunately, the use of linear methods is considerably reduced by the need for nonlinear tyre descriptions.

Vehicle parameters can be considered to fall into two categories, passive and active. The use of optimisation techniques to explore vehicle parameter settings, other than to find the minimum time solution to a manoeuvre, has not been satisfactorily explored. Figure 1.2 shows a graphical summary of the current state of the literature with respect to vehicle parameter optimisation. Two groupings are given, one that includes the quasi steady state and steady state methods and one that encompasses the transient-optimal methods. The advantages and disadvantages between the two groups are highlighted by the horizontal arrows, and the vertical arrows describe how these two groups have approached the vehicle parameter optimisation work (if at all) in the literature. The base of the diagram summarises the literature on this topic, and highlights the deficiencies in the current method implementations to optimise vehicle parameters and/or systems in addition to the prevailing state vector input.

The use of active systems, while generally restricted by the sporting regulations, may offer some insight into the better choice of passive setting for the vehicle, if the maximisation of vehicle performance is used as the objective of the active control.

This thesis explores the gaps in the body of knowledge illustrated in Figures 1.1 and 1.2. The use of numerical optimisation as the basis of a quasi steady state method will be described. Optimisation of vehicle parameters will also be investigated with the objective of maximising vehicle performance capability.

1.3 Structure of thesis

Chapter 2 provides a summary of the literature surrounding the research presented in this Ph.D. thesis.

Chapter 3 describes a vehicle quasi steady state nonlinear simulation tool that has been developed during this research. Using a validated vehicle model, the method is described and checked with published results. Following this, a more accurate method

for the quasi steady state method is described. The vehicle model is extended to include ride height dependent aerodynamics, a nonlinear suspension model, and a physically significant differential model.

Using the original quasi steady state method from *Chapter 3*, *Chapter 4* explores the importance of knowing the optimal racing line, for on-limit vehicle simulations. The performance advantages gained by following the optimal line are compared with the performance advantages of changing vehicle parameters.

In *Chapter 5*, a parametric sweep of vehicle parameters is carried out and analysed in terms of expansion or contraction of the GG speed diagram. The practicality of engineering effort to bring about these vehicle changes is also discussed.

Chapter 6 looks at the advantages of actively controlling the roll stiffness distribution using the roll axis concept. Using the knowledge gained from analysis of the active roll stiffness results, a case study to improve the performance of the vehicle through a single static change to the roll stiffness distribution is conducted. The practical application of such work is also explored.

Chapter 7 uses the extended suspension model described in *Chapter 2* and a new differential model to explore the performance benefits from actively controlling (optimising) the rear differential. Following analysis of the vehicle behaviour, a practical control law is suggested to fit the hydraulic pressure profile of the vehicle with the actively controlled differential.

Chapter 8 provides a summary of the conclusions that have been made through the course of this research.

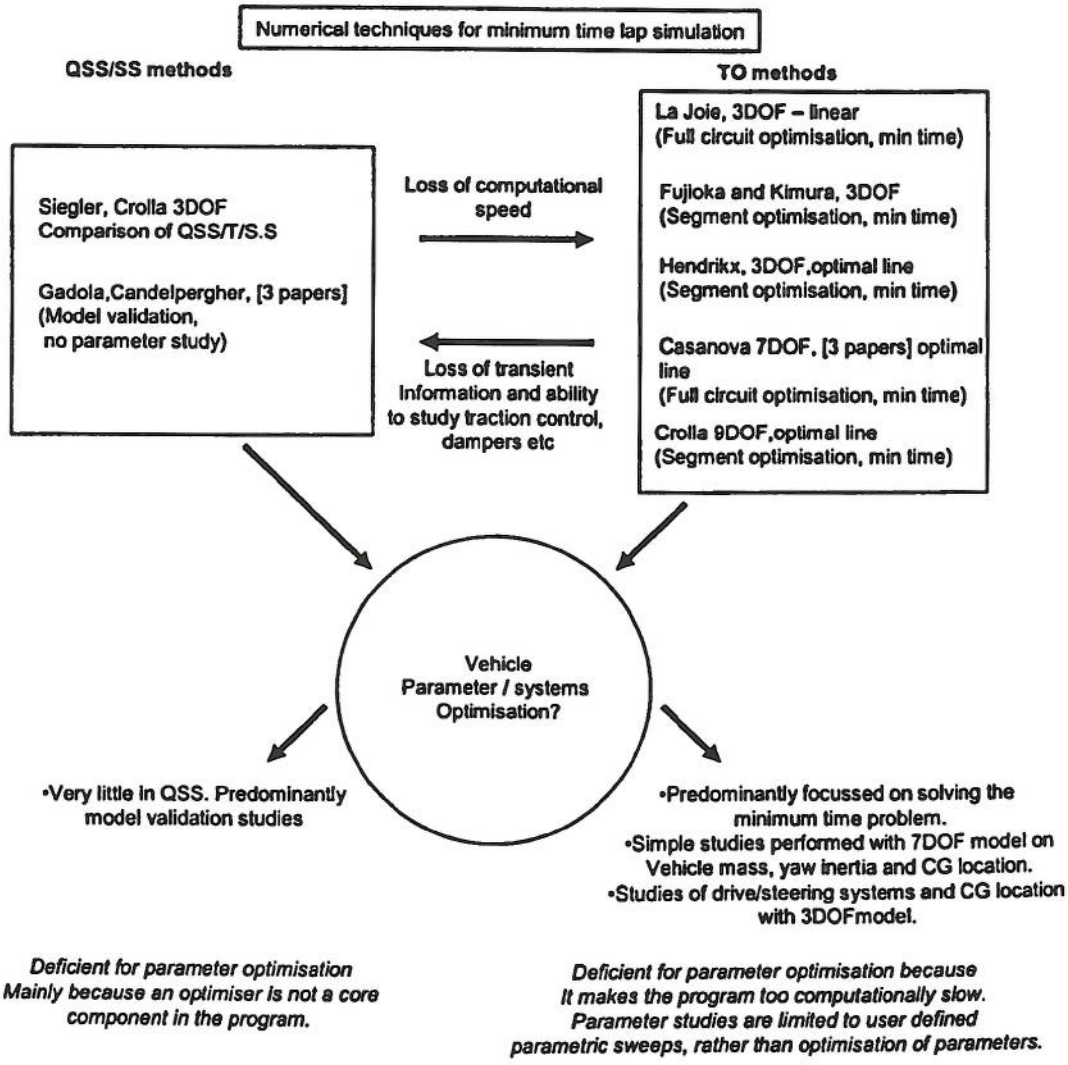

Figure 1.2: Analysis of parameter optimisation literature.

Chapter 2

Literature survey

In pursuit of the aims and objectives described in Chapter 1, the following sections introduce the reader to the current body of knowledge around the topics of this thesis. The current state of lap simulation methods are identified, and the concept of the GG speed diagram is introduced.

The use of constrained optimisation, which is a form of optimal control, is described due to its recurring inclusion in transient optimal lap simulation methods and its use in the methods developed in this thesis. This is followed by a discussion of current methods of evaluating derivatives which are a key input to the current generation of constrained optimisation tools.

Vehicle on-limit behaviour literature is covered in terms of the aims and objectives of exploring active and passive vehicle systems, and a case study on the importance of the optimal racing line is introduced. Finally the literature surrounding the field of driver modelling as it pertains to race car driving, is presented.

2.1 Lap simulation techniques

From the point of view of designers and engineers, lap time simulation needs to perform three functions: it needs to accurately model the dynamic behaviour of the vehicle, it needs to accurately predict lap times and it needs to produce lap simulation results rapidly, and to allow many different vehicle set up and configuration changes to be examined for a particular circuit.

Lap simulation methods have been produced by a variety of different researchers, notwithstanding the programs generated by race teams that are not published in the interests of maintaining a competitive advantage over other teams.

Lap simulations can be considered to fall into three main types: steady state, quasi steady state, and transient (sometimes optimal control based). Steady state models will not be discussed in this thesis because of their over simplicity and lack of ability to accurately represent the vehicle in lap time simulations, as seen in Siegler et al. [6].

2.1.1 Quasi Steady State Models (QSS)

The use of quasi steady state models has been widespread across the automotive industry [6–10]. A car that accelerates, brakes and corners in a smooth fashion can be modelled approximately by joining together a series of static equilibrium or steady state manoeuvres. The circuit is broken into segments, and the local curvature is calculated for each segment. The static equilibrium or steady state behaviours can be generated for each segment from either a dynamic or a steady state vehicle model. The overall process, regardless of the method of determining the vehicle states, is the quasi steady state approach to vehicle-circuit simulation.

Of the quasi steady state lap time simulation programs reported in the literature, it appears that there are two methods of producing the static equilibrium or steady state behaviours for a lap simulation of a circuit. Siegler et al. [6] generate the points interactively, while Candelpergher et al. [7] and Blasco-Figueroa [8] access an independently generated GG speed diagram. These diagrams are discussed by Milliken and Milliken [11], Wright [12] and are covered in section 2.1.2.

The research presented in Siegler et al. [6] is a comparison of steady state, quasi steady state and transient programs for cornering manoeuvres using a three degree of freedom (DOF) model. To find the maximum lateral acceleration that the car is able to maintain through a corner, the quasi steady state program iterates using a Newton-Raphson method, altering the steer angle until it finds the peak lateral acceleration for the given cornering radius. The quasi steady state approach was found to be a good approximation to the transient model in the cornering manoeuvres.

A quasi steady state program that operates on a GG speed diagram has been produced by Blasco-Figueroa [8]. The program requires the trajectory to be defined in terms of curvature and distance travelled. The GG speed diagram is generated from a seven DOF model [3]. The program identifies peaks in the curvature data as an apex of a corner. At each apex, the program calculates the vehicle speed profile from the acceleration data up to the next apex. Similarly, the program then calculates the vehicle speed profile from deceleration data from the second apex back to the first apex. Where accelerating and braking vehicle speeds in between two apexes reach the same value, the vehicle stops accelerating and starts braking. The program achieves this by switching at this point from the vehicle speed profile from the acceleration data to the vehicle speed profile from the braking data. The program runs very quickly (a simulation of the Barcelona Grand Prix circuit on a 266 MHz Intel processor takes just under 60 seconds) and robustly.

The program outlined in Candelpergher et al. [7] also operates from a GG speed diagram, but the vehicle model used is not described. The paper emphasises that the computational speed of their simulations was improved by estimating the GG speed diagram before simulating a lap. Like Siegler et al. [6], Candelpergher et al. [7] also use iterative methods to determine the accelerating and braking zones for the vehicle model. The program iterates to make the speed at the end of the acceleration zone meet the braking zone, if the car is not able to reach full speed before reaching the braking point for the next corner. Iterative processes can be computationally expensive, and there is no guarantee they will converge. The approach of Blasco-Figueroa [8] working backwards from the new apex to the old one for braking, and then working forwards from the old apex to the new one and identifying the crossover point appears to be simpler and more robust.

2.1.2 The GG diagram

A GG diagram can be considered a graphical map of vehicle performance, indicating how well the vehicle can corner and how fast it can brake and accelerate.

The accelerations shown on Figure 2.1 are given in units of g, for gravity. This plot is known as a GG Diagram, as it plots values of longitudinal acceleration in units of g against lateral acceleration in units of g for a particular vehicle configuration and setup. The concept of the GG Diagram has been around for a while, arising from automotive

research in the United States initially in 1958, and published articles begun appearing in the early 1970's [11].

The issue of which unit system to use can be ignored by comparing the measured accelerations with the acceleration due to gravity, which is a reasonably constant value (9.8066 m/s^2, though it varies slightly with location). The result is a number, which has no dimensions. It is the same regardless of whether S.I. or imperial units are used.

When downforce aids are used, as in many open-wheel formulae, the acceleration performance of the vehicle becomes strongly speed dependent, as the downforce and drag created are proportional to the square of the vehicle speed. GG diagrams are expanded for these vehicles to three dimensions; longitudinal acceleration, lateral acceleration and vehicle speed. This produces a 3D envelope that is termed the *GG speed diagram.*

Producing GG speed diagrams as an intermediate step for a QSS simulation to use as a lookup table, was found to improve the speed of computation of the overall program (which includes the time taken to generate the GG speed diagram) when compared with another version of the program [7]. The other version generated quasi steady state solutions, equivalent to one GG speed point on the diagram, at each time step during the simulation process [7]. The generation of GG speed diagrams also offers the opportunity for the analyst to assess the overall performance capability of the vehicle.

2.1.3 Shape of the GG speed diagram

The GG speed diagram curves are a representation of the longitudinal and lateral forces acting on the vehicle collapsed down to an equivalent longitudinal and lateral acceleration of a representative point mass, for a given constant vehicle speed. In Figure 2.1, two cases are shown, one as a solid line and one as a dotted line, representing a high and low speed case respectively for an open wheel downforce race car.

An open wheel downforce car generates vertical tyre load in addition to the vehicle's static weight in proportion to the square of the vehicle speed (Figure 2.2). Consequently at high speeds (> 40 m/s) more tyre load, and therefore comparatively more tyre force, is available for cornering and lateral acceleration is improved. However, at higher speeds, the drag created by air resistance also increases in proportion to the

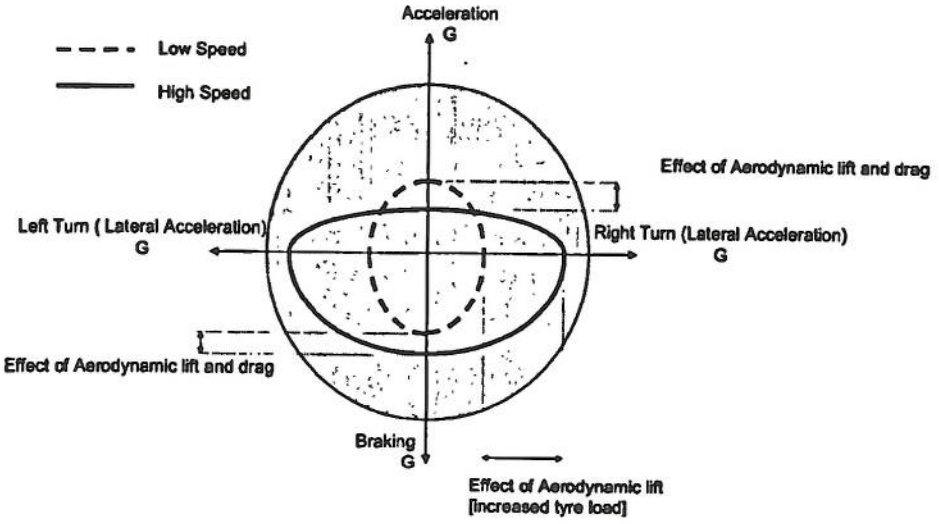

Figure 2.1: GG diagram sketched for a downforce rear wheel driven race car.

square of the speed of the car (Figure 2.2). The car is not able to longitudinally accelerate as well due to the increased resistance to forward motion at high speed, and therefore the longitudinal acceleration limit is considerably lower than the low speed result. The ideal remedies for this longitudinal acceleration constraint are a engine with more power, or a vehicle shape with less drag.

At low speeds (< 40 m/s), the aerodynamic forces of drag and lift are considerably lower than for the higher speed cases (Figure 2.2). At 40 m/s the downforce produced by the vehicle is 50% of that available at 53 m/s. At low speed a combination of low tyre load, and a high amount of engine torque that can be transferred to the tyres, creates a condition where the rear wheel speeds and therefore the vehicle acceleration, are governed by the available road friction. However, since the aerodynamic drag force increases with the square of the vehicle speed, the vehicle acceleration capability is generally higher at low speed than at high speed, due to the finite amount of engine torque. This trend is seen in Figure 2.1. At high speed the engine torque is increasingly used to overcome the aerodynamic drag force at the expense of vehicle longitudinal acceleration.

It is noticeable that the braking part of the GG curves approximate a quadrant of a circle much better than the accelerating part (Figure 2.1). This is because in the open wheel race car configuration used in this thesis, the braking torque is applied to all

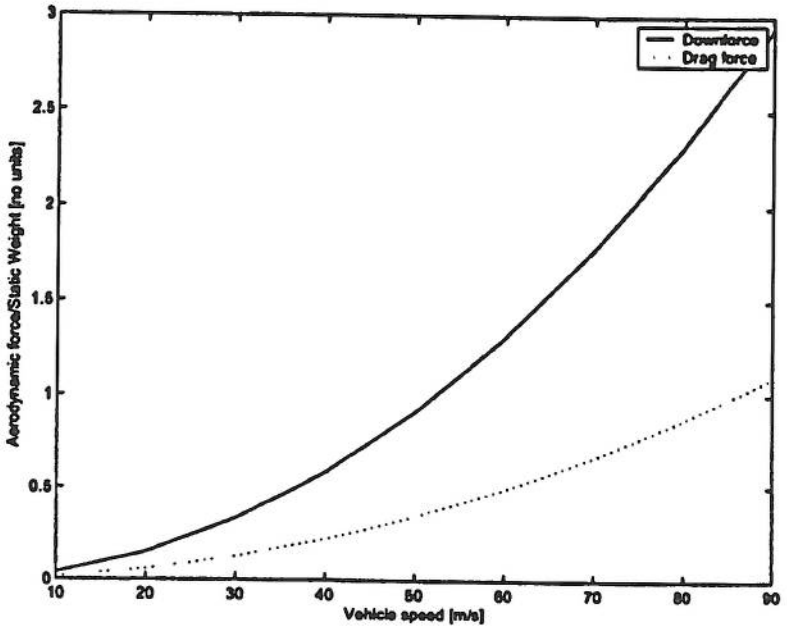

Figure 2.2: Aerodynamic dependency with vehicle speed.

four wheels during deceleration, whereas the engine torque is only applied to the rear wheels during acceleration. In addition, the total braking torque available is twenty times larger than the available engine torque.

The shape of the GG curves is determined by the shape of the tyre force curves. This is because the tyres provide the contact between the vehicle and the road. All the redistribution of forces carried out by the suspension, and all braking and tractive torques provided by the braking system and engine respectively are ultimately transferred to the tyres. How the tyres respond to these applied forces and moments directly determines the acceleration of the vehicle, and is analogous to passing a signal through a complex, nonlinear filter. Filters pass on their own characteristics during the filtering process and this also occurs with the resulting accelerations of the vehicle mass as a consequence of the tyre forces applied at the contact patch between tyre and road. Figure 2.3 shows a friction ellipse for a representative F1 vehicle tyre. A friction ellipse shows the force that a tyre is capable of generating as a consequence of a vertical load (Fz) and simultaneously applied slip angle and slip ratio inputs. This tyre was used in the generation of a GG speed diagram that is illustrated in Figure 2.4. This GG speed diagram was generated using the seven DOF vehicle model of an F1 race car described

in Casanova [3] and Section 3.1, and used the method that will be described in Chapter 3. It is seen that the shape of the ellipse in Figure 2.3 is responsible for much of the shape of Figure 2.4.

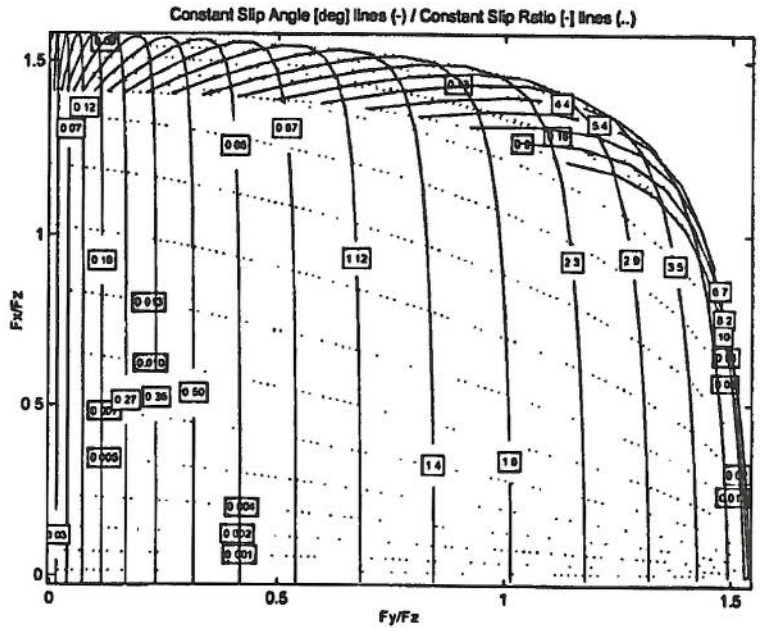

Figure 2.3: Friction circle/ellipse - A generalised F1 tyre.

2.1.4 Transient-optimal control (TO)

Transient methods of lap simulation involve the numerical integration of the vehicle equations of motion with respect to time. This is different to the QSS methods which form a simulation history from the succession of quasi steady state manoeuvres used to follow a prescribed trajectory. The simulation time, found from a QSS method, is a consequential variable evaluated from the distance travelled along the trajectory and the vehicle speed, whereas time is an independent variable in a transient simulation.

There are many computer programs like ADAMS [13], that use transient simulation to show the time varying response of a vehicle to specific manoeuvres, but for the purpose of this thesis, only a subset of the transient method research field, transient-optimal control, will be discussed. This is because this area of transient-optimal control simulation is focussed on controlling the vehicle models to produce the fastest

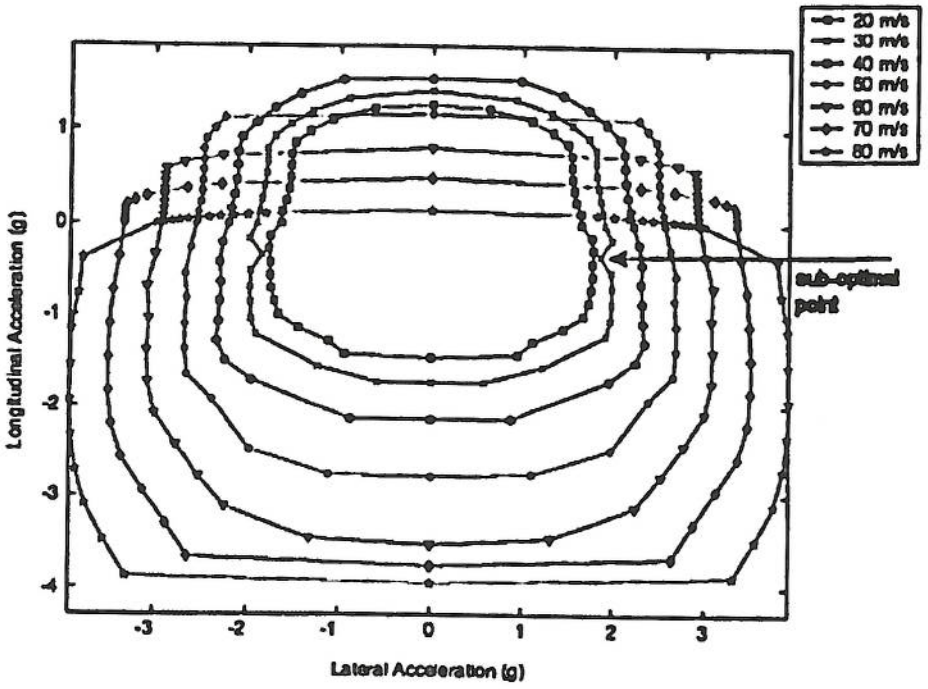

Figure 2.4: GG speed diagram - Using the generalised tyre.

lap time possible, creating the desired situation where the vehicle is controlled to its performance capability limit.

An early three DOF transient optimal control model was produced by Fujioka and Kimura [14]. This model was used to optimise simple cornering manoeuvres with different driving and steering configurations. A simple lap time optimisation using a linear three DOF vehicle model was produced by La Joie [15].

The next significant improvement was a vehicle model with three DOF, an engine torque curve, a non-linear tyre model and a steady state approximation of the aerodynamic forces and load transfer [5]. Like Fujioka and Kimura [14], the model was employed for single manoeuvres, but additionally the vehicle path was not prescribed and was only limited by constraints on the vehicle states.

A direct shooting method for employing optimal control for vehicle simulation has been investigated by Allen [16]. Direct shooting, or direct searching methods rely only on evaluation of the problem ($f(x)$) at a sequence of points $x_1, x_2, \ldots$ and comparing

values, in order to reach the optimal point x^* [17]. This method provides a discrete approximation to the continuous problem and allows the optimal control problem to be formulated as a nonlinear programming problem and is then solved using mathematical programming techniques. This method was applied to a vehicle model that is similar to Hendrikx et al. [5].

The research conducted by Casanova [3] has also focused on more efficient optimal control algorithms. His research expands on previous models, by extending the vehicle model to include seven DOF, an engine map specified by engine speed as well as throttle position, and a combined slip form of the Pacejka Magic Formula Tyre model [18]. His research extends to a complete lap optimisation of two Grand Prix circuits.

At present, Casanova [3]'s work appears to be the state of the art. No other work has been published, to the author's knowledge, that optimises a transient nonlinear race car model over a complete lap of a circuit. The vehicle model has been used to conduct mass [19], centre of gravity [20] and vehicle yaw inertia sensitivity studies [21] that have produced results that are in agreement with results obtained from an F1 car. Unfortunately the computational time for solution is very long (can be more than 24 hours) and the program's success is reliant on the users knowledge of the driver-vehicle relationship with respect to cornering and straight line negotiations to significantly improve the computational time and produce a solution. Additionally judicious choice of the circuit segmentation is necessary for the method to work reliably.

Several relevant studies have been undertaken at Cranfield University that pre-date this thesis. Griffiths [22] produced a basic lap simulation method for an open wheel race car. Minimum time optimal control for cornering, has also been investigated [16]. More recently, full lap time optimisation has been a topic of research [3]. GG speed diagram based research began being applied to race cars by Blasco-Figueroa [8] using diagrams generated from an optimal control-based method [3], and more recently a GG diagram has been produced from a series of dynamic simulations of a simple vehicle model by Murdoch [23].

2.2 Constrained optimisation

Optimisation involves the minimisation or maximisation of a particular function. A scalar performance index $f(x)$ is given that is a function of a state vector $x \in \Re^n$. In a more advanced form the use of constraints can also be accommodated. These constraints can be in the form of equality constraints, $G_i(x) = 0$ $(i = 1,\ldots,p_e)$ and inequality constraints, $G_i(x) \leq 0$ $(i = p_e + 1,\ldots,p)$. The optimisation problem is to select x to minimise $f(x)$ and simultaneously satisfy the constraint equations $G(x)$ within parameter bounds x_u, x_l.
A General Problem (GP) description is given in [24]:

$$\begin{aligned} &\underset{x \in \Re^n}{\text{minimise}} \; f(x) \\ &\text{subject to :} \quad G_i x = 0 \qquad i = 1,\ldots,p_e \\ &\qquad\qquad\quad G_i x \leq 0 \qquad i = p_e + 1,\ldots,p \\ &\qquad\qquad\quad x_l \leq x \leq x_u \end{aligned}$$

where x is the vector of design parameters,$(x \in \Re^n)$, $f(x)$ is the objective function that returns a scalar value $(f(x) : \Re^n \rightarrow \Re)$ and the vector function $G(x)$ returns the values of the constraints evaluated at x $(G(x) : \Re^n \rightarrow \Re^m)$[24].

Analytical solutions cannot be found except for simple functions $f(x)$ and $G(x)$. In most practical situations numerical optimisation methods need to be used [25].

Depending on the characteristics of the objective function and the constraints, different forms of optimisation can be used. If both the objective function and the constraints are linear functions of x the problem is formulated as a Linear Programming (LP) problem. Quadratic Programming (QP) is a method that is constrained as a linear function of x, but the objective function is quadratic. For both the LP and QP problems, reliable solution procedures are available [24].

The most difficult form of the GP is the case where the objective function and constraints are nonlinear functions of x. Solutions of the Nonlinear Programming (NP) problem require an iterative procedure to determine the direction of search at each iteration. The direction of search is usually found by solving a simplified version of the NP, in the form of a LP, QP or an unconstrained sub-problem.

The Kuhn-Tucker equations (KT) [26] are necessary conditions for optimality for a constrained optimisation problem. If the problem is a convex programming problem, then the KT equations are both necessary and sufficient for a global solution point [24]. Referring to the GP, the Kuhn-Tucker equations can be stated as [24]:

$$f(x^*)+\sum_{i=1}^{m}\lambda_i^*.\nabla G_i(x^*)=0 \tag{2.1}$$

$$\nabla G_i(x^*)=0 \qquad i=1,...,m_e \tag{2.2}$$

$$\lambda_i^* \geq 0 \qquad i=m_e+1,...,m \tag{2.3}$$

where * represents the value of the design parameters at the solution point.

If, for instance, a system with a given initial state is provided, then it will be possible that a collection of possible states can be achieved in a given time. These possible states form a set $\ell \subset \Re^n$, the set of n-dimensional vectors with real elements [27]. The set ℓ is convex if all points lying on the line joining two points j and k belonging to ℓ also belong to ℓ; if $j,k \subset \ell$, then [27]:

$$cj+(1-c)k \subset \ell \text{ for } 0<c<1$$

The set is said to be strictly convex if the line joining two points in the set lies in the interior of the set. The diagrams in Figure 2.5 indicate the definition of a convex set in two dimensions.

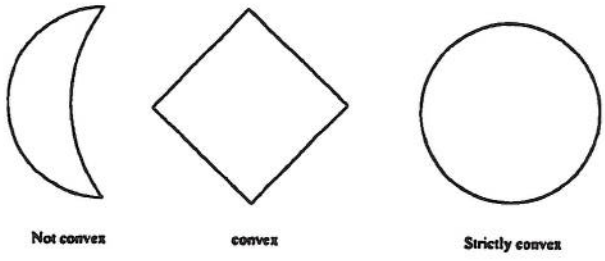

Figure 2.5: Two dimensional sets.

If the problem is not convex then the examination of the second derivative of the objective at the proposed optimal solution $\nabla^2 f(x^*)$ is required. To be a local minimum or maximum the second derivative must be positive definite.

Initially, Lagrange multipliers are introduced ($\lambda_i, i = 1,...m$). The Lagrangian is then formed and partially differentiated with respect to each x_j and each λ_i and set equal to 0, to get a system of $m+n$ equations with nm variables.

The Lagrangian is an augmented function. The objective function is augmented with Lagrange multipliers and constraints to take account of the fact that constraints are part of the problem definition. The point of doing this is the constrained problem is now defined as an unconstrained one.

So, for each variable x_j three conditions must be met. Similarly, those three conditions must also be met for each constraint (and therefore ($\lambda_i, i = 1,...m$)). Each point that is a solution to this equation system is a possible candidate for the minimum/maximum sought. The conditions are called the complementary slackness conditions [28]. This is because for each set of three conditions, either the first or the second condition can be slack (i.e. not equal to zero), but the third condition ensures that they cannot both be non-zero.

The solution of the KT equations forms the basis to many nonlinear programming algorithms. These algorithms attempt to compute the Lagrange multipliers directly. Constrained quasi-Newton methods guarantee superlinear convergence by accumulating second order information regarding the KT equations using a quasi-Newton updating procedure [24]. These methods are commonly referred to as Sequential Quadratic Programming (SQP) methods, since a QP subproblem is solved at each major iteration.

Most available nonlinear MATLAB routines use a Sequential Quadratic Programming (SQP) method. The solution of the QP subproblem is used to define a search direction where the solution is estimated to be. The problem to be solved is:

$$x_{k+1} = x_k + \alpha^* d \tag{2.4}$$

Where x_k is the current state vector, α^* is the scalar step length parameter that is the distance to the minimum, and d is the search direction vector. The specific method used in *fmincon*, the MATLAB implementation used predominantly in this research, estimates the minimum from the search direction by a cubic interpolation method. This is preferred if gradient information is readily available [24].

The step length parameter α is obtained on the basis of decreasing the value of the merit function. The merit function can take on many forms but its role is one of an error function estimate of the current iterate to the solution point. The MATLAB version uses a penalty term that is a function of the Lagrange multiplier values at the current iterate.

This section is a summary of the basic theory of nonlinear programming using the KT equations, and the practical implementation of this theory in the form of the MATLAB Optimisation toolbox, and specifically the *fmincon* SQP method. The interested reader is directed to the user guide for a full description of the implementation of optimal control in MATLAB [24].

2.3 Derivative evaluation

Optimisation routines for nonlinear programming generally use iterative methods to solve the problem. The iterations are conducted with a view to computing a search direction that determines the location of the next iterate. The search direction algorithms are constructed using the gradient of the objective function and for constrained problems the gradients of the constraint equations are also used. Therefore derivative information must be calculated in some manner as an integral part of the optimisation process.

There are three main methods of producing derivative information in mathematical programs: numerical differentiation, symbolic differentiation and automatic differentiation.

In numerical differentiation, a finite difference is evaluated to obtain an approximate numerical value for the derivative of a given function. The accuracy of finite differencing in principle depends only on the increment used to separate the function values (called the truncation error). In addition, the accuracy of the approximation also depends on characteristics of the computing environment on which the calculations are performed. Using digital computers with a defined machine precision there will also be some numerical, or roundoff error, and the combination of both determine the accuracy of the final approximation to the derivative.

2.3.1 Finite differencing

This section follows closely the reasoning of Press et al. [29].

The formula for the forward difference finite approximation is extracted from the definition of the derivative of a variable, x. As the limit of $h \rightarrow 0$ is approached the derivative converges on its true value.

$$f'(x) = \lim_{h \to 0} \frac{f(x+h) - f(x)}{h} \tag{2.5}$$

Using this definition, $f'(x)$ can be approximated by

$$\nabla f(x) = \frac{f(x+h) - f(x)}{h} \tag{2.6}$$

if h is chosen to be sufficiently small. The choice of h directly determines the magnitude of the errors in the use of this approximation.
Truncation error comes from neglecting the higher order terms of the Taylor series expansion in the evaluation of $f'(x)$
where:

$$\frac{f(x+h) - f(x)}{h} = f'(x) + \frac{1}{2} \cdot h \cdot f''(x) + \frac{1}{6} \cdot h^2 \cdot f'''(x) \ldots \tag{2.7}$$

So, for the forward difference formula, the truncation error is of the order of:

$$e_t \sim |h \cdot f''(x)| \tag{2.8}$$

The roundoff error varies with each application. If it is assumed that e_f is the fractional accuracy with which the function $f(x)$ can be evaluated with, then the round off error of Equation 2.6 will be of the order of:

$$e_r \sim e_f |f(x) \ / h| \tag{2.9}$$

In the instance of a simple function, $e_f \approx e_m$, the machine accuracy, but it can be larger if the function is complex.
Varying the value of h allows the minimisation of the summation of the errors e_t and e_r. The optimal choice of h is:

$$h \sim \sqrt{\frac{e_f \cdot f(x)}{f''(x)}} \approx \sqrt{e_f} x_c \tag{2.10}$$

where x_c is the 'curvature scale' of the function $f(x)$ over which it changes, which is generally unknown. Usually x_c is approximated with x. The minimum error (e_d), if h is chosen in accordance with Equation 2.10, to be expected using the finite difference formula for approximating the derivative is $e_d \sim \sqrt{e_f}$. This means that even with virtually zero truncation error, the error in the derivative using the finite difference formula of Equation 2.6 will be at best, the square root of the machine accuracy.
The use of the forward finite difference formula requires at least n+1 calls to the function $f(x)$ to evaluate the approximating derivative. If it is affordable to call the function twice to evaluate the derivative then it is better to use the central difference formula for the approximating derivative:

$$\nabla f(x) = \frac{f(x+h) - f(x-h)}{2h} \tag{2.11}$$

In this case the truncation error becomes:

$$e_t \sim |h^2 \cdot f'''(x)| \tag{2.12}$$

while the roundoff error remains of the same order as in the forward difference formula. The optimised value of h as:

$$h \sim \left(\frac{e_f \cdot f(x)}{f'''(x)}\right)^{1/3} \sim (e_f)^{1/3} \cdot x_c \tag{2.13}$$

Similarly when applying Equation 2.11 with the optimal value of h found in equation 2.13, the minimum value to be expected of the fractional error in the derivative is $e_d \sim (e_f)^{2/3}$. Depending on the value of the variable storage precision of the computer, single or double, the central difference approximation can be one to two orders of magnitude better, respectively than the forward difference formula.

The advantage of the finite difference approximation method is that it is completely general and the function to be differentiated can be treated as a 'black box'. The corresponding disadvantage is that the potential to minimise propagated errors to be transferred during the derivative evaluation is limited to selecting a suitable value of h. The approximation errors due to truncation of the Taylor series cannot be avoided.

2.3.2 Symbolic differentiation

Symbolic differentiation begins with an algebraic expression for the function and produces a formula for the derivative. Commercial symbolic differentiation products

such as Mathematica and Maple are now widely available. The advantage of using symbolic methods is that the resulting formula can give insight into a problem whereas the corresponding numerical derivative value cannot.

In general, symbolic mathematics programs manipulate formulas to produce new formulas, rather than performing numeric calculations based on formulas. The implementation on a computer is deceptively simple [30]:

- If the problem to be solved is an easy problem, solve it at once.
- If the problem to be solved is a hard problem, break the problem into smaller sub-problems.
  - Use the problem-solver recursively to solve the sub-problems.
  - Combine the solutions of the sub-problems to make a solution for the larger problem.

This method avoids truncation errors but usually a computer implementation has problems in handling large expressions and the time/space usage for computing derivatives can be enormous. In the worst case it can cause the program to crash. In the situation where common sub-expressions are not identified in the main expression this leads to unnecessary computations during the evaluation of the derivatives.

The disadvantages are that some important functions cannot be described by expressions. The useful method of data storage, the lookup table, is one such example. This is a significant short-coming because the use of lookup tables allows accuracy in evaluating variables without requiring an analytical, expression based relationship defined as a function of other variables. In most instances this is too complex to achieve, or in the more usual case, the variable cannot be defined as a function of other variables because the relationship is unknown. The research presented in this thesis relies on the definition of engine torque and gear ratios as lookup tables and in the absence of accurate empirical relationships, this makes the use of symbolic differentiation impossible at the current time. Therefore this method will not be discussed further.

2.3.3 Automatic differentiation

Automatic Differentiation (AD) is a set of techniques based on the repetitive application of the chain rule to numerical expressions rather than symbolic values to obtain

derivatives of a function. AD exploits the fact that every computer program, no matter how complicated, executes a sequence of elementary arithmetic operations such as (+,-,x,/) or elementary functions such as *log* and *exp* [31]. AD is a process that obtains numerical values without generating a formula for the derivative and without the truncation error of numerical differentiation. AD might be considered as somewhere between symbolic and numerical differentiation.

There are two main methods of implementing AD, the forward mode and the reverse mode. In the forward mode the function variables of a program are stored as both a value and a partial derivative vector referred to as the *Jacobian*. As the function is evaluated the program variables are updated with new values as a result of algebraic operations. In the forward mode the corresponding partial derivative vectors are also updated at the same time, and at the end of the function evaluation the partial derivative vectors will contain the gradient of the function with respect to the program variables.

The reverse mode differs in that the partial derivative information is evaluated in the opposite order to the corresponding function evaluation. While the function is evaluated, a record is kept of the values held by program variables. Each record is termed a node [32]. The reverse mode calculates the partial derivative of the function value with respect to the node.

AD works using chain rule propagation. Two examples of the implementation of these rules are shown below:

$$\begin{aligned} a &= x^T \cdot y \\ \dot{a} &= \dot{x}^T \cdot y + \dot{y}^T x \\ b &= x + y \\ \dot{b} &= \dot{x} + \dot{y} \end{aligned} \tag{2.14}$$

As far as the computer program is concerned, the program is unchanged except for the fact that it is now operating with a new function class which is stored as a structure of two double precision variables. Using the example in 2.14:

$$a = (a.value, a.derivative) \tag{2.15}$$

$$b = (b.value, b.derivative) \tag{2.16}$$

All the elementary functions are overloaded to ensure that while the 'value' is being computed, the derivative output is being consistently updated at the same time.
This means that there are no Taylor series truncations and the only source of error will be due to the roundoff error e_r, which is a function of the computer machine precision.

2.4 Vehicle on-limit behaviour

Vehicle simulation is the standard tool for investigating aspects of vehicle behaviour. In this thesis the interest lies in the on-limit behaviour of the vehicle as this is the primary area of interest in race car handling behaviour analysis. This very premise unfortunately negates the majority of the linear analyses that can be conducted in investigating vehicle dynamic behaviour. The reason for this is due to the lack of realism when using linearised slip angle and tyre force approximations in the vehicle models. These approximations have been shown to be valid when investigating normal driving conditions [1, 2, 33], but the fact that on the performance limit the tyres have a nonlinear response to slip angle and slip ratio, limits their use in race car handling analysis.

2.4.1 Minimum time programs

The use of optimal control to solve the minimum time manoeuvre/lap problem has mainly been documented as an applied mathematics treatise, which has increased the toolkit available to the vehicle dynamics engineer. The research conducted and summarised in Section 2.1.4 has produced very few contributions to the body of knowledge in terms of understanding vehicle behaviour. The early work of Fujioka and Kimura [14] employed a double lane change manoeuvre to produce a set of time histories of a range of drivetrain configurations. A similar approach and manoeuvre was taken by Hendrikx et al. [5], using a more sophisticated vehicle model. More recently research by Casanova [3] and Siegler and Crolla [34] have used seven and nine DOF respectively to solve the minimum time problem and the extent of reporting has been limited to vehicle model/simulation validations. This is due to the application of optimal control for race car simulation being in its infancy and due to computational difficulties that exist when solving the minimum time problem. Additionally it has been, and still remains, a challenge to prove that the result found is truly optimal. As a result the use of the minimum time solution to date, has been limited to preliminary investigations of vehicle mass, centre of gravity location and yaw inertia sensitivity [19–21].

2.4.2 Steady state cornering behaviour

The steady state solution of the equations of motion are often used in vehicle research because it allows the vehicle handling to be characterised in terms of understeer, oversteer or neutral steer. The key parameter that determines this is called the *stability margin*, which was originally identified by Segel [33] as a key variable in the mathematical definition of the understeer and oversteer concepts. The sign of the stability margin for the standard two DOF system (bicycle model) directly determines the sign of K_{us} which is known as the understeer coefficient [35].
The definition of K_{us} as given by Crolla [1] for the 2DOF handling model is:

$$K_{us} = \frac{M(l_r C_r - l_f C_f)}{W_b C_f C_r} \tag{2.17}$$

where the stability margin is:

$$(l_r C_r - l_f C_f) \tag{2.18}$$

Equations 2.17 and 2.18 are central to the definition of steady state vehicle handling behaviour. The three conditions are as follows:

1. Neutral steer - $K_{us} = 0$, where the stability margin is zero. This is equivalent to the front and rear axle slip angles being equal.

2. Oversteer - $K_{us} < 0$, where the stability margin is negative. This is equivalent to the rear axle slip angle being larger than the front axle slip angle.

3. Understeer - $K_{us} > 0$, where the stability margin is positive. This is equivalent to the rear axle slip angle being smaller than the front axle slip angle.

The stability of the vehicle is a function of the stability margin and K_{us}. When the vehicle is understeering the vehicle response is always stable, but may be oscillatory. However when the vehicle is oversteering there is a critical speed beyond which the vehicle becomes unstable. Because the link between steady state behaviour and the transient response of the vehicle is very strong, there has been a continued reliance on steady state methods to the current day [1].

The characterising of a vehicle's steady state behaviour and high speed stability have been fundamental to the history of vehicle dynamics. Passenger vehicles are always designed to maximise safety and therefore in most instances the vehicles are

configured to ensure that the vehicle has an understeer characteristic at all plausible vehicle speeds, due to its unconditional stability.

2.4.3 Passive systems

Inspection of the equations of motion for a vehicle model provide obvious starting points for exploring the limits of performance and how to improve it. The three DOF vehicle model described by Crolla [1], Genta [2] is given in equations 2.19 to 2.21 and illustrated in Figure 2.6 using the SAE vehicle axis definitions [36].

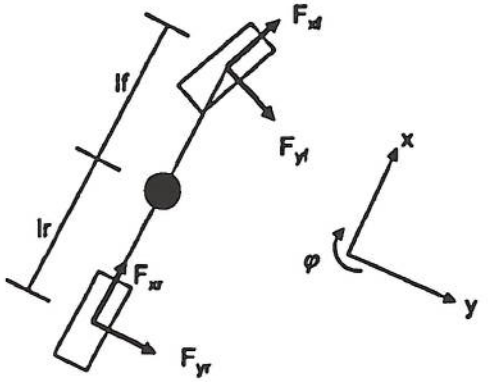

Figure 2.6: Three DOF vehicle model. [1, 2]

$$M(\ddot{x} - \dot{y}\dot{\varphi}) = F_{xf} + F_{xr} \tag{2.19}$$

$$M(\ddot{y} + \dot{x}\dot{\varphi}) = F_{yf} + F_{yr} \tag{2.20}$$

$$I_{zz}\ddot{\varphi} = l_f \cdot F_{yf} - l_r \cdot F_{yr} \tag{2.21}$$

The terms in the equations of motion M,I_{zz}, and the tyre forces are obvious choices. By reducing the vehicle mass, the acceleration of the vehicle automatically improves, if everything else remains the same. Whether or not reducing the yaw inertia to make the vehicle more sensitive in yaw is performance enhancing is still not certain. It has been shown that the value of I_{zz} does not affect the minimum time performance [20], but whether the behaviour of the vehicle is fundamentally changed still remains to be seen. The longitudinal location of the centre of gravity also appears in the equations

of motion through l_f and l_r, and has been shown by other researchers to be very influential in the vehicle behaviour [1, 20, 33, 37]. These parameters are regarded in this thesis as passive elements of the vehicle setup for race cars. For vehicles that generate aerodynamic downforce this also falls into the passive category as the aerodynamic components can not be actuated on the race car for most racing formulae. Once the vehicle is prepared, there is no form of control that can be applied to the vehicle that can vary these parameters at will to meet a control objective during a race. As the vehicle traverses a circuit, the mass of the fuel will reduce and depending on the fuel tank location, it may affect the yaw inertia of the vehicle as well, but this cannot be controlled beyond taking into account these affects during the designing of the vehicle.

However, there is merit in making a performance based choice of these parameters for a particular circuit or racing strategy. For instance, depending on the vehicle fuelling strategy and engine fuel consumption requirements, the sizing of the fuel tank can be optimised for the car and circuit to minimise weight, and thus improve the vehicle acceleration capability. The choice of values for all of these parameters in the racing environment is investigated by this research.

2.4.4 Active systems

The use of active systems hit a peak in Formula One in the early 1990's. This was characterised by Wright [12] as the era of the control system (1984-1993). During this period the performance lost by the banning of skirts, the requirements of a flat underside, and the phasing out of turbo engines pushed engineers to make the vehicles more driveable at the limit of the vehicle performance, thereby utilising more of the performance potential of the vehicle more often.
The list of parameters that were 'actively' controlled at some point during this era were [12]:

- Active suspension.
- Automatic and semi-automatic gear changing.
- Engine control: ignition, fuel, throttles, and intake lengths.
- Drive-by-wire.
- ABS.

- Traction control.
- Four-wheel steer.
- Differential control.

The only ones to have survived to this day from this list are differential control, drive-by-wire, semi-automatic gearboxes and traction control. In this thesis, the term active has a specific meaning. By active it is meant that the time varying control of a parameter or component is conducted in a manner where the continuous maximisation of the performance of the vehicle is the main objective.

2.4.5 Roll stiffness distribution

The contribution of roll to lateral load transfer, and therefore the normal force applied to the tyres is well established [38, 39]. The use of active systems for controlling suspensions has been used before in Formula One and other open wheel racing series with the specific aim of controlling the ride height of the vehicle to produce consistent and advantageous aerodynamic downforce [12, 40, 41]. At present this form of active control is not allowed by Formula One regulations, but the roll stiffness distribution is a key variable in determining dynamic weight transfer [40]. The enhancement of vehicle handling via suspension control has been investigated recently [42]. Through a study using double lane change manoeuvres, their simulation results suggested that by kinematically controlling links in the suspension the roll centre migration could be adjusted by which the roll angle, lateral acceleration and yaw rate were improved.

When equations for roll motion are derived for basic handling models, it is normally found that there is very little inertial coupling between the yaw mode and the roll mode. However, modifications to the vehicle handling characteristics may occur [39]. This is because the relative roll stiffnesses of the front and rear axles affect the proportion of the vertical load transfer carried by the front and rear axles.

To investigate the effects of load transfer on the GG speed diagram, one can begin with the roll centre concept.

> For a two dimensional representation of a suspension there exists an instantaneous centre for which it is possible to rotate the body cross sec-

> tion while the points of tyre/road contact do not slide. This centre is the *roll centre* [39] (p97).

In the literature there appears to be some confusion over the actual definition of the roll centre. It has been suggested in Dixon [43] that the method of calculation of the roll centre, which can be performed using suspension geometry or in terms of applied forces [36], should be correctly identified as either a *kinematic* roll centre or a *force* roll centre, respectively. In this thesis, and from this point forward, the term roll centre is assumed to mean the kinematic roll centre. This has been chosen because the intended use of the roll centre analysis is to determine the lateral load transfer component of the tyre load for nonlinear tyre force evaluation. The force roll centre uses tyre force information to infer the lateral load transfer, which is the reverse of what is required of the suspension model. The relative advantages and disadvantages of both methods have been well documented by Dixon [43].

Using a simple suspension design, as depicted in Figure 2.7, it is possible to show how the roll centre vertical height is derived from the geometry of the suspension locations on the body and wheel assembly. The roll centre method begins by extending a line through the current position of the upper and lower wishbones (as the roll centre moves with suspension articulation), through their wheel and body connections, to find the instantaneous centre of rotation of the wheel unit relative to the body. The centre of rotation is where these two lines converge, because the wishbones are assumed to be perfectly rigid and therefore the wheel position relative to the body will always be perpendicular to each wishbone. In reality the wishbones are connected by rubber bushes which do allow movement of the wishbone relative to the wheel and to the body, but this is assumed to be negligible. The aim of the roll centre analysis is to end up with a description of the roll centre which is the instantaneous centre of rotation of the body relative to the road. If it is assumed that the wheel is considered to pivot at the centre of its contact patch, then the instantaneous centre of rotation of the wheel/road pair will also occur at this point. According to Dixon [43] (p70):

> The centro of each of the three pairs selected from three objects lie in a straight line.

The *centro* is an abbreviation for the instantaneous centre of rotation. This theorem states that the roll centre (the centro of the body/road pair) must lie on a line between the centro of the wheel/road pair and the centro of the wheel/body pair. This is also

equivalent to assuming a third rigid link between the contact patch and the lower wheel suspension wishbone (Figure 2.7). The assumption that the vehicle is symmetric determines the lateral location of the roll centre on the centreline of the vehicle.

If the roll centre is located for both the front and rear axles of the vehicle, then a line drawn between these two centres, from axle to axle, is termed the *roll axis*.

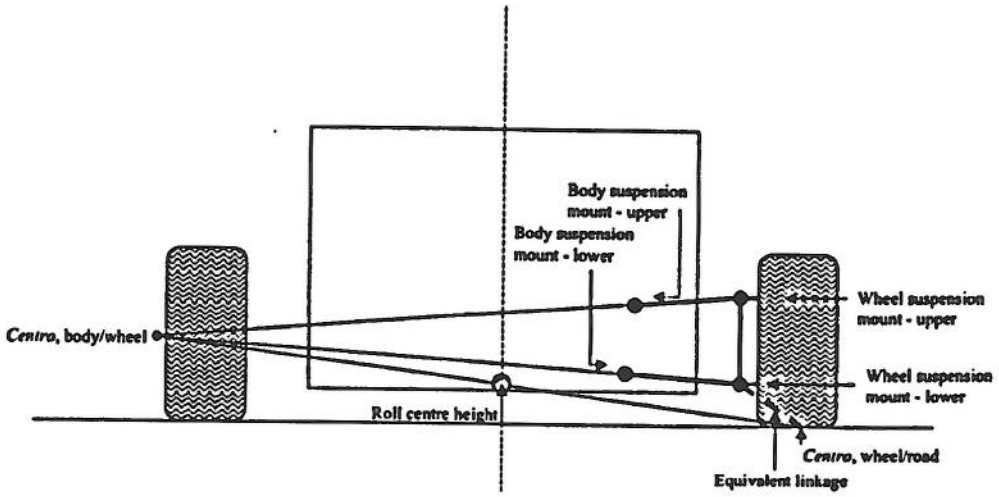

Figure 2.7: Roll centre analysis - one axle.

It should be noted that the use of the roll axis concept must be undertaken with care and respect for the underlying conditions under which it is valid. Strictly, the roll axis method embodies a group of assumptions:

- Small roll angles.
- Vertical compliance of the tyres is ignored.
- Inclination of the roll axis is neglected.
- Gyroscopic effects of the wheels and engine are neglected.
- Torsionally rigid body.
- Approximation of longitudinal tyre forces using the torque applied to each wheel.
- The lateral deflection of the wheel and tyre are neglected.

The assumption of a torsionally stiff chassis allows the supposition that the roll moment will be distributed according to the ratio of the roll stiffnesses between front and rear axles. This assumption effectively requires the two axles to adopt the same roll angle. This is usually possible for cars but the torsional compliance of a truck can be significant and will make the analysis significantly more complicated [44]. An open wheel race car, characterised by stiff springs with ride height dependent aerodynamics, rolls significantly less than a standard car and as such the assumption of a torsionally stiff chassis is believed to be valid for the research in this thesis.

In reality, as soon as the vehicle rolls, the assumption of symmetry is no longer valid and the roll centre migrates from the centre line. The assumptions of small roll angles and negligible inclination of the roll axis can be held on the basis that the combined suspension and tyre stiffnesses are very high (175-250 kN/m [12]) and therefore the roll angle of the vehicle will be quite small. Because the compliances are high it is also assumed that the lateral deflection of the wheel and tyre can also be considered negligible.

The use of nonlinear tyres in the form of the Magic Tyre Formula [18] requires the tyre load to be provided as an input rather than the linear method of assimilating it into a cornering stiffness coefficient. To calculate the load transfer which affects the load on the tyres, the moments generated from the longitudinal tyre forces applied at their respective contact patches are needed. This is a circular dependency requiring either an iterative solution to find the correct tyre loads and longitudinal tyre forces, or either the tyre loads or longitudinal tyre forces are estimated by other means to allow the calculation to be made. The method used here is a first approximation of the longitudinal tyre forces, using the torque applied to each wheel divided by the wheel radius. This assumption results in the contribution of the inertia of the rotating masses being neglected, but this is only significant at low speeds. For a race car this is not particularly often and so the assumption is also valid for the areas of interest in this thesis.

The roll axis and kinematic roll centre concepts are very simplified means of characterising the roll mode of a vehicle. The choice of this method is purely due to the computational economy offered through its use.

This thesis will explore the significance of the roll stiffness distribution at a representative front and rear roll centre height from a roll centre analysis to determine how important this parameter is with respect to the performance capability of the vehicle.

2.4.6 Differentials

The differentials used in Formula One and also in the World Rally Championship (WRC), are rather unique. The cost of producing electro-hydraulic differentials is very high, therefore these are the only two forms of racing that employ them. They are not fitted in passenger vehicles. As a result information about them is sparse, with Wright [12] giving a broad overview of this type of differential. To avoid banning the use of electronic differentials, the rules of the Formula One championship up until recently [45], stipulated that the electronic differential could only be a electronic analog of a mechanical equivalent limited slip differential. The purpose of a limited slip differential is worthy of discussion.

The basic premise of the differential is to transmit power from a single power source to two drive axles (or shafts) and permitting independent rotation of the two driven axles (i.e. differentiation) [46]. The original version of this is the open differential, shown in terms of a power balance in Figure 2.8. The open differential aims to split the incoming torque equally to the two driveshafts, while allowing the two driveshafts to spin at different speeds if required. The side gears allow the two driveshafts to spin at different speeds. The only difficulty with this arrangement occurs when one of the wheels attached to a driveshaft loses traction for some reason. Due to the balancing of torque design of the open differential, the low traction wheel accelerates, the side gear accelerates as well, but the high traction wheel does not accelerate in a similar fashion. The side gear absorbs the excess incoming torque and the total torque that can be transferred by the differential is only twice the torque provided to the low traction wheel. The crux of the problem with this scenario is that the high traction potential of the other wheel on the axle is not exploited.

The Limited Slip Differential (LSD) is a solution to this problem with the open differential. There are many varieties of LSD that exist. They fall into two categories, those that are torque sensitive and those that are speed sensitive, but both generate a transfer torque to the high traction wheel from the low traction wheel through the differential, facilitating improved traction over that capable by the open differential

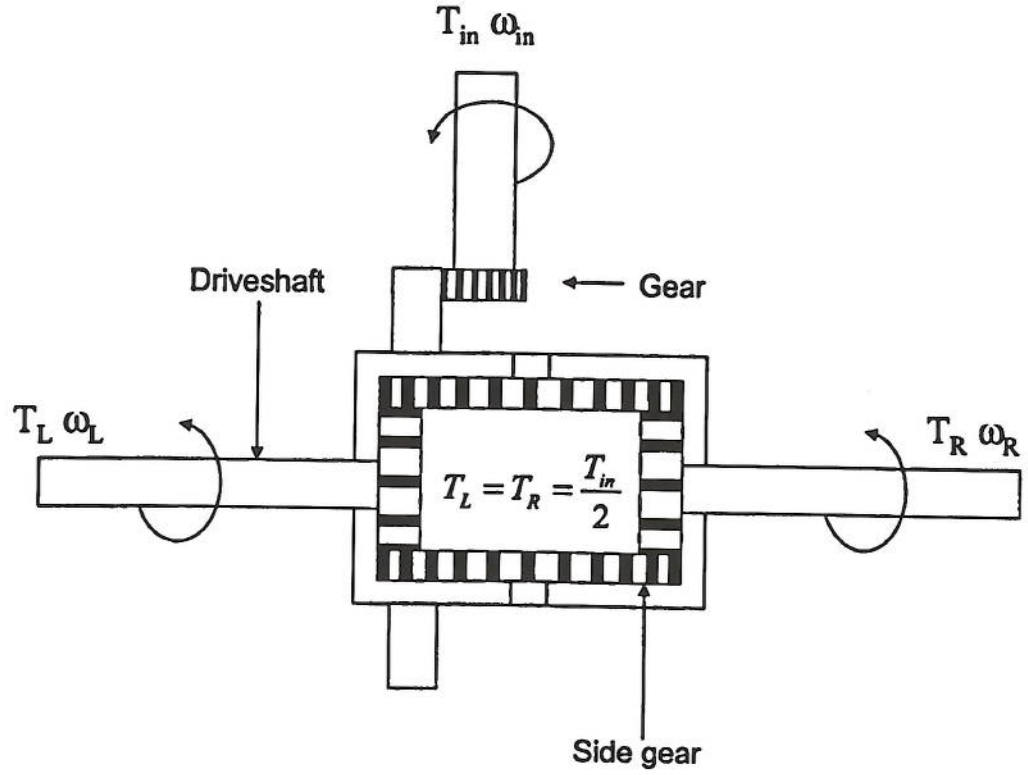

Figure 2.8: Open differential power balance.

(Figure 2.9). Since speed sensitive differentials are more commonly used for centre differentials the discussion will be restricted to torque sensitive differentials. The simplest example of the LSD is the Salisbury differential [11]. This LSD produces ΔT_{LSD} through splining a series of clutches to the driveshafts and the differential housing. Engaging the clutches locks the driveshafts to the differential housing forcing the driveshafts to rotate at the same speed as the housing. The driveshafts can still rotate independently of each other if they can overcome the locking torque provided by the clutches.

Another solution is the Torsen differential [46]. The Torsen differential provides a torque proportioning characteristic between driven axles by interconnecting the drive axles with a worm-type gearing arrangement. This arrangement is designed to support a predetermined ratio of torques between drive axles. This ratio is a measure of the amount of torque that can be delivered to the wheel with high traction when compared with the torque that can be supported in the low traction situation. The Torsen system is very elegant but to change the bias ratio a new gear train is necessary. With the

clutch plate system it is easy to set up using electro-hydraulic actuation allowing any form of control strategy to be employed, and as a result it is used in Formula One [12].

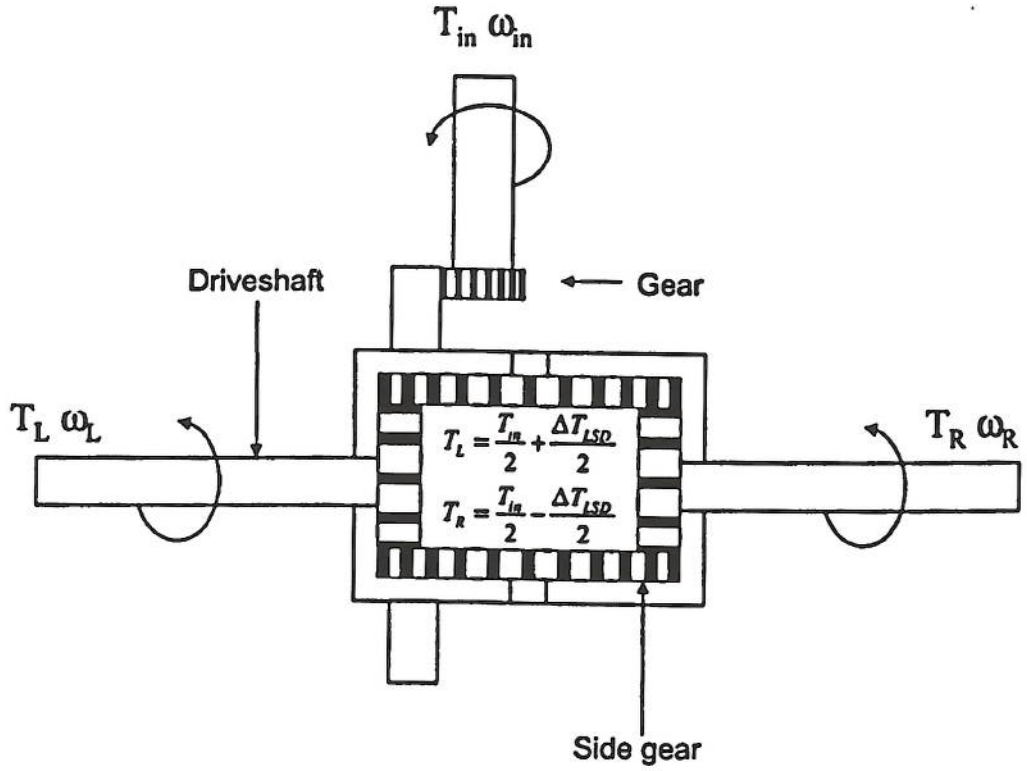

Figure 2.9: General Limited Slip Differential power balance.

In addition to the two primary objectives of differentiation and torque transfer, it has become increasingly obvious that the differential situated on the rear axle can be used in a manner to affect the vehicle dynamics. Differential braking (using the brake torque of each individual wheel to control individual wheel spin) is a similar concept. The use of mechanical forms of clutch pack LSD differentials, which have an inherent resistance to turning caused by the preload torque, was deemed disadvantageous with respect to torque transfer provided by differential braking via the ABS control mechanism [47]. However, the use of LSDs for controlling vehicle stability has been explored. One set of researchers has made the case for using a Torsen differential instead of differential braking for affecting vehicle stability and complementing a traction control system [48]. As mentioned earlier, these types of differentials are not commonly used in Formula One but the argument is valid. The general point made by Holzwarth and May is that traction in general can only be improved by either propor-

tioning the torque across the driven axle or by limiting the input torque to the axle. The natural domain of the differential is to proportion torque. The simple answer to limiting the torque is to reduce the engine torque supplied to the differential. The study by Holzwarth and May concluded that a torque sensitive differential coupled to a traction control system was equal to the performance of a equivalent differential braking system plus traction control. Because a electro-hydraulic differential can be controlled according to any definable strategy, it appears that complementary vehicle stability control and traction control could be possible. In addition, the differential could be operated in a manner which actually improves the vehicle performance envelope. Differential control is an area that will be investigated further in this research.

2.4.7 Vehicle stability

A system is (Lyapunov) stable if the system states will remain bounded for all time, for any finite initial condition [49]. In terms of the vehicle:

> Following a disturbance the vehicle should return to its previous steady condition without undue time lag and in a well damped fashion [1](p7).

Most vehicle stability studies fall into one of two categories: linear analysis via the solution of the equations of motion to find the eigenvalues of the system, or simulation studies using indicators of vehicle stability to make comparative studies.

The use of linear models allows a very insightful view of vehicle stability. Traditionally the vehicle model's equations of motion are solved with the inputs set to zero, producing a set of homogeneous equations which can be solved to find the roots of the equations. These roots are called eigenvalues and can be plotted in the real-imaginary plane for a series of parameter changes (for instance different vehicle speeds). Depending on the location of the roots in the real-imaginary plane the vehicle model stability can be characterised as a combination of stable or unstable, and oscillatory, and non oscillatory due to inspection of the eigenvalue plot. As mentioned earlier linear analysis is not generally valid at the limit of vehicle performance, but in some cases, as seen frequently in aircraft modelling linearisation about an operating point can extend the use of linearisation to particular manoeuvres with success [50, 51].

The other option is to run vehicle simulations with demanding vehicle manoeuvres to find the limit of 'stability'. Examples of commonly used manoeuvres include the

conventional constant radius (variable speed) test and the "infinite skid pad" (constant speed) test, and are well documented in Milliken and Milliken [52]. It is evident from the literature that the term 'stability' has been used in different contexts by researchers [1, 47, 53]. Stability, when using linear models, tends to apply to straight line running, where the vehicle transient response to small perturbations arising from wind gusts and road camber, etc, are investigated [1].

Research using vehicle simulations for the development of vehicle stability control suggests that the vehicles yaw response and/or its sideslip angle are direct measures of vehicle stability and should be included in the objective for a vehicle stability control system [54–56]. Considering that the stability control strategies are all aimed at ensuring that the driver is able to maintain directional control of the vehicle at all times, then it appears that the stability being referred to is an on-limit vehicle stability. The vehicle simulations are provoking the vehicle up to and beyond its tractive and cornering capabilities to establish the vehicle stabilising abilities of the controllers. This second measure of stability is more applicable to the current research direction of on-limit performance of race cars as it allows the use of nonlinear models which is crucial if saturating tyre models are to be used.

2.4.8 Vehicle stability control

To control vehicle stability effectively means that the tyres must be used at less than their maximum tractive force to ensure lateral force capability to enable directional control of the vehicle to be maintained [47, 57–59].
The most common example of tyre force control is traction control, and is used in automotive systems to meet two fundamental goals: [47, 58, 59]:

1. To ensure directional/lateral stability.

2. To provide effective transmission of the tractive force to the road surface.

This order of importance is imposed because keeping the vehicle within its stability limits is more important than producing optimum traction. This is also the case for racing cars, because although the optimum traction is of vital importance, the realisation of it causes the driven tyres to be utilised close to saturation. This leaves very little tyre force capacity for cornering and will result in a vehicle which will be directionally

unstable [60]. This will be especially evident on exit from a corner. Finding the correct balance between the two objectives is vitally important to ensure a fast, stable race car.

Traction control algorithms

The slip ratio is the independent variable that determines the amount of longitudinal tyre force for a given vertical load. It is a measure of the deviation of the tyre from a pure rolling condition. The slip ratio, κ is defined as:

$$\kappa = \frac{\dot{x} - R_w \cdot \dot{\theta}_w}{\dot{x}} \tag{2.22}$$

The basis of traction control is to maintain the vehicle slip ratio beneath a predetermined maximum or within a narrow band depending on vehicle stability considerations (Figure 2.10). To ensure vehicle stability, the band is situated below the maximum available longitudinal tyre force capability, allowing lateral force to be generated if required.

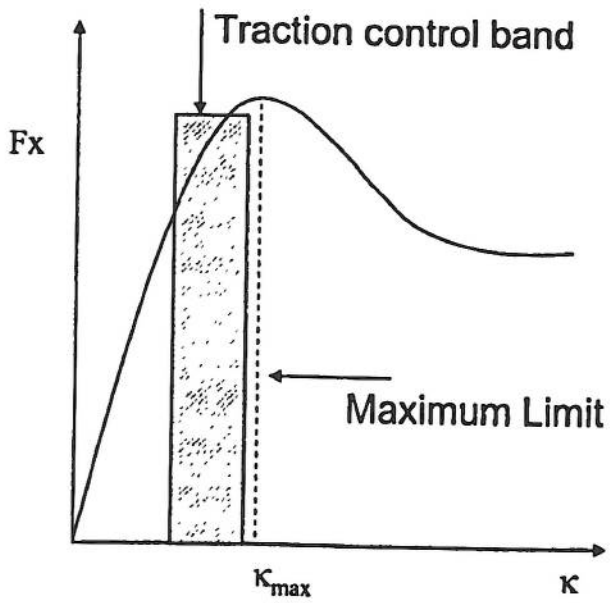

Figure 2.10: General relationship between longitudinal tyre force and slip ratio, κ.

For reasons of commercial sensitivity not many algorithms used to produce traction control are published. The manner in which they are installed, mode of operation, sensors used and general strategy are often published, an example of which is the

Bosch ASA system which has been improved through the 1990's to the current day [61-63].

One of the rare occurrences in the literature is the algorithm used by Toyota for traction control of the Crown model [64] and the improved version for the Lexus model [47]. The Lexus version will be discussed here. The Lexus traction control system uses a Proportional plus Integral controller to meet a target wheel speed, $`V'''$ which is found from a target slip ratio maximum value. The targets are set from extensive vehicle testing on various p road surfaces. Differential braking is used to control the spinning driven wheel when the driven wheels on an axle are on split p surfaces. It is not mentioned in the Lexus article but other researchers suggests that this is only practical if differential braking is used only at low speed (below 40m/s) [62, 65, 66]. Unfortunately differential braking is not allowed in Formula One so it cannot be employed. However, at high speed most systems only use a form of engine control for traction control response, due to the high thermal load required by the braking system to carry out the traction control [62, 65, 66].

The Proportional plus Integral controller produces a modification to the throttle angle, with the throttle control provided by a step motor acting on a sub-throttle valve, which is adjacent to the main throttle valve in the throttle body [47]. The results of the traction control system showed in testing that the corresponding steer angle and yaw rate response for specific manoeuvres were reduced when compared with the vehicle without the system.

Due to the banning of traction control in 1994 it became possible for a Formula One team to publish their approach to the problem [67]. In similar fashion to Ise et al. [47], the solution entailed the use of an automatic control approach choosing a PID controller (Proportional plus Integral plus Derivative), but in this instance the controller provided an engine torque reduction estimate. The input deviation to the PID controller was calculated as the difference of the measured slip and the slip goal value. The slip goal values were stored in a map as a function of vehicle speed/throttle operating points.

Interestingly, the practical application of traction control has highlighted an interdependent relationship with vehicle handling behaviour. Frequently in test sessions, improved traction control response came at the expense of degradation in chassis stability.

Power-on understeer and the inability to position the car with power-on oversteer were cited as the chassis problems. Additionally the proper employment of traction control required the driver to 'commit' to the corner at a higher speed and accelerate out of the corner sooner, thus requiring the driver to 'trust' the traction control system to intervene and eliminate the excess wheelspin that can cause a spinout.

For passenger vehicles the use of stability control has taken on many forms, initially with traction control and ABS focussing on the wheel as the plant to be controlled in some fashion [61-63, 68] to a fixed slip ratio target. A method of varying the slip ratio target for a TC (Traction Control) system as a function of slip angle is described in Park and Kim [57]. Their results showed that the path deviation of a vehicle on a limited ,14. surface was lower with the slip angle dependent target rather than a fixed slip ratio target method. More recently the use of these vehicle subsystem controllers have been employed to provide an additional control function for an outer loop control of the vehicle as the plant, in addition to the controller duties to meet ABS and TC requirements.

In the wheel-plant focussed systems, the aim was to meet a slip ratio target [47, 57] to help optimise performance without impairment of stability and steerability, whereas the next generation of systems has sought to meet a vehicle stability criteria through anticipation/determination of the course that the driver intends to follow [69]. Comparison with the actual vehicle position resulted in control commands to avoid excessive understeering and oversteering.

For racing cars, developments in vehicle stability control have been similar to the early ABS and TC methods with a view to extracting as much performance from the tyres without losing directional stability [67].

Yaw rate or sideslip angle?

In order to control a plant a target must be provided. **In** the literature, two vehicle parameters used to measure vehicle stability are yaw rate and/or sideslip angle [5456, 70-74] (Figure 2.11).

The yaw rate of the vehicle, (0, represents the rate of change of the vehicle turning about its imposed vehicle fixed axis system (Figure 2.11). As (j) increases, there will

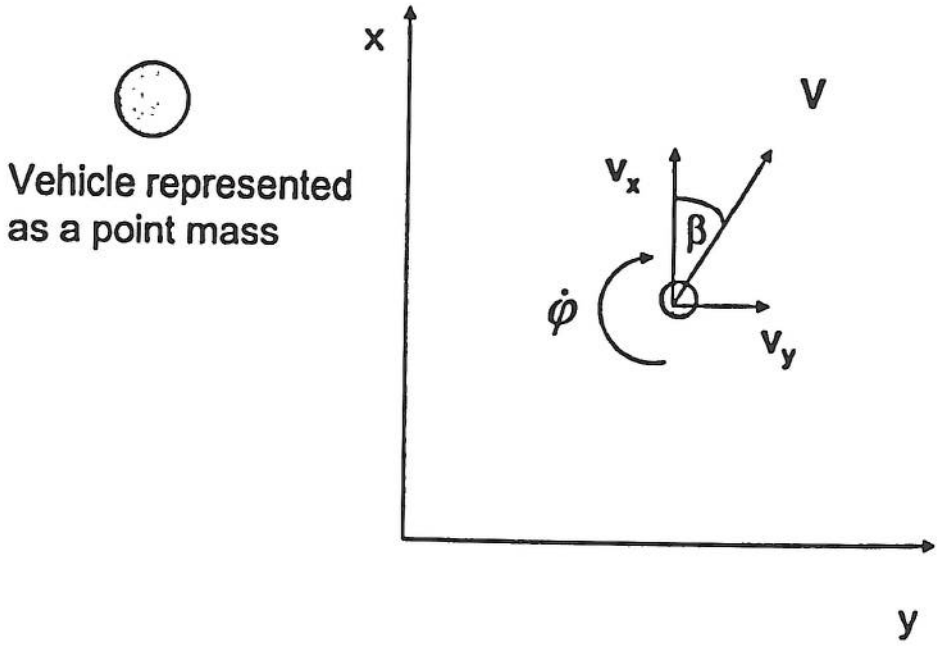

Figure 2.11: Sideslip angle β and yaw rate $\dot{\varphi}$

come a point where the vehicle will become unstable and the vehicle could spin out of control. The sideslip angle is a measure of the proportion of lateral planar motion with respect to the total planar translational motion of the vehicle. This is described by the angle the velocity vector of the vehicle forms with the imposed vehicle axis system. Therefore as the proportion of lateral velocity increases with respect to the longitudinal velocity, β will increase towards infinity. As β increases, the vehicle progresses towards complete lateral drift which is generally undesirable for regular drivers. As Figure 2.11 shows, β can increase without $\dot{\varphi}$ increasing and vice versa.

The majority of research to date started with yaw rate as the main variable of interest [70, 71]. This is partly due to its comparatively lower cost of measurement compared with sideslip angle [74–76]. Another significant reason is that for normal driving conditions (i.e in the linear range) a yaw rate goal of neutral steer is straight forward to produce from a two DOF linear vehicle model in real time, and it is implied in the published literature that the neutral steer condition forms a big part of the desired yaw rate target [54, 69–71]. Yaw rate control appears to be the dominant variable for passenger vehicle stability control [72].

In emergency situations, the value of the sideslip angle is necessary to detect a sliding or skidding vehicle, which may have normal yaw rates [75]. Leffler et al. [69] showed that the steady increase of the sideslip angle for a car may lead to instability, and it can be concluded from Shibahata et al. [77]'s work that the sensitivity of the yaw moment of the vehicle, with respect to changes in the steer angle, decreases rapidly as the sideslip angle of the vehicle increases [72]. The difficultly of controlling the vehicle characteristics in the nonlinear region led to the development of the β method of Shibahata et al. [77] which suggests that the mechanisms of vehicle behaviour in the linear and nonlinear region can be described as a function of sideslip angle, for a given steer angle.

Combinations of side slip angle and yaw rate has been quite common in the literature, with Yi et al. [56], using sliding mode control to stabilise a vehicle with a linear combination of sideslip angle and yaw rate in the objective. Using a state space version of the 2DOF bicycle model Tseng et al. [54] controls both sideslip angle and yaw rate in their version of VSC (Vehicle Stability Control), on the basis that a vehicles yaw dynamics and sideslip angle value must be limited to make the vehicle manageable by average drivers. This same argument is used by van Zanten et al. [72, 78] to explain their combined limitation of vehicle yaw rate and sideslip angle for the average driver.

There are many articles centred around the measurement of β and $\dot{\phi}$, [73–76] due to the inherent difficulties and costs associated with practical control and instrumentation on mass produced vehicles. However little attention is given to the application of vehicle stability control on the performance limit to race cars. There is the obvious argument that vehicle stability is a secondary concern in the pursuit for performance, but the counter argument is that if the vehicle is made to be more stable at the vehicle performance limit, the driver may feel more comfortable operating at that limit and the laptime may improve.

This thesis takes a different approach to the vehicle stability limit problem, by focussing on the effect of implementing a stability algorithm solely based on β. This is chosen because it is the belief that in Formula One the majority of vehicles spinning out of control will occur at low speeds (< 40 m/s) and therefore this phenomena can be controlled via the TC system design. The TC system has significant control of the high acceleration of the vehicle at low speeds because the engine torque available is more than capable of saturating the rear tyres. The level of saturation of the rear tyres

generated by transfer of the engine torque to the tyres via the TC system affects the leftover amount of tyre force available for lateral force generation, and therefore the ability of the vehicle to resist a spinout at low speeds. At higher speeds the additional tyre load due to aerodynamic supplementation ensures that the vehicle is more likely to experience unwanted lateral drift before the vehicle reaches the conditions conducive to spinning out. Therefore if the lateral drift which is characterised by β but not $\dot{\varphi}$, is used for vehicle stability control then the path tracking requirements of the driver following the racing line could be enhanced if the driver is operating the vehicle close to the performance limit.

Transient control methods will be investigated in this research, with regards to improving vehicle stability on the performance limit, for Formula One cars.

2.5 The optimal path (racing line)

The optimal path (racing line) is important because it is part of the objective in the search for the fastest possible lap time that can be achieved by the vehicle, in its current set up condition, for a particular circuit.

It is theoretically possible to determine the optimal line by experiment. Extensive testing of the vehicle at the circuit with a world class driver who spends hours trying to improve his/her laptime would approach the optimal line eventually, if sufficient time was available and the driver's skill was sufficient to control the vehicle on the limit of the cars performance envelope. In general the huge cost of testing and the inherent variability in driver performance negate this as a genuine method for determining the optimal line. Also, finding ways of capturing actual racing lines has never been easy, and even with the aid of global positioning systems (G.P.S) the task is both expensive and difficult [79].

Computer simulation offers another possibility. Optimal control techniques have begun to be applied to this problem with reasonable success. This method has been employed from negotiating simple manoeuvres [5, 9, 34] to the full circuit racing line [3], using optimised control of the vehicle inputs to control a vehicle model, and find the optimal line. Gadola et al. [80] used a genetic-based algorithm for calculating the optimal line by finding the combination of turn-in, brake release, throttle application,

and exit to maximise the minimum cornering radius. This method does not appear to be vehicle dependent, so whether a vehicle can actually follow the line at the limit of its capability is unknown. These methods remove the variability of driver skill but to make the problem solvable in a reasonable time, it requires simplified mathematical models of the vehicle to be used. Removing the variability of driver skill is helpful to compute an optimal vehicle setup for a particular track, which provides a starting point for the vehicle setup that can be further refined by the driver during track testing. The importance of the optimal line in simulation studies will discussed in this research.

2.6 Driver Modelling for transient vehicle dynamics

The mathematical modelling of human car driving appears to have begun in the early seventies [81]. Driver models have been reviewed by Guo and Guan [82], highlighting those that utilised single point preview. A preview tracking experiment was conducted by Tomizuka and Whitney [83], which showed that the availability of preview information significantly improved the tracking performance of the human operator compared to the non preview case. Their research also suggested that a particular preview length of $0.3 - 0.7$s was sufficient for almost all of the improvement.

Research on active suspensions using multiple point preview has been carried out by Prokop and Sharp [84], indicating that the usefulness of preview information in the active control of suspensions follows an exponential decay with increasing distance in front of the vehicle. This finding has been carried over into driver modelling [85] and an association between linear optimal preview control and driving has been found, utilising saturation functions to account for nonlinearities in the vehicle and limits on control input bounds. The saturations were tuned through trial and error, and satisfactory path tracking was found to be possible for a racing vehicle at racing speeds using an exponentially decaying function of increasing preview distance information.

Linear optimal preview steering control using a linear vehicle model [86] showed that as the vehicle travelled faster, the steering control became more oscillatory. It was concluded that if sharp changes in direction were required, then departures from perfect tracking would occur.

A nonlinear SQP optimisation algorithm was used by Prokop [81] to set up the driver control process as one of trajectory planning based on preview information, which is then followed by the driver modelled as a PID controller, to minimise deviations from the planned path. It was shown that the level of driver understanding of the vehicles on-limit non-linear behaviour was crucial in controlling the yaw dynamics of the vehicle during high-speed manoeuvres.

From an assessment of the literature, it is clear that non-linear feedback control with preview information and knowledge of the on-limit vehicle dynamics is necessary for the racing driver to be successful in high speed manoeuvring [87]. To this end, the empirical driver model of Sharp et al. [85] is chosen to model the on-limit behaviour of the driver in this thesis. This method does not require a linear vehicle model and was specifically implemented on an open wheel race car. Consequently the driver model is available and ready to use with minimal adjustment to ensure robust nonlinear preview path following control.

Chapter 3

The QSS method

This chapter describes a vehicle quasi steady state (QSS) nonlinear GG speed diagram generator and simulation tool that has been developed during this research. Using a published vehicle model, the method is described and checked against published results. The simplifying assumptions of quasi steady state are critically examined for this application to a particular open wheel race car.

Once the QSS method is checked against published results, the simplified mathematical modelling of a group of vehicle components and control strategies is discussed, and where possible, the models are developed to be more physically representative and realistic.

3.1 The published vehicle model

When developing new computer programs, validation is an essential element of the process. The QSS method has been developed initially with a published vehicle model from previous research. The full description of the model implementation is described in [3], and a summary is provided below. The equations of motion were derived by AutoSIM [4] for the previous research, but have been derived by hand for this research for checking purposes. The hand derivation is given in Appendix A.

Chassis

The model has seven degrees of freedom. Four wheels (one rotation freedom relative to the chassis per wheel), as well as yaw, lateral and longitudinal displacements.

Suspension movement is considered minor and can be neglected. The lateral and longitudinal load transfer are included as steady-state approximations. The model is shown in Figure 3.1.

Aerodynamic forces

Drag and lift coefficients are constants. Drag is applied at the height of the centre of gravity of the vehicle. The down force distribution between the front and rear axle is held at a constant value. The proportion of the downforce applied to an axle is applied equally to each wheel on the axle.

Tyre forces

The tyre lateral and longitudinal forces are produced from the Magic Formula Tyre Model which uses weighting functions to provide combined slip conditions [18]. Static wheel camber angles of -3 and -1°, at the front and rear axles respectively, are included.

Wheel vertical loads

Wheel loads are evaluated from the vehicle static weight distribution, aerodynamic downforce distribution and longitudinal and lateral load transfer.

Powertrain and Transmission

A two dimensional engine map characterises engine torque by engine speed and throttle position. The throttle position is characterised by a value between 1 and -1, where 0 marks the transition between accelerating (0 to 1) and braking (0 to -1). This is done for computational economy. Gear ratios are selected based on vehicle speed. Braking torque is characterised by a maximum braking torque and is delivered as a function of negative throttle position. The braking torque is applied to the front and rear wheels based on a constant front/rear distribution. The model utilises a limited slip differential.

3.2 GG speed diagram generation

The GG speed diagram is generated from the results of a series of dynamic equilibrium problems that are solved by the constrained nonlinear optimisation routine

Figure 3.1: Vehicle Model - 7DOF.

fmincon implemented in MATLAB [24].

The optimiser is supplied with an initial guess of the vehicle limit states. These states are a mixture of system inputs and unknown quantities, and the unknowns vary depending on the application. Equation 3.1 shows the possible components of the optimisation vector, P:

$$P = [\dot{x}, \ddot{x}, \dot{y}, \dot{\varphi}, \dot{\theta}_{LF}, \dot{\theta}_{RF}, \dot{\theta}_{LR}, \dot{\theta}_{RR}, \delta, T_P]^T \tag{3.1}$$

Initially the GG diagram program finds the maximum possible speed of the vehicle. It is clear that the vehicle will travel in a straight line to achieve this. This assumption allows us to reduce the optimisation vector, P to:

$$P = [\dot{x}, \dot{\theta}_F, \dot{\theta}_R, T_P]^T \tag{3.2}$$

where $\dot{\theta}_F$ and $\dot{\theta}_R$ are the front and rear wheel angular speeds which are assumed to be identical for each side of the vehicle.

The objective function is simply:

$$f = -\dot{x} \tag{3.3}$$

The solver is a minimiser, therefore a negative sign is required in Equation 3.3. Once the maximum possible speed of the vehicle is known, the next task is to evaluate the maximum positive and negative longitudinal accelerations possible with the vehicle operating at increments of the maximum speed in order to take account of aerodynamic forces that change with vehicle speed. The optimisation vector, P and the objective function, f now become:

$$P = [\ddot{x}, \dot{\theta}_F, \dot{\theta}_R, T_P]^T \tag{3.4}$$

$$f = \pm\ddot{x} \tag{3.5}$$

Once the longitudinal acceleration and deceleration capabilities of the vehicle at various speeds have been calculated, the task of filling the remainder of the GG speed diagram can be split into a set of optimisations at increments of the maximum longitudinal acceleration/deceleration for each speed increment. This is the most difficult task, because the number of variables in the optimisation vector increases significantly:

$$P = [\dot{y}, \dot{\varphi}, \dot{\theta}_{LF}, \dot{\theta}_{RF}, \dot{\theta}_{LR}, \dot{\theta}_{RR}, \delta, T_P]^T \tag{3.6}$$

The objective function becomes the maximum steady state lateral acceleration that the vehicle is capable of. Given the requirement of steady state cornering, Equation 2.20 can be rearranged with the acceleration terms removed to give:

$$\dot{x}\dot{\varphi} = \frac{F_{yf} + F_{yr}}{M} \tag{3.7}$$

Therefore the objective of the optimiser to maximise, given the condition of steady state cornering is:

$$f = -\dot{x}\dot{\varphi} \tag{3.8}$$

At all times the optimiser is constrained to find the solution to the equations of motion that gives the static equilibrium or steady state condition required. The constraint vector G is given as follows:

$$G = \begin{bmatrix} \ddot{y} & = & 0 \\ \ddot{x} & = & -\text{Target Longitudinal Acceleration} \\ \ddot{\varphi} & = & 0 \\ \ddot{\theta}_{LF} & = & f_1(\ddot{x}) \\ \ddot{\theta}_{RF} & = & f_2(\ddot{x}) \\ \ddot{\theta}_{LR} & = & f_3(\ddot{x}) \\ \ddot{\theta}_{RR} & = & f_4(\ddot{x}) \\ \text{Engine Torque} & \leq & \text{Max Engine Torque} \end{bmatrix}$$

$\ddot{y}$ and $\ddot{\varphi}$ are sideways (y axis) and yaw accelerations which must be zero. These are conditions of steady state cornering. $f_i(\ddot{x})$ represents a function that describes the wheel accelerations in terms of the longitudinal acceleration of the vehicle. The engine torque is also included as a constraint because of the tendency of the optimiser to explore throttle positions beyond fully open. The fully open throttle is assigned the value of 1 and full braking is assigned the value of -1. The engine map is stored as a two dimensional lookup table with a maximum throttle position of 1, so there are times when this constraint is required to keep the optimiser within the limits of the problem.

The GG speed diagram generation process is shown diagrammatically in Figure 3.2. When these optimisations are solved for both tractive and braking conditions all the necessary information to produce a GG speed diagram is available.

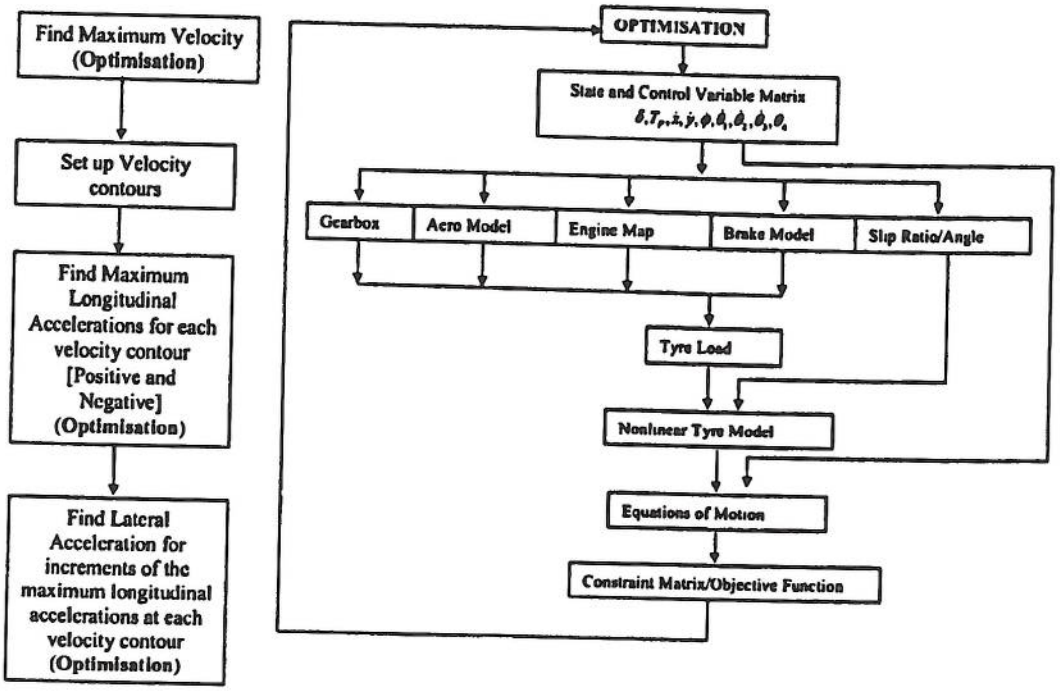

Figure 3.2: The optimisation routine.

The seven DOF vehicle model is quite comprehensive and as a result a large quantity of information is available for analysis. Table 3.1 shows the primary variables that are produced by the optimisation program either as an optimal set of the vector P or as system inputs to the model. It is possible to produce, in conjunction with a lap simulation program, data histories for an entire lap for all the vehicle states and forces listed.

GG speed diagram

The base vehicle set up is the original specification for a particular open wheel race car at the Barcelona circuit [3]. This particular vehicle set up and circuit was chosen because it has been validated by a Formula One team with telemetry data. The vehicle model, in this condition, is used to produce the GG speed diagram to be used as the vehicle performance envelope for a lap simulation program. The result is shown in Figure 3.3.

The GG speed diagram shows that the vehicle performance envelope is quite smooth, but the longitudinal acceleration is sensitive to small changes in lateral acceleration near the maximum lateral acceleration values. In some cases the computation of a

Programme Output	Variables
Primary Variables (State and control variables)	Throttle position, steer angle, individual wheel speeds, yaw rate, lateral velocity, lateral and longitudinal acceleration
Consequential Variables	Individual longitudinal and lateral tyre forces, aerodynamic lift and drag forces, brake and engine torques, slip angle and slip ratio and individual tyre loads.

Table 3.1: GG speed optimisation output.

point on the diagram clearly converges on a sub-optimal point, and requires further optimisation to remedy the final position of the resulting lateral acceleration point. An example of this is shown on Figure 3.3.

In the tractive part of the diagram, the engine torque limitation of the vehicle generates a physical limit at 50 m/s which is not seen in the braking part of the diagram. This is because the engine torque is only applied to the rear wheels and is significantly lower than the torque available in braking. In addition, the braking torque is applied to all four wheels, and the increasing force due to aerodynamic drag is additive to the braking force but acts to restrict the tractive force provided by the engine to the rear tyres.

The optimiser has been effective in maximising the lateral acceleration for a given vehicle speed and longitudinal acceleration in most cases, showing the trends expected for this type of race car [12].

3.3 QSS simulation

Assumptions

To find a sensible balance between computational speed and accuracy of simulation, it is important to consider the assumptions that have been made in the simulation

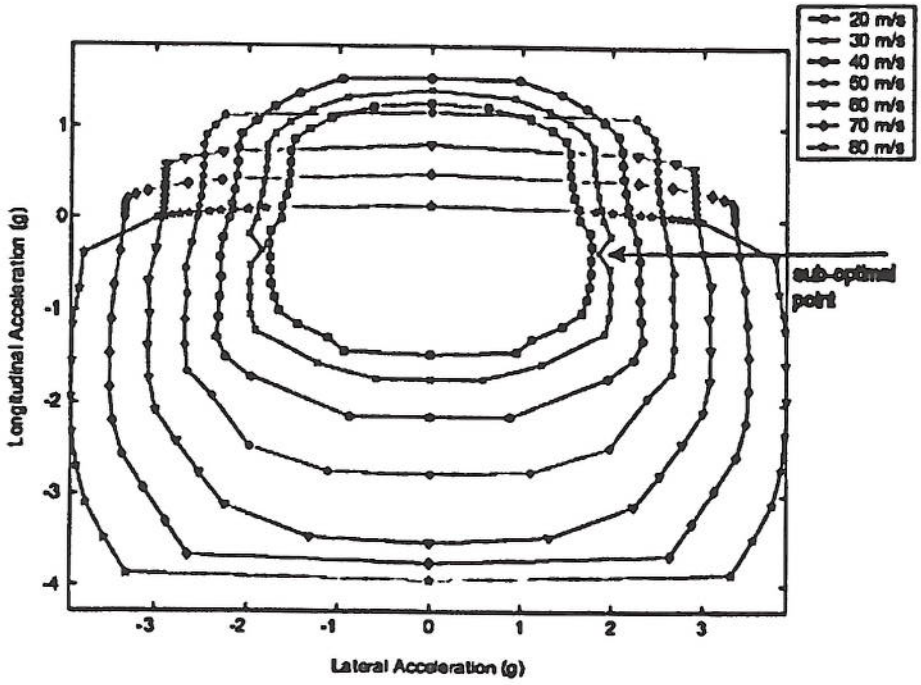

Figure 3.3: GG speed diagram - base setup.

method, and what influence they will have on the results obtained.

The term quasi steady state, as it is applied here, means that the vehicle can be modelled traversing a racetrack, split into segments, as a set of dynamic equilibrium manoeuvres. The condition that must hold for the quasi steady state assumption to be valid is that the changes in vehicle states occur slowly between adjacent segments. This can be achieved by making the segment spacing small.

The racing line is described in terms of curvature. This can be done in three ways. Firstly, it can be produced from a set of telemetry based lateral acceleration and vehicle speed data, or secondly a sensible racing line can be drawn on a facsimile of the track profile and the curvature information calculated using basic geometry or thirdly, it can be produced from a transient optimal control simulation.

The transient effects of changing the state of the vehicle are neglected in the simulation. A step change in steer angle and throttle position in the simulation from one segment to the next results in the vehicle assuming its new state instantly. Even with

fine segmentation of the track description, this is an approximation. When the car is braking and accelerating, the car is assumed to respond instantly to the longitudinal forces provided by the tyres. This is an approximation of the real situation.

As discretised segments are used to represent the race track there is constant acceleration between segments. Therefore the QSS simulation will produce smoother acceleration profiles than those generated by a real race car.

Description of the current lap simulation program

The basis of the lap simulation program is a calculated GG speed diagram. The lap simulation program interpolates between the points on the GG speed diagram to find the vehicle acceleration that is possible given the track description.

The program identifies peaks in the curvature data as an apex of a corner. Between a pair of apexes, the program calculates the maximum acceleration possible from apex (i) up to apex $(i+1)$ (Figure 3.4). This procedure is carried out for all apex pairs encountered over the entire lap.

The program then calculates the maximum braking deceleration possible between all apex pairs. Given the maximum possible accelerations and decelerations between apex pairs, acceleration and deceleration speed profiles can be calculated. This method implies braking right up to the apex of the corner which makes the computation simpler, but may not necessarily be an accurate representation of a real driving style. Many drivers choose a more classical style of only braking in a straight line and cornering in steady state. A discussion of these two styles is given in Milliken and Milliken [11].

The crossover point is where the accelerating and braking speeds between two apexes reach the same value (Figure 3.4). At this point, the program switches from the acceleration data to the braking data, providing a realistic transition point from acceleration to braking.

Effects of curvature

The main difficulty with this lap simulation method is that the results are very sensitive to small changes in the track curvature information. Initial trials showed that a

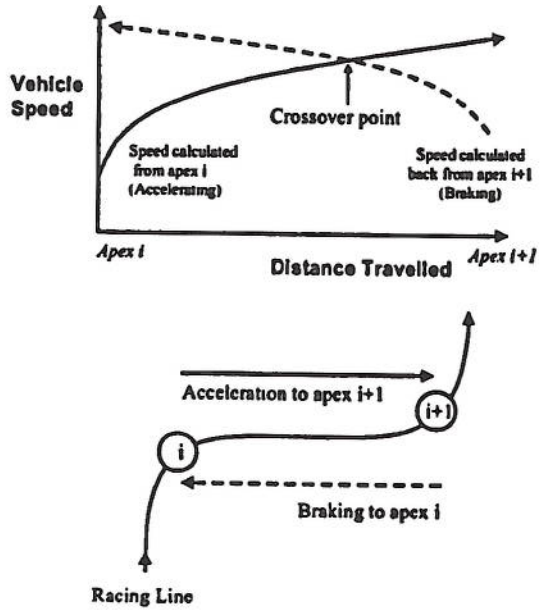

Figure 3.4: QSS simulation principle.

smooth trajectory data set was vital for the program to produce realistic results. Curvature information can be obtained from telemetry, or from a cartesian co-ordinate description of a racing line that has been drawn from experience, or from results of a transient optimal control lap simulation method.

Telemetry results can readily produce a racing line in terms of curvature. If it is assumed that the vehicle is cornering in steady state the track curvature can be calculated from the time histories of the lateral acceleration and vehicle speed data using the relationship:

$$r = \frac{\dot{x}^2}{a_y} \tag{3.9}$$

Telemetry noise from vehicle vibrations, measurement errors and calibration errors make it difficult to find the actual curvature from the data. These errors are manifested as both high frequency noise and offset in the recorded data. Therefore it is important to exercise caution when evaluating curvature from telemetry information in this manner.

To find track curvature from a set of cartesian points (as might be obtained from a transient optimal simulation), the first step is to calculate the yaw angle, φ, of the car on the given trajectory.

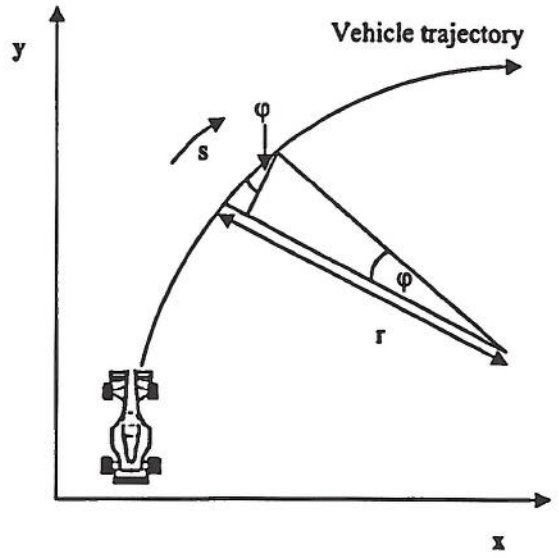

Figure 3.5: Trajectory coordinate relationships.

The geometry of the trajectory causes the following relationships:

$$\varphi = \arctan\frac{dy}{dx} \tag{3.10}$$

Differentiating φ with respect to distance travelled:

$$\frac{d\varphi}{ds} = \frac{1}{r} \tag{3.11}$$

To produce a curvature versus distance representation, φ is evaluated for each set of cartesian co-ordinates, and the distance travelled between the co-ordinates is approximated by a straight line.

In the QSS simulation method described here, a second order polynomial is fitted to the relationship between φ and s. Good results are obtained with a number of points that represent approximately half of the length of the tightest corner on the circuit when the spacing between points is 2 metres. Taking the analytical derivative of the polynomial, Equation 3.11 can be evaluated producing the curvature information required.

Track curvature calculated from a set of cartesian points includes errors from the polynomial fitting procedure and the approximation of s, but this can be controlled by sensible discretisation of the lateral and longitudinal distance points. Therefore this method was preferred to one based on telemetry data and was used to produce the results here.

3.4 Results

3.4.1 Validation using the published vehicle model

To initially validate the GG speed diagram calculation and the lap simulation method, a comparison of distance based acceleration histories with the validated and published results of a TO method (Figure 3.6) [3] are shown in Figure 3.7. These are for a simulation of the Grand Prix Barcelona circuit, Catalunya. The racing line used in both methods is shown in cartesian form in Figure 3.8.

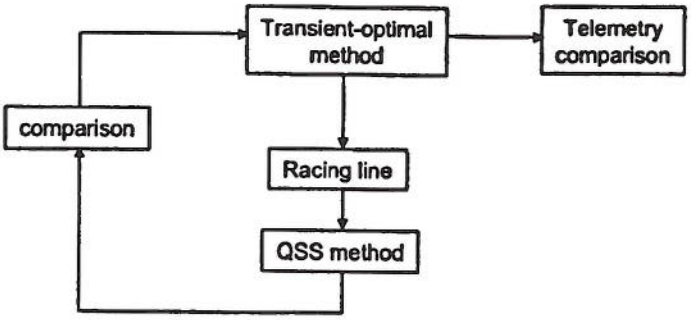

Figure 3.6: QSS method validation.

The agreement in the acceleration calculations shown in Figure 3.7 is generally very good. The main differences can be seen in the longitudinal accelerations when the vehicle is experiencing high lateral acceleration. This can be accounted for by the shape of the GG speed diagram at high lateral accelerations where the gradient with respect to longitudinal acceleration is very steep. The QSS results oscillate around the value produced by the TO method [3].

There also appears to be a constant delay in some corner entry and exit points, when comparing the two method's results. This is attributed to different braking and

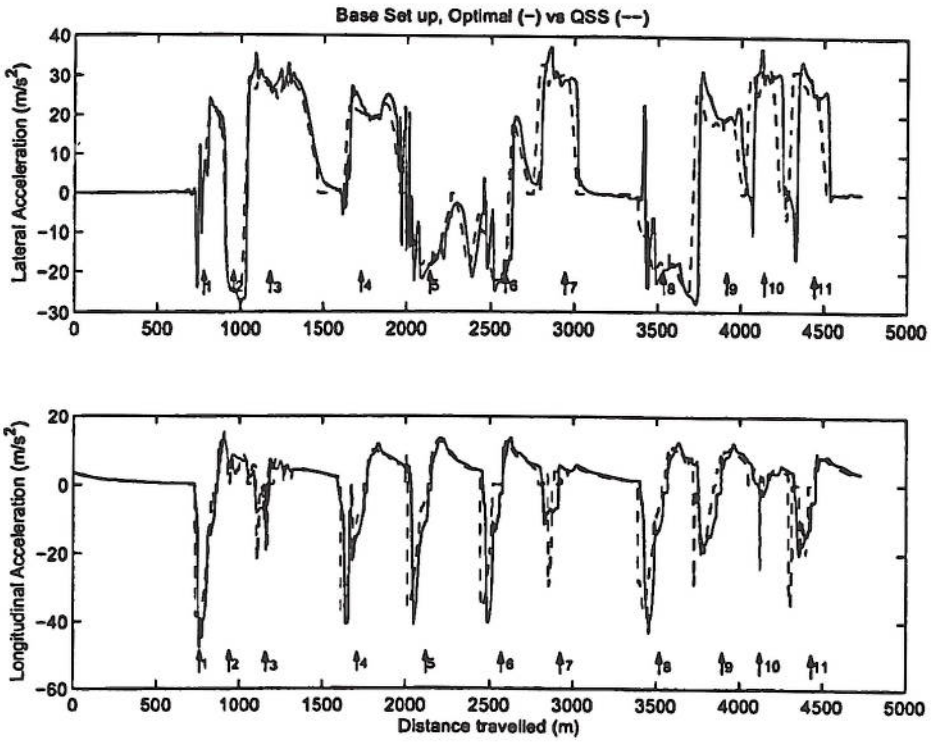

Figure 3.7: Comparison of QSS and TO methods (arrows show corner locations [see Figure 3.8]). The TO method is from [3].

acceleration crossover points used by the two methods, especially in corners 9,10 and 11.

The lap time difference between the two methods is 2.19 seconds (Table 3.2), which is a significant difference. This appears to be a function of the different braking/accelerating crossover points used by the two methods, and is not easy to remedy using the current simulation method. However, the close agreement of the acceleration magnitudes during cornering suggests that the vehicle is traversing the path on, or very close to, the limit capability of the vehicle. Therefore, for comparative analysis of vehicle setup and configuration changes for a given trajectory, the method will be suitable for determining whether the vehicle is comparatively faster or slower due to those changes. Since the accurate modelling of tyres and friction coefficients is so difficult to achieve, lap time simulation programs are generally not employed for the purposes of determining the expected laptime of an actual vehicle. The purposes of laptime evaluation are generally for determining whether changes to that vehicle have made the vehicle faster or slower around the circuit due to set up changes to the vehicle [7].

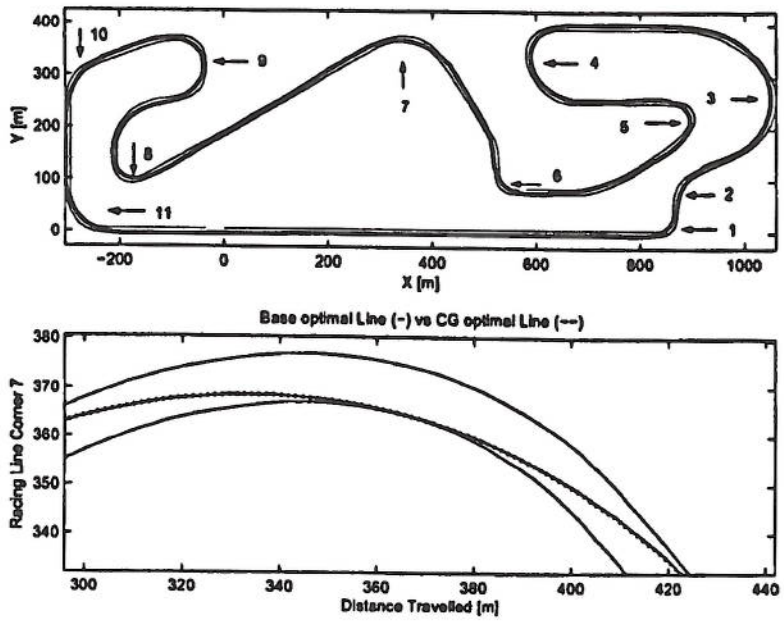

Figure 3.8: Racing line, Barcelona Grand Prix circuit.

Lap time (s) QSS	Lap time (s) T.O
82.904	80.714
Difference	2.19

Table 3.2: Lap time at Barcelona Grand Prix circuit for QSS and TO methods.

While the results produced by the current QSS method are very similar to those produced by Casanova [3], more simplifying assumptions have been made. The driver for this was the saving in computational time required to produce the result. Over an average of 24 individual optimisation runs for the Barcelona circuit, the processing time was 39.8 hours on a Sun workstation for the method in Casanova [3]. The QSS method took for an average of 10 complete runs with different vehicle set ups, only 16 minutes on an Intel 1000MHz PC. The processing time can vary due to the iterative nature of the optimisation process when the vehicle set up is changed. The simplifying assumptions of the QSS method have allowed a dramatic improvement in computational time, allowing more vehicle set up and vehicle design scenarios to be performed by the analyst, without great changes in the results obtained with respect to the TO method.

3.5 QSS method improvements

The optimisation algorithm does struggle to solve the problem in some instances, as seen in Figure 3.3. Numerical optimisation of a smooth function is more efficient and robust if the derivatives are known [31]. At present the derivatives are approximated numerically by finite differences which requires a choice of step size. This is inherently a tradeoff between truncation error accuracy and floating point round-off errors. The following section discusses the improvements made to the method of determining the derivatives for the optimisation program using automatic differentiation. Following this the mathematical modelling of the rear differential, gear change strategy and the vehicle suspension model are discussed.

3.5.1 Derivative evaluation

As mentioned in Section 2.3.1 there are two types of AD available, forward mode and reverse mode. This research has utilised a beta release of an AD tool for MATLAB that exploits the use of operator overloading in versions of MATLAB 5.0 and above. MAD, or *Matlab Automatic Differentiation* [88] is a version of the forward mode of AD. The choice of forward mode over reverse mode for this research was made for two reasons. The first reason was that the original version of the QSS method was coded in MATLAB making any AD methods for MATLAB 'm' files considerably simpler to convert to AD from the original finite differencing implementation. The second reason for not using the reverse mode was the difficulties found by Casanova [3] with large computer memory allocation requirements. Additionally, the method of implementing AD with a program that utilised lookup tables was to de-link the AD part of the index into the table to allow the interpolation routines to work. Consequently, the codelist was only viable for the current iteration and incorrect for subsequent iterations. The MAD implementation of the forward mode allowed the use of active indexing into an interpolation routine, removing one source of possible derivative evaluation error, and additionally, the memory requirements for codelist storage were not required.

This is not to say that the forward mode is not prone to its own set of problems. The reverse mode is generally preferred if the implementation is possible, mainly because the number of function evaluations and matrix manipulations can be dramatically reduced when compared with the forward mode. This is because for every operation carried out on an active 'AD' variable, i.e. the value and derivative pair, the entire

derivative matrix must be updated. This can be inefficient if the jacobian matrix contains many variables because in many instances the evaluation of the derivatives in the jacobian matrix will be dominated by the propagation of zeros (i.e most derivatives in the matrix are not affected by the operation and are just being updated with zeros). As the reverse mode records the program execution, the sparsity can be exploited and only the necessary derivative operations are executed. For the implementation in this research however, the forward mode tool MAD was chosen as providing a reasonable compromise between speed and accuracy of the two AD methods. MAD is the result of ongoing research conducted by S.A. Forth and his colleagues at the Shrivenham campus of Cranfield University. His expertise and willingness to help has made a large contribution to the success of this program implementation.

MATLAB has been constantly improved since its inception and since the release of version 6.5, the earlier versions problem of slow execution of logic statement loops (for, while etc.) have been successfully accelerated to near compiled language speeds of execution. Unfortunately one of the conditions of this acceleration being useable is that no operator overloading functions are used in the programs. This is the very basis of MAD's operation, and virtually every implementation of AD. As a result the program execution speed is slower than an equivalent FD method in MATLAB. This loss can be minimised by reducing the number of logic based loops using high level MATLAB programming matrix operations, but these methods cannot be used in all instances. Fortunately the loss in acceleration has been kept to manageable levels, and the improvement in the number of successful converged optimisation runs has doubled from 44.8% to 95.9% of the runs [89]. From this point forward GG speed diagrams are evaluated using AD for evaluating gradients.

3.6 Extensions to the vehicle model

3.6.1 Rear differential model

The basic rear differential model for open wheel race cars, described by [3], is based on the limited slip Salisbury-type differential [11] with electro-hydraulic actuation [12]. Inputs for the control system are limited by racing regulations for this era of vehicle (1999), to input torque, wheel speed difference and output shaft torque difference [45]. The control algorithm sends a signal to the hydraulic valve to actuate a piston that engages the friction plates in the differential.

The basic rear differential model in [3] has a constant gain term that responds to the input engine torque to determine the amount of dynamic torque that must be overcome by the wheels to allow the differential friction plates to slip. This model is very basic and is justifiably so to ensure fast execution for the large optimisation problems that it was intended for.

It was felt necessary to upgrade the differential model to give it physical significance and hopefully allow some insight into the effect of the differential on the vehicle dynamics.

Flat plate clutch theory and the relationship between axial load and torque is well described in the literature [90]. Depending on the assumption of the relationship between pressure and flat plate radius, two equations hold for the relationship between axial load and torque. One is based on the assumption of uniform rate of wear across the sliding surfaces, and the other is based on the assumption of uniform pressure across the sliding surfaces. Here, the assumption of constant rate of wear is chosen because of the two methods, this assumption leads to a slightly lower torque value and is therefore more conservative [90].

The relationship between friction and sliding velocity of the flat plates can be approximated by a straight line with a negative slope [91] giving:

$$\mu = \mu_0 - mv \tag{3.12}$$

The derivation of the torque - axial load relationship for constant rate of wear is given in [90] and expanded in [91] to include the friction term with a dependency on sliding velocity. The system of interest is shown in Figure 3.9.

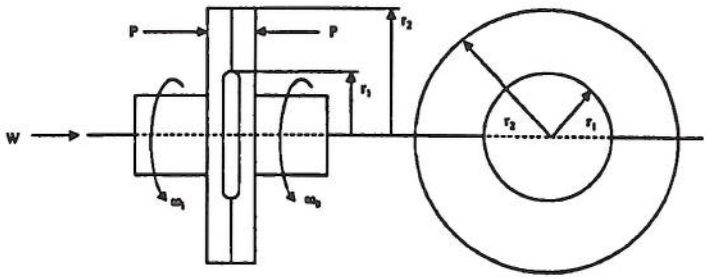

Figure 3.9: Forces and torques on a friction clutch.

The total torque on the shaft using the approach in [91] is:

$$T = \frac{\mu_0 W n(r_1 + r_2)}{2} - \frac{mWn(r_1^2 + r_2^2 + r_1 r_2)(\omega_i - \omega_0)}{3} \tag{3.13}$$

for n pairs of frictional surfaces. Using Equation 3.13 it is straight forward to extract the pressure required, P_H, to supply T, the torque on the shaft.

$$P_H = \frac{W}{\pi(r_2^2 - r_1^2)} \tag{3.14}$$

3.6.2 Gear change strategy

The original gear change strategy was based on a change in gear once pre-specified vehicle forward speeds were reached [3, 92]. Realistic gear change strategies are based on changing gear at a target engine speed to maximise engine power and to ensure that after the gear change, a favourable position on the torque curve is realised. The gear box function has been modified to ensure that gear changes occur only when a target engine speed has been reached, and is not a direct function of vehicle speed. This is achieved using *if-then-else* statements.

3.6.3 Ride height sensitivity

In the seven DOF vehicle model the tyre load model assumes a constant ride height, much like an active suspension race car. However there are very few racing formulae that allow the use of active suspension and as such the assumption of constant ride height is generally not valid. To take account of the effects of the aerodynamic loads, due to ride height changes, a pitch/bounce model is necessary.

For clarity the following terms will be used to describe particular vehicle models and suspension model analysis:

published model / seven DOF vehicle model This is the seven DOF vehicle model outlined in Section 3.1.

4DOF suspension analysis This is the four DOF pitch/bounce suspension model described in Appendix B.

7DOF suspension vehicle model This is the seven DOF vehicle model outlined in Section 3.1 but uses the four DOF suspension analysis described in Appendix B, to allow a ride height dependent aerodynamic lookup table to be used in the tyre load model instead of constant drag and lift coefficients.

7DOF suspension analysis This is the coupled pitch/roll seven DOF suspension model that is used to evaluate tyre vertical loads, using linear springs to represent suspension and tyre vertical compliances. This is produced by an AutoSIM script.

14DOF vehicle model The 14DOF vehicle model is the published model with the 7DOF suspension analysis used to evaluate the tyre vertical loads. This model also allows a ride height dependent aerodynamic lookup table to be used in the tyre load model instead of constant drag and lift coefficients.

3.6.4 4DOF suspension analysis

Suspension and wheel stiffnesses are high in open wheel race cars (approximately 175N/mm and 300 N/mm respectively [12, 41]) and as a result the suspension movement is small. If it is assumed that the pitch/bounce mathematical model is derived about some equilibrium position, then the changes about the equilibrium position will be so small that a linear analysis will be sufficiently accurate for an initial treatise to include the ride height changes due to suspension movement. The small angle approximation is required to linearise the equations of motion and this is valid for angles $\leq 10°$. Pitch angles of less than $2°$ are expected, so the approximation will hold over the range of interest.

This initial model assumes that the roll and pitch/bounce motions are decoupled which is not a bad assumption according to Ellis [39], and this is especially true for downforce race cars according to Metz and Maddock [41].

Linear analysis makes the pitch/bounce model easy to solve using simple matrix inversion techniques allowing a result to be calculated in a very short period of time. This is important to keep the additional computational overhead on the optimisation process low. If this pitch/bounce model indicates that ride height sensitivity is important, then a coupled roll/pitch/bounce model should be employed to more accurately determine tyre vertical loads.

The values of the spring constants that represent the vertical stiffnesses of the wheels and suspension components were obtained from Wright [12] as his values are from the same era and type of open wheel race car that this research has been based on.

The pitch/bounce model hand derivation is given in Appendix B, and is termed the 4DOF suspension analysis.

The first task is to ensure that the 4DOF suspension analysis is valid for the system that it has been designed for. The model is validated using two tests. The first is a check on the bounce and pitch frequencies of the model, as approximate F1 bounce and pitch vehicle frequencies are available for comparison in Wright [93].

Bounce and pitch frequency analysis: 4DOF suspension analysis

This frequency analysis follows a similar method to that of Gillespie [94].
The equations of motion are re-written below for convenience from the appendix:

$$m_f\ddot{x}_1 + x_1(k_1+k_2) - k_2x_3 - k_2l_f\theta = 0 \tag{3.15}$$

$$m_r\ddot{x}_2 + x_2(k_3+k_4) - k_4x_3 + k_4l_r\theta = 0 \tag{3.16}$$

$$\begin{aligned} &M\ddot{x}_3 - k_2x_1 - k_4x_2 + (k_2+k_4)x_3 \\ &+(k_2l_f - k_4l_r)\theta = 0 \end{aligned} \tag{3.17}$$

$$\begin{aligned} &I\ddot{\theta} - k_2l_fx_1 + k_4l_rx_2 + (k_2l_f - k_4l_r)x_3 \\ &+(k_2l_f^2 + k_4l_r^2)\theta = 0 \end{aligned} \tag{3.18}$$

To calculate the bounce and pitch frequencies the equations of motion need to be reduced from four to two.
First, the equations for x_1 and x_2 are re-written in terms of the two required coordinates (bounce and pitch coordinates, x_3 and θ). This requires the unsprung masses to be neglected. Considering that $m_f, m_r \ll M, I$ this is a reasonable assumption.

$$x_1 = \frac{k_2x_3 + k_2l_f\theta}{k_1+k_2} \tag{3.19}$$

$$x_2 = \frac{k_4 x_3 + k_4 l_r \theta}{k_3 + k_4} \tag{3.20}$$

Now if these relationships are inserted into Equations 3.17 and 3.18, it is then possible to use the derivation results of Gillespie [94] directly. This gives:

$$\ddot{x}_3 + \alpha x_3 + \beta\theta = 0 \tag{3.21}$$

$$\ddot{\theta} + \gamma x_3 + \varepsilon\theta = 0 \tag{3.22}$$

Where:

$$\alpha = \frac{k_2 + k_4 - \frac{k_2^2}{k_1+k_2} - \frac{k_4^2}{k_3+k_4}}{M} \tag{3.23}$$

$$\beta = \frac{k_2 l_f - k_4 l_r - \frac{k_2^2 l_f}{k_1+k_2} - \frac{k_4^2 l_r}{k_3+k_4}}{M} \tag{3.24}$$

$$\gamma = \frac{k_2 l_f - k_4 l_r - \frac{k_2^2 l_f}{k_1+k_2} + \frac{k_4^2 l_r}{k_3+k_4}}{I} \tag{3.25}$$

$$\varepsilon = \frac{k_2 l_f^2 + k_4 l_r^2 - \frac{k_2^2 l_f}{k_1+k_2} + \frac{k_4^2 l_r}{k_3+k_4}}{I} \tag{3.26}$$

Now that Equations 3.21 and 3.22 are in the same form as the Gillespie [94] derivation, a direct substitution can be made into the relevant equations for the pitch and bounce vibration modes:

$$f_1 = \frac{\sqrt{\frac{(\varepsilon+\alpha)}{2} + \sqrt{\frac{(\varepsilon-\alpha)^2}{4} + \frac{\beta}{\gamma}}}}{2\pi} \tag{3.27}$$

$$f_2 = \frac{\sqrt{\frac{(\varepsilon+\alpha)}{2} - \sqrt{\frac{(\varepsilon-\alpha)^2}{4} + \frac{\beta}{\gamma}}}}{2\pi} \tag{3.28}$$

Using the stiffness values described in Wright [12], the vibration modes are:

$$f_1 = 5.57\text{Hz}$$
$$f_2 = 2.83\text{Hz}$$

These mode frequencies are lower than those published in Wright [93] (Pitch > 8Hz and bounce > 5Hz). This published data relates to F1 vehicles which relied on side-skirts for downforce. As a consequence these vehicles required stiffer suspension and would be expected to have higher bounce and pitch frequencies. A range of 4-6Hz is given in a later reference Gadola et al. [95] for ground effect cars but it does not differentiate between open wheel and sports car vehicles. Put into context, the literature tends to support the calculated values of f_1 and f_2.

The second test is an operational test to determine whether the 4DOF suspension analysis returns sensible values in operation. A comparison of the aerodynamic map from the base car in this research and published ride height data [96] indicates that ride height experiments tend to be conducted on the assumption that the minimum value for the front ride height will be 10mm. In addition, Wildi [96] gives a high speed, open wheel downforce race car setting of 17.5mm for the front ride height and an angle of attack of 0.3°. This knowledge allows one to test the sensibility of the 4DOF suspension analysis results under the highest pitch moment that can be generated in normal operating conditions; a high speed hard braking manoeuvre. The four DOF suspension model predicts a front ride height of 11mm under 7400Nm of braking torque. This level of braking torque has brought the front suspension almost down to its lower limit of 10mm. This adds further weight to the supposition that the 4DOF suspension analysis is a good representation of the pitch motion of an open wheel, downforce race car.

Aerodynamic map subroutine

Now that the 4DOF suspension analysis has been derived and validated the model must be incorporated into the existing GG speed diagram program. This has been achieved through a revision of the tyre load model.

The 4DOF suspension analysis, has been installed where the steady state constant ride height longitudinal load transfer model once was. A lookup table that holds the ride height dependent lift, drag and longitudinal centre of pressure location coefficients is accessed via a cubic interpolation routine. This map is derived from authentic wind tunnel data. This interpolation method is used because the ride height dependent coefficients are smooth, nonlinear functions.

This method makes the old separate aerodynamic function (aerodynamic model in Figure 3.2) redundant, and allows a simple swap of the tyre load subroutines. This new vehicle model is called the 7DOF suspension vehicle model. The remaining optimisation program is unaffected. However it still remains to be seen how the optimiser handles this new addition.

GG speed diagram effects

Figure 3.10 contains two GG speed diagrams. The solid line is the base set up of the original car using the published vehicle model, and the dotted line is the same set up but using the 7DOF suspension vehicle model incorporating the ride height dependent aerodynamic map. The differences are quite significant.

Under longitudinal acceleration the change in pitch is quite low as the maximum longitudinal acceleration that can be achieved is 1.5g. The results are therefore quite similar to those of the constant ride height vehicle running in a straight line. However the maximum lateral acceleration capability is comparatively reduced with increasing speed. Since there is no apparent difference due to pitch under longitudinal acceleration the only remaining variable that can change is the longitudinal location of the centre of pressure *cp*. In maximum lateral acceleration, i.e. zero longitudinal acceleration, there is a difference between the two models. In the 7DOF suspension vehicle model, the location of the *cp* has moved 2% rearward, placing more of the aerodynamic downforce on the rear axle.

Looking at the deceleration curves, the gap in the lateral acceleration capability (beyond $\pm$ 1.2g) between the constant ride height result and the new model increases at higher longitudinal decelerations. This is mainly due to the increasing ride height of the rear wing with pitch in deceleration, generating much less negative lift due to a loss of ground effect. The rear wing helps to generate low pressure behind the vehicle, which interacts positively with the flow underneath the car [97]. The flow underneath the car is reduced due to the forward pitching of the sprung mass. The change in pitch is significantly higher in braking because the deceleration capability is nearly 4.5g.
The GG speed diagram, calculated using the 7DOF suspension vehicle model, is used to run a simulation at the Barcelona Grand Prix circuit. The acceleration and speed histories are presented in Figures 3.11 and 3.12 respectively. Figure 3.11 shows that the differences are mainly in high lateral accelerations as was noted in the analysis of

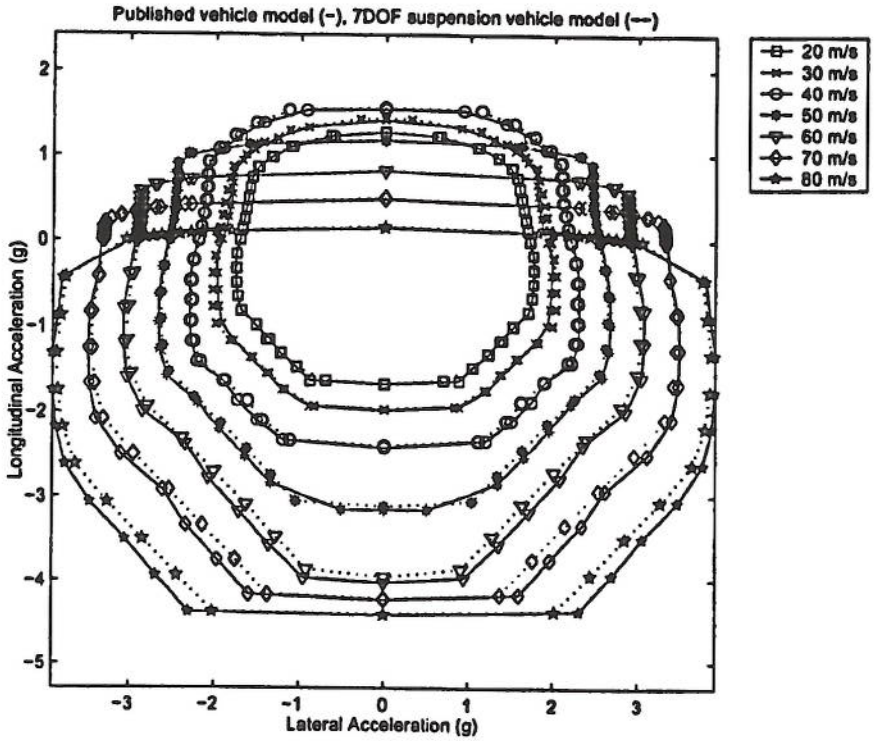

Figure 3.10: GG speed diagram - 7DOF suspension vehicle model.

Figure 3.10. Figure 3.12 shows that in corners 3,7,9 and 11 higher cornering speeds, and therefore later braking points, were possible with the vehicle using the constant ride height model.

The overall effect of using this new 7DOF suspension vehicle model is a slower vehicle, but a more accurate representation of that vehicle. The laptime has been found to be nearly two seconds slower (Table 3.3) and has confirmed that the effect of variable ride height aerodynamics is significant for vehicle simulations. The next step is to re-couple the roll motion and produce a more accurate suspension model, which also allows the roll centre concept to be disbanded, removing a set of intrinsic assumptions and again further improving the accuracy of the vehicle model.

3.6.5 Coupled pitch and roll suspension model

The suspension was originally modelled with a constant ride height assumption, constant roll stiffness distribution and fixed roll axis position. The dynamics of the un-

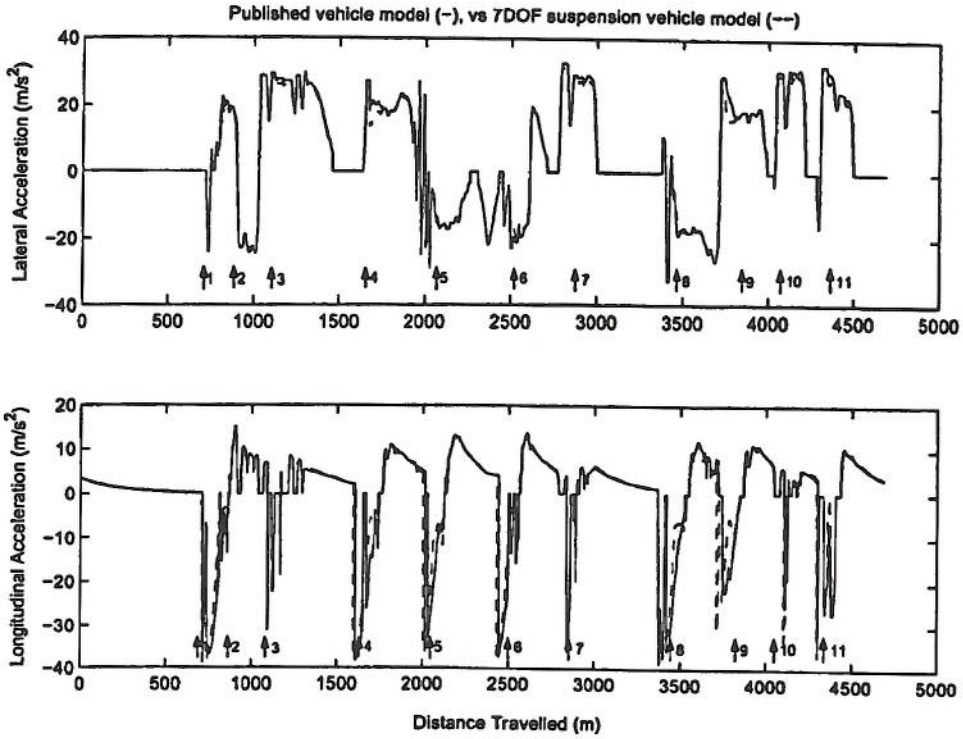

Figure 3.11: Acceleration comparison - Base published vehicle model and Base 7DOF suspension vehicle model. Barcelona Grand Prix Circuit.

sprung masses were neglected. The desirable addition of a lookup table for the aerodynamic drag, lift and longitudinal location of the centre of pressure as functions of ride height requires the pitch degree of freedom for the sprung mass to be added to the model. The inclusion of ride height dependent aerodynamics has been shown to be significant in Section 3.6.3. To also include the roll motion in the suspension a more complex model is required. Figure 3.13 shows a schematic of the 7DOF suspension analysis that has been employed to address this.

Linear springs are used in the model in the present incarnation but a modification to the AutoSIM [4] script would allow the use of a polynomial or lookup table function to describe a nonlinear spring application. In addition to the pitch DOF, the roll DOF and the unsprung masses' vertical displacement with respect to the sprung mass are included. This 7DOF suspension analysis is incorporated into the program as a substitution for the tyre load model in the published model in a manner similar to the 4DOF suspension analysis. While the springs are modelled with linear coefficients,

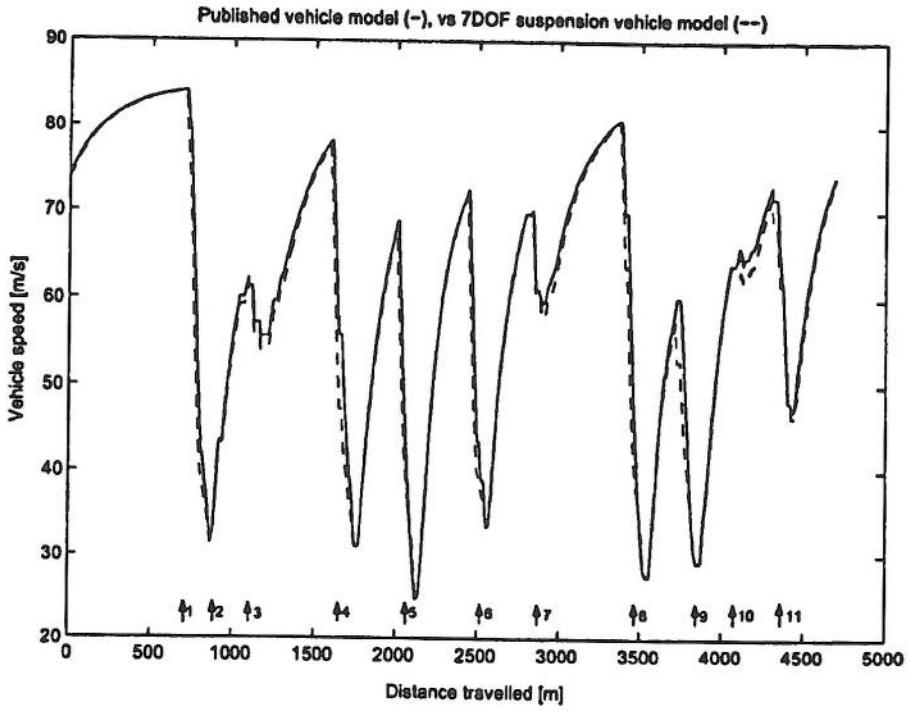

Figure 3.12: Speed comparison - Base published vehicle model and Base 7DOF suspension vehicle model. Barcelona Grand Prix Circuit.

the effects of second order terms due to the coupled pitch/roll motions could not be neglected and the suspension model is nonlinear. This requires the addition of the suspension seven DOF (Figure 3.13) to the optimisation vector. The resulting optimisation program is now characterised as a 14DOF system, and the vehicle model is termed the 14DOF vehicle model.

3.6.6 14DOF vehicle model validation - The double lane change

Understeer coefficient - K_{us}

The QSS method finds the on-limit performance of the vehicle for all feasible combinations of steady state lateral acceleration and longitudinal acceleration. Therefore, the conventional method of analysing steady state manoeuvring, the understeer coefficient, can be applied quasi statically to produce a time varying result for a specified manoeuvre.

Set up	Lap time (s) QSS Barcelona G.P. Circuit
Published model (using QSS method)	82.904
7DOF suspension vehicle model	84.894
Difference	1.99

Table 3.3: Simulated lap time using the published model and the 7DOF suspension vehicle model.

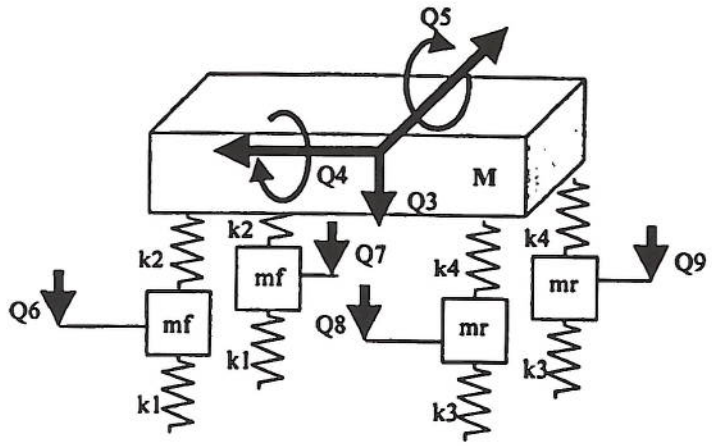

Figure 3.13: 7DOF suspension analysis.

The understeer coefficient is one of a group of terms that can be used to describe the turning response properties of the vehicle [11, 35, 38, 94]. It is commonly used in conjunction with linear vehicle models. Using linear tyres, it is a function of the weight distribution between the front and rear axles and the tyre cornering stiffnesses for each axle. The understeer coefficient allows the analyst to determine if the vehicle is understeering (positive K_{us}) , oversteering (negative K_{us}) or is in a state of neutral steer ($K_{us} = 0$).

In steady state cornering [35],

$$K_{us} = \frac{W_f}{C_{\alpha f}} - \frac{W_r}{C_{\alpha r}} \tag{3.29}$$

$$\begin{aligned}\alpha_f - \alpha_r &= \frac{W_f v^2}{C_{\alpha f} gR} - \frac{W_r v^2}{C_{\alpha r} gR} \\ &= \left(\frac{W_f}{C_{\alpha f}} - \frac{W_r}{C_{\alpha r}}\right)\frac{v^2}{gR} \\ &= K_{us}\frac{v^2}{gR}\end{aligned}$$

$$K_{us} = \frac{(\alpha_f - \alpha_r)gR}{v^2} \tag{3.30}$$

This is the generalised form of K_{us} and holds as long as the vehicle is cornering in steady state. Expressing K_{us} in terms of slip angles makes it easier for non-linear tyre models to be used.

The double lane change

The results from a full circuit analysis are complex, and in the interests of producing a general result, a full circuit analysis will not be used. Instead, a double lane change manoeuvre will be examined. Lane change tests are useful for evaluating vehicle directional control and handling performance, especially during on-limit manoeuvres [98]. Figure 3.14 illustrates the double lane change manoeuvre used for this analysis. This is based on a simplification of the standard normal distribution function that can be described by:

$$y = \frac{A}{\sigma} \cdot e^{-\frac{(x-\bar{x})^2}{2\sigma^2}} \tag{3.31}$$

where $\bar{x}$ and σ are the equivalent mean and standard deviation of the resulting function. This formula is chosen because it is a good approximation of a double lane change shape, is continuously differentiable for both the first and second derivatives and these derivatives can be derived analytically without much difficulty. Having these derivatives available makes the radius of curvature evaluation significantly more accurate.

The differences between the published vehicle model and the 14DOF vehicle model is shown in a comparison of the results of the vehicle models employed in the base configuration [92], which is for a particular 1999 open wheel race car, through a double lane change. The significant difference in terms of input information for the 14DOF

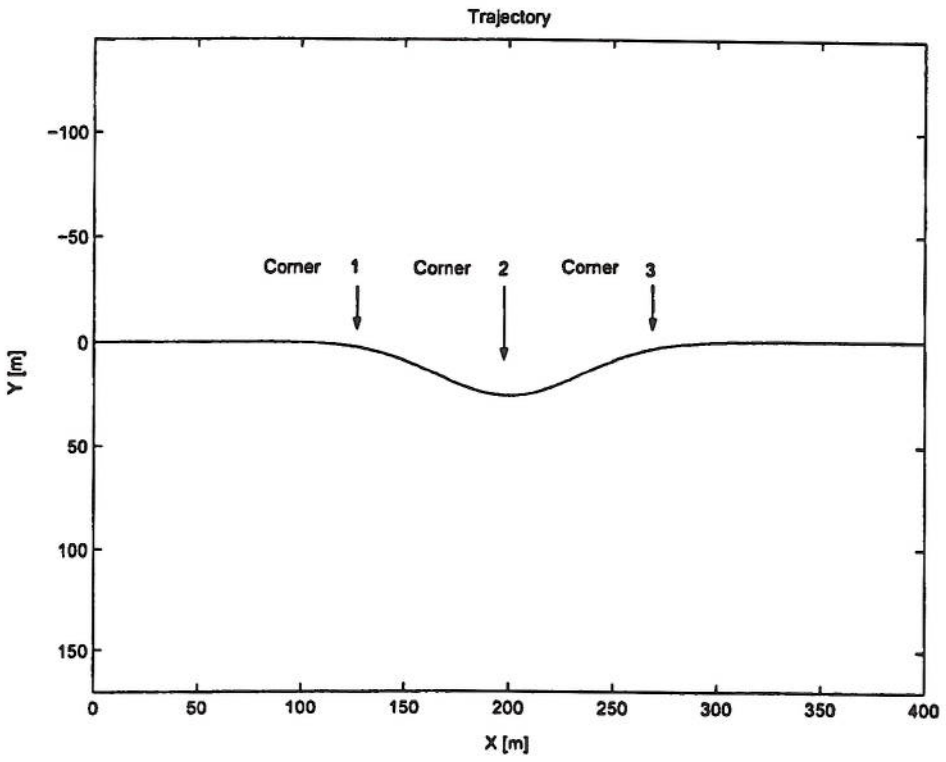

Figure 3.14: Double lane change trajectory.

vehicle model is the aerodynamic lookup table that supplies the longitudinal location of the centre of pressure, and the drag and negative lift characteristics of the vehicle in response to ride height changes. The sensitivity of this type of Formula One vehicle is, on average, $190\frac{N}{deg}$ of pitch for aerodynamic downforce and $72\frac{N}{deg}$ of pitch for aerodynamic drag.

Under pure longitudinal acceleration, where aerodynamic downforce and drag forces are similar for both models, Figure 3.15 shows that the tyre load distributions are in close agreement. The first 100 metres of distance travelled is an example of this situation.

Under braking at corner 1, towards corner 2 (100 to 200 metres of distance travelled), the drag and downforce is much higher for the 14DOF vehicle model (Figure 3.16) and the tyre loads are increased (Figure 3.15). Due to the change in pitch of the vehicle, the longitudinal location of the centre of pressure moves forward (Figure 3.16)

and the vehicle transfers more weight to the front axle. This change in proportion of aerodynamic load is quite low (up to 4%) and suggests good agreement in the proportioning of aerodynamic load between the front and rear axle, between the seven and 14DOF models. The 14DOF vehicle model exhibits oversteer during this phase, while the published vehicle model produces an understeering vehicle. This is a fundamental difference between the two models, and will be examined shortly.

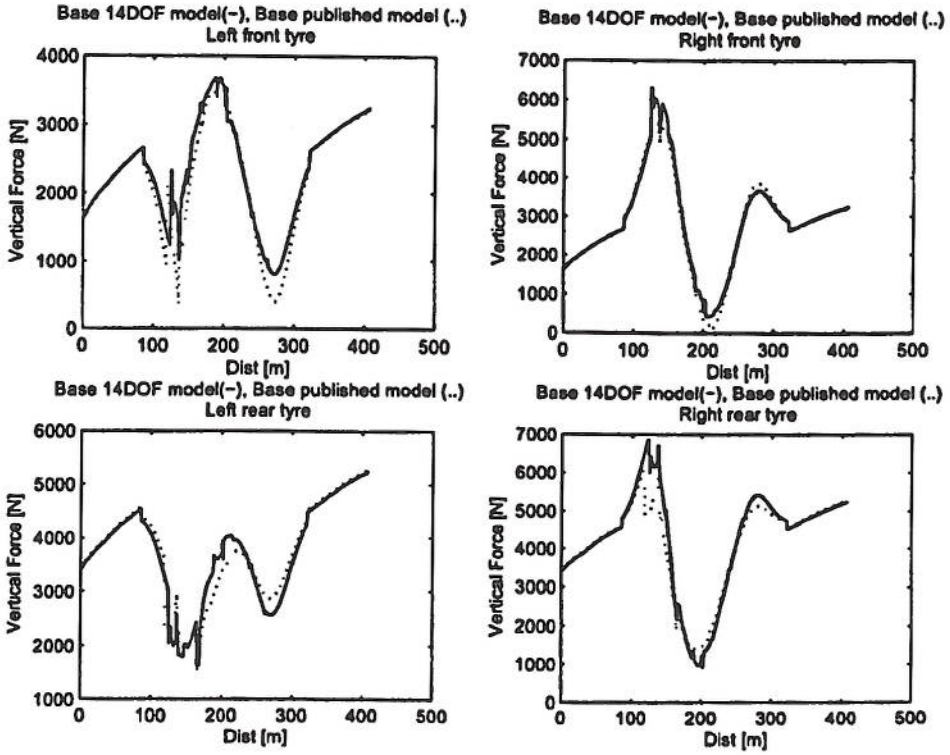

Figure 3.15: Tyre loads - published vehicle model and the 14DOF vehicle model.

The vehicle accelerates through corner 3 at approximately 280m distance travelled. The aerodynamic loads are very similar between the two models but the load distribution is quite different. The load differences could be due to differing pitch and/or roll behaviour. This can be determined from a direct comparison of the values of K_{us} for the entire GG speed diagram for the published vehicle model and the 14DOF vehicle model.

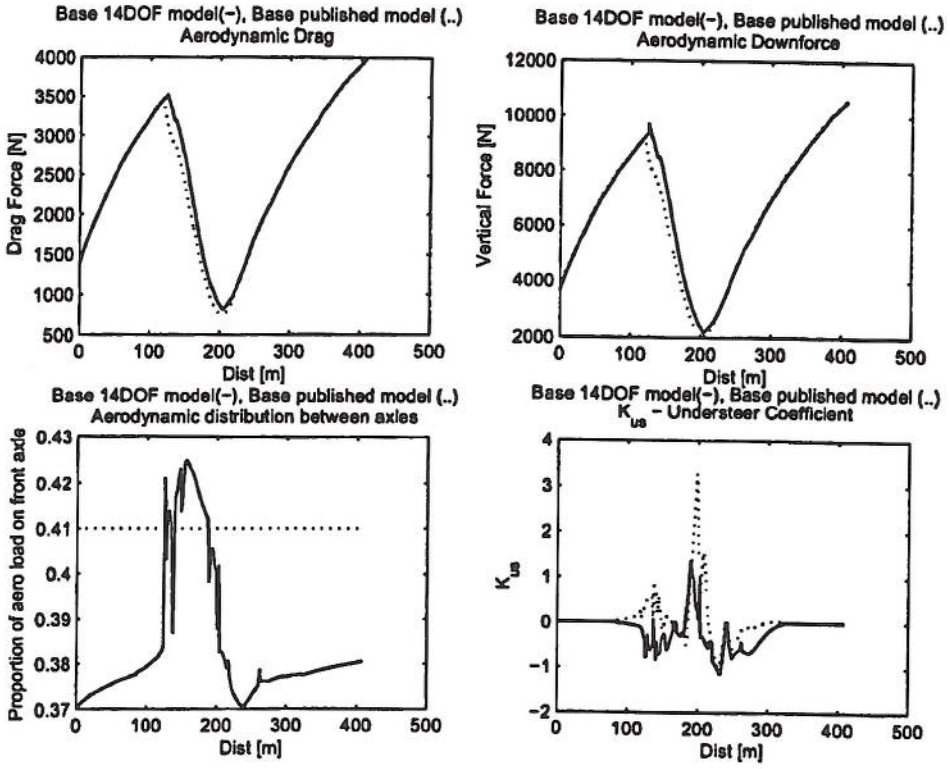

Figure 3.16: Aerodynamic loads, K_{us} - published vehicle model and the 14DOF vehicle model.

Figure 3.17 highlights clearly that the 14DOF vehicle model is fundamentally an oversteering vehicle for the majority of the vehicle performance capability, whereas the published vehicle model is fundamentally an understeering vehicle. The dotted and dash polygons indicated the difference in the location and shape of the two envelopes containing the K_{us} values for each model.

The inclusion of the ride height dependent aerodynamic map may have brought about this fundamental vehicle behaviour change. This can easily be checked by comparison of the K_{us} values for the GG speed diagram of the published vehicle model as shown in Figure 3.17, and the K_{us} values for the 7DOF suspension vehicle model. This version retained the previous roll axis based roll model but used the ride height sensitive aerodynamics wind tunnel data. Therefore the only difference in the two vehicle models is the pitch sensitive aerodynamics.

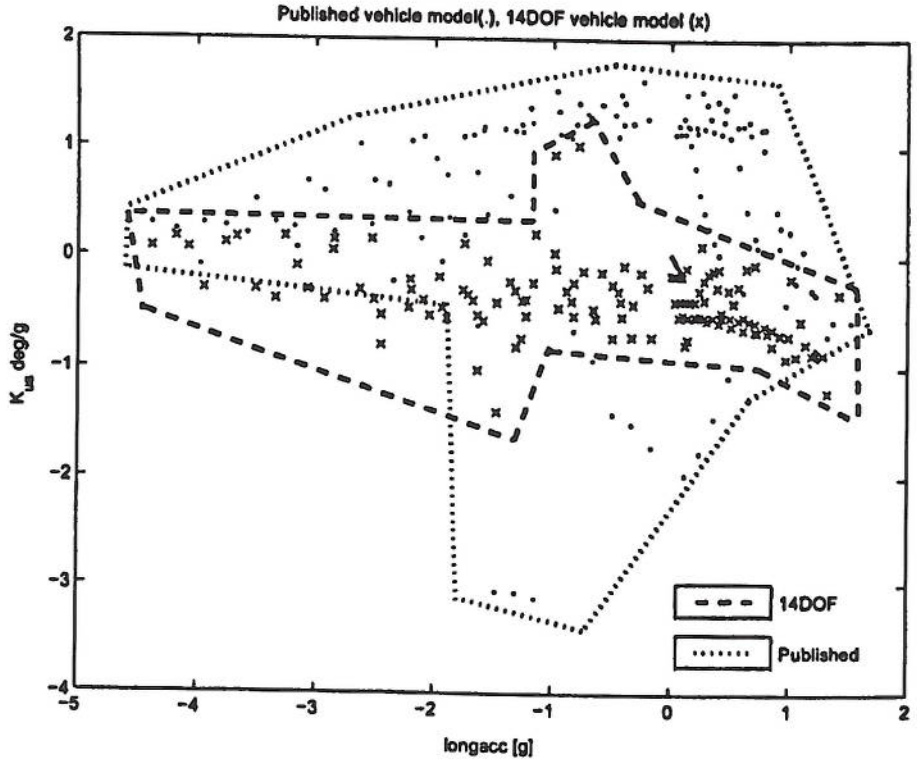

Figure 3.17: K_{us} - Published vehicle model and the 14DOF vehicle model.

Figure 3.18 is a plot of the K_{us} values for the two seven DOF models, the published vehicle model and the 7DOF suspension vehicle model. Figure 3.18 does not show the same trend seen in Figure 3.17, and the values of K_{us} for both seven DOF models are very similar. This indicates that the fundamental vehicle behaviour change is not due to the inclusion of the ride height dependent wind tunnel data.

The change in vehicle behaviour seen in Figure 3.17 must be due to differences in the roll behaviour, as this is the only other difference between the published vehicle model and 14DOF vehicle model. The original seven DOF roll dynamics have not been matched by the current choice of linear spring coefficients in the 14DOF vehicle model. This is because the spring coefficients have been found from other sources [12, 41], as the settings for the base vehicle configuration were not known. Additionally, the roll and pitch dynamics are now coupled and the load model does not rely on a roll axis implementation or constant roll stiffness description as is the case for the published vehicle model and 7DOF suspension vehicle model.

The GG speed diagram for the 14DOF vehicle model is shown in Figure 3.19. The

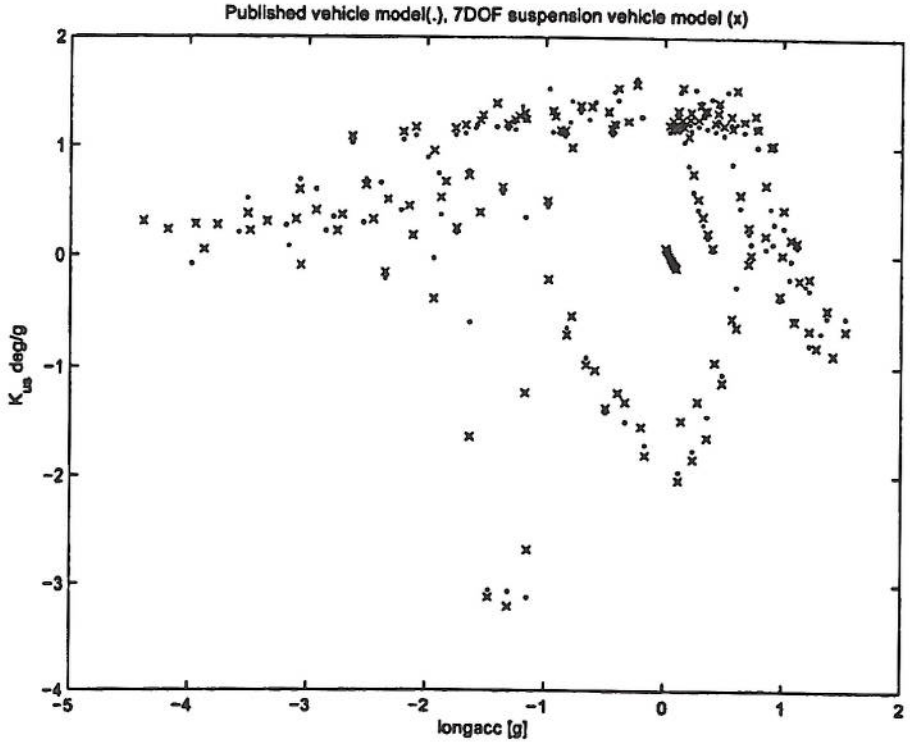

Figure 3.18: K_{us} - Published vehicle model and 7DOF suspension vehicle model.

fundamental change in vehicle performance as a result of the new 7DOF suspension analysis over the published seven DOF model is significant. The fundamental change in cornering behaviour is evident in Figure 3.19 and shows that the vehicle performance capability is significantly better than the published seven DOF model.

The 14DOF vehicle model in the base configuration has a significant oversteer bias when compared with the published seven DOF model through this double lane change manoeuvre. As the aerodynamic table is a realistic setup for the vehicle being modelled, and in the absence of experimental validation, the 14DOF system is believed to be a better representation of the vehicle being modelled than the published seven DOF model. Results shown in Casanova et al. [20] also suggest that a F1 vehicle will be faster if oversteer is promoted, and therefore it appears sensible that the fundamental nature of a F1 car will have a bias towards oversteer.

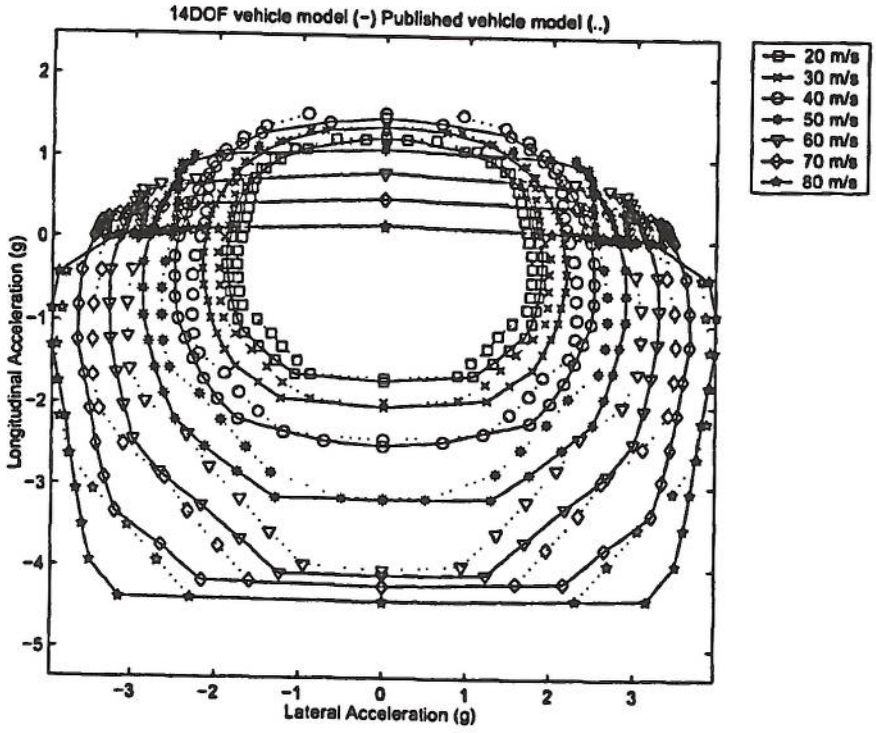

Figure 3.19: GG speed diagram 14DOF vehicle Model and published vehicle model.

Chapter 4

The optimal path (racing line)

This chapter uses the seven DOF published vehicle model. This choice allowed the inclusion of optimal path information from published results [3] that used this version of the vehicle model.

4.1 Accuracy of optimal racing line calculation

Optimisation is an iterative process. An objective function is minimised or maximised subject to a set of constraints being met. Termination criteria are set as part of the computer program. The termination criteria normally define the worst case constraint violation that is acceptable at the solution and also the precision required of the independent variables in order to call the solution optimal [24]. Consequently the simulation engineer must decide the level of accuracy and precision that is required. This will generally be a trade-off based on achieving an acceptable computational time and accuracy at the solution.

It is first prudent to determine the accuracy of the optimal solution given the available information. The 'student t' distribution will be used because the true standard deviation about the optimal solution is not known. To determine whether an optimal solution is likely to be a global or local minimum (or maximum) the TO program is started from different values of the optimisation vector variables. The results are replicate solutions. If the optimiser converges on the same solution from many different starting points, then this adds weight to the supposition that the solution found is global.

As mentioned in section 3.4.1, the computational time for an existing method for an entire lap is quite long. Of the results produced by Casanova [3], only four replicates were able to be produced in the time available for each vehicle parameter that was studied.

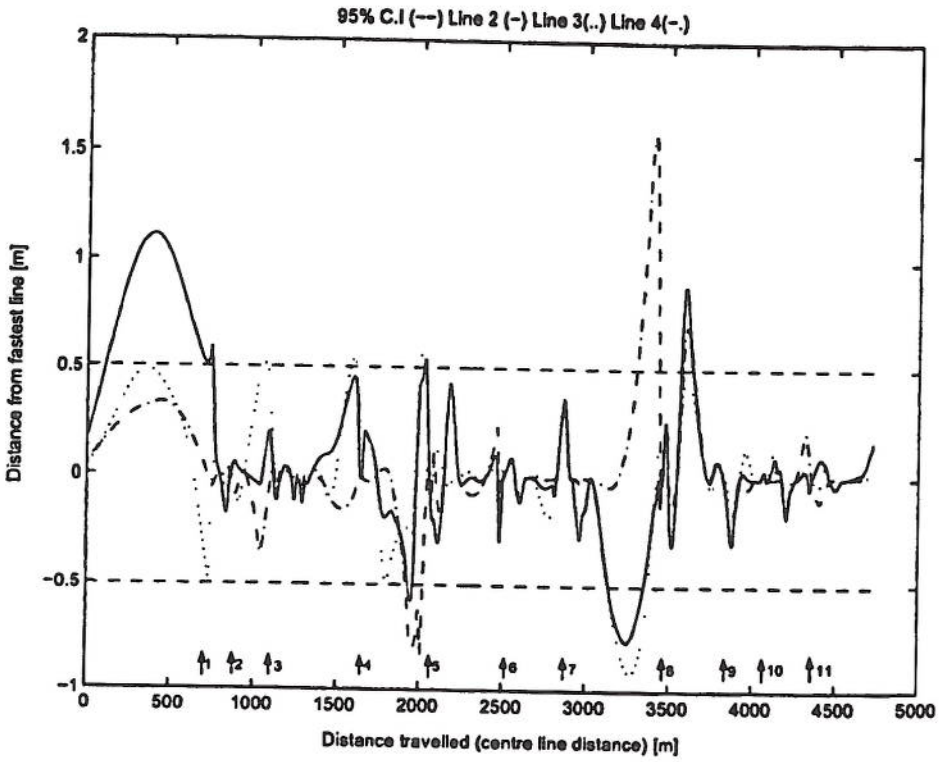

Figure 4.1: Difference in optimal racing lines calculated by the TO method.

Figure 4.1 shows the differences in the three replicate optimal racing lines with respect to the candidate global line that produced the fastest lap time. The dotted line represents the 95% confidence interval for the differences in the racing lines about the fastest line, which was found to be ±0.5m. This is relatively small in the context of a circuit that is nominally 10m wide.

4.2 Vehicle parameter changes

Now that the size of the optimal path zone can be described (±0.5m), it is possible to apply the optimal line results to the QSS simulation method and investigate the effects

of changing vehicle parameters.

The location of the centre of gravity (CG) is a sensitive and therefore dominant design variable in automotive design [37]. The general trend, not withstanding the nonlinear effects of vertical load on the tyre forces, is that a move of the CG rearward will promote oversteer [1]. In effect the car will be harder to control on the limit, but could be potentially faster round the circuit. A rearward weight bias can improve traction for a rear wheel drive vehicle. Although the effect of the CG position has been investigated elsewhere [20] the use of the current QSS method on two alternative racing lines has identified further behavioural attributes of the racing car worthy of discussion.

4.2.1 GG speed diagram

A modest change of 6% towards the rear in the location of the CG has been introduced as a change to the base vehicle setup. The GG speed diagram is recalculated and the result is shown in Figure 4.2.

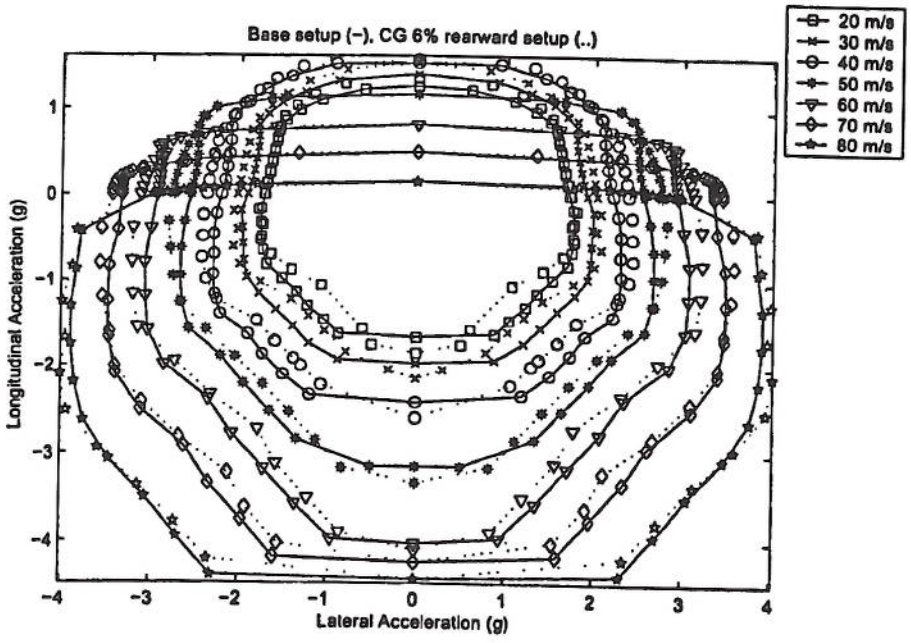

Figure 4.2: GG speed diagram - Base setup vs CG setup

The differences between the new GG speed diagram and the base car (Figure 4.2) can be summarised as follows:

1. Lateral acceleration generation capability has improved for the tractive part of the diagram.

2. Lateral acceleration generation capability has improved at low to moderate deceleration values (0 to -2g), but this degrades into a loss in lateral acceleration capability as full deceleration is approached.

The lack of smoothness in the velocity contours in Figure 4.2 of the 6% rearward CG result, when compared with the base result, is indicative of the difficulty the optimisation routine had in trying to solve the equations of motion to produce the GG speed diagram. It is obvious that the model performance is not a smooth function of the state variables. It is often difficult to find the optimum. Clearly, the method struggles with this task, and a similar difficulty was found by Casanova et al. [20] with their TO method. The natural conclusion is that under this new setup, the model is extremely sensitive to small changes in the control inputs. This is mainly evident in the braking part of the diagram. Instability under braking does not inspire any driver to brake late into corners, and one could imagine that this setup change would not be a desirable one to increase driver confidence in the vehicle.

4.2.2 New optimal line

When vehicle parameters are changed, it is reasonable to assume that there will now be a new optimal line to extract the fastest possible laptime from the vehicle. The results of Casanova et al. [20] indicate that this was indeed the case.

For clarity, the optimal line found for the base set up will be referred to as the 'base optimal' line, and the optimal line found for the set up shown in Figure 4.2 will be referred to as the 'CG optimal' line. The CG set up will be referred to as the 'CG vehicle' and the base set up will be called the 'base vehicle'.

When plotted in terms of cartesian coordinates as in Figure 3.8 the differences between the two optimal lines are very hard to see. Instead the distance from the centre line of the track has been calculated at each time step for both optimal lines and the difference between the two is shown in Figure 4.3.

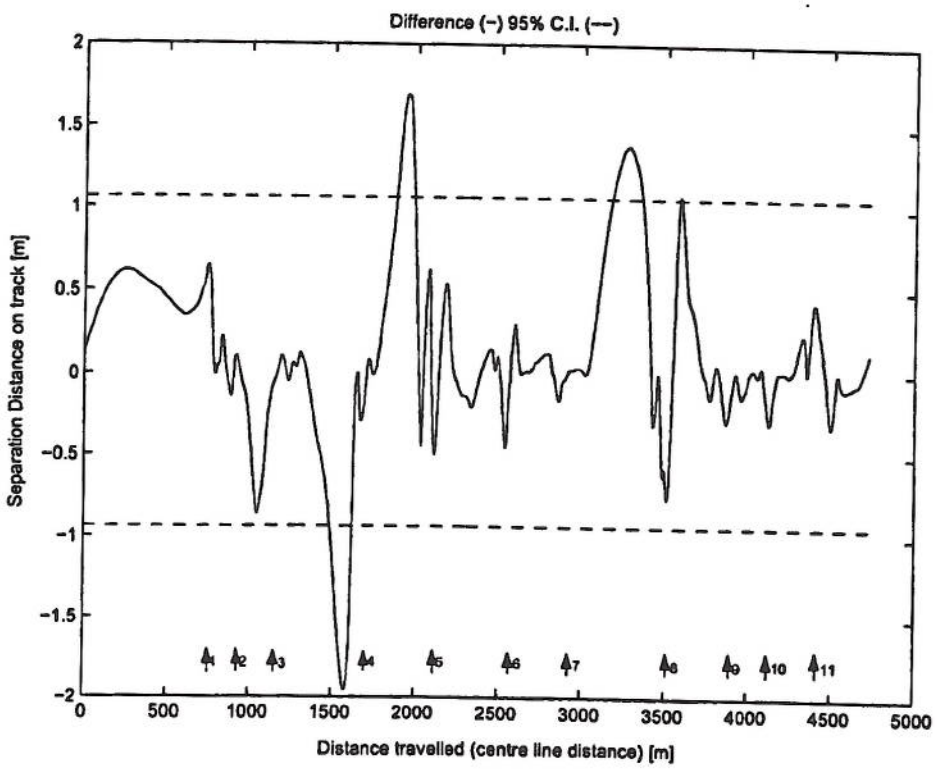

Figure 4.3: Differences in optimal line due to a 6% CG set up change

The majority of the points are very similar and this explains why the 95% confidence interval is only ± 1.0m. Drivers will struggle to follow the optimal path to ± 1.0m at racing speed, so a knowledge of the change in optimal line may not be useful to them.

In section 4.1 it was found that an estimate of the average variability about the optimal line for the base set up was ± 0.5m at the 95% confidence level. The differences between the CG optimal line and the base optimal line are ± 1.0m at the 95% confidence level. Both of these intervals are not particularly large considering the actual circuit width of 10m, and the variability in the optimal line calculation represents half of the observed difference between the base optimal and CG optimal lines. The interesting point will be the effect on the overall laptime of the CG car set up and the racing line change. To make the comparison, the fastest lines from both the base and CG set ups were used.

Set up	Lap time (s) QSS	Lap time (s) T.O [20]
Base	82.904	80.714
CG change	81.471	80.177
Difference	1.433	0.537

Table 4.1: Simulated lap time at Barcelona Grand Prix circuit

The lap times are calculated using the QSS method and are given in Table 4.1. The laptimes, as found using the TO method [20], are also given for comparison. The agreement with the TO method lap times is good (within 3%), and it appears that a positive set up change has been made because the laptime has reduced in both cases.

To determine the reasons for this improvement it is necessary to inspect the acceleration time histories for the two set ups (Figure 4.4).

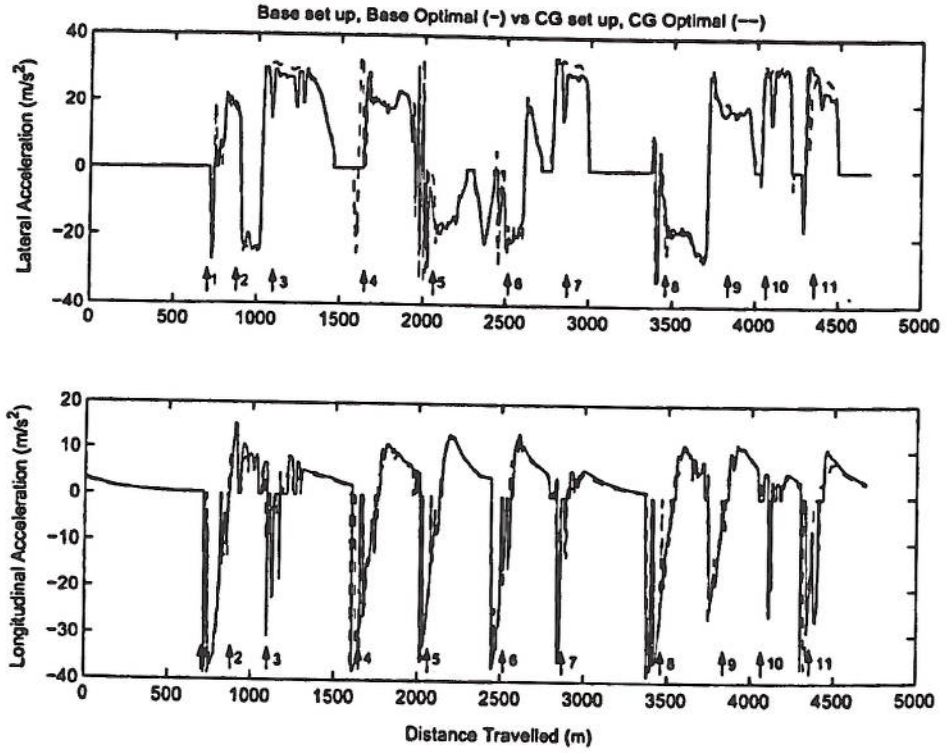

Figure 4.4: Accelerations comparison - base setup and CG set up

The main differences in the accelerations between the two set ups are the higher lateral acceleration peaks and the correspondingly higher (or lower if decelerating) longitudinal acceleration peaks in the CG optimal line results when compared with the base optimal line results. The CG vehicle on the CG line utilises the improvements in lateral acceleration under tractive acceleration seen in Figure 4.2 in corners 3,7, and 11 (Figure 4.4). The loss of lateral acceleration in braking appears to have very little impact. This is probably because the majority of braking is conducted in a straight line or close to it. As one would expect, this results in a better overall lap time for the CG optimal line (Table 4.1). The improvements in the three corners mentioned is confirmed in Figure 4.5. This figure is a measure of the distance between the two cars as if they were racing each other. As can be seen, the CG vehicle creates gaps in corners 3,7 and 11 that by the end of the lap results in a separation distance of 108 metres which at the start/finish line speed of 76 m/s accounts for the 1.43 second lap time difference.

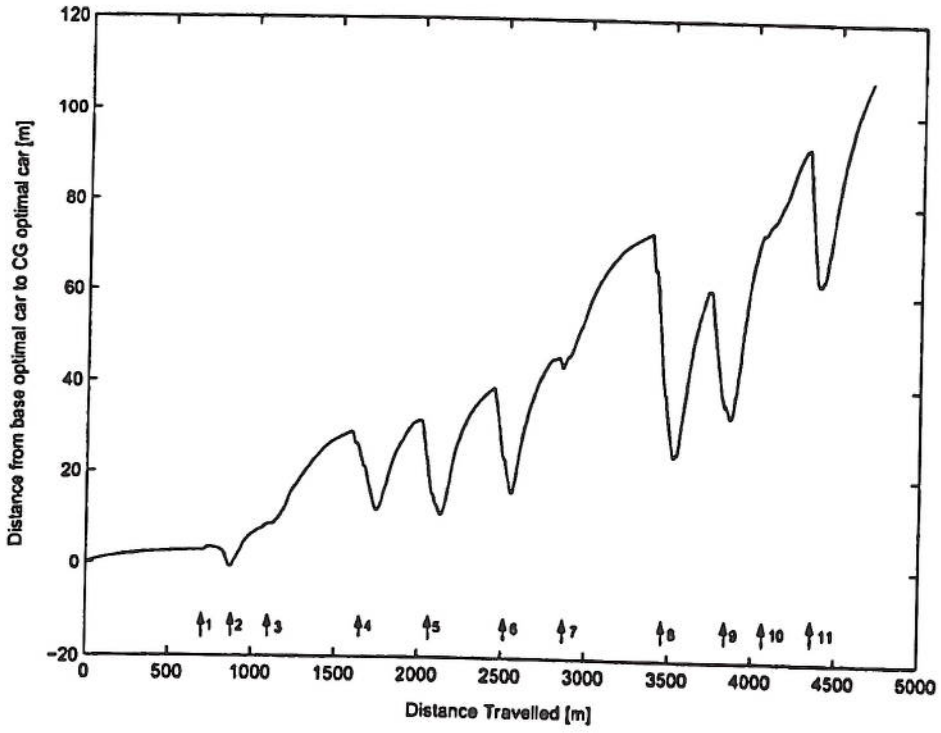

Figure 4.5: Distance from base optimal vehicle to CG optimal vehicle

Set up	Lap time (s) QSS
Base optimal line	81.531
CG optimal line	81.471
Difference	0.06

Table 4.2: Simulated lap time using the CG vehicle at Barcelona Grand Prix circuit

It is important to note that there is a significant oscillation at 1600m travelled and even more dramatically at 2000m where the lateral acceleration appears to oscillate between $\pm 30 m/s^2$. These apparent anomalies are inherent in the original path description taken from the TO method optimised results, where the optimiser has tried to excite the vehicle in yaw before entering corners 4 and 5 (Figure 3.8). Whilst this is not a conventional driving style found in F1 it is more common in rally car driving styles on loose surfaces and it appears that the optimiser has been able to control the vehicle on the limit in a similar manner here. This highlights one of the difficulties with minimum time control solutions, where the result may suggest a control of the vehicle which is beyond the reach of even experienced motor racing drivers.

4.2.3 Vehicle change or line change?

The fact that the QSS method requires a line to be provided as an input can be exploited in a manner that is difficult with an optimisation method that has the racing line and control inputs coupled together as in Casanova et al. [20]. The QSS method can run the CG vehicle behavioural characteristics which are stored as a vehicle dependent, circuit independent GG speed diagram with any choice of racing line. This allows the running of the CG vehicle with the base optimal line instead of the CG optimal line. This uncoupling allows the determination of the reason for the lap time improvement to be broken down into its potential causes, new optimal line and new vehicle, and analysed separately.

Interestingly, the results show that the lap time of the CG vehicle on the base optimal line was virtually identical to that of the CG vehicle on the CG optimal line (Table 4.2).

A similar analysis of acceleration profiles and virtual car separation distances, as in Section 4.2.2, will be used here to explain why this result occurred.

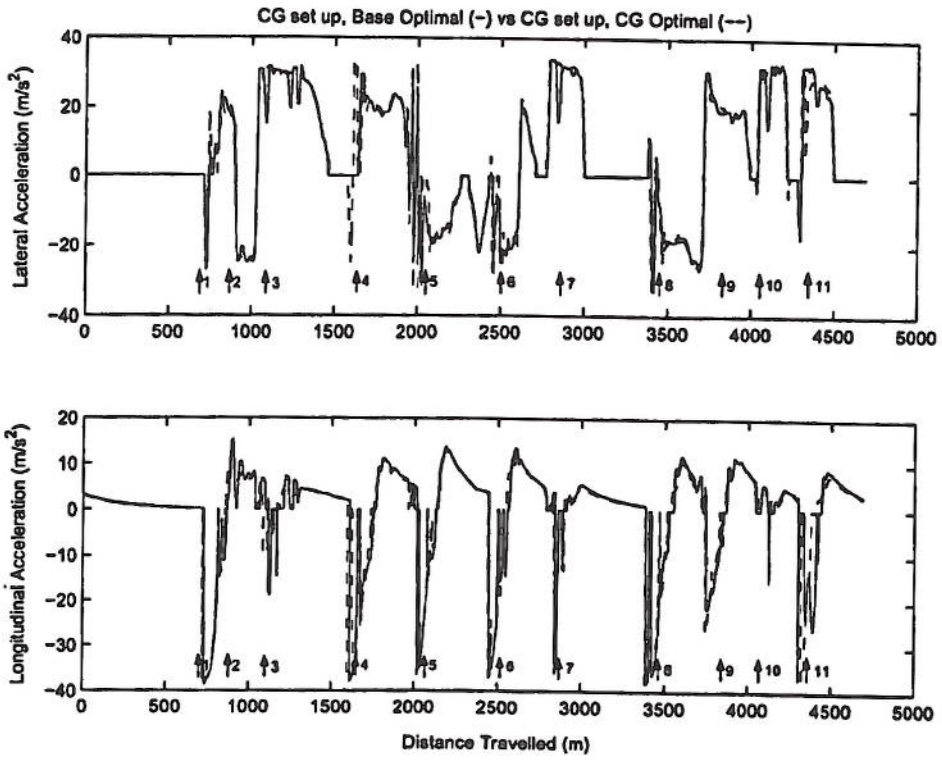

Figure 4.6: Accelerations comparison - CG vehicle on base optimal and CG optimal racing lines

Figure 4.6 shows the acceleration histories for the CG vehicle using the base optimal and CG optimal racing lines. Unlike in Figure 4.4, there are very few differences between the acceleration profiles. The differences are in corners 3,7 and 11 again, but they are much smaller this time.

Looking at the car separation distance plot in Figure 4.7 it can be seen that the car separation distance never exceeds 8 metres.

Figure 4.8 shows the speed history of the CG vehicle calculated for the base optimal and CG optimal racing lines. The speed profiles confirm that the differences are in corners 3,7, and 11 and that they are relatively small. These corners are all high speed corners ($\geq$ 50 m/s) and inspection of Figure 4.2 shows that in traction, this is one of the areas where the GG speed diagram has expanded significantly. Looking back at Figure 4.3 at these corners, it can be seen that they all vary by $\leq$ 0.5m from the base optimal line. This means that it is not possible to determine whether the small differences in lap time are due to exploitation of the new vehicle characteristics or variability in the

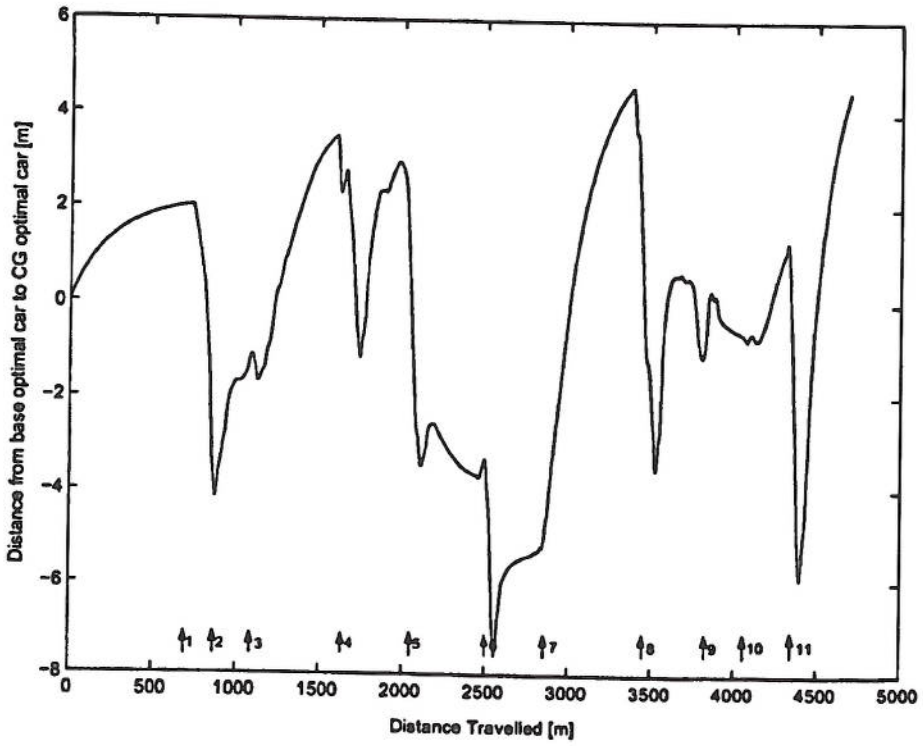

Figure 4.7: Distance from base optimal, CG vehicle to CG optimal, CG vehicle optimal line calculation.

However, the results in Table 4.1 and 4.2 suggest that moving the CG rearwards makes the car quicker around the circuit, as long as the path taken is very close to (but not necessarily exactly equal to) the optimal path. It would seem from this result that more attention should be placed on the track-dependent handling characteristics of the car than on attempting to find a new optimal line for every setup. The QSS method presented here is well suited to that approach. It would also seem that a method of producing faster lap times is to move the CG rearwards and then to find a driver who is able to get within half a meter of the notional optimal racing line, with a car that is now much harder to control on the limit.

The ability to separate the analysis of the vehicle set up to that of the racing line is a useful feature of this QSS method. The analysis of the results has shown that the 6% change in CG location towards the rear of the vehicle has produced a significant lap time improvement at the Barcelona Grand Prix circuit. The analysis of the racing

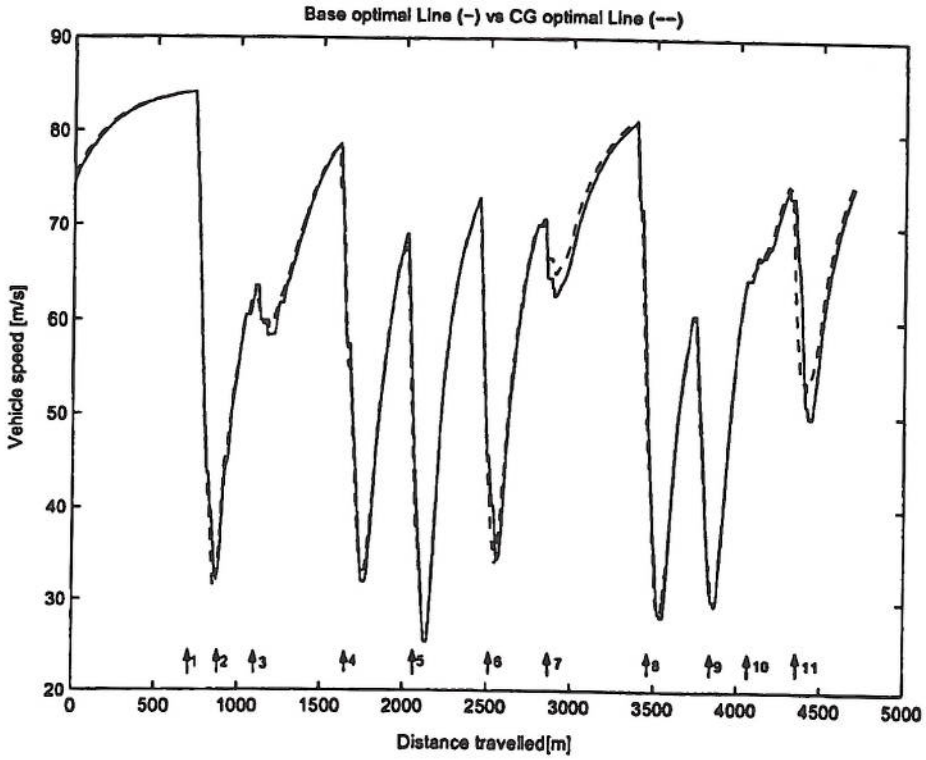

Figure 4.8: Base optimal and CG optimal racing lines, speed history

line while using the CG vehicle has shown that very little of this improvement was due to the new optimal line. There is no reason to suspect that this is not a general result applicable to all open wheel race cars that have a long wheel base and a well damped yaw response.

The quasi steady state method and the transient optimal method both show improvements in lap time due to a 6% centre of gravity set up change and the quasi steady state method produces a lap time that is within 3% of the transient optimal method result.

The difference in optimal lines caused by a 6% CG change is shown to be so small that the driver is unlikely to find the information useful. In light of this observation the computational effort required to generate a new optimal line for each set up change may be misspent.

4.3 Practical racing line experiment

The research presented so far has been based purely on numerical modelling and analysis. As an interesting exercise that supplements the racing line argument, a small group of four experienced racing drivers were provided with a two-corner section of the Barcelona Grand Prix circuit and asked to draw their preferred racing line with a permanent marker. The drivers were interviewed separately. Each driver attempted to draw their best line through the two corners based on their driving experience of the circuit.

The marked lines were then digitised on a PC and thinner digital lines were constructed from the averages of the marked lines. This made the comparison easier to make through the use of different line styles, and the reduction in line thickness created a small allowance for the vehicle track width which was deemed more realistic. The result is shown in Figure 4.9.

The four drivers are current professional racing drivers, and all the racing lines are based on a line taken with a similar type of open wheel race car.

This experiment while interesting, suffered some obvious shortcomings in the method, with the most obvious one being that drawing the line as accurately as the driver intended was difficult. However, if one uses the result to look at driving trends then useful qualitative information can be extracted from the experiment.

The differences in the lines taken by the four drivers are more than ± 1m, which adds further weight to the conclusion that a change in racing line of ± 1m may be of limited practical value to a racing driver.

Three of the four drivers suggest a very late turn into the first corner, to allow for a very tight exit of the corner, with the aim of improving exit speed. Driver 1 chose an earlier turn into corner 1 and to sacrifice hitting the corner apex and following a wider mid-corner and corner exit trajectory. Driver 1, who took the earlier corner entry trajectory, suggested that the line taken in a traction controlled vehicle would depend very much on the behaviour of the traction control system. If the traction control system cut in relatively early, driver 1 would adopt a wider trajectory through corner 1 to help improve the traction and therefore speed through the corner.

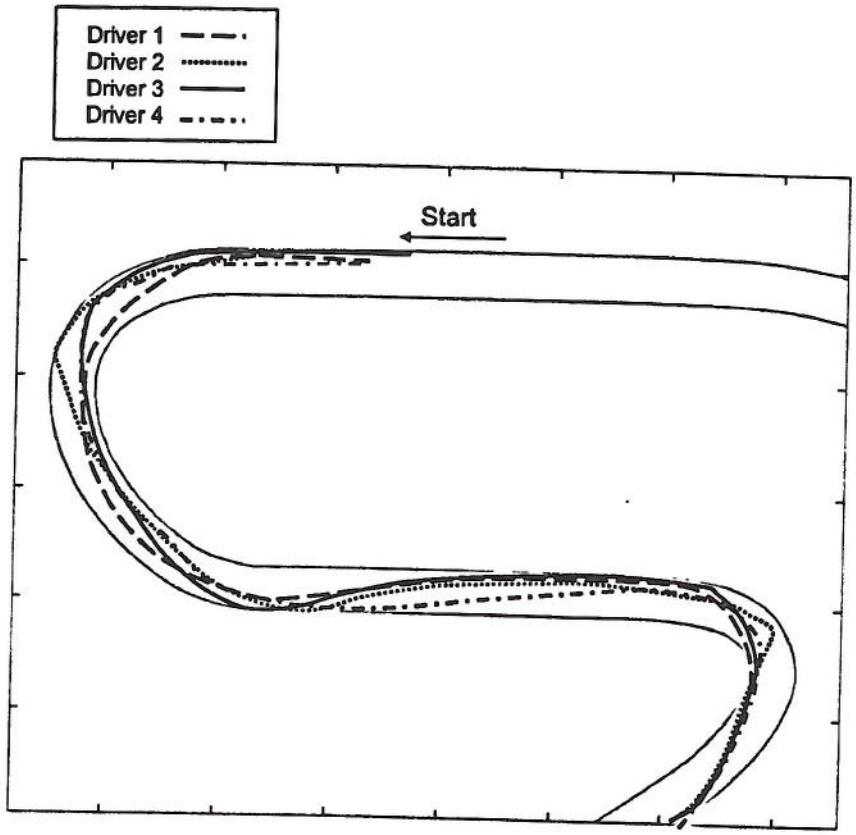

Figure 4.9: Racing Line experiment - Experienced racing drivers

Through corner 2, three of the drivers appear to converge on the same trajectory with corner entry started out at the edge of the circuit, before turning in tight as close as possible the apex of the corner, and then reducing the steer angle to control the vehicle towards the outside of the track on corner exit. Again one driver, this time Driver 2, took a later turn in to corner 2 although the same mid-corner and corner exit trajectory was suggested as the other three drivers. The severity of the change in trajectory towards the apex of corner 2 of Driver 2's trajectory, suggests that this was likely to be a drawing error, and if redrawn would more closely approximate the other three driver trajectories.

This analysis of the racing lines shown in Figure 4.9 indicates that there is more to the process of driving the racing line than just putting the car on the limit at all times, as the optimal path finding methods do. Other relevant factors include: low road friction conditions off from the most frequently used racing line, the effect of active systems and driver prejudice.

Chapter 5

Parametric study

This study is conducted with the seven DOF published vehicle model. This implementation of the QSS method is based on the first method described in Chapter 3, but uses automatic differentiation for evaluating the derivatives as required by the optimiser, and uses the updated differential and gear selection models. The aim of this chapter is to conduct a sensitivity study based around a true vehicle set up. The only validated race car data available during this research was for the published vehicle model.

5.1 Introduction

The real benefit of the GG speed diagram approach described in this thesis has been the relative ease in changing key parameters in the published vehicle model to determine the effect on the GG speed diagram shape. In this chapter a group of key parameters that represent the major areas of open wheel race car design have been chosen to be included in a parametric sweep. The aim of this study is to quantify and rank the areas in terms of possible vehicle performance improvements and consequently, identify where resources could best be utilised in vehicle development and research. Whilst the following analysis only relates to a specific vehicle, trends are likely to be true for Formula One vehicles, and the method could easily be applied to another vehicle configuration or setup as required.

The following six areas have been included in this study.

- Vehicle mass (Fuelling and race strategy).

- Yaw inertia (Chassis design).
- Tyres (Tyre materials and construction, and the effects of wear).
- Engine (Power train).
- Longitudinal centre of gravity location (Chassis design).
- Aerodynamic Downforce (Aerodynamic packaging).

Based on the engineering effort required to bring about changes in these areas, the following ranking is suggested in terms of least effort required to the largest:

1. Vehicle mass.
2. CG location.
3. Yaw inertia.
4. Aerodynamic downforce.
5. Tyre force sensitivity.
6. Engine torque.

Underlying this list are the following assumptions:

- The base vehicle configuration is the starting point for additional engineering effort required.
- Vehicle mass must not be lower than the rules allow. Therefore changes to vehicle mass are limited to changes in fuelling strategies.
- CG location is restricted to the range tested and can be achieved by relocation of ballast and easily relocatable items, such as the ECU, battery etc.
- Tyre development is less expensive than engine development.

Given that the engineering effort required to bring about changes in these key areas can be characterised based on a set of assumptions, it is now necessary to determine the sensitivity in vehicle performance as a result of changes in these areas.

5.2 Vehicle mass

The minimum allowable weight of the vehicle is 600kg [45]. If an allowance is made for fuel storage, a plausible maximum weight for the vehicle would be 700kg. These two limits were used to define the vehicle mass range to be studied. The base setting for the vehicle is 650kg.

Five GG speed diagrams have been generated for each of the six areas of enquiry in this chapter. The parameter sweep can be a percentage change from the current set up or, as in this case, equally spaced points between two realistic variable upper and lower settings. For the vehicle mass analysis 600,625,650,675 and 700 kg were computed using the QSS method.

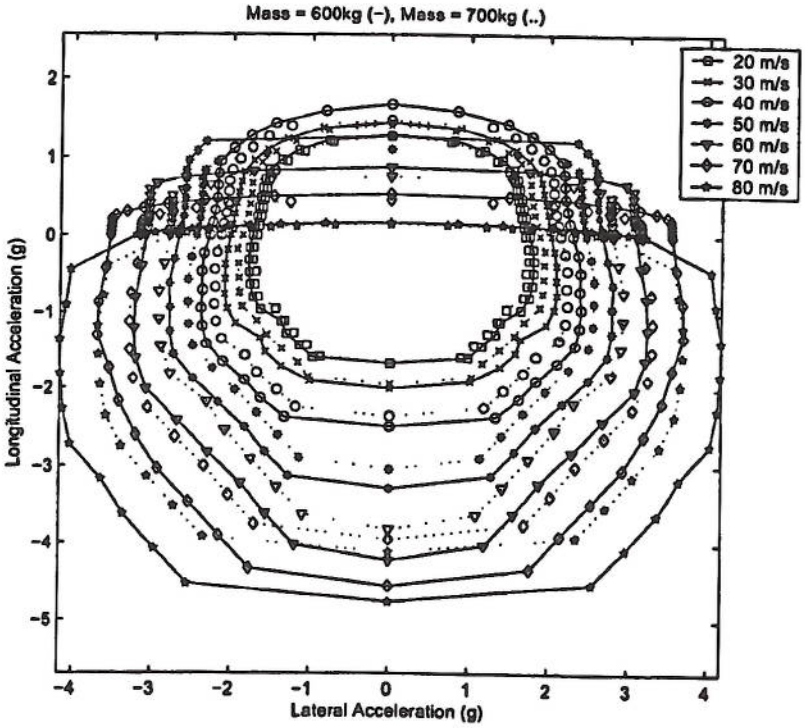

Figure 5.1: Vehicle mass sensitivity analysis - GG speed diagram.

Figure 5.1 shows the range in performance at the two extremes of the mass sensitivity analysis, 600 and 700kg. As one would expect, the lighter vehicle is significantly

better in both positive acceleration and braking. It is very easy to quantify this phenomena for a vehicle travelling in a straight line and in pure steady state cornering, but in combined longitudinal and lateral acceleration the task is more difficult. However, this is easily determined with the QSS method.

This thesis focusses on interpretation of GG speed diagrams for determining improvements and losses due to changes in the published vehicle model and the use of optimised terms. As soon as more than two diagrams are presented in the form shown in Figure 5.1 it becomes very difficult to see the differences between the diagrams without confusion. A quantitative comparison would be better than a qualitative comparison so a method of quantitatively comparing GG speed diagrams has been devised.

Each particular constant velocity contour as calculated by the QSS method is a closed polygon. An improvement for a particular velocity contour results in the polygon expanding in size, and conversely, a decline in performance capability results in the polygon shrinking. By measuring the area of each polygon/velocity contour (as illustrated in Figure 5.2) and comparing the values found from other GG speed diagrams a quantitative comparison at each particular velocity contour is possible. Averaging of the percentage differences across the velocity contours gives a single scalar term that represents the global performance difference between two GG speed results.

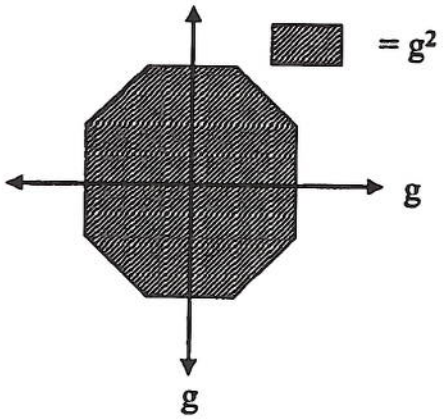

Figure 5.2: GG speed diagram - area evaluation.

Table 5.1 is a summary of the 600kg result shown in Figure 5.1 compared with the base result. As Table 5.1 shows, the GG speed diagram has expanded by 9% on

Speed m/s	Mass = 600kg g^2	Base g^2	% Improvement
20	8.852	8.643	2.42
30	12.028	11.236	7.05
40	16.802	15.633	7.48
50	21.435	19.319	10.17
60	26.501	23.793	11.38
70	30.887	27.645	11.73
80	35.304	31.286	12.84
Global average			9.01

Table 5.1: Area of constant velocity contours - GG speed diagram for vehicle mass = 600kg (Figure 5.1).

average.

Since the five results are to be compared, it is easier to show the differences in an *XY* plot rather than in a table. Figure 5.3 shows the percentage change in the areas of the GG speed diagram constant velocity contours compared to the base vehicle GG speed diagram result.

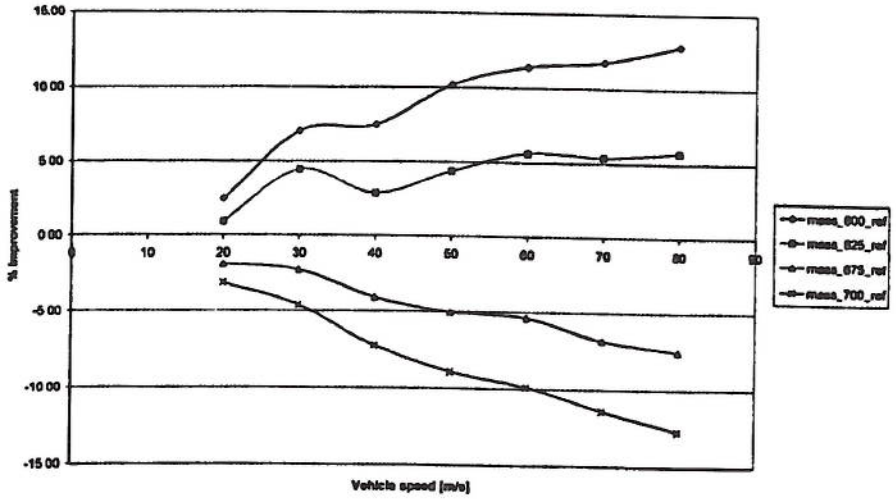

Figure 5.3: Vehicle mass sensitivity analysis - Percentage Improvements.

The most noticeable feature of Figure 5.3 is the dip seen in the 600kg and 625kg results at 40 m/s. Around 40 m/s, in positive acceleration, there are two active constraints operating, whereas at speeds lower and higher than this value one of the two constraints dominates the vehicle performance capability. The first constraint is the saturation limit of the tyres and the second is the limit of the available engine torque. At low speeds the level of road friction dominates the size of the GG speed diagram. At high speeds, the available engine torque limits the vehicle performance capability. This accounts for the two distinct slopes seen in Figure 5.3, above and below 40m/s.

In general, the relative vehicle performance improves with speed with reducing mass. This is due to the simple expression of Newton's second law of translational motion:

$$\sum F = Ma \tag{5.1}$$

As M reduces, the acceleration capability proportionally increases. By changing the vehicle mass in the published vehicle model as was done here, the percentage differences in acceleration should correspond to ±4% per ±25kg using Equation 5.1. However, the GG speed diagram results illustrate a different trend. At low speeds the acceleration capability is lower than expected, but this is due to the longitudinal acceleration limit being dominated by μ_{road}, the road friction coefficient. The tyres are saturated at 20-30 m/s at 1.8-2 longitudinal g. As the speed increases to 40-50 m/s the improvement in tyre load due to the aerodynamic vertical load component helps realise the ±4% change expected. However, at speeds beyond 50 m/s the improvements/losses are larger in magnitude than would be predicted by Equation 5.1. Bearing in mind that the aerodynamics are not ride height dependent in this model, the first place to check for differences is the tyre force response to variations in tyre load because as M changes the static component of F_z is changed in direct proportion. Inspection of the friction circle for the type of tyre used in the vehicle optimisations, shown in Figure 5.6, highlights the nonlinear response of the tyre to a change in $\frac{F_x}{F_z}$ and $\frac{F_y}{F_z}$. In fact the area of the diagram where the tyre force sensitivity to tyre load is greatest is at $0.5 < \frac{F_{x,y}}{F_z} < 1.3$ which is precisely the area of tyre operation at high speed.

At 80m/s, the majority of the tyre force is longitudinal in direction, maintaining the high vehicle speed to overcome the aerodynamic drag force. In terms of Figure 5.6 $\frac{Fx}{Fz} \approx 1$ and $\frac{Fy}{Fz} < 0.1$ indicating that the tyre is in the nonlinear region of operation

around the maximum longitudinal tyre force value for the given tyre load. With a 600kg vehicle mass, the actual tyre forces produced are lower than the base vehicle result, but the resulting acceleration vectors per unit vehicle mass are higher for all four tyres in both longitudinal and lateral directions. However, over 90% of the improvement is due to changes in the longitudinal tyre forces. The mechanism is purely a function of the tyre properties in the nonlinear region and illustrates the difficulty in determining quantatively, the effects of changing a relatively well understood parameter like the vehicle mass when the vehicle is in combined longitudinal and lateral acceleration. Using the QSS method, this can be determined quite simply as in Figure 5.3, and comparisons can be made with ease.

5.3 Yaw inertia

This section is included because early research into the effect of yaw inertia highlighted that it was rather unimportant in terms of improving the manoeuvre time through a double lane change using a transient open wheel race car model [21]. What was left undetermined was the mechanism for this result and if it was manoeuvre specific or an underlying feature of the vehicle dynamic performance of this type of vehicle.

A subset of the range of yaw inertias tested in Casanova et al. [21] was used here to investigate Casanova et al. [21]'s finding using the QSS method. Yaw inertias of $100, 250, 750, 1000\ \text{kgm}^2$ were used to generate GG speed diagrams for a comparative analysis. These diagrams are not shown here because the differences between the constant velocity contours were negligible.

The relative performance of the five yaw inertia cases, compared to the base vehicle result, is shown in Figure 5.4. The level of variability and the magnitude of the differences of the results compared to the base vehicle result suggests that this is purely noise within the QSS method. The QSS method, by definition, is insensitive to the value of the vehicle yaw inertia I_{ZZ}. This is because of the imposed constraint of steady state cornering which requires that the yaw moment be equal to zero, and therefore the value of I_{ZZ} is not particularly important (from Appendix A):

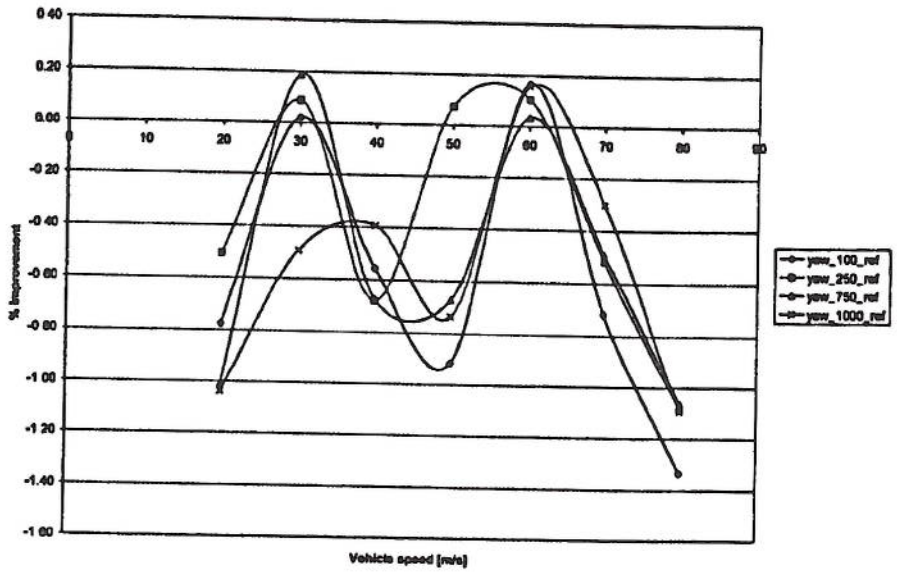

Figure 5.4: Vehicle Yaw sensitivity analysis - Percentage Improvements.

$$
\begin{aligned}
Izz\dot{r} \;=\; & \frac{tf}{2}\Big[Fx_1\cos(\delta) - Fx_2\cos(\delta) - Fy_1\sin(\delta) + Fy_2\sin(\delta)\Big] \\
& + \frac{tr}{2}\Big[Fx_3 - Fx_4\Big] + a\Big[Fy_1\cos(\delta) + Fy_2\cos(\delta) + Fx_1\sin(\delta) + Fx_2\sin(\delta)\Big] \\
& - b\Big[Fy_3 + Fy_4\Big] = 0 \qquad (5.2)
\end{aligned}
$$

Figure 5.4 is an illustration of the error in the QSS method. In its current state, the error in evaluating a velocity contour's true area is shown to be $\pm 1.4\%$.

The fact that Casanova et al. [21] found the transient model of the open wheel race car was insensitive to changes in yaw inertia through a double lane change is a validation of the trimmed steady state cornering condition assumption of the QSS method, for this type of vehicle configuration. It also explains why the manoeuvre time was found to be insensitive to yaw inertia value changes. It is theorised here that in most cases the yaw acceleration of the vehicle is approximately zero and therefore the yaw inertia value is not significant in the majority of vehicle manoeuvres, and therefore is a vehicle model feature and not a circuit dependent result.

Clearly the QSS method is deficient in being able to determine this assertion due to the assumption of steady state cornering, but it can be used indirectly by evaluating the numerical derivative to the value of β, the vehicle sideslip value, from a circuit simulation result.

The transient lateral acceleration of the vehicle model is:

$$a_y = V\dot{\varphi} + \ddot{y} \tag{5.3}$$

$$a_y = V\dot{\varphi} + V\dot{\beta} \tag{5.4}$$

$$\dot{\varphi} = \frac{V}{R} \tag{5.5}$$

Therefore for steady state cornering, $\dot{\beta}$ must be zero. As a result, the theory of circuit insensitivity to yaw inertia for the open wheel race car configuration used in this thesis can be checked using the QSS method. Since numerical differentiation is used, the result in Figure 5.5 is very noisy but the trend is clearly seen, $\dot{\beta}$ is normally very close to zero, except for brief periods of transient vehicle dynamics where the vehicle is changing state very quickly due to combined high lateral acceleration and longitudinal acceleration/deceleration, corresponding to corner exit and entry manoeuvres.

5.4 Tyres

Tyres provide the contact between the vehicle and the ground. All the forces applied to the vehicle are reacted by the chassis and suspension components and ultimately are transferred to the tyres. Tyre force is expressed as a function of slip angle for lateral force and slip ratio for longitudinal force. These relationships are generally nonlinear and are strongly dependent on both construction methods and environmental conditions like tyre vertical load [99], tyre pressure, tyre temperature, and state of tyre wear [100], as well as the underlying road surface type and condition [1]. Early research on tyre force calculation focused on simple models [101], and for use with repetitive vehicle simulations, linear tyre models that provide the tyre force as a linear function of slip angle or slip ratio or as a tyre stiffness $\frac{F_{x,y}}{F_z}$ were, and still are, used in current research [80, 85]. The tyre stiffness term is used to allow for the variation in tyre force with tyre load, but like most influencing factors, this mechanism is also nonlinear, and loses its validity as the tyre approaches saturation. The general consensus for repetitive

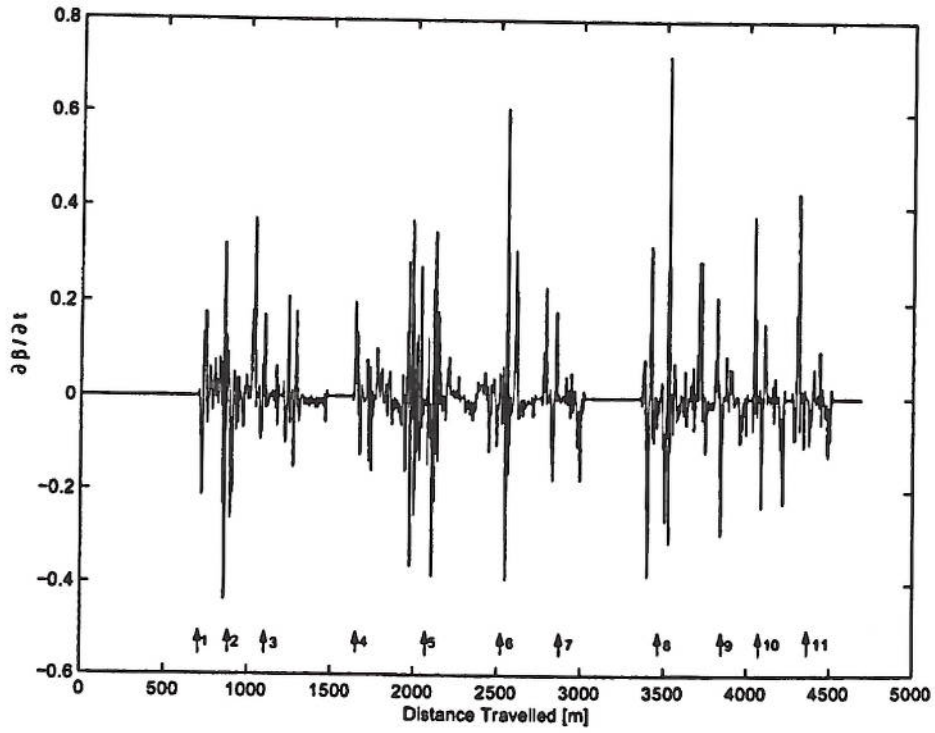

Figure 5.5: $\dot{\beta}$ QSS simulation - Barcelona GP circuit.

vehicle simulation studies is to use a empirical or semi-empirical model. The Pacejka Magic Formula Tyre Model has been used more frequently since its first publication [102] and its subsequent updates [18, 103], because the formula can be made to fit experimental results well, and the key terms in the formula correspond to particular physical attributes of the tyre [102].

As tyre information is particularly difficult to get, without great expense and effort, this research has continued with the use of the Magic Formula Tyre Model from previous work in race car performance at Cranfield University [3]. This is used because of the availability of realistic coefficients for the Magic Formula for the types of tyre used on the open wheel race cars, which are the subject of this thesis. The coefficients used here are an amalgamation of real data from a series of Magic Tyre coefficient fitting results to actual F1 vehicle tyre force data.

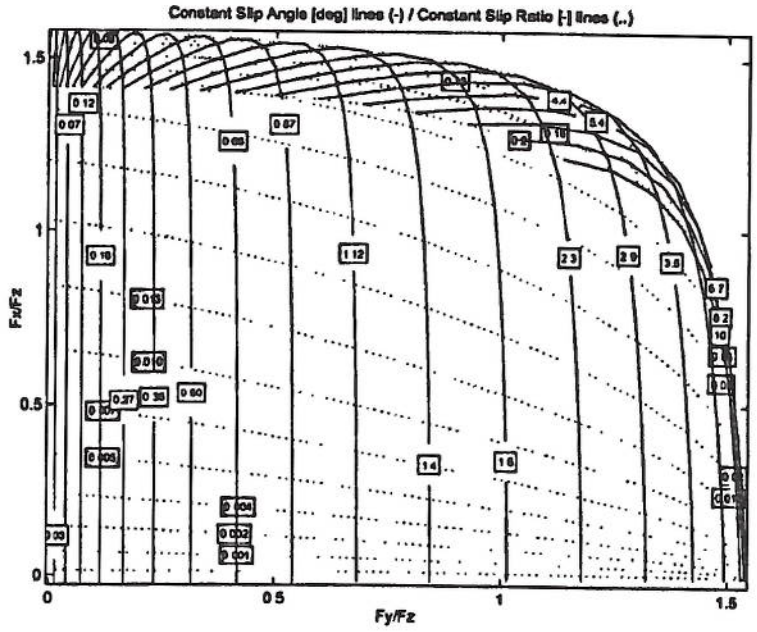

Figure 5.6: Friction circle/ellipse - Representative tyre.

The friction circle (Figure 5.6), used to characterise a tyre's longitudinal and lateral tyre force capability [2, 11], is a key component in the GG speed diagram and much of the shape of the GG speed diagram constant velocity contours is attributable to the shape of the friction circles of the tyres.

This study, of the vehicle response to changes in tyre performance, has been conducted by adding (or subtracting) 5% additional tyre force to each of the four tyres to the values calculated by the Magic Formula Tyre Model. The aim is to evaluate the sensitivity of the vehicle performance, as described by the GG speed diagram, of a change in the tyres' performance due to tyre wear, or a new construction method, or equivalently a change in the road friction coefficient, μ_{road}. The areas of the constant velocity contours of the five resulting GG speed diagrams have been measured and are shown graphically in Figure 5.8. The GG speed diagrams for the 90% and 110% tyre force results, where 100% is the original Magic Formula tyre force values, are given in Figure 5.7 to give an indication of the range in results.

The effect of improving the force capability of the tyres is very significant. The magnitude of improvement (up to 17%) when compared with the mass sensitivity re-

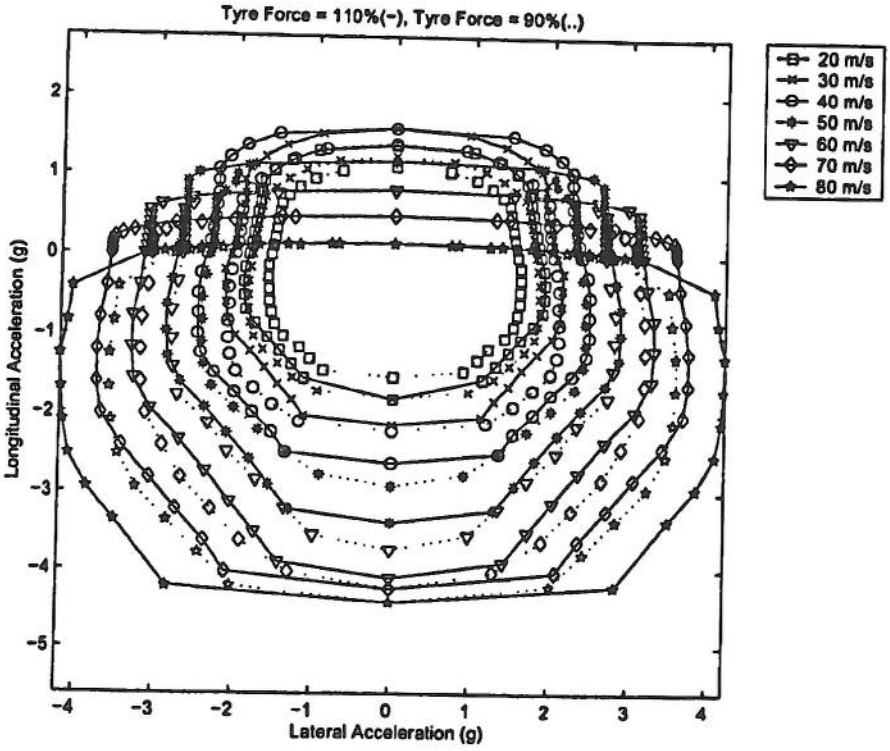

Figure 5.7: 90% and 110% GG speed diagram results.

sult is similar, but it must be remembered that the engineering effort required to bring about these improvements would be vastly different. Changing the vehicle mass in the range explored in Section 5.2 is achieved by a different fuelling strategy, as 600kg is a minimum weight specified by the regulations. Whereas the engineering effort required to produce new compounds of rubber, and possibly new construction methods to better utilise the rubber, could be very large.

As was seen in Section 5.2, there is another noticeable dip at 40m/s for the configurations with lower tyre force generation capacity than the base vehicle, which appears out of line with the adjacent speed results (Figure 5.8). In this instance, the transition from traction limited conditions to engine torque limited conditions is very severe, as represented by the dip. Conversely, in the result for the increased tyre force capacity situation, due to the increased tyre force capability, the engine torque constraint is reached at a higher vehicle speed. At higher vehicle speeds the vertical load on the tyres is higher due to the additional downforce, and the switch from traction limited conditions to engine torque limited conditions is less severe (Figure 5.8).

The improvements over the base vehicle result of the increased tyre force trials are not restricted to particular speeds. There is a tendency to move towards the base result at high speeds but this is due to the finite amount of engine torque, restricting the expansion of the positive acceleration section of the GG speed diagram, which is illustrated in Figure 5.7. In braking, where the available torque for deceleration is much higher than the available engine torque for positive acceleration, the additional tyre force capability can be utilised.

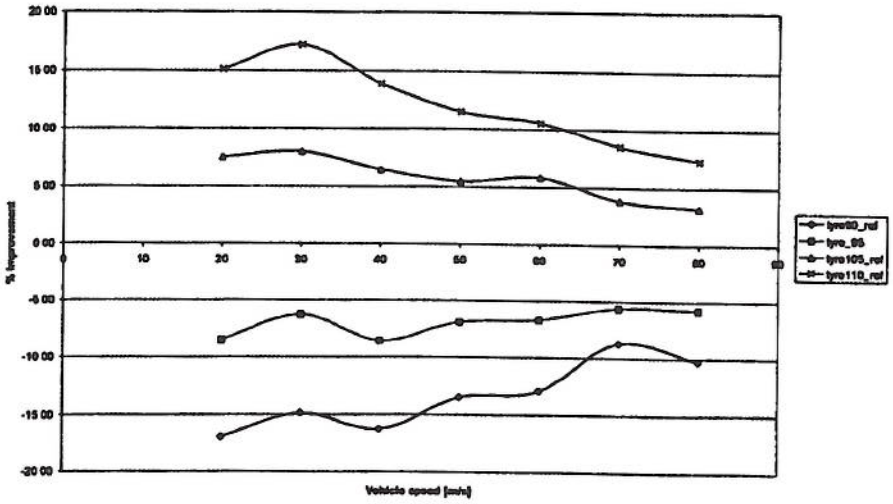

Figure 5.8: Vehicle tyre sensitivity analysis - Percentage Improvements.

The highest gains over the base vehicle results are seen at low speed. Again, this is because at low speeds the tyre vertical load is limited and the brake and engine torque available are in excess of that required to saturate the rear tyres. Therefore the increased tyre force capability is exploitable and a peak at 30 m/s of 17% for the 110% result is seen.

Above 40 m/s, increasing aerodynamic downforce increases the tyre load available and the tyre force demanded is lower than the maximum force available. There is still a substantial improvement though, and this is increasingly provided in braking as the vehicle speed rises. Since the braking torque is provided to all four wheels, and the magnitude of the braking torque available is 20 times that available from the engine, the increased tyre force capability can be exploited in high speed braking and cornering (Figure 5.7).

5.5 Engine torque

In a manner similar to the tyre force sensitivity study, the entire engine torque curve has been decreased and increased in increments of 5% from the original baseline value for a given throttle position and engine speed. The two dimensional areas of the constant speed contours were measured and have been plotted as percentage differences relative to the base vehicle GG speed diagram constant speed areas. This result is shown in Figure 5.9.

The engine torque sensitivity will only be seen in the positive acceleration part of the GG speed diagram and therefore it is possible to show the five positive acceleration curves on one GG speed diagram (Figure 5.10).
Figure 5.10 shows that at speeds below 40m/s the GG speed surface is very similar for the different engine curves. This is because the engine torque available in all configurations (90% to 110%) at these low vehicle speeds is in excess of the torque that can be transmitted to the rear tyres without tyre force saturation occurring. In the 40-60 m/s speed range the aerodynamic drag is low, and the aerodynamic downforce contribution to the wheel vertical loads allows the available engine torque to be effectively transmitted to the ground by the tyres. Beyond this speed the drag force, which is proportional to the square of the vehicle speed, overcomes the torque created by the engine that is transferred to the tyres as longitudinal force and the comparative benefits diminish with further speed increases.

The shape of the percentage change curves in Figure 5.9, for each engine torque curve, are quite dissimilar to those in the previous parameter studies. There is no particular geometric pattern that describes the change in vehicle performance, but the trends can be explained with reference to Figure 5.10. The GG speed contours in the speed range below 40m/s are similar for all five cases due to traction limitations and excess engine torque. At 50m/s, the available engine torque can be transmitted to the tyres and the improvement that can be achieved from an additional 10% engine torque across the entire torque curve is a 3.5% expansion of the 50 m/s constant speed contour over the base result. However, the gains at 80m/s are lower, heading back towards the same level of performance as the base engine torque curve result (Figure 5.9). This can be explained by the drag force increasing with the square of the vehicle speed. However, there is a very large drop seen in the results of the reduced engine torque cases, especially at 80m/s. This apparent anomaly can be explained through examination of

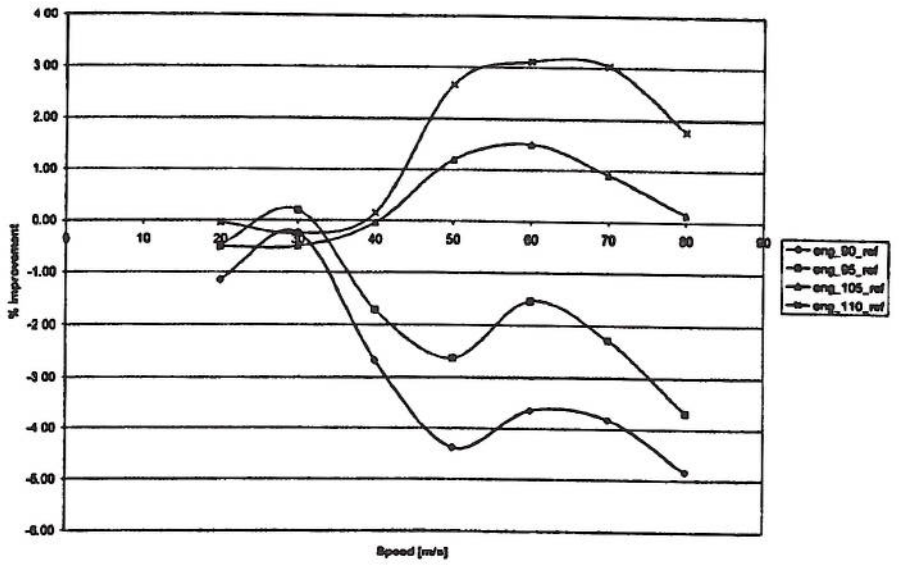

Figure 5.9: Vehicle Engine torque sensitivity analysis - Percentage Improvements.

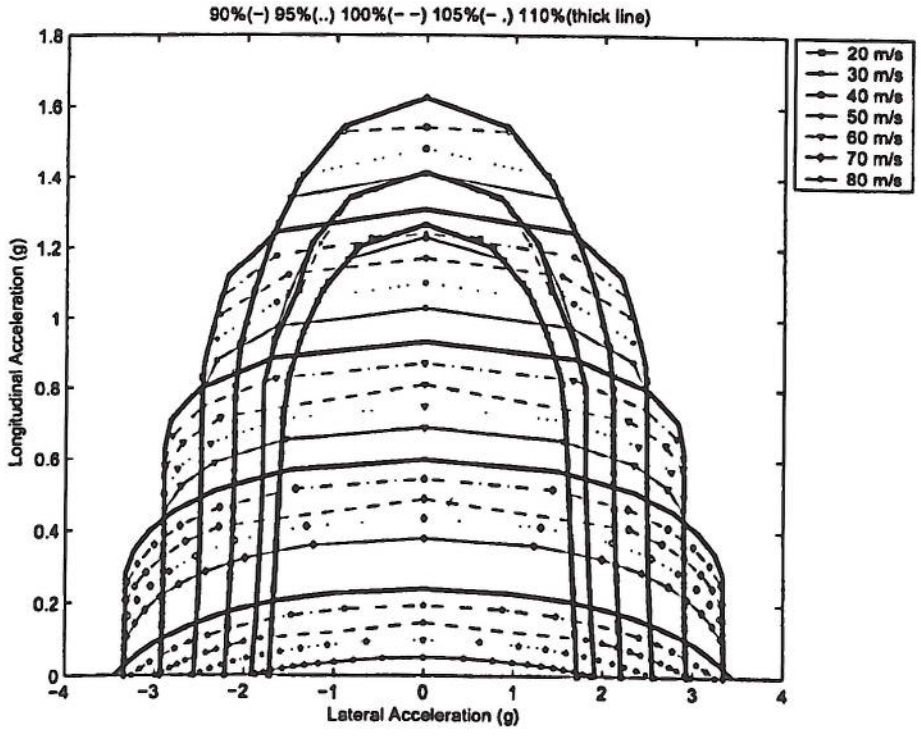

Figure 5.10: Vehicle Engine torque - Positive acceleration only, GG Diagram.

the change in lateral acceleration capability of the vehicle due to the changes in engine torque availability. From 20m/s to 70 m/s the maximum lateral acceleration capability is virtually identical for all of the five engine torque curve runs. The improvements in vehicle performance, indicated by Figure 5.9, are predominantly attributable to the extension of the longitudinal acceleration capability of the vehicle. However, at 80m/s this is not the case. The GG diagram of the 10% increased engine torque case has a maximum lateral acceleration capability of 3.4g, compared with 3g of the base vehicle result. The reduced engine torque configurations, -5% and -10% have a proportionally greater drop in maximum lateral acceleration capability, when compared with the base vehicle, than the corresponding increase as a result of the higher engine torque cases. Additional engine torque of 10% gives a 13% increase in maximum lateral acceleration capability, whereas a 10% reduction in engine torque produced a 33% loss in maximum lateral acceleration capability. This indicates that the use of the engine torque via throttle control is an important factor in exploiting the lateral acceleration capability of the vehicle. This analysis is not suggesting that changes in engine torque directly affect the lateral acceleration capability of the vehicle. However, when the vehicle is using all the available engine torque to attain the current vehicle speed of 80m/s, then any change in the yaw rate and ultimately, the lateral acceleration capability of the vehicle, reduces the longitudinal force contributing to maintaining the constant longitudinal speed condition. Since the constant speed condition is a constraint that cannot be compromised, the lateral acceleration capability of the vehicle is limited by the available engine torque.

5.6 Longitudinal location of the centre of gravity (CG)

The longitudinal location of the centre of gravity has been found to be an influential term in vehicle dynamics [1, 20, 37]. Early work with this published vehicle model, in the open wheel race car configuration, showed that a movement rearward of the CG made the base vehicle potentially faster [92] and possibly a more difficult car to control. A similar result is shown in [20].

In Figure 5.11, the changes in shape of the GG speed performance envelope due to movements of up to $\pm 10\%$ of the longitudinal location of the CG from the base vehicle position can be seen. Figure 5.11 is presented in terms of the percentage of the vehicle static load on the front axle. These choices of CG locations were made to

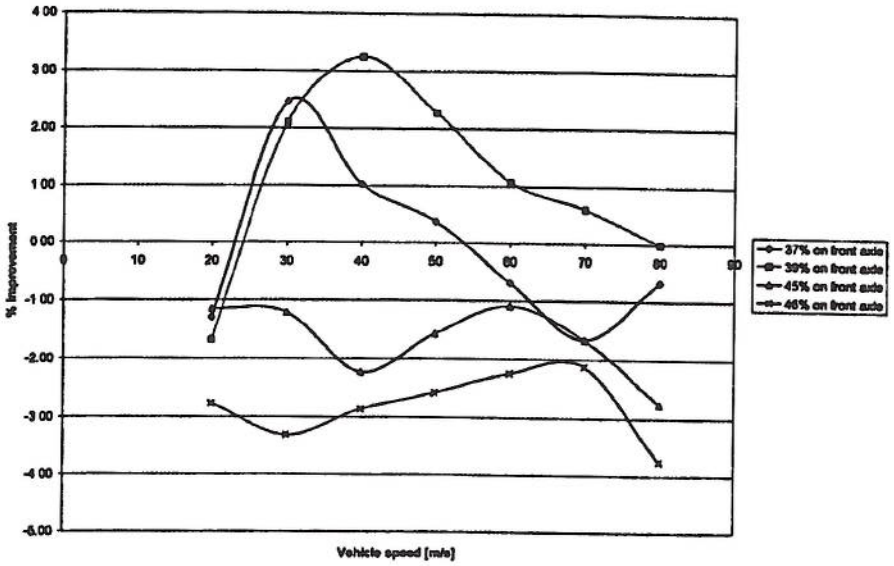

Figure 5.11: Vehicle C of G sensitivity analysis - Percentage Improvements.

allow comparisons between the results found here and the results of Casanova [3] and Casanova et al. [20]. The results are particularly variable and it is difficult to determine from Figure 5.11 whether or not this variability is due to the optimiser finding non global optimums or is an illustration of the true sensitivity of the vehicle dynamics to changes in this parameter. The easiest way to determine if the optimiser has found a poor local optimum is to investigate the GG speed diagram (Figure 5.12). The GG speed diagram shape is predominantly due to the shape of the friction circle of the tyres, as seen in Figure 5.6. When the resulting GG speed diagram constant velocity contours do not show smooth continuous curves, like the friction circle, it is a sign that the optimiser has found a local optimum which could be improved on, and generally means the optimiser has struggled to solve the equations of motion.

Figure 5.12 shows that the curves are not as smooth as the base vehicle result and therefore there is probably an element of error in the results. Figure 5.12 shows the underlying trend for the published vehicle model performance response to moving the CG rearward. High lateral acceleration, combined with low to moderate positive acceleration/braking, is improved at the expense of low lateral acceleration and high braking performance.

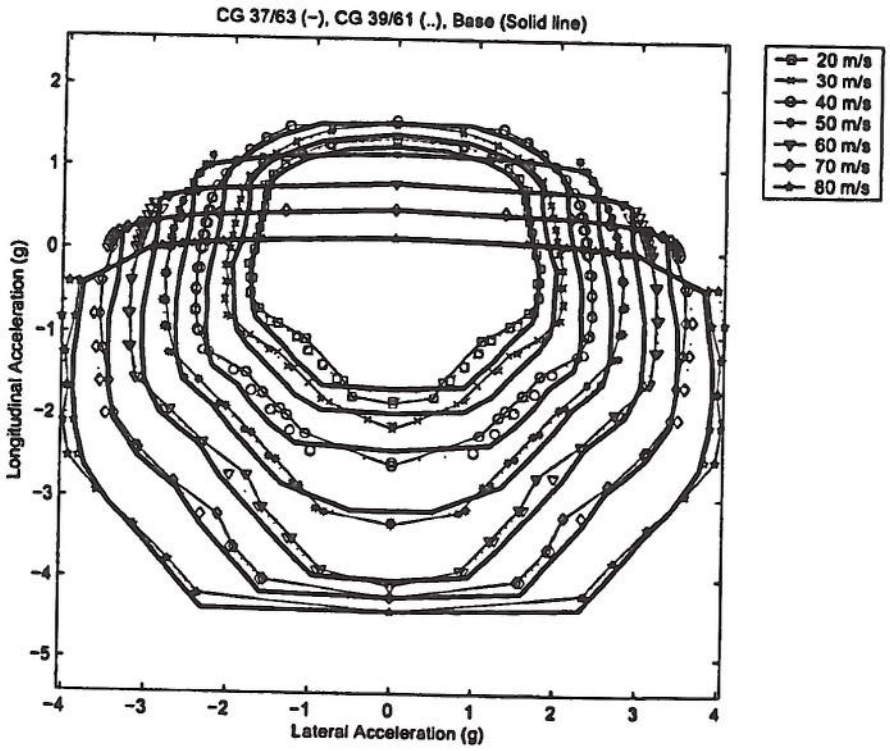

Figure 5.12: Vehicle C of G sensitivity - GG diagrams.

The dip seen in the other studies at 40m/s is evident in Figure 5.11 and although the improvements for the CG rearward cases over the base result are very low when compared with changing the vehicle mass or the tyres used, the transition from traction limited to engine torque limited conditions is pronounced. Since the static load over the driven wheels is now higher, in positive acceleration there is more vertical load on the tyres of the driven axle, enhancing traction at low speed for the rearward CG cases.

Previous research has suggested that this vehicle, with the CG moved rearward from its base position, could be more difficult to control [20]. This was hypothesised because the computer program that solved the optimisation problem found the solution more difficult to find with the CG moved rearward. This is also a possible source of the lack of smoothness in the GG speed diagram in Figure 5.12. To investigate this possibility the stability of the vehicle model, through the possible vehicle speed range, was conducted with a linearised version of the seven DOF model. This study is provided in Appendix C. The study showed that in straight line running the vehicles with the base set up and with the modified CG set ups, were seen to be stable and overdamped,

indicating oversteer [1] at all realistic vehicle speeds. In steady state cornering, the base vehicle set up was shown to be lightly damped but stable in the lateral velocity and yaw rate dependent modes in the 20-70m/s vehicle speed range. However, using the largest rearward CG result, 37/63% front to rear respectively, the vehicle model was shown to be unstable in the 20-70m/s vehicle speed range in steady state cornering. This instability makes the task of the optimiser very difficult to achieve at the performance limit and this will contribute to the lack of smoothness in the rearward CG set up GG speed diagram in Figure 5.12. As the numerical optimiser moves closer to the solution of the optimisation problem, the changes it makes to the vehicle state and input values reduces in magnitude. If the vehicle is fundamentally unstable at the solution (performance limit), then a small change in vehicle states and inputs can result in large fluctuations in the value of the objective function. These fluctuations impede the convergence of the search direction calculation towards the location of the solution to the problem.

The effects of changing the location of the CG are very complex and, while it is a comparatively easy parameter to modify, if the changes are small enough to be achieved by moving ballast around the vehicle locations, the benefits/losses of such a change are likely to be circuit specific. This is because the GG speed diagram shape has changed (Figure 5.12), and this appears to be more significant than the increase/decrease in the speed contour areas. In Section 4.2.2 a notional rearward movement of 6% improved the laptime on the Barcelona Grand Prix circuit by 1.4 seconds. Additionally, the performance benefits illustrated by the change in GG speed diagram area are not linear or near-linear with speed, as evidenced in the mass and tyre sensitivity studies. The base vehicle CG setting is a good compromise when compared with the results from other CG locations used in this parametric analysis. Of the five settings used, only the 6 and 8% rearward shifts from the base vehicle setting produced a positive net improvement over the base vehicle. Moving the CG further forward was worse for all constant speed contours trialled (Figure 5.11). The stability study described in Appendix C showed that the CG rearward shift to 37/63%, front to rear, also made the vehicle unstable at the steady state cornering limit.

An expected feature of the rearward CG GG speed diagram results is that under braking, especially from zero to 50 m/s, there is an improvement in straight line braking of the vehicle. This is because more vehicle weight is closer to the rear axle and

therefore this counters the loss in rear axle vertical load, due to longitudinal load transfer towards the front axle in braking.

5.7 Aerodynamic downforce

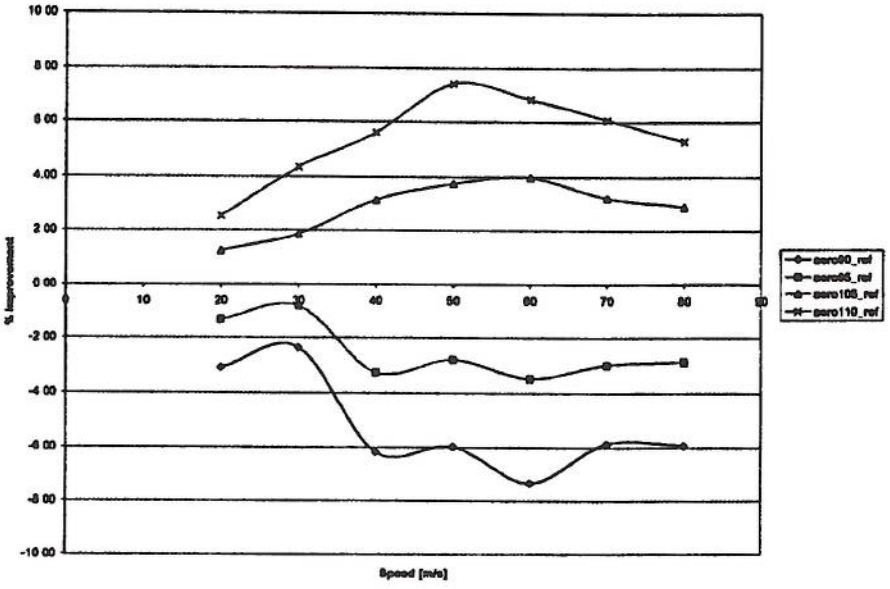

Figure 5.13: Aerodynamic downforce sensitivity analysis - Percentage Improvements.

In this section the aerodynamic downforce has been modified to be lower and higher than the value used in the base vehicle configuration. The aerodynamic downforce is evaluated using the equation for speed dependent pressure:

$$F_{az} = \frac{1}{2} \cdot \rho \cdot C_z \cdot S \cdot \dot{x}^2 \tag{5.6}$$

Whilst in the aircraft industry the lift coefficient is normally referenced to the wing area and the drag coefficient is referenced to the frontal area, in automotive applications the frontal area is commonly used as the reference area for both [104], and this is also assumed in this research.

The negative lift coefficient, C_z, for the base vehicle configuration, is increased and decreased in 5% increments to produce a range of speed dependent downforce evaluations for up to ±10% around the base aerodynamic setting.

These modifications increase or reduce the vertical load provided to the tyres. Figure 5.13 shows the size of the constant velocity contours, compared to the base vehicle velocity contours at the same vehicle speed. Intuitively, the results are predictable. A vehicle with increased downforce generation capacity should have a comparatively higher tyre force generation capacity when compared with the base vehicle result, and therefore an expanded GG speed diagram.

Following the familiar discussion of vehicle speed dependent tyre performance at lower speeds and engine torque limited performance at high speed, the percentage change as a result of the 5% and 10% increases in the values of C_z, show a peak performance advantage at 50 m/s of 4% and 7.5%, respectively.

For the cases where the value of C_z has been reduced by 5% and 10% below the base value the peak performance loss is -3.5% and -7.2% respectively. However, both of these reduced C_z results contain a dip at 60 m/s. To investigate this the GG speed diagram for the 90% value of C_z and the base vehicle are plotted in Figure 5.14.

Inspection of Figure 5.14 shows why there is an apparent extra loss in vehicle performance at 60 m/s. The difference in straight line braking ability, between the base vehicle and the 90% C_z result, is at its highest at 60 m/s, compared to the differences in braking capability at other speeds.

The dip at 60 m/s is also exaggerated in Figure 5.13 because of the discretisation of the deceleration points chosen by the QSS method at 50 m/s. The QSS method evaluates the maximum longitudinal deceleration capability and then splits this value into 10 equally spaced points to populate the GG speed diagram between maximum deceleration and the maximum lateral acceleration. Unfortunately, at 50 m/s, point 9, (approximately -3g) the base vehicle result slightly misses the 'corner' where the constant velocity contour turns sharply towards the lateral acceleration axis. For the 90% C_z result the spacing is better and the true turning point of the contour is captured. Therefore the 50 m/s contour is slightly smaller than it should be for the base vehicle result. This has the effect of reducing the apparent percentage loss of the 90% C_z

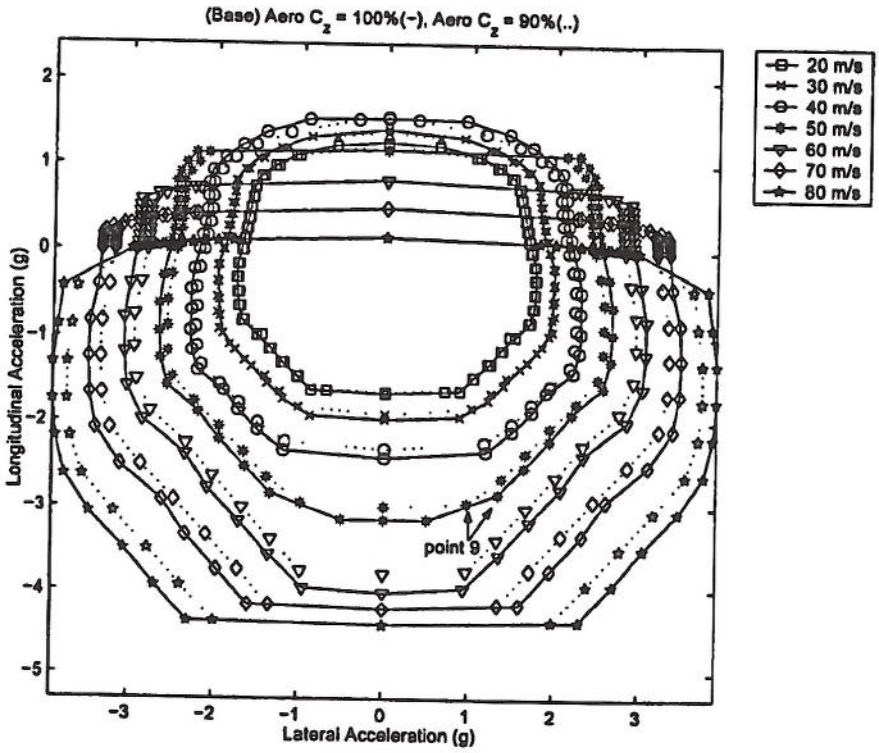

Figure 5.14: Aerodynamic downforce sensitivity - GG speed diagram.

result compared to the base vehicle result at 50 m/s, and making the dip at 60 m/s more pronounced in Figure 5.13.

A simple solution to this is to calculate more GG points for each GG speed diagram using the QSS method, but at the expense of increased computational effort. Although it has not been shown, the same dip at 60 m/s for the 95% case is also attributable to the better braking capability of the base vehicle at 60 m/s.

5.8 Summary

This chapter has explored the effects on vehicle performance of permutations of particular vehicle settings around the base vehicle configuration. This configuration is based on a realistic vehicle setup. As a result these results are very specific to a particular vehicle, but the trends are likely to be true for Formula One vehicles.

The vehicle performance sensitivity, due to vehicle mass changes, was found to linearly increase or decrease with vehicle speed, if the mass was reduced or increased respectively.

Changing the vehicle yaw inertia was found to be relatively ineffective, and this was determined to be a function of the vehicle configuration, and not due to any particular type of manoeuvre. The lack of vehicle performance sensitivity is due to the vehicle approximating trimmed steady state cornering in the majority of manoeuvres, which does not create significant yaw accelerations and therefore, in these situations, the vehicle yaw inertia is irrelevant.

The changing of the tyre's ability to generate longitudinal and lateral forces resulted in a near linear response, but with increasing speed the performance gains begin to converge on the base vehicle result. This is due to the comparatively low engine torque available, resulting in under utilised tyres at high speed. The majority of the engine torque is used to offset the vehicle drag, which is increasing with the square of vehicle speed. The benefits from increased tyre force generation capability at high speed were exploited predominantly in braking.

The benefits of increased engine torque across the engine speed range is shown to be most effective (or detrimental with the reduced torque cases) at higher speeds, particularly between 50-70 m/s. This is because tyre force generation capability, due to aerodynamic downforce supplementation, is sufficient to transfer the available torque provided by the engine to the road.

The effects of CG relocation were found to be rather complicated when compared with the other parameters studied. Moving the CG forward of the current base position was found to be a backward step in vehicle performance, at all vehicle speeds. Moving the CG rearward, as found in other research, could make the vehicle faster, but this is suggested to be a circuit specific rather than a general performance improvement. The general trend was that moving the CG rearward improved the lateral acceleration capability at low longitudinal accelerations (both in traction and braking), at the expense of lateral acceleration capability in high speed braking. The base vehicle has been shown to be stable using linear analysis of the vehicle lateral velocity and yaw rate modes, but the analysis of the 37/63% front to rear CG balance whilst stable in straight line running, was found to be unstable in steady state cornering. This is believed to have

made the optimisation task more difficult, and explains some of the errors noticed in the GG speed diagrams during the CG location study.

Studying the downforce generation capacity of the vehicle was achieved by proportionally increasing and decreasing the aerodynamic downforce coefficient, C_z. The effects of improving the downforce capability increases with increasing speed, to reach a peak at 50 m/s. As found in the engine torque curve and tyre sensitivity tests the lack of engine torque, coupled with the increasing drag force at high speed, reduces the vehicle's ability to capitalise on the additional vertical load provided by the aerodynamic downforce package. Reducing the C_z below the base value linearly reduced the vehicles performance with respect to increasing vehicle speed below 50 m/s. The comparative loss in performance stopped increasing with speed beyond 50 m/s.

Notwithstanding the huge variation in engineering effort that would be required to bring about some of these changes, it is still an interesting exercise to summarise the results of the parametric study areas on one graph. For brevity, only the maximum positive improvement and the maximum loss setups, when compared with the base vehicle, will be shown [1].

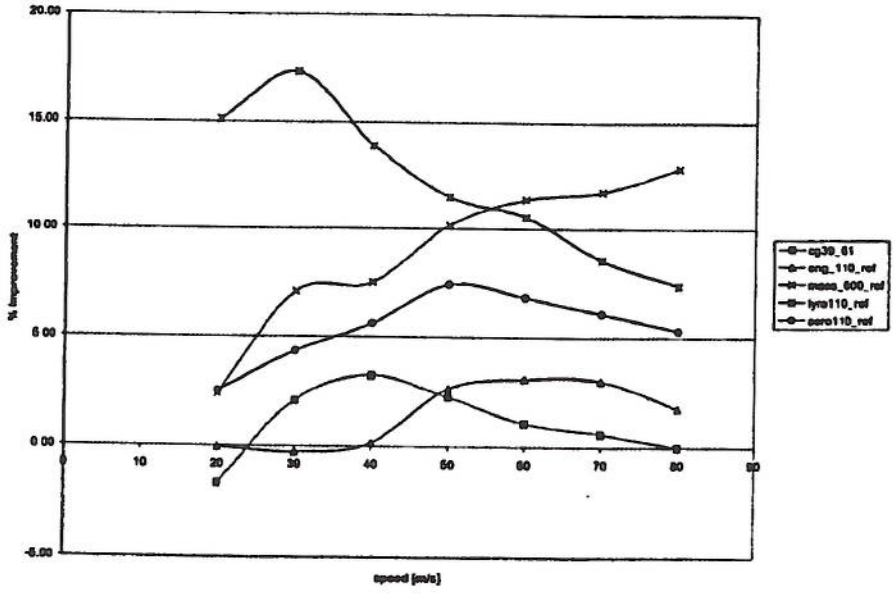

Figure 5.15: Vehicle sensitivity - Positive improvements.

[1] Yaw inertia results are not shown

From Figure 5.15 a ranking of sensitivity to vehicle performance of the six areas looked at in this chapter can be made (from highest to lowest sensitivity):

1. Tyre force generation.
2. Vehicle mass.
3. Aerodynamic downforce.
4. Engine torque.
5. CG location.
6. Yaw inertia.

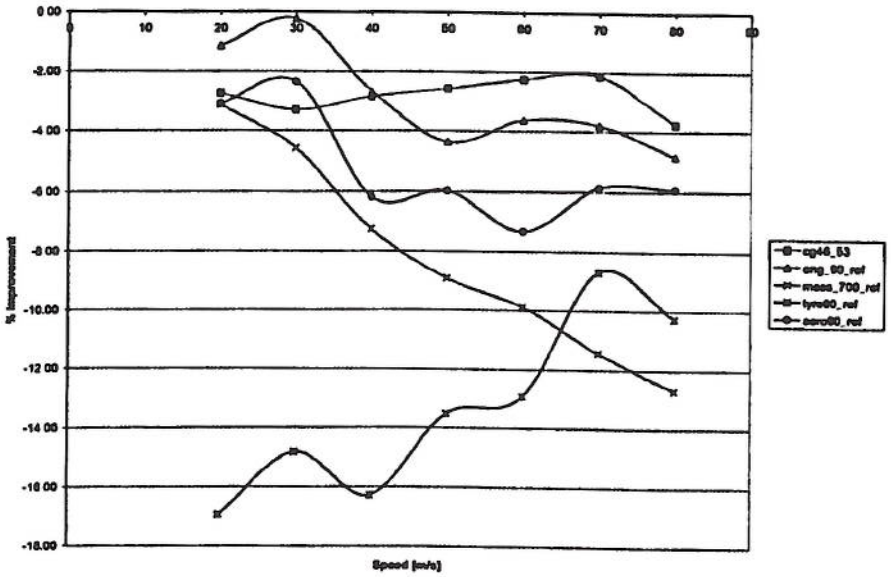

Figure 5.16: Vehicle sensitivity - Loss of performance.

This ranking can be checked by plotting the worst performing ends of the parameter sweep, to see if the vehicle performance loss is in the same order (Figure 5.16). Figure 5.16 complements the results of Figure 5.15 indicating the same order of parameter sensitivity to vehicle performance. Whilst this ranking is true for the current vehicle setup, this could change for a different vehicle setup for other circuits and therefore the analysis should be repeated in those cases.

Chapter 6

Roll stiffness distribution

This study is conducted with the seven DOF published vehicle model. This implementation of the QSS method is based on the first method described in Chapter 3, but uses automatic differentiation for evaluating the derivatives, as required by the optimiser, and uses the updated differential and gear selection models as described in Chapter 3.

Inspection of Equations 6.1 and 6.2 taken from Casanova [3], and Figure 6.1 for this model shows that the lateral load transfer is dependent on the magnitude of the lateral acceleration, the longitudinal location of the centre of gravity of the vehicle and the proportion of the total roll stiffness carried by each axle.

$$\Delta F_{fz\_lat} = \frac{\dot{\varphi} \cdot \dot{x} \cdot M}{t_f}[(l_r \cdot h_{rf})/W_b + R_{sf}(h_g - h_{rc})] \tag{6.1}$$

$$\Delta F_{rz\_lat} = \frac{\dot{\varphi} \cdot \dot{x} \cdot M}{t_r}[(l_f \cdot h_{rr})/W_b + R_{sr}(h_g - h_{rc})] \tag{6.2}$$

The effectiveness of the roll stiffness distribution parameter to influence the load transfer is dependent on the difference in vertical height of the roll axis, with respect to the vertical height of the centre of gravity. This chapter will explore the significance of the roll stiffness distribution, at a representative front and rear roll centre height, from a roll centre analysis. This is to determine how important this parameter is, with respect to the GG speed surface shape, and therefore the performance capability of the vehicle. Numerical optimisation will be used to achieve this.

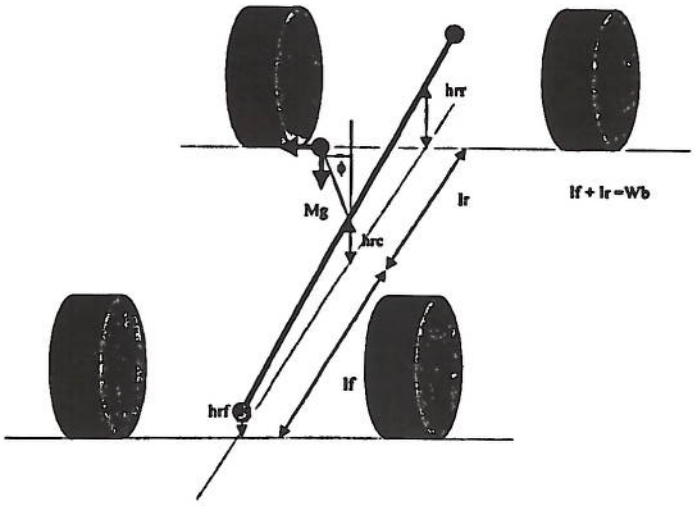

Figure 6.1: Roll axis implementation - 7DOF model.

6.1 Optimisation of the roll stiffness distribution

To determine the influence of the roll stiffness distribution on the dynamics of the vehicle, the front roll stiffness, R_{sf} is allowed to be manipulated by the numerical optimiser between zero and one, with zero being 100% of the roll stiffness located on the rear axle. To achieve this, R_{sf} is inserted into Equation 3.6. The updated optimisation vector is shown in Equation 6.3. For brevity, the result with the optimised roll stiffness distribution will be referred to as the 'active roll stiffness' result.

$$P = [\dot{y}, \dot{\phi}, \dot{\theta}_{LF}, \dot{\theta}_{RF}, \dot{\theta}_{LR}, \dot{\theta}_{RR}, \delta, T_P, R_{sf}]^T \tag{6.3}$$

The GG speed diagram for the active roll case is shown in Figure 6.2 with the original base case for comparison. The expansion of the GG speed diagram, due to the active roll term, is very significant.

Table 6.1 is a summary of the two diagrams shown in Figure 6.2. As Table 6.1 shows, the GG speed diagram has expanded by 10% on average, with the largest improvements attributable to significant lateral acceleration capability improvement under braking at high speeds (50 - 80 m/s, Figure 6.2). It is possible to look at the resulting roll stiffness distribution values for the GG speed diagram of the active roll vehicle that has produced this significant improvement. Figure 6.3 is a frequency plot of the roll stiffness distribution values found by the optimiser.

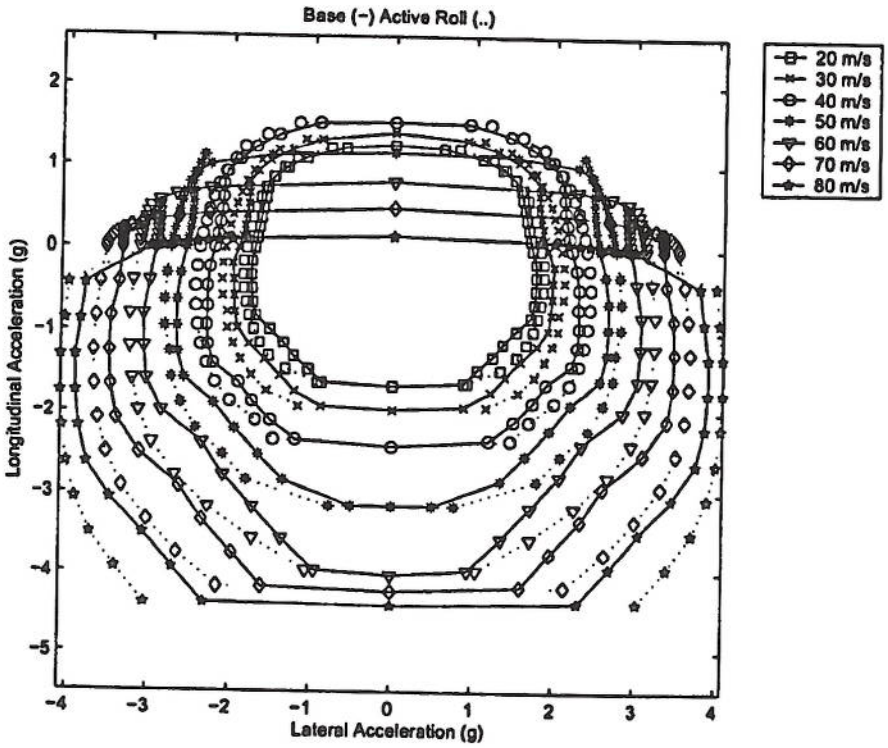

Figure 6.2: GG speed diagram - Active roll.

Figure 6.3 shows that with active roll stiffness control the population distribution of the roll stiffness on the front axle is skewed towards the rear. Therefore, for most of the time, the majority of the sprung mass roll moment is carried on the rear axle. The mean front axle roll stiffness found from this analysis, R_{sf}, is 0.478 (Table 6.2). Conversely, the base vehicle static value from the original vehicle data is front axle biased at 0.58.

The majority of the R_{sf} values have migrated away from the base static value. These changes in R_{sf} have resulted in lateral acceleration improvements of up to 0.8g in braking, with smaller but significant improvements in traction. To make use of this finding it must be determined how this improvement was realised, in terms of the vehicle dynamics.

One method of inspecting the vehicle dynamics is to look at one vehicle speed and interrogate the state vectors that together form the constant velocity contour.

Speed m/s	Active roll g^2	Base g^2	% Improvement
20	9.373	8.643	8.45
30	12.398	11.236	10.34
40	16.844	15.633	7.75
50	21.445	19.319	11.00
60	26.544	23.793	11.56
70	30.960	27.645	11.99
80	34.287	31.286	9.59
Average			10.10

Table 6.1: Area of constant velocity contours - GG speed diagram.

	GG speed diagram points	Barcelona circuit history
Mean	0.478	0.526
Median	0.475	0.519
Variance	0.018	0.014

Table 6.2: Active roll population statistics.

To determine the reasons for the expanded diagram with active roll stiffness, the state vectors of a significantly improved constant velocity contour are interrogated. The state vectors for the 70m/s velocity contour in braking are shown in Tables 6.3 and 6.4, for the active roll stiffness result and the base case result, respectively.

The most noticeable differences between the two sets of results are the much higher vehicle attitude angle, β, yaw rate $\dot{\phi}$, and the increased slip angles for the active roll stiffness vehicle when compared with the base vehicle. The active vehicle is yawing significantly more than the base vehicle and this is provided by the tyres, as indicated by the increased slip angles of the wheels. To determine how the tyre forces have changed, as a result of changing the roll stiffness distribution, the individual tyre forces will be examined.

The tyre saturations are calculated from the combined slip tyre forces evaluated in both the x and y directions. The maximum longitudinal and lateral forces that are possible, given the combined slip condition, are also calculated from the Magic Tyre Formula [18]. The saturation is then a simple proportion calculation, given in Equation

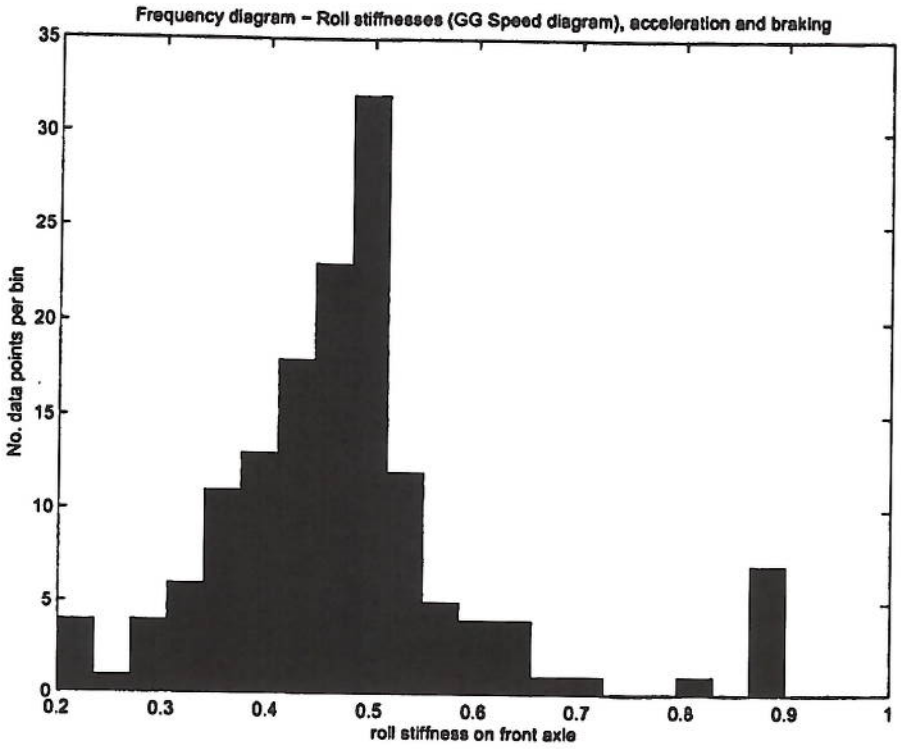

Figure 6.3: Active roll stiffness GG speed diagram - Roll stiffness distribution.

6.6, using the values found from an analysis, as described in Figure 6.4:

$$F = \sqrt{Fx^2 + Fy^2} \tag{6.4}$$

$$F\max = \sqrt{Fx_{\max}^2 + Fy_{\max}^2} \tag{6.5}$$

$$\text{Tyre saturation} = \frac{F}{Fmax} \tag{6.6}$$

The tyre saturations for all four wheels, for the 70m/s braking velocity contour, are given in Figure 6.5. There is very little difference between the active roll stiffness and the base vehicle on the front axle, in terms of comparative tyre force saturation. However, the rear axle tyre saturations are significantly different between the two cases. The tyre saturations are shown for a right hand manoeuvre, and there is a significant increase in the saturation of the rear axle and specifically the left rear tyre, in the active roll case. The increased tyre saturation at this corner at all lateral accelerations,

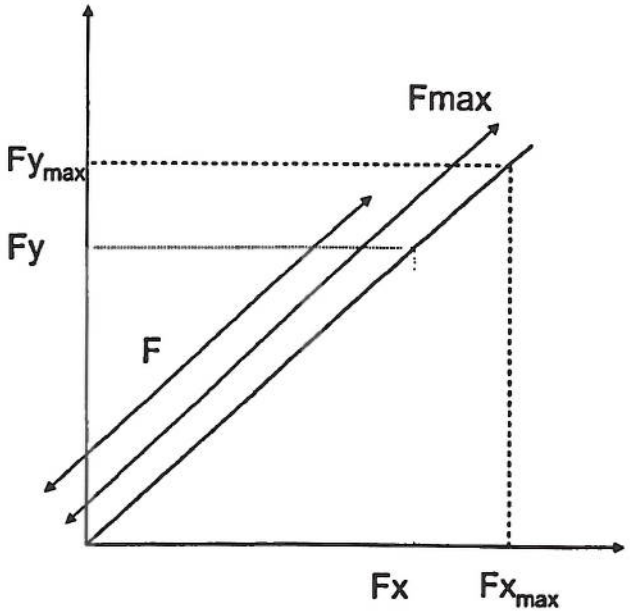

Figure 6.4: Tyre saturation calculation.

coupled with the improvement in the right rear tyre saturation at lateral accelerations below 3g increases the yaw rate of the vehicle across the velocity contour. This facilitates an increased steady state lateral acceleration over the base vehicle result. This is an interesting finding because the rear axle is usually considered to be comparatively lightly loaded, due to longitudinal load transfer under braking towards the front axle. The result indicates that the rear tyres in the base configuration are under utilised and are capable of carrying significantly more of the lateral load transfer due to roll. Figure 6.2 shows how much the GG speed surface has expanded as a result.

6.2 Practical implications

Section 6.1 has quantified and shown the magnitude of improvement possible in the GG speed performance of the base vehicle, if the roll stiffness distribution could somehow be controlled. The interrogation of the tyre force saturation values has shown how the improvements have been realised. The base vehicle, however, is an F1-type open wheel race car which, in line with most other forms of open wheel race car formulae, shares a series of rule restrictions on active technologies. In this form of motorsport, the implementation of any form of active roll stiffness system is not permitted under current regulations. The suspension and roll systems must be of mechanical operation,

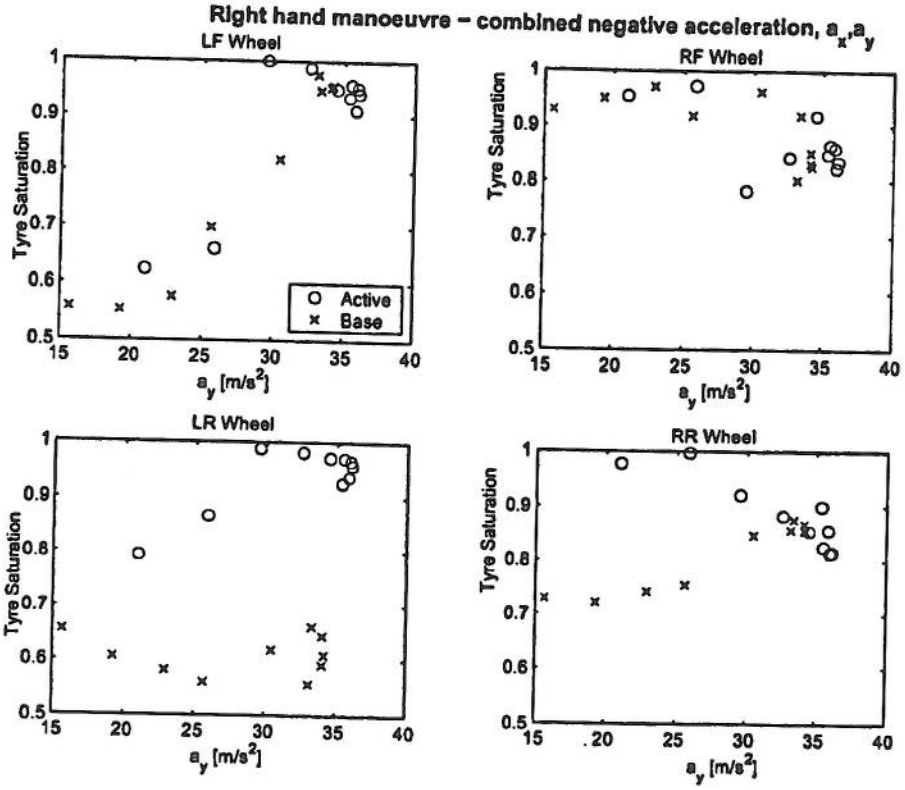

Figure 6.5: Tyre saturation plots Active and Base vehicle 70 m/s - Braking.

with no external influence from electronic control systems. This ensures that the roll stiffness distribution, as an actively controlled parameter, has limited practical use for these vehicles. The roll stiffness distribution is a static setting which is determined by suspension geometry and conventional roll bar designs. If one was to implement such a system, the best way would still be by using electronically controlled actuators either in parallel or instead of conventional springs and dampers. These components formed the basis of the 'active suspension' systems used in the nineties on Formula One cars [12]. This is the best option because the technology and implementation issues have been resolved by Formula One teams in the past and the reintroduction would be straight forward. A less technology intensive method would be to fabricate an electronically controlled variable roll bar system that would have central control over the actuated roll bars at both axles.

Notwithstanding the current regulations, the benefit offered through knowledge of the results attainable by the optimised roll distribution can still be exploited. Figure

6.3 showed that the mean found from the GG speed diagram derived points for the active roll stiffness vehicle was substantially different from the base vehicle setup. This indicates that there are potentially better choices for the static setting of the roll stiffness distribution.

Using the GG speed diagram, for the active roll result, the vehicle can be simulated for a lap of a circuit using the QSS simulation described in Section 3.3. If the values of R_{sf} are calculated during the simulation, then a track history of the optimised values of R_{sf} can be obtained. This history of R_{sf} will be racing line dependent, and if it is considered that the aim of a good racing driver is to find straight lines through curves to maintain high longitudinal acceleration at all times, then it is possible that the GG speed diagram area that will be used for the circuit simulation could be quite small.

The circuit history of the optimised values of R_{sf} for a lap of the Barcelona Grand Prix circuit have been plotted as a frequency plot in Figure 6.6 to compare with Figure 6.3 and to highlight the underlying population distribution shape.

The population of R_{sf} values around Barcelona is more symmetric than was seen in Figure 6.3, but the data set is now significantly larger (160 points $\rightarrow$ 1400 points) so the population of R_{sf} values is expected to more closely approximate a normal distribution. The other improvement offered by the increased size of the data set is the reduction in population variance (Table 6.2). More importantly, it is also found that the mean of the values from the GG speed diagram derived points of 47.8% for the active roll stiffness result (Figure 6.3) and the mean of the R_{sf} values of the active roll vehicle used for from the simulation around Barcelona shown in Figure 6.6, are quite different. The Barcelona result placed more of the mean roll stiffness on the front axle at 52.6% (Table 6.2).

While the population distribution should closely approximate the bell shaped normal distribution, it was also expected that the means would be similar, as the Barcelona results are sampled from the underlying GG speed diagram. One plausible reason for this difference in means, as mentioned earlier, is a skewed sampling of the active roll GG speed diagram by the QSS simulation. To examine in detail how the GG speed diagram is sampled for a given trajectory, the lateral and longitudinal acceleration can be tracked during the QSS simulation in the same way as the R_{sf} values and a circuit-dependent GG speed diagram can be constructed. This is shown in Figure 6.7. The

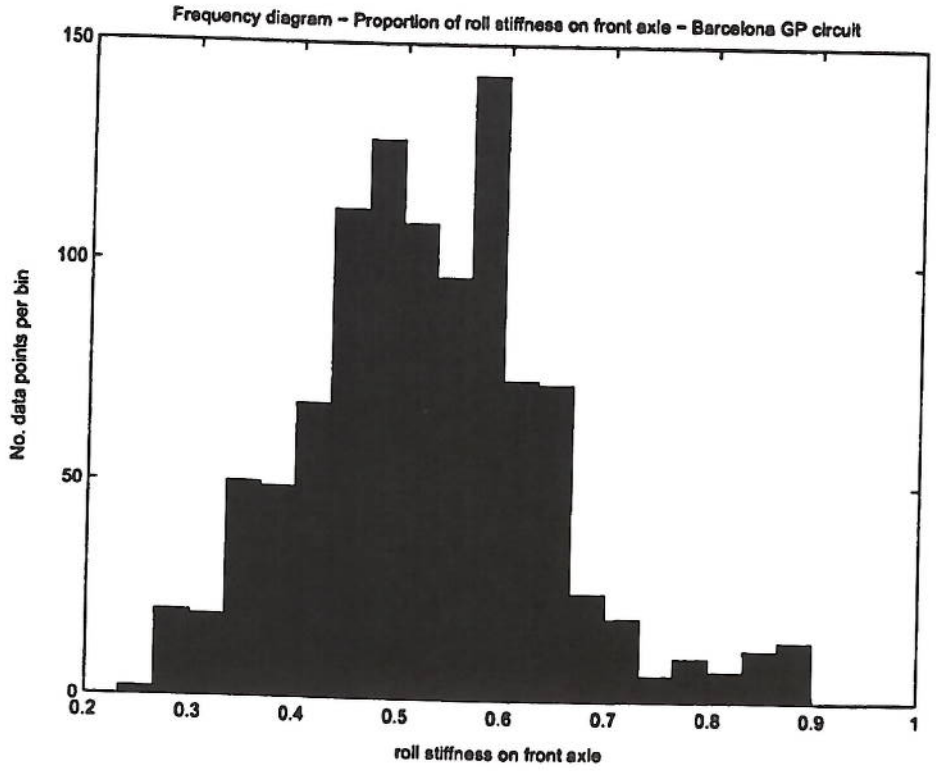

Figure 6.6: Active roll Barcelona GP circuit - Roll stiffness distribution.

reasons for the differences are now very clear. Lateral acceleration in braking is low, with a maximum of 3.5g compared with the possible 4g at high speed. The vehicle is in positive acceleration more often than in braking, and the general conclusion made from Figure 6.7 is that the lateral acceleration capability of the vehicle in braking cannot be fully exploited at this particular circuit.

To investigate the usefulness of determining optimised static settings from the above analysis of the circuit dependent roll stiffness distribution settings, a new GG speed diagram was calculated. This GG diagram has a static setting of R_{sf} set to 0.526, the mean found from the simulation results of the active roll stiffness vehicle around the Barcelona circuit (Figure 6.6 and Table 6.2). The resulting GG speed diagram is overlayed with the base vehicle result for comparison in Figure 6.8.

As can be seen in Figure 6.8 the the braking portion of the GG speed diagram has been significantly improved at lateral accelerations greater than 1g, and, in positive

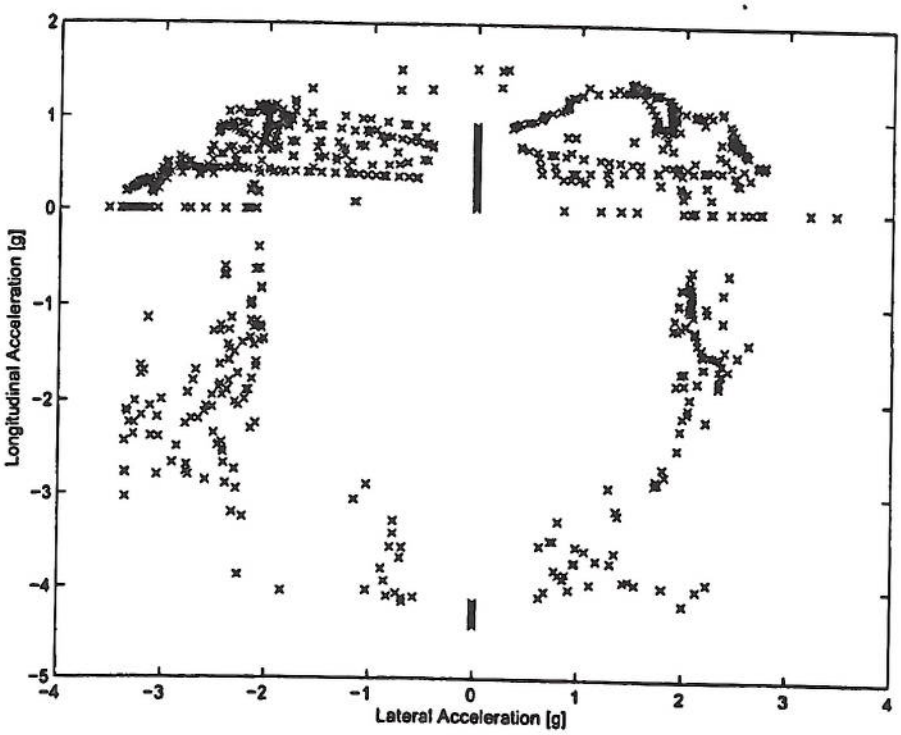

Figure 6.7: Circuit history GG speed diagram - Active roll - Barcelona.

acceleration, improvements can be seen at lateral accelerations for all vehicle speeds where the lateral acceleration is within 20% of the speed dependent lateral acceleration capability at zero longitudinal acceleration. When this new result is used as a basis for a QSS simulation on the base trajectory, the vehicle laptime improves around Barcelona by 1.03 seconds per lap compared to the base vehicle (Table 6.5 and Figure 6.9). This is still slower than the active roll stiffness vehicle, which is 2.71 seconds per lap quicker than the base vehicle, but it is a useful improvement and can be realised on a passive suspension vehicle without the need for active suspension technologies. This can be illustrated with a simple example.

6.2.1 Practical calculation example

In this section a simple example based on the assumption that the nonlinear suspension and tyre vertical compliance of a real vehicle can be approximated by linear spring terms, which, considering the very high stiffnesses for these components provided in the literature [12], is quite reasonable, a straightforward analysis is possible.

Using an amalgamation of data, the values given in Table 6.6 will be used.

Using the simple expression for the roll rate of the sprung mass on an axle using linear spring terms, given in Milliken and Milliken [52], but additionally considering the vertical tyre compliance, Equation 6.11 gives the front roll stiffness distribution expression. The roll rates of the anti roll bars are assumed to be inboard and acting in parallel with the roll rate of the suspension springs.

$$\frac{1}{k_f} = \frac{1}{k_1} + \frac{1}{k_2} \tag{6.7}$$

$$\frac{1}{k_r} = \frac{1}{k_3} + \frac{1}{k_4} \tag{6.8}$$

$$K_{\phi f} = \frac{1}{2} k_f \cdot t_f^2 + k_{f-roll} \tag{6.9}$$

$$K_{\phi r} = \frac{1}{2} k_r \cdot t_r^2 + k_{r-roll} \tag{6.10}$$

$$R_{sf} = \frac{K_{\phi f}}{K_{\phi f} + K_{\phi r}} \tag{6.11}$$

Substituting the values of Table 6.6 into Equations 6.7 to 6.11, the current base vehicle setting for R_{sf} of 0.58 is found. To modify this setting, to give the new static setting of 0.526, either or both roll bars or the suspension springs and tyres could be changed. If it is assumed that the setting of the vehicle is well suited to a particular driver and the current handling characteristics are acceptable, then a sensible solution would be to simply modify the anti roll bars. One such change that arrives at $R_{sf} = 0.526$ is the change of anti roll bar at the rear, to give a rolling rate of 159 N/mm. This is a stiffening of the roll motion of the rear axle to force the rear axle to carry more of the sprung mass lateral load transfer due to lateral acceleration. Many methods of arriving at this new R_{sf} setting could be chosen, but the point to be made is that the new value of R_{sf} is realisable with simple suspension component changes. A typical range for anti roll bars, for this type of vehicle, is given in Wright [12] as 0-1000 N/mm.

Additionally, as a further check on the calculations, a large lateral acceleration of 4g was used to determine the maximum roll angle ϕ, in steady state lateral acceleration, to

check the assumption of small roll angles (Equation 6.12). The value of ϕ was found to be 0.91 degrees, which is small.

$$\phi = \frac{M \cdot (hg - h_{rc}) \cdot a_y}{K_{\phi f} + K_{\phi r}} \tag{6.12}$$

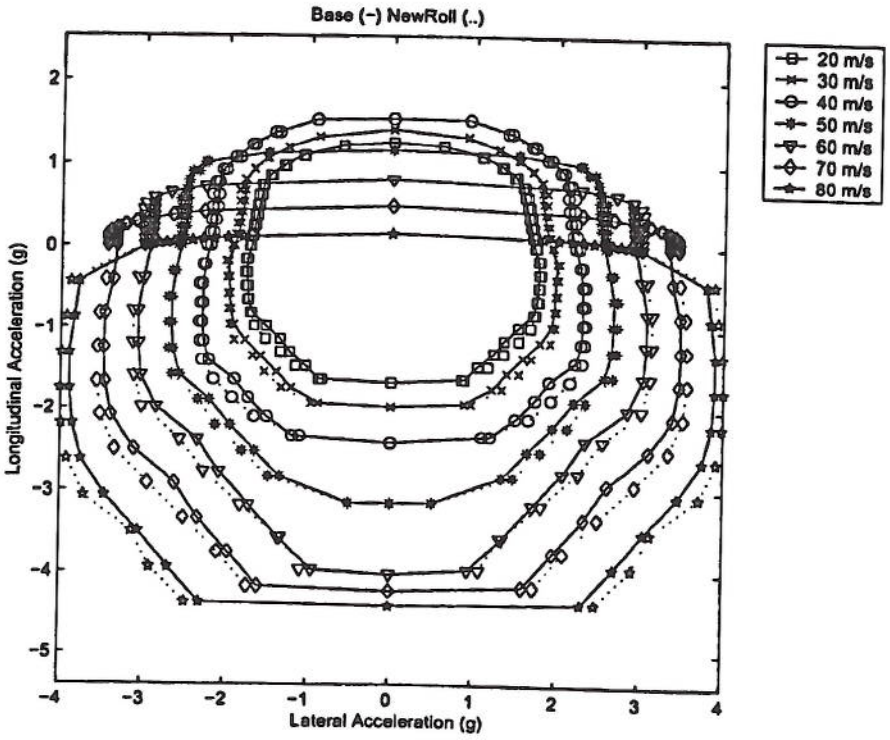

Figure 6.8: GG speed diagram - R_{sf} set to 0.526.

6.3 Summary

In this chapter the roll stiffness distribution has been optimised, during the GG speed diagram calculation process, to simulate and quantify the possible benefits of controlling the distribution of roll stiffness between the front and rear axles of an open wheel race car. The roll axis concept has been used to provide the roll component to the lateral load transfer evaluation. The shortcomings of this method have been highlighted, but the assumptions have been analysed in view of the type of vehicle model employed and are believed to be acceptable for the range of operation of the published vehicle model. The benefits shown by the optimisation of the roll stiffness distribution have

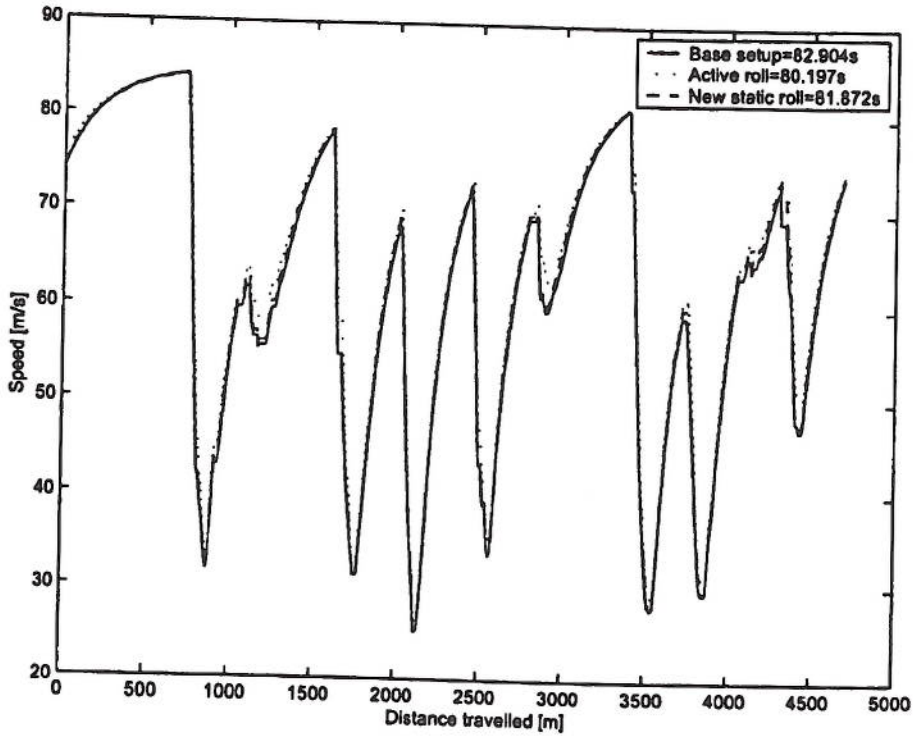

Figure 6.9: New static roll ($R_{sf} = 0.526$), Active roll and the base vehicle - speed history.

created a mean improvement over the base vehicle of over 10%, which on the base Barcelona circuit trajectory yielded a lap time improvement of 2.71 seconds. Additionally, it has been shown how this improvement has been realised in terms of the change in vehicle dynamics. In view of current rules, in the forms of motorsport applicable to this type of open wheel race car, any form of active roll distribution control would not be allowed. However, it has been shown that circuit dependent analysis is possible to exploit the value of the static setting of the roll stiffness distribution. Using the QSS simulation method, with this new static R_{sf} setting on the base trajectory, a significant improvement of 1.03 seconds per lap was realised. Further work and validation is required to explore this avenue of vehicle setup optimisation, but it does appear that the optimised GG diagram approach offers a way of helping make an objective choice of static R_{sf} setting for particular circuits.

Parameter		Vehicle Active				
		1	2	3	4	5
Steer Angle	[deg]	1.0108	2.3059	3.6137	0	0.315
Throttle Position		-0.3462	-0.4696	-0.6007	-0.8107	-0.9563
LF wheel speed	[rad/s]	-210.2	-206	-199.4	-209.7	-209.3
RF wheel speed	[rad/s]	-184.6	-165.1	-147.9	-189	-193.7
LF-RF wheel speed	[rad/s]	-25.6	-40.9	-51.6	-20.7	-15.6
LR wheel speed	[rad/s]	-207.8	-206	-204.7	-207.8	-208.1
RR wheel speed	[rad/s]	-205.4	-200	-183.8	-192.5	-190
LR-RR wheel speed	[rad/s]	2.4	6	20.9	15.4	18.1
LF slip angle	[rad]	0.133	0.1549	0.1763	0.0534	0.0389
RF slip angle	[rad]	-0.1341	-0.156	-0.1773	-0.0538	-0.0391
LR slip angle	[rad]	0.1382	0.1364	0.1329	0.0706	0.0474
RR slip angle	[rad]	-0.1396	-0.1376	-0.134	-0.0711	-0.0477
Vehicle velocity	[m/s]	70	70	70	70	70
Vehicle lateral velocity	[m/s]	-9	-8.9	-8.7	-4.4	-2.9
Yaw rate	[rad/s]	0.493	0.4659	0.422	0.3699	0.3001
Longitudinal Acceleration	[m/s^2]	-24.6	-28.7	-32.8	-36.9	-41
Engine Torque	[Nm]	35.249	35.249	35.249	35.249	35.249
Vehicle Attitude Angle	[Deg]	-7.345	-7.2678	-7.1176	-3.6247	-2.3736
Hydraulic Pressure	[Bar]	23.1	23.1	23.1	23.1	23.1
Torque Transfer	[Nm]	-280.7	-342.7	-368.5	-365.3	-367.1
Roll Stiffness (front)		0.5117	0.4363	0.3306	0.4122	0.4102
Data Point number		6	7	8	9	10

Table 6.3: Active roll vehicle state vector 70 m/s - Braking.

Parameter		Vehicle Base				
		1	2	3	4	5
Steer Angle	[deg]	3.3026	2.5416	1.5966	1.2703	0.9683
Throttle Position		-0.417	-0.5662	-0.7044	-0.8382	-0.9699
LF wheel speed	[rad/s]	-211.3	-211	-211	-210.5	-209.8
RF wheel speed	[rad/s]	-184	-176.3	-192.5	-193.4	-195.3
LF-RF wheel speed	[rad/s]	-27.4	-34.8	-18.5	-17	-14.5
LR wheel speed	[rad/s]	-212.3	-211.9	-211.2	-210.4	-209.2
RR wheel speed	[rad/s]	-210.6	-210.2	-209.3	-208.5	-207.4
LR-RR wheel speed	[rad/s]	1.7	1.7	1.9	1.9	1.8
LF slip angle	[rad]	0.0916	0.0665	0.0464	0.0365	0.0281
RF slip angle	[rad]	-0.0919	-0.0667	-0.0465	-0.0366	-0.0282
LR slip angle	[rad]	0.0542	0.0392	0.0338	0.0271	0.0217
RR slip angle	[rad]	-0.0546	-0.0395	-0.034	-0.0273	-0.0217
Vehicle velocity	[m/s]	70	70	70	70	70
Vehicle lateral velocity	[m/s]	-3.2	-2.2	-1.9	-1.5	-1.2
Yaw rate	[rad/s]	0.4356	0.3664	0.3274	0.2754	0.2238
Longitudinal Acceleration	[m/s^2]	-24.6	-28.7	-32.8	-36.9	-41
Engine Torque	[Nm]	35.249	35.249	35.249	35.249	35.249
Vehicle Attitude Angle	[Deg]	-2.6079	-1.829	-1.5588	-1.2388	-0.9827
Hydraulic Pressure	[Bar]	23.1	23.1	23.1	23.1	23.1
Torque Transfer	[Nm]	-238.4	-238.5	-248.6	-246.9	-241.6
Roll Stiffness (front)		0.58	0.58	0.58	0.58	0.58
Data Point number		6	7	8	9	10

Table 6.4: Base vehicle state vector 70 m/s - Braking.

	Barcelona Lap time (s)	Improvement over base (s)
Base setup	82.904	N.A.
Active roll	80.197	2.71
New static roll	81.872	1.03

Table 6.5: Lap times - Barcelona Grand Prix circuit.

Component	Linear stiffness	Units
Front suspension vertical rate, k_1	175	N/mm
Front tyre vertical rate, k_2	130	N/mm
Front roll bar rate, k_{f-roll}	205	N/mm
Rear suspension vertical rate, k_3	230	N/mm
Rear tyre vertical rate, k_4	260	N/mm
Rear roll bar rate, k_{r-roll}	110	N/mm

Table 6.6: Hypothetical suspension and roll settings - open wheel race car.

Parameter		Vehicle Base				
		1	2	3	4	5
Steer Angle	[deg]	3.3026	2.5416	1.5966	1.2703	0.9683
Throttle Position		-0.417	-0.5662	-0.7044	-0.8382	-0.9699
LF wheel speed	[rad/s]	-211.3	-211	-211	-210.5	-209.8
RF wheel speed	[rad/s]	-184	-176.3	-192.5	-193.4	-195.3
LF-RF wheel speed	[rad/s]	-27.4	-34.8	-18.5	-17	-14.5
LR wheel speed	[rad/s]	-212.3	-211.9	-211.2	-210.4	-209.2
RR wheel speed	[rad/s]	-210.6	-210.2	-209.3	-208.5	-207.4
LR-RR wheel speed	[rad/s]	1.7	1.7	1.9	1.9	1.8
LF slip angle	[rad]	0.0916	0.0665	0.0464	0.0365	0.0281
RF slip angle	[rad]	-0.0919	-0.0667	-0.0465	-0.0366	-0.0282
LR slip angle	[rad]	0.0542	0.0392	0.0338	0.0271	0.0217
RR slip angle	[rad]	-0.0546	-0.0395	-0.034	-0.0273	-0.0217
Vehicle velocity	[m/s]	70	70	70	70	70
Vehicle lateral velocity	[m/s]	-3.2	-2.2	-1.9	-1.5	-1.2
Yaw rate	[rad/s]	0.4356	0.3664	0.3274	0.2754	0.2238
Longitudinal Acceleration	[m/s^2]	-24.6	-28.7	-32.8	-36.9	-41
Engine Torque	[Nm]	35.249	35.249	35.249	35.249	35.249
Vehicle Attitude Angle	[Deg]	-2.6079	-1.829	-1.5588	-1.2388	-0.9827
Hydraulic Pressure	[Bar]	23.1	23.1	23.1	23.1	23.1
Torque Transfer	[Nm]	-238.4	-238.5	-248.6	-246.9	-241.6
Roll Stiffness (front)		0.58	0.58	0.58	0.58	0.58
Data Point number		6	7	8	9	10

Table 6.4: Base vehicle state vector 70 m/s - Braking.

	Barcelona Lap time (s)	Improvement over base (s)
Base setup	82.904	N.A.
Active roll	80.197	2.71
New static roll	81.872	1.03

Table 6.5: Lap times - Barcelona Grand Prix circuit.

Component	Linear stiffness	Units
Front suspension vertical rate, k_1	175	N/mm
Front tyre vertical rate, k_2	130	N/mm
Front roll bar rate, k_{f-roll}	205	N/mm
Rear suspension vertical rate, k_3	230	N/mm
Rear tyre vertical rate, k_4	260	N/mm
Rear roll bar rate, k_{r-roll}	110	N/mm

Table 6.6: Hypothetical suspension and roll settings - open wheel race car.

Chapter 7

Differentials

7.1 Introduction

The QSS method is capable of completing the GG speed diagram calculation very quickly. As a result, improvements to the vehicle model are realisable using the QSS method with an acceptable computational load penalty. In this chapter the 14DOF vehicle model with the modelling improvements to the rear differential, gear change strategy and suspension model, as described in Chapter 3, are implemented. The computational time has subsequently increased from 16 minutes to 35 minutes, which is still acceptable. This chapter aims to investigate the effect of rear differential control on the vehicle handling behaviour of the base vehicle using numerical optimisation.

In addition, the use of differentials can be taken one step further. All wheel drive (AWD) or four wheel drive systems, incorporating a mix of open and limited slip differentials, are used on many current production vehicles. These systems are not allowed by most forms of motorsport. AWD systems are full time four wheel drive vehicles. Some four wheel drive systems allow the engagement of either four wheel or two wheel drive, through the use of a transfer case. Rally type vehicles are unrestricted in the use of these systems and the corresponding methods of control. How much extra performance could be attained from an AWD system installed on modern open wheel race cars with aerodynamic aids is not readily known. Due to the ease of modification of the equations of motion in the QSS method, the use of AWD systems will also be discussed in this chapter.

7.2 Open versus locked differentials

Using the differential model described in Section 3.6.1, which is now fundamentally controlled by the hydraulic pressure P_H, it is possible to begin to describe the effects of the differential in a quasi steady state manner.

The differential is simply a torque splitting device. How the torque is split between the two output shafts to the wheels depends on the mechanical configuration. Explanations of inner workings of the open differential are given in Wright [12] and Milliken and Milliken [11], but these explanations are not particularly clear. Another explanation is offered here.
The so-called open differential is the simplest type of differential. It consists of:

- A differential housing to which torque from the gearbox output shaft is applied.
- A pinion shaft that passes across the diameter of the differential housing.
- Two bevelled pinion gears that rotate freely around the pinion shaft.
- Two bevelled side gears that mesh with the pinion gears. Each side gear is splined with a driveshaft.

Torque from the gearbox is applied to the differential housing, which in turn, acts on the pinion shaft. Torque from the pinion shaft acts on the pinion gears and in turn on the side gears and hence the driveshafts.

The pinion gears mesh with the two side gears. High torque to each side gear can be realised when the two side gears spin with the same velocity. This is because the pinion gears do not rotate under this condition and a high contact pressure between the teeth of the pinion gears and those of the meshed side gears can be produced and maintained.

Once one side gear spins at a higher velocity than the other, torque delivery to the side gears will be limited. This is because the pinion gears now rotate. The torque transferred to either side gear is limited by a rotating pinion gear because torque that might have been passed to the side gears is now expended in rotating the pinion gears.

In the open differential, the torque delivered to one side gear is equal to the torque delivered to the other. As a result, the driving torque to a pair of wheels is limited to twice the torque delivered to one wheel. This torque limitation is commonly attributed to the wheel that spins the fastest as this causes the pinion gears to rotate. When one wheel spins faster than the other, due to a loss of traction, then the faster wheel is clearly the cause of the limited torque. In this case, the torque delivered to the wheels will be strongly limited because the engine will have to be operated at only part load to avoid a rapid increase in engine speed. An example of this phenomenon is a car with one of the driven wheels on ice and the other wheel on tarmac. Every time the throttle pedal is depressed, the wheel on the ice spins, the engine speed increases but the car hardly moves.

A difference in the spin velocities of the driven wheels will frequently occur in racing. Wet conditions could cause one tyre to break traction. Alternatively, lateral weight transfer under moderate speed cornering (where aerodynamic downforce is limited) will reduce the vertical load on the inner driven tyre, which might break traction. The negotiation of very tight corners will generate a significant wheel speed difference even without loss of tyre grip.

The use of an open differential will allow significant wheel speed difference, whilst maintaining smooth cornering but it will hamper the racing driver by limiting tractive effort.
Figure 7.1 is a GG speed diagram result using the 14DOF model with P_H set to zero to simulate an open differential. The shape of the diagram is significantly smaller than the result for the 14DOF model with a Salisbury differential in Figure 3.19. As expected, the vehicle with an open differential is significantly penalised when the vehicle is in combined lateral and longitudinal acceleration, on the limit.

The opposite to the open differential is the locked differential or *spooled* differential. This simply means that the two driveshafts of the differential are locked together and cannot rotate with respect to each other. This is simulated using a very high P_H of 200Bar on the limited slip differential model. This pressure forces the clutch plates to lock with the two driveshafts, so that they spin together at the same speed. The resulting GG speed diagram of the use of a locked differential is shown in Figure 7.2. There is very little difference between this locked differential result and the limited slip Salisbury differential result in Figure 3.19. This indicates that the limited slip Salisbury

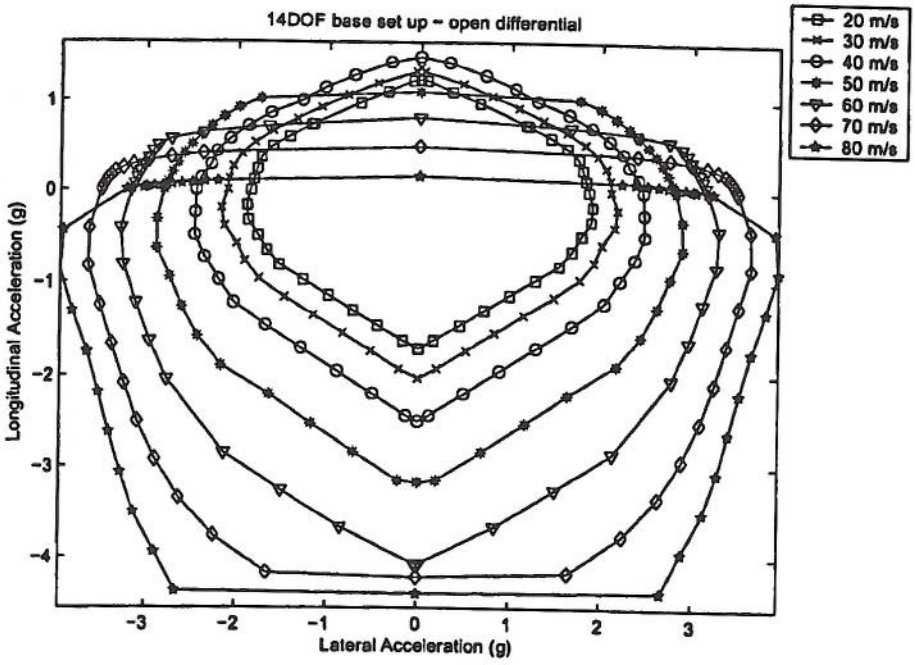

Figure 7.1: Open differential GG speed diagram.

differential is locking up very quickly when significant engine or braking torque is applied to the vehicle. The reason for persisting with a compromise between locked and open differentials, rather than using a locked differential, is that one ideally requires an open differential for cornering to allow the rear wheels to turn at different speeds. This ensures that the inside tyre does not spin or drag across the road surface, since it has a smaller path to traverse than the outside wheel. However, race cars operate as close as possible to the limits of adhesion. This is analogous to the ice/tarmac example but obviously on a much less extreme level. Therefore, when the wheel speed difference becomes significant, ideally the differential progressively locks to ensure that the available engine torque is transferred to the driveshafts and not to spinning the pinion gears.

The Salisbury differential is one example of an effective compromise between locked and open differentials. The conventional Salisbury limited slip differential is the same as an open differential but inside the differential case a set of friction disks are splined alternately to a driveshaft and the differential cage. When the disks are engaged by an axial load that is produced by P_H, the driveshafts are progressively locked to the differ-

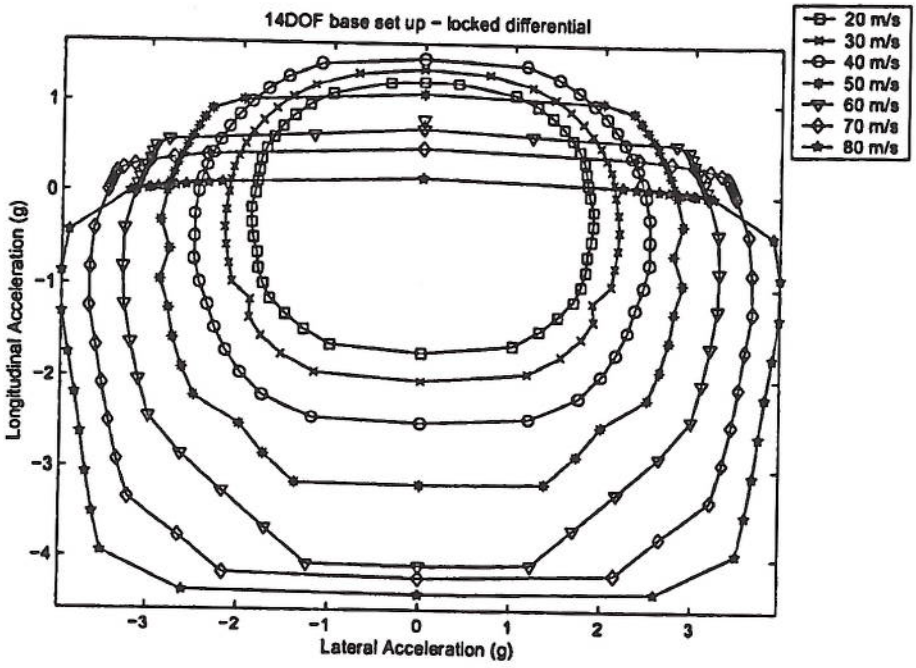

Figure 7.2: Locked differential (spool) GG speed diagram.

ential case, and consequently to each other once the disks lock to the point where there is no slippage between the adjacent disk surfaces. The Salisbury mechanical differential is input torque sensitive, so when the engine torque is increased this ultimately results in the differential responding by trying to lock the drive shafts together.

To show the range of operation of the differential, a steady state cornering manoeuvre using a transient simulation of the seven DOF model is produced by setting a fixed steer angle that maximises the lateral acceleration of the vehicle. The seven DOF model is used here because a transient simulation based on this model was readily available. This is carried out with an open differential configuration (P_H = 0 Bar), the limited slip differential (LSD) and the differential operated at full pressure (P_H = 200 Bar). Figure 7.3 shows the vehicle path under these fixed steer angle, constant vehicle speed conditions.

For a standard torque sensitive limited slip differential (LSD) as used here, at constant speed and zero longitudinal acceleration the engine torque is constant and relatively small, when compared with the engine torque demand during heavy acceleration. Therefore the LSD is operating very close to the open differential configuration.

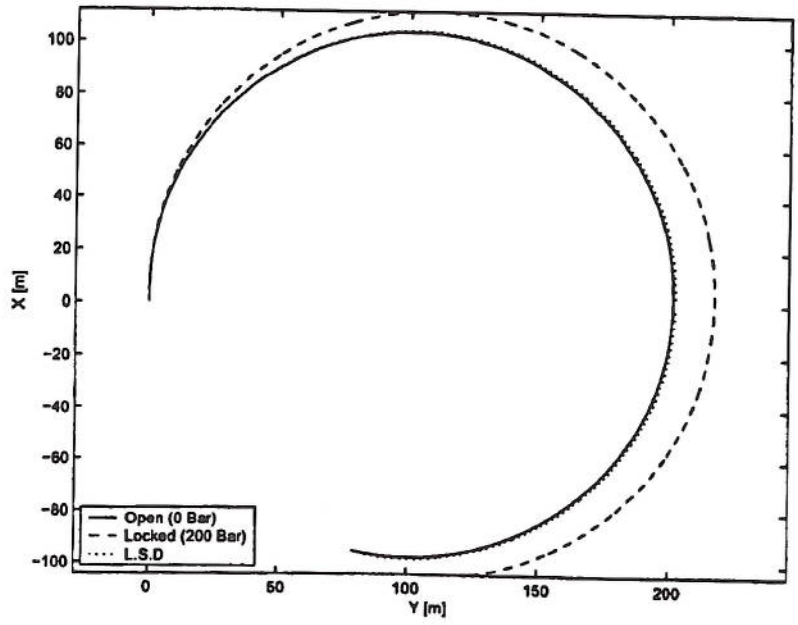

Figure 7.3: Path taken, for three cases of differential operation.

Diff operation	Steer angle [Deg]	Yaw rate [rad/s]	Lat. acceleration [m/s^2]
Open	4	0.496	24.78
LSD	4	0.493	24.65
Lock	2.6	0.462	23.53

Table 7.1: Steady state values for the on-limit vehicle operation at constant speed.

Figures 7.4 and 7.5 show the vehicle yaw rate and lateral acceleration for the steady state manoeuvre. The steady state values from these results are summarised in Table 7.1, taken at nine seconds simulation time.

In the open differential situation, the vehicle generates the highest yaw rate and lateral acceleration by virtue of its tighter cornering radius (Table 7.1). Under full differential pressure the steady state yaw rate is lower than the other two cases, and the vehicle is only capable of a manoeuvre with a reduced steer angle and a wider path radius (Figure 7.3). At constant speed the LSD is very close to an open differential situation, although once the vehicle with the torque sensitive LSD is accelerated, the driven wheels will progressively lock.

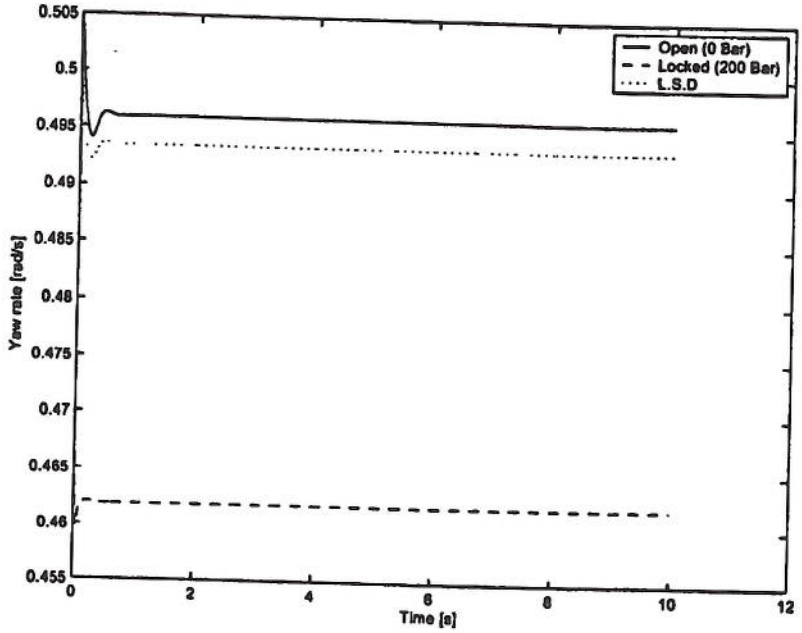

Figure 7.4: Yaw rate, $\dot{\varphi}$, for the three cases of differential operation.

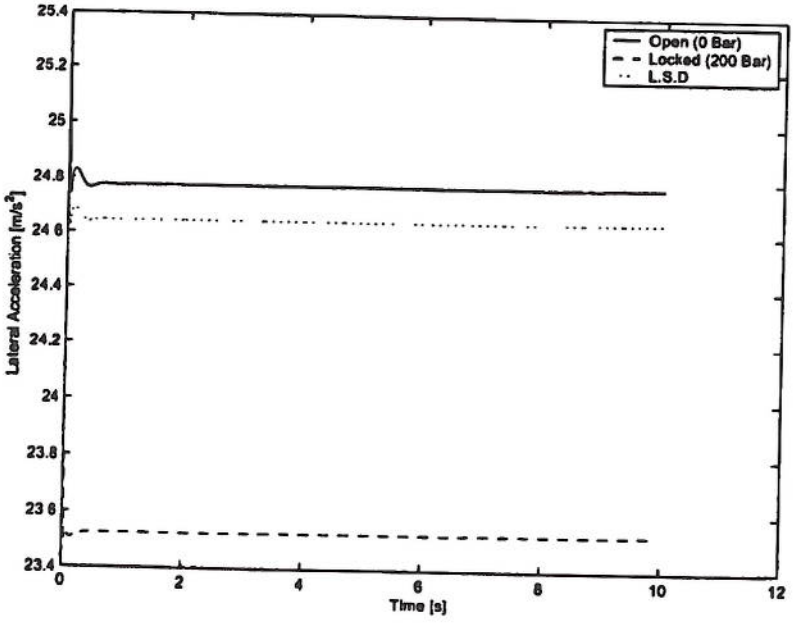

Figure 7.5: Lateral acceleration, for the three cases of differential operation.

Looking at the range of control provided by the differential in terms of the path radius of the vehicle, there is approximately 15 metres between the two extremes of differential operation. However, the effect of the differential on the vehicle during combined acceleration manoeuvres is yet to be determined.

With electro-hydraulic actuation, the control strategy is not confined to emulate a Salisbury differential. It becomes possible to cause locking and opening of the differential under any condition. It may be possible to find a control strategy which outperforms the Salisbury differential. This is the subject of the next section.

7.3 Rear differential control

Using the QSS method to find the optimal values of vehicle parameters, other than the vehicle states, has been achieved in earlier chapters by increasing the size of the P vector. The same method is used here with the hydraulic pressure, P_H, inserted in to the P vector.

The term 'Active Control' as it is used here, is the use of control methods to determine the optimal state of a parameter to meet a defined objective, rather than follow a predetermined relationship (passive) between vehicle states or inputs (like steer angle and throttle position).

The GG speed diagram of the active differential result is shown in Figure 7.6. Surprisingly, there is very little improvement on the results produced by the current Salisbury differential equipped vehicle, in terms of expanding the GG speed diagram. The only improvements seen are in braking above 50 m/s. This new differential control will now be investigated further.

Figure 7.7 illustrates the range of actuation of the differentials for two cases, the original (base) vehicle, and the same vehicle with the differential actively controlled as described above.

The key feature illustrated in Figure 7.7 is the range of actuation of the active differential result compared with the base vehicle. There is significantly more variability in hydraulic pressure. The next section will discuss the effect this new differential control has on the vehicle following a double lane change as shown in Figure 3.14.

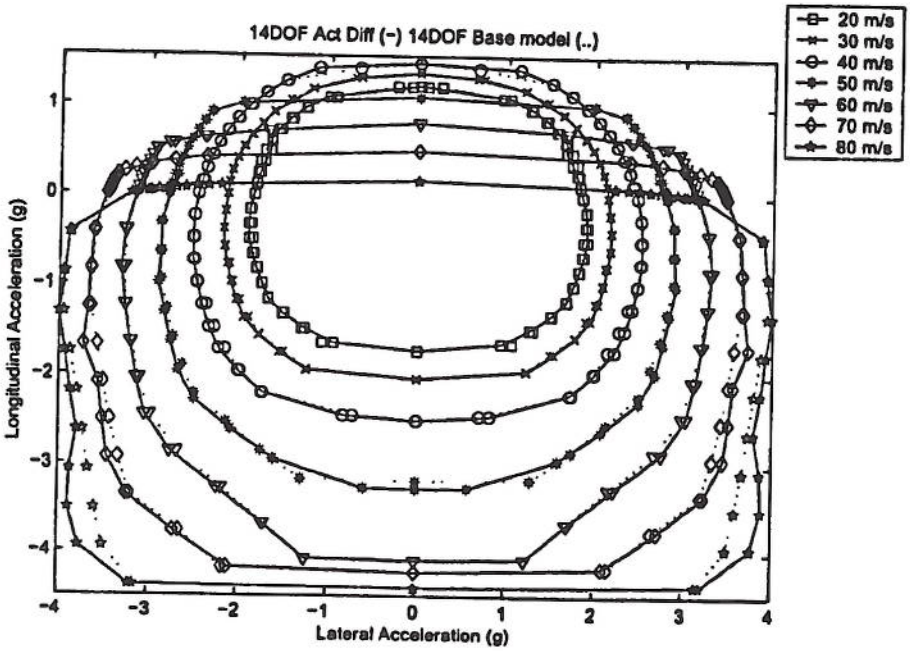

Figure 7.6: Active Differential 14DOF model - GG speed diagram.

The base configuration vehicle begins the manoeuvre as shown in Figure 7.8, at 40 m/s, accelerates to the first left hand bend 1, and then proceeds to slow down to meet the right hand apex of the double lane change 2. The vehicle then accelerates through the last left-hand corner 3 and on to the final straight, completing the manoeuvre. The understeer coefficient, K_{us}, is shown in the top of Figure 7.8, above the steer angle input of the optimal driver (as found by the QSS method). The most important observation for the base car result is that the required steer input is quite significant, showing the car is steered aggressively through the manoeuvre. Of the 500 data points that comprised this manoeuvre, 5.6% of the time the car was understeering, 49.2% of the time the vehicle was oversteering, and the balance was straight line running of the vehicle either side of the double lane change. The vehicle changes very quickly from understeer to oversteer within a 400m long manoeuvre and this places a high work load (in terms of decision processing) on the driver when the car is driven on the limit, as it is here.

As the apex of corner 1 is approached the vehicle progresses from low to moderate oversteer, while the vehicle is accelerating and responding to the steer input. Once through the apex, the car moves closer to a neutral steer condition under braking while

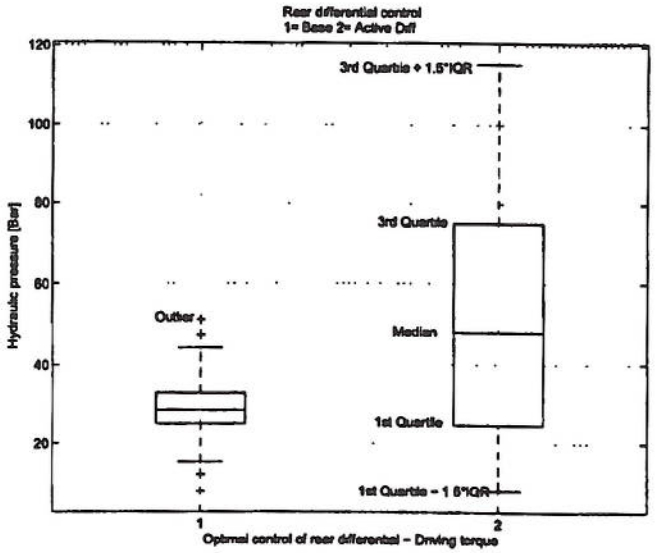

Figure 7.7: Box plot of rear limited slip differential control.

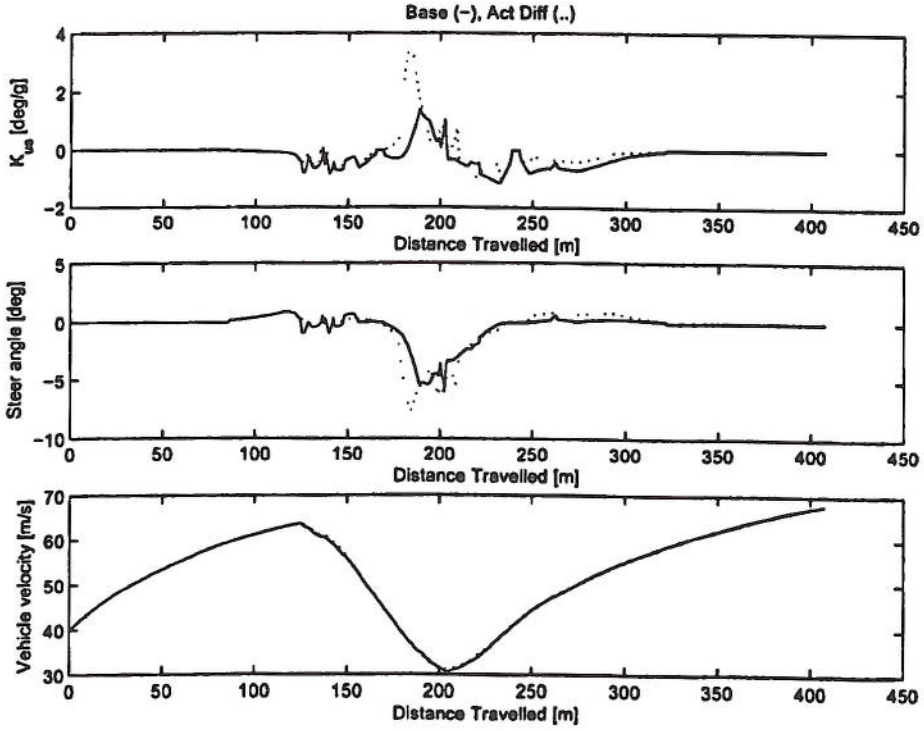

Figure 7.8: Double lane change manoeuvre.

	Base Car	Active Differential
Manoeuvre Time (sec)	8.1094	8.0952

Table 7.2: Manoeuvre time, double lane change.

heading towards the apex of corner 2. Just before the apex of corner 2 the steer angle input climbs exponentially and the vehicle responds, producing $1.5\frac{deg}{g}$ of understeer. Upon exiting corner 2 the car begins to accelerate again, the understeering vehicle switches to $-1.2\frac{deg}{g}$ of oversteer and then slowly reduces towards neutral steering, as the car accelerates through corner 3 and onto the straight.

Figure 7.9 shows the lateral tyre force utilisation as a percentage of the maximum amount of lateral tyre force available, given the longitudinal force required to maintain the longitudinal acceleration of the vehicle. Through the apex of corner 1 the front and rear axles both approach their lateral tyre force capacity, but there is unutilised lateral tyre force capacity in the front right tyre. The rear axle is closer to full utilisation than the front axle. This explains why the values of K_{us} show the vehicle in a mild oversteer condition.

The most difficult aspect of controlling the vehicle through the double lane change is the negotiation of corner 2. After the apex, the car goes from an understeering vehicle to a moderately oversteering vehicle, as the steering input is reduced from six degrees to zero. This is a very quick change in vehicle cornering behaviour from the perspective of a driver, and is not desirable.

7.3.1 Active differential control

The vehicle response under active rear differential control is shown in Figures 7.8 and 7.9 as a dotted line. The key difference, with respect to the base vehicle result, is the damping of the peaks in the understeer coefficient.

The one notable exception is an understeer spike just before the apex of corner 2. Inspection of the steer input shows that the steer angle is significantly higher during turn in, compared to the base vehicle configuration. The highly utilised front left tyre experiences a small drop in lateral force, necessitating the steer input to be increased, to increase the yaw rate of the vehicle to follow the racing line. Figure 7.10 shows that

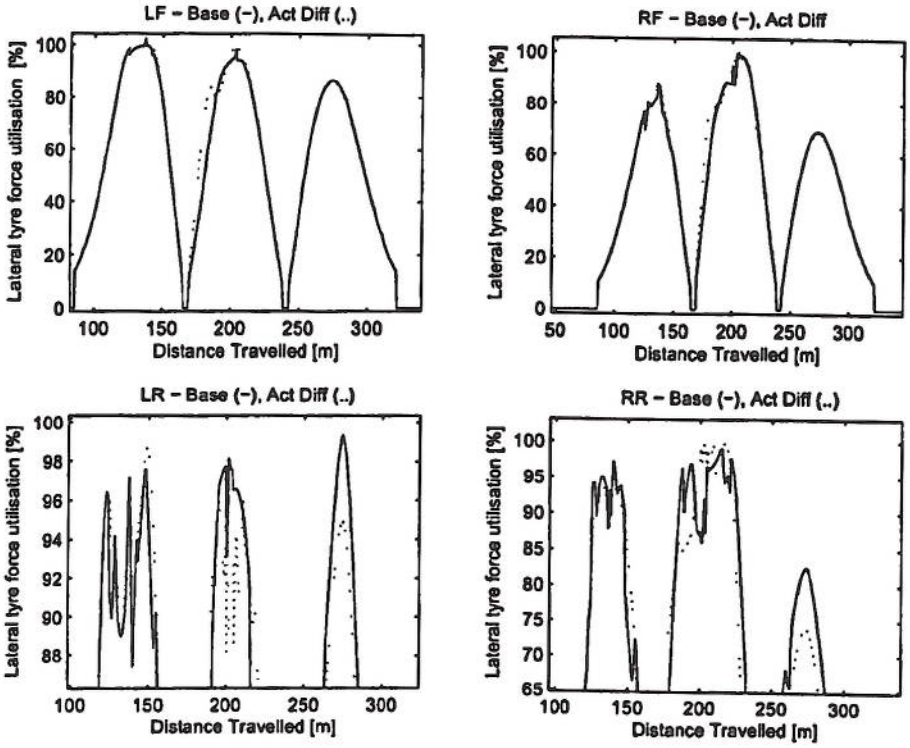

Figure 7.9: Lateral tyre force utilisations.

this coincides with an increased demand in longitudinal braking force for this tyre, at 184m distance. The active differential vehicle is slightly faster than the vehicle in the base configuration, as shown in Table 7.2. This is mainly due to a slightly higher cornering speed through apex 1 and 2.

The vehicle is in understeer for 10.0% of the time and in oversteer 44.8% of the time with the active differential under optimal control. The hydraulic pressure is markedly higher through corner 1 (Figure 7.11) making it much more difficult for the rear wheels to rotate at different speeds. The differential action reduces the oversteer and the amplitude of the oscillations seen in the values of K_{us} under braking.

Approaching corner 1, the differential pressure increases significantly, compared to the basic Salisbury differential, requiring the rear wheels to rotate at similar speeds (Figure 7.11). Exiting the corner at approximately 150m distance travelled the optimised hydraulic pressure is 10Bar higher than the base vehicle result. The lateral tyre force utilisation of the two rear wheels, due to the action of the active differential,

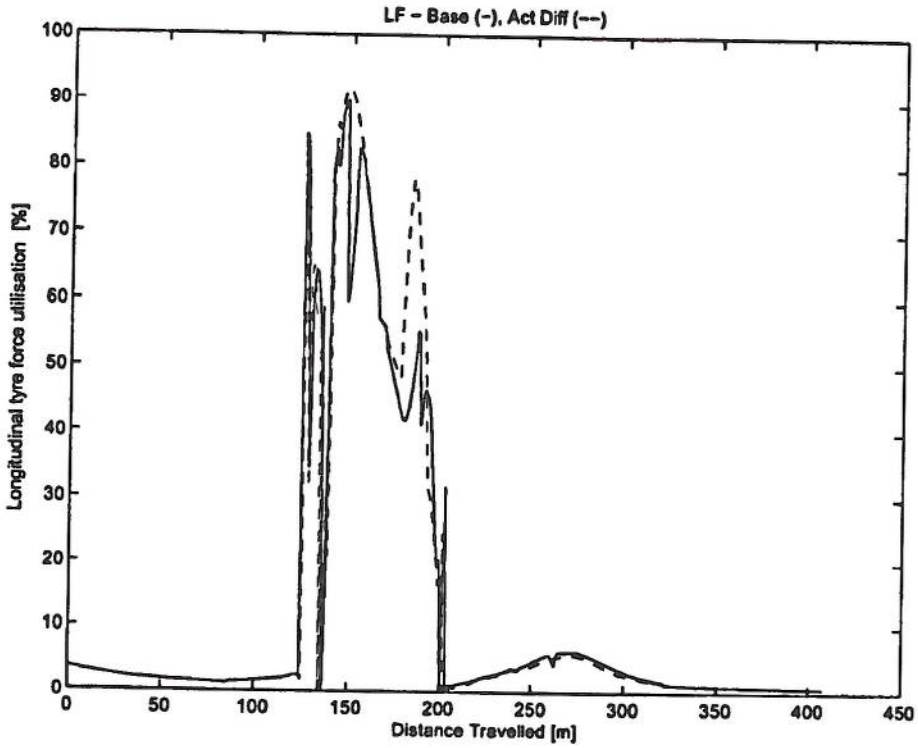

Figure 7.10: Longitudinal tyre force utilisation.

is a reversal of the base vehicle result exiting corner 1. The active differential control causes the left rear (highly loaded) tyre to be operated closer to 100% lateral tyre force utilisation. In addition, the right rear lateral tyre force utilisation does not reduce as quickly as the base result (Figure 7.9) at 150m distance travelled. The result is a slightly higher cornering speed as shown in Figure 7.8.

Similarly in corner 2, the highly loaded right rear tyre is operated much closer to the 100% lateral tyre force utilisation limit, and the lightly loaded left rear tyre is comparatively reduced. As a result of the optimised differential control through these two corners, the larger lateral tyre force utilisation of the outside rear tyre forces creates a higher yaw rate and increases the lateral acceleration of the vehicle. In this instance however, the optimised hydraulic pressure is reduced to 10Bar through corner 2 (distance travelled = 200m) as shown in Figure 7.11. This is lower than the base result at 40Bar, allowing the rear wheels speed difference to increase.

The manoeuvre time was found to be only marginally faster (Table 7.2) but the differences in K_{us} indicate that the vehicle's steady state cornering behaviour is less oscillatory than the base vehicle. The differential action under optimal control brings the vehicle closer to neutral steer in nearly all situations during the manoeuvre. According to a current F1 team, the advantage gained from differential control allows one to implement a more 'aggressive' vehicle set-up by using the differential to help stabilise an otherwise unstable vehicle, from the drivers point of view [105]. This appears to be possible based on the findings presented here.

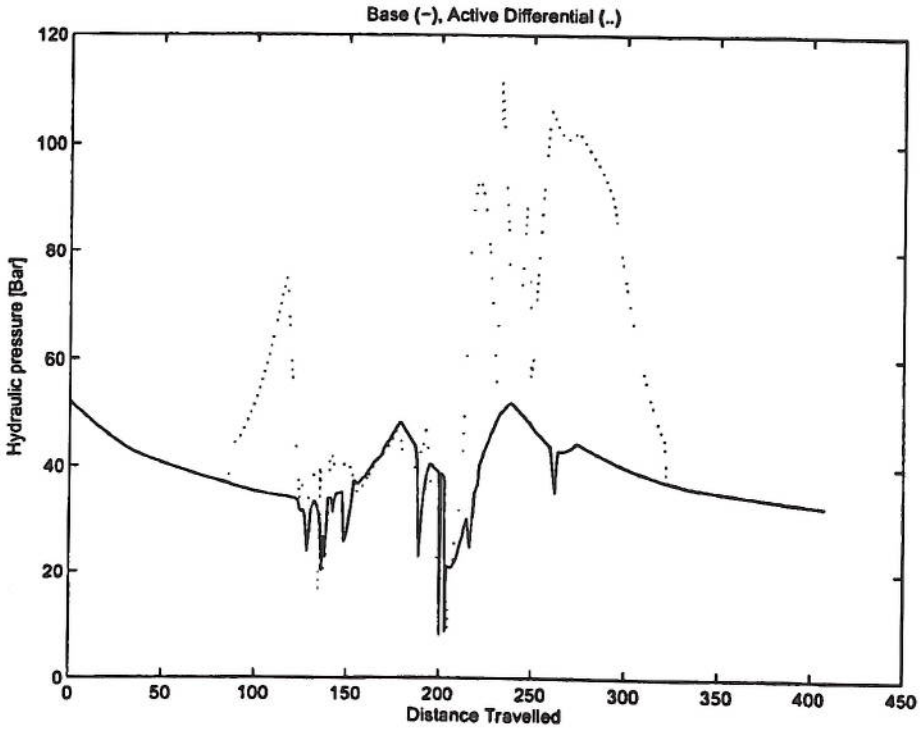

Figure 7.11: Rear differential hydraulic pressure.

7.3.2 Practical control

The use of optimal control to find the hydraulic pressure for the differential is very difficult to apply to a race car in real time. The solver is required to iterate to find the result because the vehicle model is nonlinear. Possible options for implementing the knowledge gained through the QSS method are to linearise the model to enable quick solution times, to access a stored map of all the optimal settings, or to imple-

ai^3+bi^2+ci	a	b	c
$\ddot{x}$	0.0024	0.1166	4.5236
δ	-0.0879	1.7650	-7.7993
$\dot{\varphi}$	178.3855	-485.4871	326.8772
$\omega_i-\omega_o$	0.1444	-2.6054	6.2490
T_p	6.1412	56.2584	-81.0117

Table 7.3: Polynomial coefficients - Active differential control law.

ment an empirical control law that produces the same results as the optimal control. The method described here is an empirical control law as it does not require model simplification and it is easier to implement than a multidimensional lookup table.

A realistic control law using only the sensors allowed by the FIA, to control the differential in Formula One, proved to be difficult. Instead, a set of relevant parameters were used that can be measured easily with current sensor technology. The variables are, longitudinal acceleration ($\ddot{x}$), throttle position (T_p), steer angle (δ), yaw rate ($\dot{\varphi}$) and rear wheel speed difference ($\omega_i-\omega_o$).

The aim used to direct the control law development was to keep the function as simple as possible, whilst maintaining the highest possible accuracy. Trials, with various types of polynomials and periodic functions, resulted in a 3rd order polynomial being selected as the best compromise. The MATLAB least squares nonlinear fitting algorithm *lsqnonlin* was used to find the coefficients of the polynomial. Table 7.3 shows the coefficients(a,b,c) for the resulting polynomial.

The QSS method was employed in the same manner as the base (passive differential) configuration, but with the differential being operated by the control law instead of the original passive differential. The result is compared with the active differential result for the double lane change as shown in Figure 7.12.

Figure 7.12 shows that while there are differences between the two hydraulic pressure results throughout the manoeuvre, the optimised control of the rear differential can be used to develop practical control laws for rear differentials.

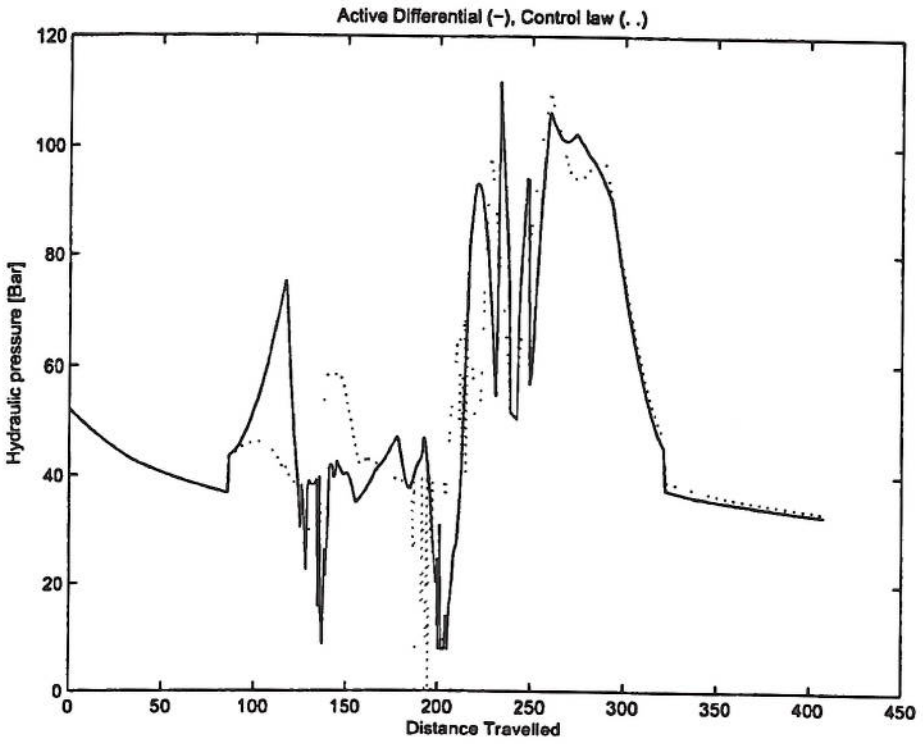

Figure 7.12: Rear differential hydraulic pressure - Control law and Active differential (Corner 1= 136m, Corner 2= 204m, Corner 3= 271m).

Through the double lane change the performance of the vehicle, under the control law actuation, produces significantly different results under braking (Figure 7.13) compared with the active differential result. As can be seen in Figure 7.12 the hydraulic pressure in the differential from corner 1 to corner 2 is markedly different. The vehicle speed suffers and corner 2 is negotiated at a lower speed. Before corner 2 there is no large increase in steer angle in the control law based result, as seen in the active differential result. In addition, at corner 2 the steer angle becomes very oscillatory. In traction conditions, before corner 1 and up to and through corner 3, the control law based differential appears to work well. Overall the vehicle is slower through the manoeuvre, when the differential is operated by the control law, but its handling behaviour is more uniform as manifest by the relatively constant understeer coefficient shown in Figure 7.13.

The implementation of the polynomial-based control law has shown varied effects; good control in traction, but difficulties under braking. This test case has demonstrated

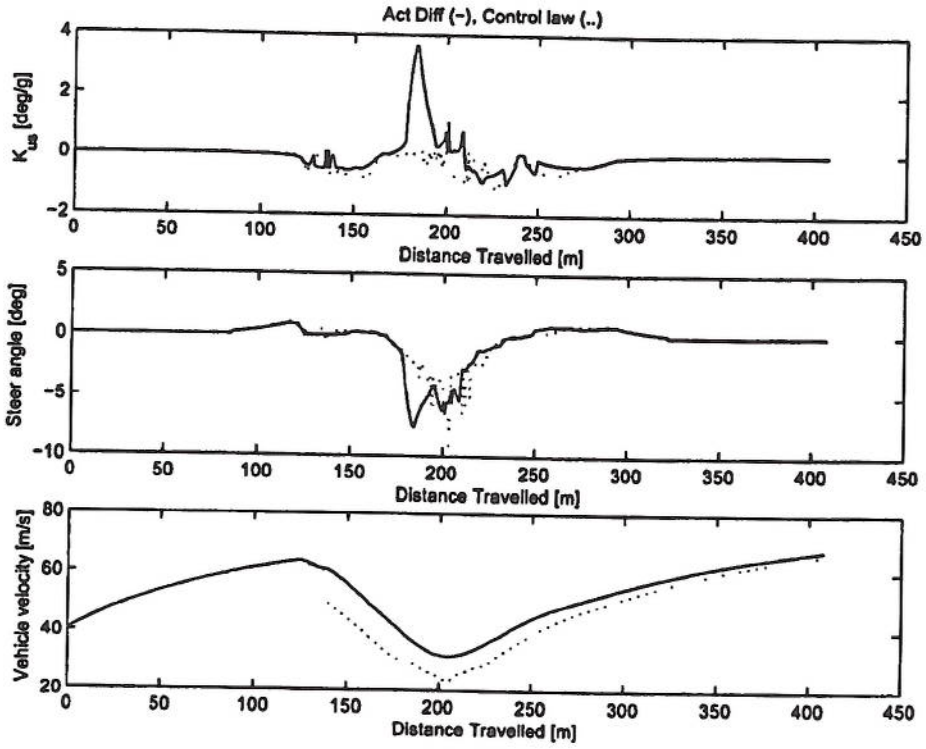

Figure 7.13: Double lane change comparison - Control law and Active differential (Corner 1= 136m, Corner 2= 204m, Corner 3= 271m).

that it is possible to use the QSS method as a tool to develop control strategies for a limited slip differential. However, relatively small changes in the control manifest themselves as significant changes in vehicle speed and handling characteristics that are not always beneficial. This suggests that the practical control of hydraulic limited slip differentials is a difficult task.

The principal finding in this differential work is that a controlled locking differential improves the performance of an open wheel race car (by increasing the area of the GG speed diagram) but only when braking hard (neglecting any cases that might occur in practice where the traction at one of the driven wheels is broken). This perhaps surprising result merits some further discussion.

The locking differential provides a mechanism whereby torque may be transferred from a driven wheel that is spinning quickly to a driven wheel that is spinning more slowly. Neglecting the cases involving broken traction, there will only be a differ-

ence in wheel speed under cornering. Therefore, one can anticipate the result shown in Figure 7.6, that the active differential only affects cases where there is combined longitudinal and lateral acceleration.

The locking differential affects vehicle performance through the mechanism of torque transfer. In a practical differential the magnitude of transferred torque must be less than the torque delivered to the differential. Therefore, to have any significant effect on the performance of a vehicle with race car inertias, the transfer torque must be large and hence the torque to the differential must be larger still. Large traction torque is delivered to the differential under wide open throttle, in low gears at low ground speed. Notwithstanding this, from the results in Sections 7.3.1 and 7.3.2, the torque transfer created under such conditions is not great enough to influence vehicle performance. However, much greater torque is applied to the differentials via the driveshafts under heavy braking from high speeds. The substantial torque transfer that can occur when braking and cornering is enough to alter vehicle performance, as noted in Sections 7.3.1 and 7.3.2.

The above discussion suggests that for the case of open wheel race cars, the locking differential plays a role as a braking performance enhancer for combined high speed braking and cornering manoeuvres. Unfortunately, as the double lane change results demonstrate, the advantages of enhanced braking performance are not always seen as it is difficult to realise a control algorithm that can be implemented on a practical differential.

Another observation begs attention. Close inspection of the state vectors that make up the GG speed diagram reveals that even when longitudinal and lateral accelerations are unaffected by the operation of the active differential, other elements of the state vector (throttle / brake position, steer angle, vehicle attitude angle) are affected. This is an expected result as the numerical optimiser manipulates all of these quantities as well as the hydraulic pressure in the differential. Changes to these other elements of the state vector alter the driver's feel of the race car.

In summary a controlled locking differential can be used to enhance vehicle performance in a limited set of braking manoeuvres but also can be used to alter the driver's feel of the vehicle. The effects on driver feel are particularly interesting and deserve further attention. However, this is beyond the scope of this research study.

7.4 All wheel drive (AWD)

In the past, the use of AWD on open wheel race cars has been briefly explored. The first instance of a vehicle with four wheel drive for Formula One appears to have been the Cisitalia, Porsche-designed Type 360, constructed in the 1940's [106]. In the 1960's Ferguson built a four wheel drive Formula One car, which won a wet-weather, non championship race. [12]. In 1969 Lotus explored the use of four wheel drive, and was subsequently followed by Matra, Mclaren and Cosworth. These cars were not particularly successful in Formula One events [12]. With the appearance of four wheel drive Formula One cars with six wheels the use of four wheel drive was banned from 1983 [12].
As an interesting exercise, the AutoSIM script for the base model with 14DOF was expanded to include two further differentials; an open differential for the front axle and a centre differential to distribute the engine torque between the other two differentials. The limited slip differential was retained on the rear axle and an open differential was selected for the front axle, to reflect current practice. The open differential is used to ensure that the wheel speed differences are not regulated, and that the proportion of engine torque destined for the front axle is split equally between the two wheels.

The modelling of the two new differentials was kept very simple. The proportion of engine torque sent to each axle, C_{diff}, is added to the state/control optimisation vector as shown in Equation 7.1.

$$P = [\dot{y}, \dot{\varphi}, \dot{\theta}_{LF}, \dot{\theta}_{RF}, \dot{\theta}_{LR}, \dot{\theta}_{RR}, \delta, T_P, P_H, C_{diff}]^T \tag{7.1}$$

The rear differential remains the same and the proportion of engine torque destined for the front axle is split evenly between each wheel. However, the equations of motion become very complex. This model neglects the drive train and engine power losses that accompany the implementation of such systems. The rotational inertias of all differentials are also neglected.

Under the AWD system the vehicle still has a heavy rear wheel drive bias. Figure 7.14 shows that on average, 73% percent of the drive torque is sent to the rear axle. The AWD active rear differential has a higher average hydraulic pressure (63%) than the two wheel drive with active rear differential control (44%). But in most respects the magnitude of the rear differential control is very similar to the two wheel drive optimised result as evidenced by a comparison of Figure 7.15 and Figure 7.11.

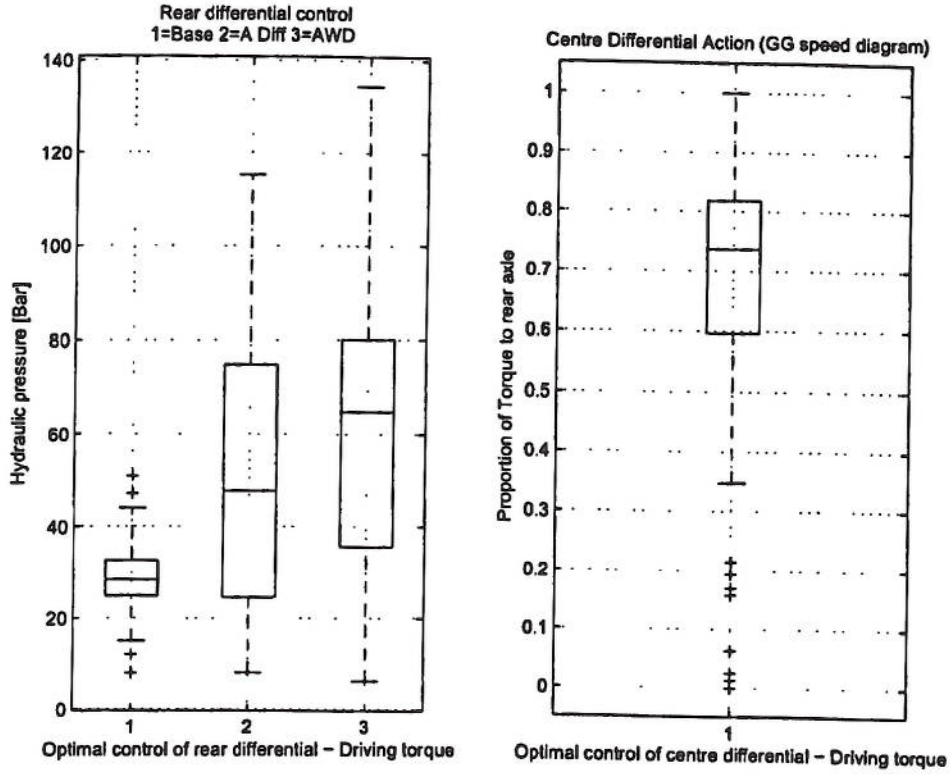

Figure 7.14: Box plot of differential control.

To make a judgement on the effectiveness of the model implementation the longitudinal tyre force utilisations are examined, as the front tyres now accept driving torque from the centre differential.

Figure 7.16 highlights the effect of the AWD system. The interesting feature is the degree of utilisation at the front axle in the straight running condition. The centre differential has sent the majority of the drive torque (Figure 7.18) to the front axle. Considering the load transfer under acceleration favours more tyre load at the rear axle this is a surprising result, but the vehicle speed shown in Figure 7.17 confirms that the vehicle is indeed faster in a straight line than the other two cases.

The vehicle speed difference is largest just after the onset of braking between corners 1 and 2. The AWD system is able to begin braking later than the other two cases, and also maintains a higher cornering speed through corner 2. Closer inspection of the longitudinal tyre force utilisations shows that the AWD system has utilised the front

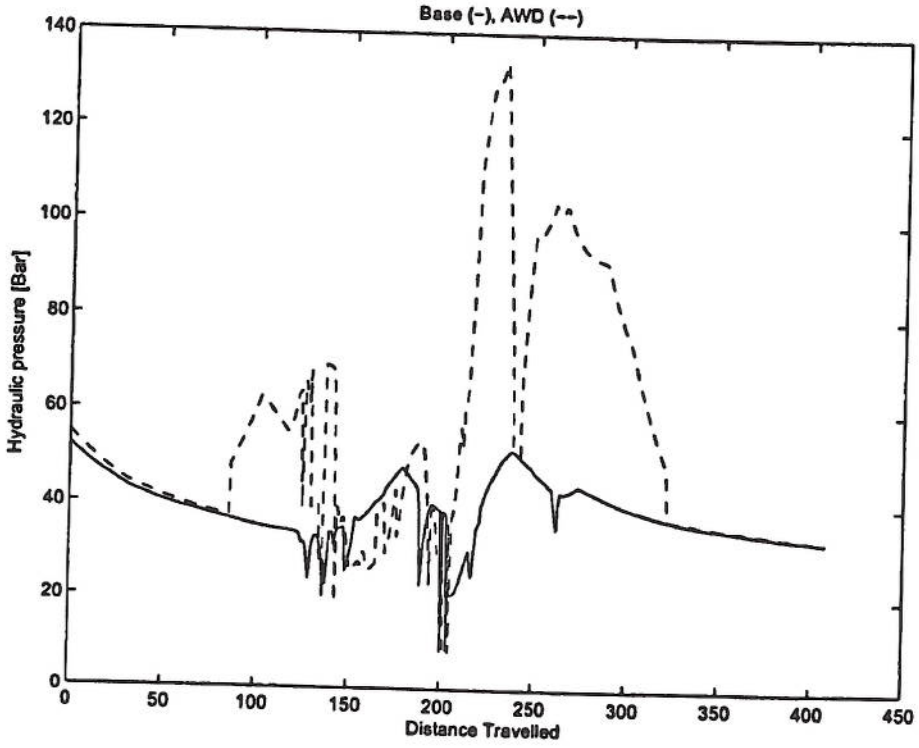

Figure 7.15: Rear differential hydraulic pressure - AWD.

	Base Car	Active Differential	All Wheel Drive
Manoeuvre Time (sec)	8.1094	8.0952	7.9056

Table 7.4: Manoeuvre time, double lane change.

tyres better. This appears to be due to a transfer of available drive torque to the front axle during the switch from acceleration to braking (130-144m, Figure 7.18). This theory is reinforced by the drop in longitudinal tyre force utilisation on the rear axle and corresponding gain on the front axle in Figure 7.16.
The re-direction of torque to the front axle (30-58% of available drive torque) after corner 2 and through corner 3 also creates speed gains for the AWD system over the other two cases.

The use of AWD does not add any further torque to the system, it just affects how the torque is distributed. Therefore, the gain in tractive force on the front tyres reduces their ability to generate lateral tyre forces. This requires the front tyres to operate much

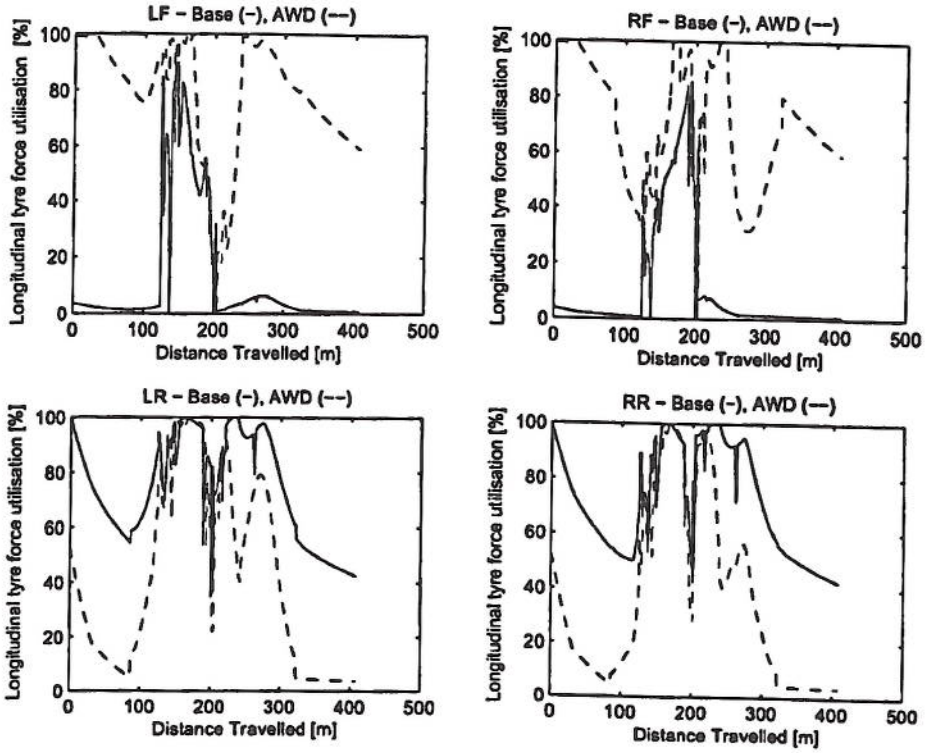

Figure 7.16: Longitudinal tyre force utilisations - AWD.

closer to their lateral limit (Figure 7.19). To follow the prescribed trajectory the steer angle through corners 1 and 3 has increased significantly to compensate. The tyres have been utilised much more effectively and the vehicle has traversed the manoeuvre 0.2 seconds quicker than the other two configurations (Table 7.4). This is a 2.5% improvement and potentially significant over an entire lap of a Grand Prix circuit.

The cornering behaviour of the vehicle has also changed significantly. The vehicle with AWD has become a predominantly understeering vehicle with 44.4% of the data showing the vehicle in understeer and only 10.5% of the data showing the vehicle in oversteer, through the double lane change. The oversteer is generated mainly during braking where the load transfer increases the load on the front axle and reduces the load on the rear axle. Track testing of the Formula One cars fitted with these AWD systems highlighted the amount of understeer generated as a problem [12]. The drivers also pointed out that the ability to induce oversteer with the throttle was now not possible. More throttle induced more understeer [12]. The additional weight of the systems required to implement AWD, and the complexity of locating a drive shaft alongside

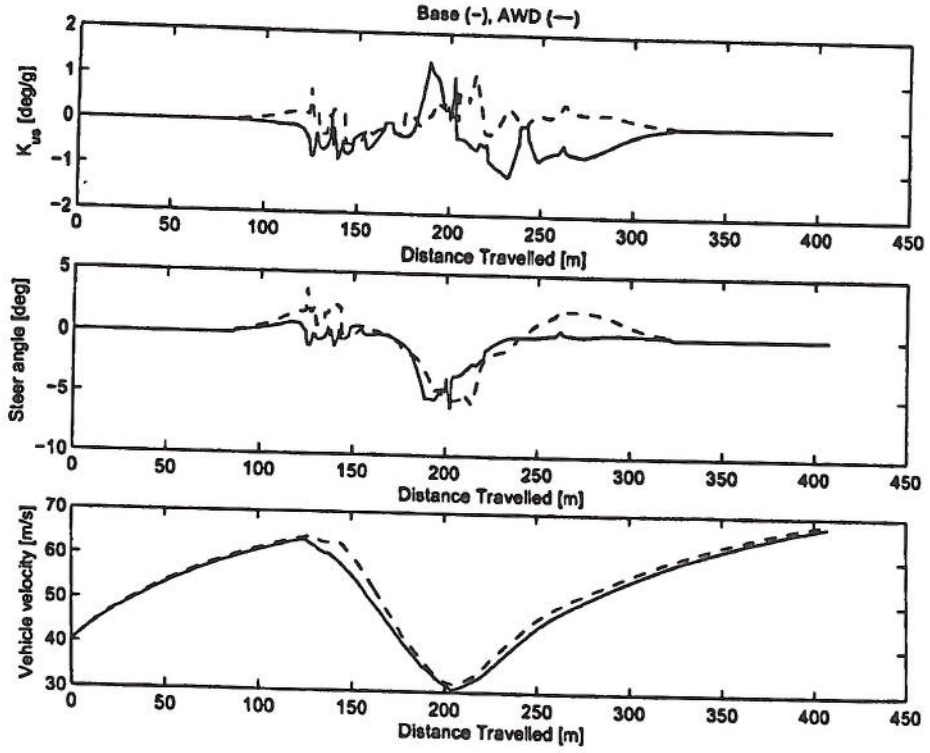

Figure 7.17: Double lane change manoeuvre - AWD.

the driver, all added to the reluctance to persist with AWD in Formula One in the late sixties [12]. Since AWD systems remain banned to this day this exercise remains academic, but the 2.5% improvement in manoeuvre time indicates that there are potential performance gains to be realised in applying AWD systems to Formula One vehicles. This study of AWD does not allow the complete control of the torque across an axle, it only follows the current principles of allowing torque to be sent from the faster wheel to the slower wheel. Investigating the possibility of improved performance due to complete control over the torque across an axle may also have advantages. The capability of directing torque across an axle in either direction is termed *torque vectoring*, and whilst this is the logical next step, an investigation is beyond the scope of this study.

7.5 Summary

The controlled locking differential is useful for enhancing vehicle performance when traction is broken at low ground speeds and when braking hard in a cornering manoeu-

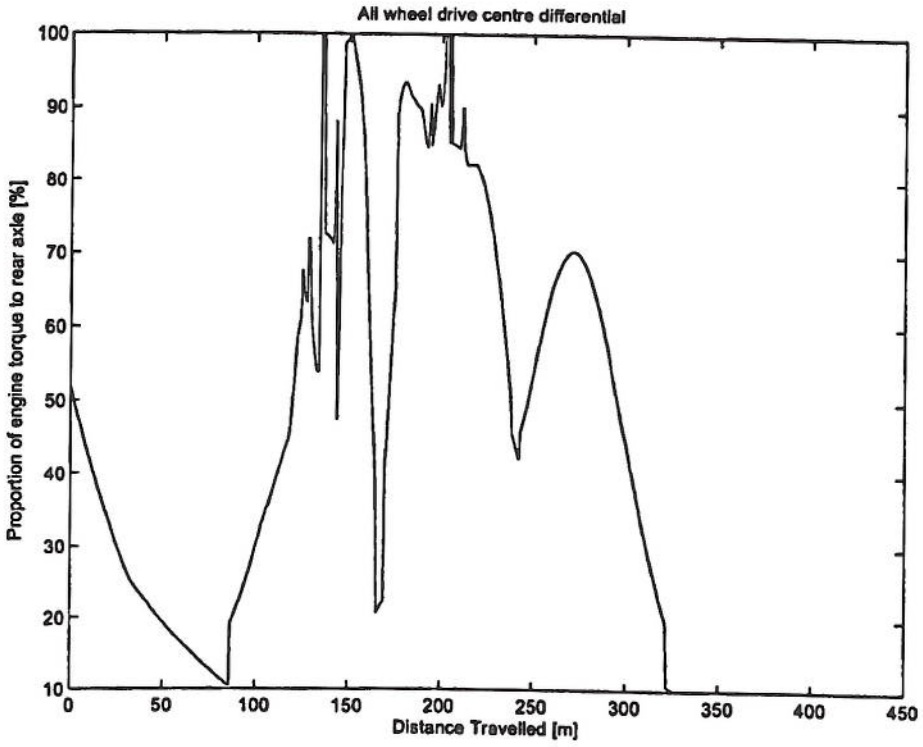

Figure 7.18: Centre differential control - double lane change manoeuvre.

vre.

The results suggest that optimising the action of the locking differential improves the braking performance of a race car, when cornering, but these benefits are difficult to realise when implementing practical differential control laws. The controlled locking differential is seen to alter the handling characteristics of the vehicle.

An all wheel drive system applied to the new 14DOF model has been shown to improve the time to complete a double lane change manoeuvre by 2.5%. The cornering behaviour of the vehicle has changed from a predominantly oversteering vehicle to an understeering one, due to this system.

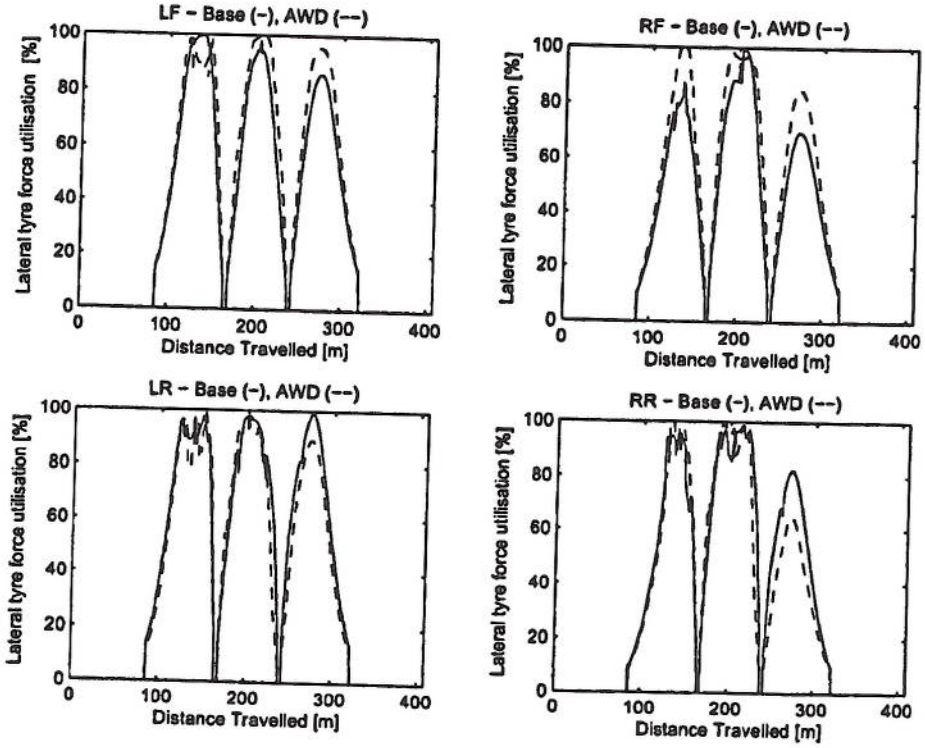

Figure 7.19: Lateral tyre force utilisations - AWD.

Chapter 8

Discussion and conclusions

This thesis is constructed around a set of objectives and an overall aim to investigate the on-limit behaviour of an open wheel downforce type race car using the best compromise of modelling accuracy with computational effort. The following sections update how the research objectives were met and state the key findings of the research, and the conclusions drawn.

8.1 Research objective 1

To design, build, and validate fast numerical optimisation race car simulation programs for the purposes of defining vehicle setup parameters, as well as the minimum laptime, using appropriate vehicle models.

This thesis described the current options in numerical modelling of vehicle dynamics in terms of simulation to achieve the fastest possible laptime. Transient and quasi steady state programs were reviewed, and the best compromise between accuracy and computational effort was determined to be a quasi steady state method. A method was developed using a validated seven degree of freedom vehicle model, and checked for accuracy against a published method. The developed method generated a GG speed diagram as an intermediate step. The vehicle model was then expanded, where possible, to make the mathematical descriptions more realistic and physically significant, and to reduce the number of inherent assumptions in the published vehicle model. Using the extended models approximately doubled the computational time on the 1000MHz PC.

Additionally, a transient near-optimal method was developed using a nonlinear driver preview model, and the published seven DOF vehicle model. The resulting program followed a prescribed racing line and followed a near optimal vehicle speed profile, generated by the quasi steady state method. The method computational time was comprised of the quasi steady state method computational time plus the time for a standard numerical integration initial value problem to be computed. This method known as the PI method, was used to conduct a transient case study on the potential benefit of introducing a vehicle stability control system to a contemporary open wheel race car. The key findings were:

- The quasi steady state method was found to be valid when compared with a published transient optimal method, using a published vehicle model.
- The quasi steady state method was found to be significantly faster to compute than the transient optimal method.
- A transient near-optimal path following method (PI method) has been shown to produce a lap simulation result that is comparable with both the quasi steady state method and the published transient optimal path finding method.
- The PI method was significantly faster to compute than the transient optimal path finding method.

8.2 Research objective 2

To explore race car vehicle on-limit behaviour with the vehicle optimisation programs, by analysing the sensitivity of specific vehicle parameters and/or systems on vehicle performance. The following vehicle parameters will be analysed over a wide range of values:

1. **Vehicle mass.**
2. **Yaw inertia.**
3. **Tyres properties.**
4. **Engine.**
5. **Longitudinal centre of gravity location.**
6. **Aerodynamic downforce.**

The vehicle parameters listed above were varied around their original values, which are based on actual vehicle settings. The published seven degree of freedom vehicle model was used to take advantage of the existing parameter information available. Whilst the following findings only strictly relate to a specific vehicle, trends are likely to hold for all Formula One type vehicles.
The key findings were:

- The vehicle performance sensitivity due to vehicle mass changes was found to linearly increase or decrease with vehicle speed, if the mass was reduced or increased respectively.

- Changing the vehicle yaw inertia was found to be relatively ineffective, and this was determined to be a function of the vehicle configuration, and not due to any particular type of manoeuvre. The lack of vehicle performance sensitivity is due to the vehicle approximating trimmed steady state cornering in the majority of manoeuvres, which does not create significant yaw accelerations and therefore in these situations the vehicle yaw inertia is irrelevant. This study did contribute an analysis of the potential error in the use of the QSS method. The potential error in evaluating a velocity contour's true area was found to be $\pm 1.4\%$.

- The changing of the tyre's ability to generate longitudinal and lateral forces resulted in a near linear response with respect to vehicle speed, but with increasing speed the performance gains begin to converge on the base vehicle result. This is due to the comparatively low engine torque available resulting in under utilised tyres at high speed. The majority of the engine torque is used to offset the vehicle drag, which is increasing with the square of vehicle speed. The benefits from increased tyre force generation capability at high speed were exploited predominantly in braking.

- The benefits of increased engine torque across the engine speed range is shown to be most effective (or detrimental with the reduced torque cases) at higher speeds, particularly between 50-70 m/s. This is because the tyre force generation capability, due to aerodynamic downforce supplementation, is sufficient to transfer the available torque provided by the engine to the road.

- The use of the engine torque via throttle control is an important factor in exploiting the lateral acceleration capability of the vehicle.

- The effects of CG relocation were found to be rather complicated when compared with the other parameters studied. Moving the CG forward of the base position was found to be a backward step in vehicle performance at all vehicle speeds. Moving the CG rearward, as found in other research, could make the vehicle faster, but this is suggested to be a circuit specific result rather than a general performance improvement. The general trend was that moving the CG rearward improved the lateral acceleration capability at low longitudinal accelerations (both in traction and braking) at the expense of lateral acceleration capability in high speed braking. The base vehicle has been shown to be stable using linear analysis of the vehicle lateral velocity and yaw rate modes, but the analysis of the 37/63% front to rear CG balance whilst stable in straight line running, was found to be unstable in steady state cornering. This is believed to have made the optimisation task more difficult.

- The effects of improving the downforce capability increases with increasing speed to reach a peak at 50 m/s. As found in the engine torque curve and tyre sensitivity tests, the lack of engine torque, coupled with the increasing drag force at high speed, reduces the vehicle's ability to capitalise on the additional vertical load provided by the aerodynamic downforce package.

8.3 Research objective 3

To investigate an aspect of vehicle on-limit *control* using a case study on the importance of the optimal path (path finding) to lap simulation studies.

The suite of vehicle simulation programs developed during the course of this research were utilised for two case studies centred around the on-limit control of a race car. The quasi steady state method was used to investigate the value of calculating the new optimal line for a centre of gravity location change to a baseline vehicle set up. This was conducted because the ability to calculate the optimal line was lost using the quasi steady state method, and the value of this information needed to be quantified. The key findings were:

- The quasi steady state method and the transient optimal method both show improvements in lap time due to a 6% centre of gravity set up change. The quasi steady state method produces a lap time that is within 3% of the transient optimal method result.

- The difference in optimal lines caused by a 6% CG change is shown to be so small (±1m) that the driver is unlikely to find the information useful. In light of this finding the computational effort required to generate a new optimal line for each set up change may be misspent.

A simple experiment involving four professional racing drivers was conducted during this study. The drivers were asked to draw their preferred racing lines on a section of the Barcelona Grand Prix circuit.
The key finding was:

- There is more to the process of driving the racing line than just putting the car on the limit at all times, as the optimal path finding methods do. Other relevant factors include: low road friction conditions off from the most frequently used racing line, the effect of active systems and driver prejudice.

8.4 Research objective 4

To determine the usefulness of certain active control technologies. These are:

1. **Active control of the roll stiffness distribution.**
2. **Active control of electronically controlled limited slip differentials.**

Active control technologies, as used in Formula One have, in general, been very restricted. However, it was determined that value from the simulation of active control technologies lay in the understanding of how the potential increase in vehicle performance was attained. This knowledge could then be used to provide an objective method of improving the passive setting up process at racing circuits. The active control of the differential and the roll stiffness distribution was achieved by expansion of the optimisation variable vector to accommodate the hydraulic pressure of the differential and the proportion of the roll stiffness carried by the front axle, as required. The seven degree of freedom model was used for the roll stiffness distribution research, and the extended modelling of vehicle systems conducted after the QSS model validation, was used for the differential study.
The key findings were:

- The benefits shown by the optimisation of the roll stiffness distribution have created a mean improvement in performance capability over the base vehicle

of over 10%. It has been shown that circuit dependent analysis is possible to exploit the value of the static setting of the roll stiffness distribution to improve lap times.

- Further work and validation is required to explore this avenue of vehicle setup optimisation, but it does appear that parameter optimisation using numerical optimal control methods offers a way of helping make an objective choice of static R_{sf} setting for particular circuits.

- The controlled locking differential is useful for enhancing vehicle performance when traction is broken at low ground speeds and when braking hard in a cornering manoeuvre.

- The results suggested that optimising the action of the locking differential improves the braking performance of a race car when cornering, but these benefits are difficult to realise when implementing practical differential control laws. The controlled locking differential is seen to alter the handling characteristics of the vehicle.

- An all wheel drive system applied to the new 14 DOF model has been shown to improve the time to complete a double lane change manoeuvre by 2.5%. The cornering behaviour of the vehicle has changed from a predominantly oversteering vehicle to an understeering one, due to this system.

- The use of active systems, while generally restricted by the sporting regulations, does offer insight into the better choice of passive setting for the vehicle, if the maximisation of vehicle performance is used as the objective of the active control.

This thesis has identified gaps in the current practice of open wheel race car simulation, and the above findings are taken to be new contributions to the understanding of on-limit race car dynamic simulation.

8.5 Conclusions

Quasi steady state methods are capable of quantifying the effects of vehicle setup changes, for open wheel race cars, to a similar level of accuracy as a transient optimal result.

Numerical optimisation methods can be used to construct a quasi steady state, GG speed diagram based, laptime program that is capable of optimising vehicle parameters, for an acceptable computational effort. The optimised parameter values can be used to both understand on-limit vehicle behaviour, and to help determine vehicle parameter changes to minimise laptimes.

The path finding algorithm, in the minimum laptime calculation, can be replaced with a path following and imposed racing line algorithm with a significant computational advantage and minimal loss of accuracy, when compared with an optimised path finding result. This can be achieved using a quasi steady state vehicle history as a reference for the path following algorithm.

8.6 Further work

The use of vehicle stability control systems should be explored. A new transient path following method and a case study using sideslip angle control are provided in Appendices D and E of this thesis as an initial exploration into this area of research. Further work is required to conclusively decide on the usefulness of vehicle stability control in the racing environment.

The development of a linear quadratic tracker/regulator optimal control based method is possible using a linearised form of the seven degree of freedom model about a trimmed steady state point. This would allow the optimisation of two parameters, if the current system of steer angle and throttle control were maintained as the only control inputs to the system. The simulation would integrate the nonlinear equations of motion, and then, at each time step, the values of the state vector and control inputs would be passed to the linearised model, to find the control perturbations to minimise an optimal control objective. The value in pursuing this line of research is that it could provide a real-time optimisation method that could be practically implemented on a race car. This type of approach is currently used in the real-time control of aircraft.

References

[1] D.A. Crolla. An introduction to vehicle dynamics. Vehicle dynamics group, Department of mechanical engineering, University of Leeds, UK, 1991.

[2] G. Genta. *Motor Vehicle Dynamics Modelling and Simulation*. Series on advances in mathematics for applied sciences. World Scientific Publishing, Singapore, 1997.

[3] D. Casanova. *On Minimum Time Vehicle Manoeuvring: The Theoretical Optimal Lap*. PhD thesis, School of Engineering, Cranfield University, 2000.

[4] M.W. Sayers. *Introductory guide to AUTOSIM Version 2.0*. The Regents of the University of Michigan, December 1992.

[5] J.P.M. Hendrikx, T.J.J. Meijlink, and R.F.C. Kriens. Application of optimal control theory to inverse simulation of car handling. *Vehicle System Dynamics*, 26:449–462, 1996.

[6] B. Siegler, A. Deakin, and D. Crolla. Lap time simulation: Comparison of steady state, quasi-static and transient racing car cornering strategies. In *Proceedings of the 2000 SAE Motorsports Engineering Conference and Exposition*, number SAE:2000-01-3563. Society of Automotive Engineers, 2000.

[7] A. Candelpergher, M. Gadola, and D. Vetturi. Developments of a method for lap time simulation. In *Proceedings of the 2000 SAE Motorsports Engineering Conference and Exposition*, number SAE:2000-01-3562. Society of Automotive Engineers, 2000.

[8] J.R. Blasco-Figueroa. Minimum time manoeuvre based on the g-g-speed envelope. Master's thesis, School of Engineering, Cranfield University, 2000.

[9] M. Muehlmeier and N. Mueller. Optimization of the driving line on a race track. In *Proceedings of the 2002 SAE Motorsports Engineering Conference and Exposition*, number SAE:2002-01-3339. Society of Automotive Engineers, 2002.

[10] T. Butz, M. Ehmann, O. von Stryk, and T. Wolter. Realistic road modelling for the real-time simulation of vehicle dynamics. *Automobiltechnische Zeitschrift*, 106:118–125, February 2004.

[11] W.F Milliken and D.L Milliken. *Race car vehicle dynamics*. Society of Automotive Engineers, 400 Commonwealth Drive, Warrendale, PA 15096-001 U.S.A, 1995.

[12] P Wright. *Formula 1 Technology*. Society of Automotive Engineers, 400 Commonwealth Drive, Warrendale, PA 15096-001 U.S.A, 2001.

[13] ADAMS Software - http://www.mscsoftware.com/products/products_detail.cfm, Accessed Nov 8 2004.

[14] T. Fujioka and T. Kimura. Numerical simulation of minimum-time cornering behaviour. *JSAE Review*, 13(1):44–51, 1992.

[15] J.E. La Joie. Race car performance optimization. Technical Report SAE:942492, Society of Automotive Engineers, 1994.

[16] J. Allen. Computer optimisation of cornering line. Master's thesis, School of Engineering, Cranfield University, 1997.

[17] G.R. Walsh. *Methods of Optimization*. John Wiley and Sons, 1977.

[18] H.B. Pacejka and I.J.M Besselink. Magic formula tyre model with transient properties. *Vehicle System Dynamics Supplement*, 27:234–249, 1997.

[19] D. Casanova, R.S. Sharp, and P. Symonds. On minimum time optimisation of formula one cars: the influence of vehicle mass. In *Proceedings of AVEC'2000, International Symposium on Advanced Vehicle Control*, Ann Arbor Michigan, USA, August 2000.

[20] D. Casanova, R.S. Sharp, and P. Symonds. On the optimisation of the longitudinal location of the mass centre of a formula one car for two circuits. In *Proceedings of AVEC'2002, International Symposium on Advanced Vehicle Control*, Hiroshima, Japan, September 2002.

[21] D. Casanova, R.S. Sharp, and P. Symonds. Minimum time manoeuvring: The significance of yaw inertia. *Vehicle System Dynamics*, 34(2):77–115, 2000.

[22] R Griffiths. Minimum lap time simulation of a racing car. Master's thesis, School of Mechanical Engineering, Cranfield University, September 1992.

[23] A. Murdoch. 'G G' speed surface approach to minimum lap time simulation. Master's thesis, School of Mechanical Engineering, Cranfield University, September 2001.

[24] T Coleman, M.A. Branch, and A Grace. Matlab optimisation toolbox version 2 user guide. Technical report, Mathworks, 24 Prime Park Way, Natick, MA 01760-1500, 1999.

[25] F.L. Lewis and V.L. Syrmos. *Optimal control*. John Wiley and Sons Inc, 605 Third Avenue, New York, NY 10158-0012 U.S.A., 2nd edition, 1995.

[26] H. W. Kuhn and A. W. Tucker. Nonlinear programming. In Jerzy Neyman, editor, *Proceedings of the Second Berkeley Symposium on Mathematical Statistics and Probability*, pages 481–92. University of California Press,Berkeley, California, 1951.

[27] L.M. Hocking. *Optimal Control: An introduction to the theory with applications*. Oxford applied mathematics and computing science series. Oxford University Press, Oxford University Press, Walton Street, Oxford OX2 6DP, 1991.

[28] B. Wallace. Constrained optimization: Kuhn-tucker conditions. http://personal.rhul.ac.uk/ukte/148/teaching/ec5555/kt.pdf, Accessed 17 August 2004.

[29] W.H. Press, S.A. Teukolsky, W.T. Vetterling, and B.P. Flannery. *Numerical recipes in C: the art of scientific computing*. Cambridge University Press, 2nd edition, 1992.

[30] Symbolic Differentiation - http://www.cs.utexas.edu/users/novak/asg-symdif.html, Accessed July 27 2004.

[31] T Ringrose and S.A. Forth. Improved fitting of constrained multivariate regression models using automatic differentiation. In W Härdle and B Rönz, editors, *Compstat 2002 - Proceedings in computational statistics*, pages 1–6. Humboldt-Universität zu Berlin, 2002.

[32] A. Griewank. *Evaluating derivatives. Principles and techniques of algorithmic differentiation*. Society for industrial and applied mathematics, 2000.

[33] L. Segel. Theoretical prediction and experimental substantiation of the response of the automobile to steering control. In *Proceedings of the automobile division, Institute of Mechanical Engineers*, pages 310–330, 1956-1957.

[34] B. Siegler and D. Crolla. Lap time simulation for racing car design. In *Proceedings of the SAE 2002 World Congress and Exhibition*, number SAE:2002-01-0567. Society of Automotive Engineers, 2002.

[35] J.Y. Wong. *Theory of ground vehicles*. John Wiley and Sons Inc, 605 Third Avenue, New York, NY 10158-0012 U.S.A., 2nd edition, 1993.

[36] SAE Vehicle Dynamics Committee. Vehicle dynamics terminology -SAE J670. Society of Automotive Engineers, July 1976.

[37] J-H Jang and C-S Han. The sensitivity analysis of lateral acceleration for the front wheel steering vehicle in the frequency domain. *International Journal of Vehicle Design*, 19(4):415–435, 1998.

[38] J.C. Dixon. *Tires, suspension and handling*. Society of Automotive Engineers, 400 Commonwealth Drive, Warrendale, PA 15096-001 U.S.A., 2nd edition, 1996.

[39] J.R. Ellis. *Vehicle dynamics*. London business books, London, 1969.

[40] A. Staniforth. *Competition car suspension design, construction, tuning*. Haynes publishing, 3rd edition, 1999.

[41] D. Metz and J. Maddock. Optimal ride height and pitch control for championship race cars. *Automatica*, 22(5):509–520, 1986.

[42] S.H. Lee, U.K. Lee, and C.S. Han. Enhancement of vehicle handling characteristics by suspension kinematic control. In *Proceedings of the Institute of*

Mechanical Engineers Part D: Journal of Automotive Engineering, volume 215, pages 197–216, 2001.

[43] J.C. Dixon. The roll-centre concept in vehicle handling dynamics. *Journal of Automotive Engineering, Institute of Mechanical Engineers*, 201(D1):69–78, 1987.

[44] D.A. Crolla. Vehicle dynamics. Vehicle dynamics group, Department of mechanical engineering, University of Leeds, UK, 2004.

[45] Formula One regulations - http://www.fia.com/sport/Regulations/f1regs.html, Accessed Nov 8 2004.

[46] S.E. Chocholek. The development of a differential for the improvement of traction control. In T.P. Newcomb, editor, *Traction Control and Anti-wheel-spin Systems for Road Vehicles*, number 6, pages 75–82, Birdcage Walk, London, March 1988. IMechE, Mechanical Engineering Publications Ltd.

[47] K. Ise, K. Fujita, Y. Inoue, and S. Masutomi. The "lexus" traction control TRAC system. In R. Cass, D. Hodgson, R. Newton, and M. Rowell, editors, *ABS Traction Control and Brake Components*, number SP-90/815, pages 153–160, 400 Commonwealth Drive, Warrendale, PA 15096-0001, February 1990. SAE international.

[48] R. Holzwarth and K. May. Analysis of traction control systems augmented by limited slip differentials. In R.K. Urgent, editor, *Electronic braking, traction, and stability control*, number PT-76 in Automotive electronics series, pages 277–285. Society of Automotive Engineers, Inc., 1999.

[49] E.A. Jackson. *Perspectives of nonlinear dynamics*. Cambridge University Press, 40 West 20th Street, New York, NY 10011-4211, U.S.A., 1995.

[50] S. Park and M.G. Nagati. Approximate decoupling flight control design with output feedback. *Journal of Guidance, Control, and Dynamics*, pages 897–902, 1997.

[51] M. Paus. A general approach to optimal real-time guidance of dynamic systems based on nonlinear programming. In *AIAA Guidance, Navigation and Control Conference - Part 1*, number AIAA-92-4378-CP, pages 297–305, 1992.

[52] W.F. Milliken and D.L. Milliken. *Chassis design principles and analysis based on previously unpublished technical notes by Maurice Olley.* Society of Automotive Engineers, 400 Commonwealth Drive, Warrendale, PA 15096-001 U.S.A., 2002.

[53] H. Leffer. Traction control systems of different levels of complexity - a comparison of technical effort and system performance. In T.P. Newcomb, editor, *Braking of Road Vehicles*, number 2, pages 69–80, Birdcage Walk, London, March 1993. IMechE, Mechanical Engineering Publications Ltd.

[54] H.E. Tseng, B. Ashrafi, D. Madau, T.A. Brown, and D. Recker. The development of vehicle stability control at Ford. *IEE/ASME Transactions on Mechatronics*, 4(3):223–234, September 1999.

[55] O. Mokhiamar and M. Abe. Active wheel steering and yaw moment control combination to maximise stability as well as vehicle responsiveness during quick lane change for active vehicle handling safety. In *Proceedings of the Institute of Mechanical Engineers Part D: Journal of Automotive Engineering*, volume 216, pages 115–124, 2002.

[56] K. Yi, T. Chung, J. Kim, and S. Yi. An investigation into differential braking strategies for vehicle stability control. In *Proceedings of the Institute of Mechanical Engineers Part D: Journal of Automotive Engineering*, volume 217, pages 1081–1093, 2003.

[57] J.H. Park and C.Y. Kim. Wheel slip control in traction control system for vehicle stability. *Vehicle System Dynamics*, 31:263–278, 1999.

[58] E. Gerum. A highly dynamic anti-wheel-spin system. In T.P. Newcomb, editor, *Traction Control and Anti-wheel-spin Systems for Road Vehicles*, number 6, pages 135–140, Birdcage Walk, London, March 1988. IMechE, Mechanical Engineering Publications Ltd.

[59] H. Wallentowitz, G. Egger, E. Herb, and H. Krushche. Stability and traction control for four-wheel-drive passenger vehicles. In T.P. Newcomb, editor, *Traction Control and Anti-wheel-spin Systems for Road Vehicles*, number 6, pages 49–60, Birdcage Walk, London, March 1988. IMechE, Mechanical Engineering Publications Ltd.

[60] G.P.R. Farr. A simple traction control. In T.P. Newcomb, editor, *Traction Control and Anti-wheel-spin Systems for Road Vehicles*, number 6, pages 95–102, Birdcage Walk, London, March 1988. IMechE, Mechanical Engineering Publications Ltd.

[61] A. Sigl and A. Czinczel. ABS/ASR5 - the new ABS/ASR5 system for passenger cars. In T.P. Newcomb, editor, *Braking of Road Vehicles*, number 2, pages 81–88, Birdcage Walk, London, March 1993. IMechE, Mechanical Engineering Publications Ltd.

[62] H.J. Kraft and H. Leffler. The integrated brake and stability control system of the new BMW 850i. In R. Cass, D. Hodgson, R. Newton, and M. Rowell, editors, *ABS Traction Control and Brake Components*, number SP-90/815, pages 71–78, 400 Commonwealth Drive, Warrendale, PA 15096-0001, February 1990. SAE international.

[63] A. Sigl and H. Demel. ASR-Traction Control, state of the art and some prospects. In R. Cass, D. Hodgson, R. Newton, and M. Rowell, editors, *ABS Traction Control and Brake Components*, number SP-90/815, pages 71–78, 400 Commonwealth Drive, Warrendale, PA 15096-0001, February 1990. SAE international.

[64] Y. Inoue, H. Minegishi, and H Miyazaki. A traction control system for use in rear-wheel-drive vehicles with automatic transmissions. In T.P. Newcomb, editor, *Traction Control and Anti-wheel-spin Systems for Road Vehicles*, number 6, pages 61–69, Birdcage Walk, London, March 1988. IMechE, Mechanical Engineering Publications Ltd.

[65] E. Gohring and E.C. von Glasner. Improvements in traction and stability performance as seen by the commercial vehicle manufacturer. In T.P. Newcomb, editor, *Traction Control and Anti-wheel-spin Systems for Road Vehicles*, number 6, pages 13–22, Birdcage Walk, London, March 1988. IMechE, Mechanical Engineering Publications Ltd.

[66] B.G. Schultz and E. Lissel. Anti-slip-regulator system (ASR) with high performance and comfort. In T.P. Newcomb, editor, *Traction Control and Anti-wheel-spin Systems for Road Vehicles*, number 6, pages 69–74, Birdcage Walk, London, March 1988. IMechE, Mechanical Engineering Publications Ltd.

[67] K. Lyon, M. Philipp, and E. Grommes. Traction control for a formula 1 race car: Conceptual design, algorithm development. In R.K. Urgent, editor, *Electronic braking, traction, and stability control*, number PT-76 in Automotive electronics series, pages 333–343. Society of Automotive Engineers, Inc., 1999.

[68] P.A. Beever and C. Wiehen. The introduction of electronic traction for range-rover. In T.P. Newcomb, editor, *Braking of Road Vehicles*, number 2, pages 89–98, Birdcage Walk, London, March 1993. IMechE, Mechanical Engineering Publications Ltd.

[69] H. Leffler, R. Auffhammer, R. Heyken, and H. Roth. New driving stability control system with reduced technical effort for compact and medium class passenger cars. In R.K. Jurgen, editor, *Electronic braking, traction, and stability control*, number PT-76 in Automotive electronics series, pages 365–372. Society of Automotive Engineers, Inc., 1999.

[70] A. Seireg and H. El-Deen. Integrating mechanics and electronics to prevent skidding on icy roads. In R. Cass and M. Rowell, editors, *ABS Traction Control*, number SP-744, pages 89–94, 400 Commonwealth Drive, Warrendale, PA 15096-0001, February 1988. SAE international.

[71] S.K. Mohan and R.C. Williams. A survey of 4WD traction control systems and strategies. In R.K. Jurgen, editor, *Electronic braking, traction, and stability control*, number PT-76 in Automotive electronics series, pages 345–362. Society of Automotive Engineers, Inc., 1999.

[72] A.T. van Zanten, R. Erhardt, and G. Pfaff. VDC, the vehicle dynamics control system of Bosch. In R.K. Jurgen, editor, *Electronic braking, traction, and stability control*, number PT-76 in Automotive electronics series, pages 395–412. Society of Automotive Engineers, Inc., 1999.

[73] A. Nishio, K. Tozu, H. Yamaguchi, K. Asano, and Y. Amano. Development of vehicle stability control system based on vehicle sideslip angle estimation. In *Vehicle Dynamics and Simulation*, number SAE:2001-01-0137. Society of Automotive Engineers, 2001.

[74] A. Hac and M.D. Simpson. Estimation of vehicle side slip angle and yaw rate. In *Vehicle Dynamics and Simulation*, number SAE:2000-01-0696. Society of Automotive Engineers, 2000.

[75] J. Ryu, E.J. Rossetter, and J. Christian Gerdes. Vehicle sideslip and roll parameter estimation using GPS. In *Proceedings of AVEC'2002, International Symposium on Advanced Vehicle Control*, Hiroshima, Japan, September 2002.

[76] A.Y. Ungoren, H. Peng, and H.E. Tseng. Experimental verification of lateral speed estimation methods. In *Proceedings of AVEC'2002, International Symposium on Advanced Vehicle Control*, Hiroshima, Japan, September 2002.

[77] Y. Shibahata, K. Shimada, and T. Tomari. Improvement of vehicle manoeuverability by direct yaw moment control. *Vehicle System Dynamics*, 22:465–481, 1993.

[78] A.T. van Zanten, K. Erhardt, R. Landesfeind, and G. Pfaff. VDC systems development and perspective. In R.K. Jurgen, editor, *Electronic braking, traction, and stability control*, number PT-76 in Automotive electronics series, pages 373–394. Society of Automotive Engineers, Inc., 1999.

[79] J. How, N. Pohlman, and C-W. Park. GPS estimation algorithms for precise velocity, slip and race-track position measurements. In *Proceedings of the 2000 SAE Motorsports Engineering Conference and Exposition*, number SAE:2002-01-3336. Society of Automotive Engineers, 2002.

[80] M Gadola, D Vetturi, D Cambiaghi, and L Manzo. A tool for lap time simulation. Technical Report SAE:962529, Society of Automotive Engineers, 1996.

[81] G. Prokop. Modelling human vehicle driving by model predictive online optimization. *Vehicle System Dynamics*, 35(1):19–53, 2001.

[82] K Guo and H. Guan. Modelling of driver/vehicle directional control system. *Vehicle System Dynamics*, 22(3–4):141–184, 1993.

[83] M. Tomizuka and D.E. Whitney. The human operator in manual preview tracking (an experiment and its modelling via optimal control). *Journal of Dynamic Systems, Measurement and Control*, pages 407–413, 1976.

[84] G. Prokop and R.S. Sharp. Performance enhancement of limited bandwidth active automotive suspensions by road preview. *IEE Proceedings - Control Theory and Applications*, 142(2):140–148, 1995.

[85] R.S. Sharp, D. Casanova, and P. Symonds. A mathematical model for driver steering control, with design, tuning and performance results. *Vehicle System Dynamics*, 33:289–326, 2000.

[86] R.S. Sharp and V. Valtetsiotis. Optimal preview car steering control. In H. Aref and J.W. Phillips, editors, *Mechanics for a New Millenium - The 20th International Congress of Theoretical and Applied Mechanics*, pages 101–117, Chicago, MI, U.S.A, 2000.

[87] D.L. Brayshaw and M.F. Harrison. The driver's control of high performance vehicles on the limit, the influence of vehicle setup, and the effects of active chassis systems. In P.R.N Childs and R.K. Stobart, editors, *Proceedings of the Total Vehicle Technology Conference*, pages 3–13, University of Sussex, Brighton, U.K., 2004.

[88] S.A. Forth. MAD - a matlab automatic differentiation toolbox, version 1, beta release, the forward mode. Technical Report AMOR Report 2001/5, RMCS Shrivenham, Cranfield University, 2001.

[89] D.L. Brayshaw, M.F. Harrison, and A.P. Moore. The effects of optimal differential control on the performance of open wheel race cars. In refereeing: Journal of Automotive Engineering, Institute of Mechanical Engineers.

[90] G.H. Ryder and M.D. Bennett. *Mechanics of Machines*. Macmillan Education Ltd, Houndmills, Basingstoke, Hampshire RG21 2XS, 2nd edition, 1990.

[91] Z.J. Jania. Friction-clutch transmissions - factors in clutch performance. *Machine Design*, pages 132–136, November 1958.

[92] D.L. Brayshaw and M.F. Harrison. A quasi steady state approach to race car lap simulation to better understand optimal racing line and centre of gravity location. In refereeing: Journal of Automotive Engineering, Institute of Mechanical Engineers.

[93] P.G Wright. The influence of aerodynamics on the design of formula one racing cars. *International journal of vehicle design*, 3(4):383–397, Nov 1982.

[94] T.D. Gillespie. *Fundamentals of Vehicle dynamics*. Society of Automotive Engineers, 400 Commonwealth Drive, Warrendale, PA 15096-001 U.S.A, 1992.

[95] M. Gadola, A. Candelpergher, D Armellin, and R. Adami. The impact of non-linear aerodynamics on racecar behavior and lap time simulation. In *Proceedings of the 2002 SAE Motorsports Engineering Conference and Exposition*, number SAE:2002-01-3339. Society of Automotive Engineers, 2002.

[96] J. Wildi. Wind tunnel testing of racing cars - the importance of the road simulation technique. In *Vehicle aerodynamics*, pages 11.1–11.12. The royal aeronautical society, Loughborough University of Technology, 1994.

[97] J. Katz and D. Garcia. Aerodynamic effects of indy car components. Technical Report SAE:2002-01-3311, Society of Automotive Engineers, 2002.

[98] N.H. Sledge Jr and K.M. Marshek. Comparison of ideal vehicle lane-change trajectories. In *Research into Vehicle Dynamics and Simulation*, number SAE:971062, pages 233–256, 1997.

[99] S.K. Clark. *Mechanics of pneumatic tires*. Office of Vehicle Systems Research, Institute for Applied Technology, National Bureau of Standards, 1971.

[100] B.L. Collier and J.T. Warchol. The effect of inflation pressure on bias,bias-belted and radial tire performance. In *SAE Congress and Exposition, Cobo Hall, Detroit*, number SAE:800087, 400 Commonwealth Drive, Warrendale, PA 15096-001 U.S.A., 1980. Society of Automotive Engineers.

[101] G.H. Nybakken, R.N. Dodge, and S.K. Clark. A study of dynamic tire properties over a range of tire constructions. Technical Report NASA CR-2219, University of Michigan, Ann Arbor, Michigan, 48105, 1973.

[102] E. Bakker, L. Nyborg, and H. Pacejka. Tyre modelling for use in vehicle dynamics studies. Technical Report SAE:870421, Society of Automotive Engineers, 400 Commonwealth Drive, Warrendale, PA 15096-001 U.S.A., 1987.

[103] E. Bakker, H. Pacejka, and L. Lidner. A new tire model with an application in vehicle dynamics studies. Technical Report SAE:890087, Society of Automotive Engineers, 400 Commonwealth Drive, Warrendale, PA 15096-001 U.S.A., 1989.

[104] J. Katz. *Race Car Aerodynamics - Designing for speed*. Robert Bentley, 1734 Massachusetts Avenue, MA 02138 U.S.A, 1995.

[105] P Wright. *Ferrari Formula 1.* David Bull Publishing, 4250 East Camelback Road, Phoenix, AZ 85018, U.S.A., 2003.

[106] K Ludvigsen. *Classic Grand Prix Cars - The Front-Engined Formula One Era 1906-1960.* Sutton Publishing, 2000.

[107] H.B. Pacejka. Principles of plane motions of automobiles. In H.B. Pacejka, editor, *Proceedings of IUTAM symposium on the dynamics of vehicles on roads and on tracks*, pages 33–59, Amsterdam, 1976. Delft University, Swets and Zietlinger.

[108] I. Ebert-Uphoff and K. Kozak. Review of the role of quasi-coordinates for the kinematic and dynamic modelling of parallel manipulators. In C.M. Gosselin and I. Ebert-Uphoff, editors, *Fundamental issues and future research directions for parallel mechanisms and manipulators*, pages 328–338, Quebec City, Quebec, Canada, October 2002. The National Science Foundation and The Ministry of Research, Science and Technology of the Qubec Government, http://robot.me.gatech.edu/WORKSHOP/workshop.html. accessed at 2:41pm June 2nd, 2003.

[109] R.S. Sharp. The application of multi-body computer codes to road vehicle dynamics modelling problems. In *Proceedings of the Institute of Mechanical Engineers Part D: Journal of Automotive Engineering*, volume 208, pages 55–61, 1994.

[110] M.F. Harrison. *Vehicle Refinement: controlling noise and vibration in road vehicles.* Butterworth-Heinemann, 1st edition, 2004.

[111] G.H. Farrington. *Fundamentals of Automatic Control.* Chapman and Hall, 37 Essex Street, London, UK, 1951.

[112] D.L. Brayshaw. Virtual vehicle manoeuvring - first year review report. June 2002.

[113] D.P. Eckman. *Automatic Process Control.* John Wiley and Sons, Inc, 1958.

[114] R.P. Hunter. *Automated Process Control Systems : Concepts and Hardware.* Prentice-Hall Inc, Englewood Cliffs, New Jersey 07632, USA, 1978.

[115] S. Motoyama, H. Uki, K. Isoda, and H. Yuasa. Effect of traction force distribution control on vehicle dynamics. *Vehicle System Dynamics*, 22:455–464, 1993.

Appendix A

A.1 Seven Degree of Freedom Model Derivation

A.1.1 Assumptions

The vehicle is considered to consist of a rigid body with a longitudinal plane of symmetry, joined by perfectly stiff links to the wheel assemblies. Wheel assemblies are assumed to be rigid discs, to be following a flat surface, and to rotate, but not move laterally with respect to the body. Main body can translate but not pitch or roll. However, the body can rotate in the plane creating a yaw of the main body.

At the centre of mass of the body lies the origin, o', of the axes o', ξ, η, ζ which moves with the body. The axis o', ξ, η, ζ is a right handed, orthogonal set. This axis is described with reference to another right handed, orthogonal (earth centred) axis set o, x, y, φ in which o is in the road surface with o, φ vertically downwards.

Vehicle differential and engine are represented as separate bodies but their motion is constrained to be a function of the existing main body and wheel based generalised coordinates. As a result these two bodies do not contribute to the degrees of freedom of the model.

A.2 The Special Equations of Motion - Derivation

This derivation draws heavily on the generalised derivation of the special equations of motion by Pacejka [107]. This is a specific case for the seven degree of freedom model as used by Casanova [3] which was originally derived using the multibody code generation program, AutoSIM.

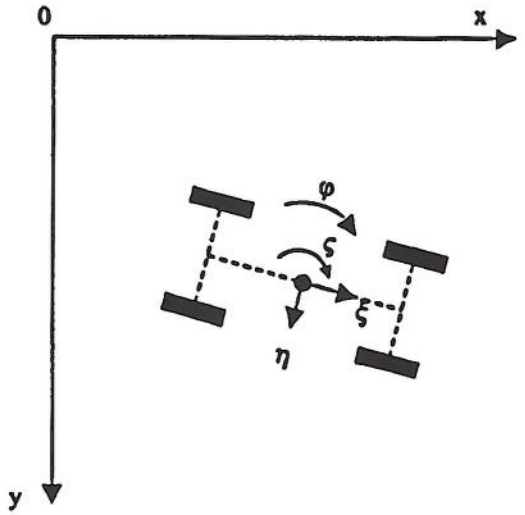

Figure A.1: Vehicle and earth centred axes.

The equations of motion in terms of the true coordinates are readily obtained by applying the equations of Lagrange:

$$\frac{d}{dt}\left(\frac{\partial T}{\partial \dot{q}_i}\right) - \frac{\partial T}{\partial q_i} + \frac{\partial U}{\partial q_i} = Q_i \tag{A.1}$$

Where q represents the generalised coordinates, Q represents the appropriate externally applied "generalised force", T represents the kinetic energy of the system and U represents the potential energy of the system.

In this system, the generalised coordinates, q_i, are defined as follows:

$q_1 = x$

$q_2 = y$

$q_3 = \varphi$

$q_4 = \theta_1$ (Front Left Wheel Position)

$q_5 = \theta_2$ (Front Right Wheel Position)

$q_6 = \theta_3$ (Rear Left Wheel Position)

$q_7 = \theta_4$ (Rear Right Wheel Position)

The kinetic and potential energy of the system are functions of these coordinates and time and can be expressed as follows:

$$T = f(q_3, q_4, q_5, q_6, q_7; \dot{q}_1, \dot{q}_2, \dot{q}_3, \dot{q}_4, \dot{q}_5, \dot{q}_6, \dot{q}_7; t) \tag{A.2}$$

$$U = 0 \tag{A.3}$$

$$Q_i = f(q_3, q_4, q_5, q_6, q_7; \dot{q}_1, \dot{q}_2, \dot{q}_3, \dot{q}_4, \dot{q}_5, \dot{q}_6, \dot{q}_7; t) \tag{A.4}$$

The generalised force, Q_i, belongs to the generalised coordinate q_i and is obtained from the virtual work δW, executed by external forces not derivable from a potential function.

$$\delta W = \sum_i Q_i \delta q_i \tag{A.5}$$

The customary Lagrangian equations are now left here, and the special equations are derived. The following (transposed) vectors are introduced:

$$\bar{q}^T = (x, y, \varphi, \theta_1, \theta_2, \theta_3, \theta_4) \tag{A.6}$$

$$\bar{v}^T = (u, v, r, \dot{\theta}_1, \dot{\theta}_2, \dot{\theta}_3, \dot{\theta}_4) \tag{A.7}$$

Their relation is

$$\bar{v} = \bar{A}\dot{\bar{q}} \tag{A.8}$$

Where the 7 by 7 transformation matrix $\bar{A}$ reads:

$$\bar{A} = \begin{bmatrix} \cos\varphi & \sin\varphi & 0 & 0 & 0 & 0 & 0 \\ -\sin\varphi & \cos\varphi & 0 & 0 & 0 & 0 & 0 \\ 0 & 0 & 1 & 0 & 0 & 0 & 0 \\ 0 & 0 & 0 & 1 & 0 & 0 & 0 \\ 0 & 0 & 0 & 0 & 1 & 0 & 0 \\ 0 & 0 & 0 & 0 & 0 & 1 & 0 \\ 0 & 0 & 0 & 0 & 0 & 0 & 1 \end{bmatrix} = \begin{bmatrix} \alpha_{11} & \cdots & \alpha_{1n} \\ . & & \\ . & & \\ . & & \\ . & & \\ . & & \\ \alpha_{n1} & & \end{bmatrix} \tag{A.9}$$

It can also be written that:

$$v_j = \sum_{i=1}^{n} \alpha_{ji} \dot{q}_i \qquad (j = 1, 2 \ldots 7) \tag{A.10}$$

Now the quantities dp_j are introduced. These are similarly related to the differentials dq_i:

$$dp_j = \sum_{i=1}^{n} \alpha_{ji} dq_i \tag{A.11}$$

These equations are not immediately integrable for $j = 1$ and $j = 2$ since the relations

$$\frac{\partial \alpha_{kj}}{\partial q_L} = \frac{\partial \alpha_{Lj}}{\partial q_k}$$

for $(j = 1,2)$ are not satisfied for all values of k and L. We shall call, therefore, $v_1 = u$ and $v_2 = v$. These are the time derivatives of the *quasi*[1] coordinates $p_1 = \xi$ and $p_2 = \eta$ respectively. The remaining p's are true coordinates.

From Equation A.11 we may solve dq_i and obtain:

$$dq_i = \sum_{j=1}^{n} B_{ij} dp_j \tag{A.12}$$

In this case, $B_{ij} = \alpha_{ji}$. Also:

$$\dot{q}_i = \sum_j B_{ij} v_j$$

or

$$\dot{q}_i = \sum_j \alpha_{ji} v_j$$

The virtual work done by external forces in an infinitesimal displacement may be expressed in terms of increments δq_i or δp_j

$$\begin{aligned} \delta W &= \sum_i Q_i \delta q_i = \sum_i Q_i \sum_j B_{ij} \delta p_j \\ &= \sum_j \sum_i Q_i B_{ij} \delta p_j \\ &= \sum_j P_j \delta p_j \end{aligned}$$

The coefficient of δp_j is the force which does the work in the displacement δp_j. We shall call this coefficient the generalised force P_j belonging to the quasi or true generalised coordinate p_j. We have

$$P_j = \sum_i B_{ij} Q_i$$

[1] A quasi coordinate, is a coordinate for which only the time derivative of the coordinate must have a physical meaning. The time derivative is called a quasi-velocity in so far that if the quasi coordinate, u, was integrated the position of the vehicle cannot be retrieved from it [108].

An equation of motion with P_j forming the right hand side is established by multiplying the n lagrangian equations (Equation A.1) with the respective B_{ij}'s and adding to give:

$$\sum_i B_{ij}\left\{\frac{d}{dt}\left(\frac{\partial T}{\partial \dot{q}_i}\right)-\frac{\partial T}{\partial q_i}+\frac{\partial U}{\partial q_i}\right\}=\sum_i B_{ij}Q_i=P_j \qquad (j=1...7) \qquad (A.13)$$

We shall now introduce the function $\bar{T}$ denoting the kinetic energy expressed in terms of the v's and q's. In this case:

$$\bar{T}=f(q_3,q_4,q_5,q_6,q_7;v_1,v_2,v_3,v_4,v_5,v_6,v_7;t) \qquad (A.14)$$

It is recalled that if $i \geq 3$, then the p's are true coordinates, i.e $p_i = q_i$.

With Equation A.10:

$$\frac{\partial T}{\partial \dot{q}_i}=\sum_k \frac{\partial \bar{T}}{\partial v_k}\times\frac{\partial v_k}{\partial \dot{q}_i} \qquad (A.15)$$

$$\frac{\partial T}{\partial \dot{q}_i}=\sum_k \frac{\partial \bar{T}}{\partial v_k}\times\alpha_{ki} \qquad (A.16)$$

Consequently, Equation A.13 becomes:

$$\sum_i\sum_k B_{ij}\left\{\alpha_{ki}\frac{d}{dt}\left(\frac{\partial \bar{T}}{\partial v_k}\right)+\frac{\partial \bar{T}}{\partial v_k}\frac{d\alpha_{ki}}{dt}\right\}-\sum_i B_{ij}\left\{\frac{\partial T}{\partial q_i}-\frac{\partial U}{\partial q_i}\right\}=P_j \qquad (A.17)$$

But

$$\sum_i B_{ij}\alpha_{ki}=\delta jk\left\{\begin{array}{l}=1 \text{ if } j=k\\=0 \text{ if } j\neq k\end{array}\right\}$$

So that Equation A.17 reduces to

$$\frac{d}{dt}\left(\frac{\partial \bar{T}}{\partial v_j}\right)+\sum_i\sum_k B_{ij}\frac{\partial \bar{T}}{\partial v_k}\frac{d\alpha_{ki}}{dt}-\sum_i B_{ij}\left\{\frac{\partial T}{\partial q_i}-\frac{\partial U}{\partial q_i}\right\}=P_j \qquad (A.18)$$

Furthermore,

$$\frac{\partial T}{\partial q_i}=\frac{\partial \bar{T}}{\partial q_i}+\sum_k\frac{\partial \bar{T}}{\partial v_k}\frac{\partial v_k}{\partial q_i}=\frac{\partial \bar{T}}{\partial q_i}+\sum_k\sum_l\frac{\partial \bar{T}}{\partial v_k}\frac{\partial \alpha_{kl}}{\partial q_i}\dot{q}_l \qquad (A.19)$$

and also

$$\frac{d\alpha_{ki}}{dt}=\sum_l\frac{\partial \alpha_{ki}}{\partial q_l}\dot{q}_l \qquad (A.20)$$

Substitution into Equation A.18 yields with $\dot{q}_l = \sum B_{lm}v_m$

$$\frac{d}{dt}\left(\frac{\partial \bar{T}}{\partial v_j}\right)+\sigma_j-\sum_i B_{ij}\left(\frac{\partial \bar{T}}{\partial q_i}-\frac{\partial U}{\partial q_i}\right)=P_j \tag{A.21}$$

In which, for abbreviation, the symbol σ_j for the second term has being used:

$$\sigma_j=\sum_k\sum_m \gamma_{jkm} v_m \frac{\partial \bar{T}}{\partial v_k} \tag{A.22}$$

where

$$\gamma_{jkm}=\sum_i\sum_l B_{ij}B_{lm}\left(\frac{\partial \alpha_{kl}}{\partial q_l}-\frac{\partial \alpha_{kl}}{\partial q_i}\right) \tag{A.23}$$

For this system $B_{ij}=\delta_{ij}$ for i or $j \geq 3$. Moreover $\bar{T}$ and U are independent of q_1 and q_2. The third term of Equation A.21 may therefore be replaced by

$$-\frac{\partial(\bar{T}-U)}{\partial q_j}$$

So that

$$\frac{d}{dt}\frac{\partial \bar{T}}{\partial v_j}+\sigma_j-\frac{\partial(\bar{T}-U)}{\partial q_j}=P_j \tag{A.24}$$

The term σ_j, containing γ_{jkm} can be reduced by considering the fact that in this problem:

$$\frac{\partial \alpha_{kp}}{\partial q_s}=0 \quad \text{for} \quad s\neq 3 \quad \text{and for} \quad p\geq 3$$

Hence Equation A.23 becomes

$$\gamma_{jkm}=\sum_{i=1}^{2}(B_{ij}B_{3m}-B_{3j}B_{im})\frac{\partial \alpha_{ki}}{\partial q_3} \tag{A.25}$$

The expression for $B_{ij}=\alpha_{ji}$ was noted earlier. We also note that for $j>3$ the quantity A.25 vanishes. Correspondingly, $m>3$ and $k>2$ also cause A.25 to vanish. The term σ_j can be reduced by utilising these facts.

Inspection of the possible combinations, will determine if the coefficients of Equation A.25 will provide a non zero result and reduce the computations.

γ_{jkm}	$(j=1)$	$k=1 or 2$		
$(B_{11}B_{31}-B_{31}B_{11})$	+	$(B_{21}B_{31}-B_{31}B_{21})$	$=0$	*(m=1)*
$(B_{11}B_{32}-B_{31}B_{12})$	+	$(B_{21}B_{32}-B_{31}B_{22})$	$=0$	*(m=2)*
$(B_{11}B_{33}-B_{31}B_{13})$	+	$(B_{21}B_{33}-B_{31}B_{23})$	$\neq 0$	*(m=3)*

$$
\begin{array}{lcll}
\gamma_{jkm} & (j=2) & k=1 or 2 & \\
(B_{12}B_{31}-B_{32}B_{11}) & + & (B_{22}B_{31}-B_{32}B_{21}) & =0 \quad (m=1) \\
(B_{12}B_{32}-B_{32}B_{12}) & + & (B_{22}B_{32}-B_{32}B_{22}) & =0 \quad (m=2) \\
(B_{12}B_{33}-B_{32}B_{13}) & + & (B_{22}B_{33}-B_{32}B_{23}) & \neq 0 \quad (m=3)
\end{array}
$$

$$
\begin{array}{lcll}
\gamma_{jkm} & (j=3) & k=1 or 2 & \\
(B_{13}B_{31}-B_{33}B_{11}) & + & (B_{23}B_{31}-B_{33}B_{21}) & \neq 0 \quad (m=1) \\
(B_{13}B_{32}-B_{33}B_{12}) & + & (B_{23}B_{32}-B_{33}B_{22}) & \neq 0 \quad (m=2) \\
(B_{13}B_{33}-B_{33}B_{13}) & + & (B_{23}B_{33}-B_{33}B_{23}) & =0 \quad (m=3)
\end{array}
$$

So the only plausible values of γ_{jkm} are: $\gamma_{113}, \gamma_{123}, \gamma_{213}, \gamma_{223}, \gamma_{311}, \gamma_{312}, \gamma_{321}, \gamma_{322}$.

When we evaluate the actual values of γ_{jkm} from the plausible options, we get the following

$$
\begin{array}{lcccl}
\gamma_{113} = & -\sin\varphi(\cos\varphi) & + & \cos\varphi(\sin\varphi) & =0 \\
\gamma_{123} = & -\cos\varphi(\cos\varphi) & - & \sin\varphi(\sin\varphi) & =-(\cos\varphi)^2-(\sin\varphi)^2 \quad =-1 \\
\gamma_{213} = & -\sin\varphi(-\sin\varphi) & + & \cos\varphi(\cos\varphi) & =(\cos\varphi)^2+(\sin\varphi)^2 \quad =1 \\
\gamma_{223} = & -\cos\varphi(-\sin\varphi) & - & \sin\varphi(\cos\varphi) & =0 \\
\gamma_{311} = & -\sin\varphi(-\cos\varphi) & + & \cos\varphi(-\sin\varphi) & =0 \\
\gamma_{312} = & -\sin\varphi(\sin\varphi) & + & \cos\varphi(-\cos\varphi) & =-(\sin\varphi)^2-(\cos\varphi)^2 \quad -1 \\
\gamma_{321} = & -\cos\varphi(-\cos\varphi) & - & \sin\varphi(-\sin\varphi) & =(\cos\varphi)^2+(\sin\varphi)^2 \quad =1 \\
\gamma_{322} = & -\cos\varphi(\sin\varphi) & - & \sin\varphi(-\cos\varphi) & =0
\end{array}
$$

So on inspection we see that $\gamma_{123}, \gamma_{213}, \gamma_{312}, \gamma_{321}$ are non zero. The next step is to calculate the corresponding values of σ_j:

$$\sigma_1 = \gamma_{123} \times v_3 \frac{\partial \bar{T}}{\partial v_2} \tag{A.26}$$

$$\sigma_1 = -r \frac{\partial \bar{T}}{\partial v} \tag{A.27}$$

$$\sigma_2 = \gamma_{213} \times v_3 \frac{\partial \bar{T}}{\partial v_1} \tag{A.28}$$

$$\sigma_2 = r \frac{\partial \bar{T}}{\partial u} \tag{A.29}$$

$$\sigma_3 = \gamma_{321} \times \nu_1 \frac{\partial \bar{T}}{\partial \nu_2} + \gamma_{312} \times \nu_2 \frac{\partial \bar{T}}{\partial \nu_1} \tag{A.30}$$

$$\sigma_3 = u\frac{\partial \bar{T}}{\partial v} - v\frac{\partial \bar{T}}{\partial u} \tag{A.31}$$

By substituting these results into Equation A.24 the following special set of Lagrangian equations of motion referred to axes ξ and η moving over the horizontal (x,y) plane have been derived.

$$p_1 = \xi: \ \frac{d}{dt}\left(\frac{\partial \bar{T}}{\partial U}\right) - r\frac{\partial \bar{T}}{\partial v} = Q_\xi \ \ (= P_1) \tag{A.32}$$

$$p_2 = \eta: \ \frac{d}{dt}\left(\frac{\partial \bar{T}}{\partial v}\right) + r\frac{\partial \bar{T}}{\partial U} = Q_\eta \ \ (= P_2) \tag{A.33}$$

$$p_3 = q_3 = \varphi: \ \frac{d}{dt}\left(\frac{\partial \bar{T}}{\partial r}\right) + u\frac{\partial \bar{T}}{\partial v} - v\frac{\partial \bar{T}}{\partial u} = Q_\varphi \ \ (= Q_3) \tag{A.34}$$

$$p_4 = q_4 = \theta_1: \ \frac{d}{dt}\left(\frac{\partial \bar{T}}{\partial \theta_1}\right) - \frac{\partial \bar{T}}{\partial \theta_1} + \frac{\partial U}{\partial \theta_1} = Q_4 \tag{A.35}$$

Noting that as planar motion is assumed (i.e no pitch and roll) which includes the links between the body and the wheel assemblies, then $\frac{\partial U}{\partial q_j} = 0$. So carrying on:

$$p_5 = q_5 = \theta_2: \ \frac{d}{dt}\left(\frac{\partial \bar{T}}{\partial \theta_2}\right) - \frac{\partial \bar{T}}{\partial \theta_2} = Q_5 \tag{A.36}$$

$$p_6 = q_6 = \theta_3: \ \frac{d}{dt}\left(\frac{\partial \bar{T}}{\partial \theta_3}\right) - \frac{\partial \bar{T}}{\partial \theta_3} = Q_6 \tag{A.37}$$

$$p_7 = q_7 = \theta_4: \ \frac{d}{dt}\left(\frac{\partial \bar{T}}{\partial \theta_4}\right) - \frac{\partial \bar{T}}{\partial \theta_4} = Q_7 \tag{A.38}$$

A.3 Applying the Equations of Motion

Remembering that:

$$\bar{T} = f(q_3, q_4, q_5, q_6, q_7; \nu_1, \nu_2, \nu_3, \nu_4, \nu_5, \nu_6, \nu_7; t)$$

Which is also equivalent to:

$$\bar{T} = f(\varphi, \theta_1, \theta_2, \theta_3, \theta_4; \nu_1, \nu_2, \nu_3, \nu_4, \nu_5, \nu_6, \nu_7; t)$$

We need to find the kinetic energy of the vehicle in terms of these coordinates.

Based on our assumptions, kinetic energy can be produced through a translation in u or v directions, a rotation about $r(\varphi)$, and rotations about the four wheel assemblies and engine. The differential is assumed to contribute very little and is assumed to have a rotational inertia equal to zero.

Remembering that the engine speed is linked to the rear wheel speeds, the equation of $\bar{T}$ is:

$$\bar{T} = \frac{1}{2}m\dot{u}^2 + \frac{1}{2}m\dot{v}^2 + \frac{1}{2}I_{zz}\dot{r}^2 + \frac{1}{2}I_{FL}\dot{\theta}_1^{\,2} + \frac{1}{2}I_{FR}\dot{\theta}_2^{\,2} + \frac{1}{2}I_{RL}\dot{\theta}_3^{\,2} + \frac{1}{2}I_{RR}\dot{\theta}_4^{\,2} + \frac{1}{2}I_E\dot{\theta}_E^{\,2} \tag{A.39}$$

Where:

$$\dot{\theta}_E = \frac{(\dot{\theta}_3 + \dot{\theta}_4)}{2} \times G_R \tag{A.40}$$

So, firstly, we need to evaluate the necessary partial derivatives of the special Lagrange equations. We need to know:

$$\frac{\partial\bar{T}}{\partial u}, \frac{\partial\bar{T}}{\partial v}, \frac{\partial\bar{T}}{\partial r}, \frac{\partial\bar{T}}{\partial\theta_1}, \frac{\partial\bar{T}}{\partial\dot{\theta}_1}, \frac{\partial\bar{T}}{\partial\theta_2}, \frac{\partial\bar{T}}{\partial\dot{\theta}_2}, \frac{\partial\bar{T}}{\partial\theta_3}, \frac{\partial\bar{T}}{\partial\dot{\theta}_3}, \frac{\partial\bar{T}}{\partial\theta_4}, \frac{\partial\bar{T}}{\partial\dot{\theta}_4}.$$

Inspection of $\bar{T}$ shows that $\theta_1, \theta_2, \theta_3, \theta_4$ do not feature in A.39 and therefore:

$$\frac{\partial\bar{T}}{\partial\theta_1}, \frac{\partial\bar{T}}{\partial\theta_2}, \frac{\partial\bar{T}}{\partial\theta_3}, \frac{\partial\bar{T}}{\partial\theta_4} = 0$$

And:

$$\frac{\partial\bar{T}}{\partial u} = mu \tag{A.41}$$

$$\frac{\partial\bar{T}}{\partial v} = mv \tag{A.42}$$

$$\frac{\partial\bar{T}}{\partial r} = I_{ZZ}r \tag{A.43}$$

$$\frac{\partial\bar{T}}{\partial\dot{\theta}_1} = I_{FL}\dot{\theta}_1 \tag{A.44}$$

$$\frac{\partial\bar{T}}{\partial\dot{\theta}_2} = I_{FR}\dot{\theta}_2 \tag{A.45}$$

$$\frac{\partial\bar{T}}{\partial\dot{\theta}_3} = I_{RL}\dot{\theta}_3 + \frac{1}{4}I_E G_R^2(\dot{\theta}_3 + \dot{\theta}_4) \tag{A.46}$$

$$\frac{\partial \bar{T}}{\partial \dot{\theta}_4} = I_{RL}\dot{\theta}_4 + \frac{1}{4}I_E G_R^2(\dot{\theta}_3 + \dot{\theta}_4) \tag{A.47}$$

To complete the left hand side of the special equations we need to find:

$$\frac{d}{dt}\left(\frac{\partial \bar{T}}{\partial u}\right), \frac{d}{dt}\left(\frac{\partial \bar{T}}{\partial v}\right), \frac{d}{dt}\left(\frac{\partial \bar{T}}{\partial r}\right), \frac{d}{dt}\left(\frac{\partial \bar{T}}{\partial \dot{\theta}_1}\right), \frac{d}{dt}\left(\frac{\partial \bar{T}}{\partial \dot{\theta}_2}\right), \frac{d}{dt}\left(\frac{\partial \bar{T}}{\partial \dot{\theta}_3}\right), \frac{d}{dt}\left(\frac{\partial \bar{T}}{\partial \dot{\theta}_4}\right).$$

Again, these are quite simple:

$$\frac{d}{dt}\left(\frac{\partial \bar{T}}{\partial u}\right) = m\dot{u} \tag{A.48}$$

$$\frac{d}{dt}\left(\frac{\partial \bar{T}}{\partial v}\right) = m\dot{v} \tag{A.49}$$

$$\frac{d}{dt}\left(\frac{\partial \bar{T}}{\partial r}\right) = I_{ZZ}\dot{r} \tag{A.50}$$

$$\frac{d}{dt}\left(\frac{\partial \bar{T}}{\partial \dot{\theta}_1}\right) = I_{FL}\ddot{\theta}_1 \tag{A.51}$$

$$\frac{d}{dt}\left(\frac{\partial \bar{T}}{\partial \dot{\theta}_2}\right) = I_{FR}\ddot{\theta}_2 \tag{A.52}$$

$$\frac{d}{dt}\left(\frac{\partial \bar{T}}{\partial \dot{\theta}_3}\right) = I_{RL}\ddot{\theta}_3 + \frac{1}{4}I_E G_R^2(\ddot{\theta}_3 + \ddot{\theta}_4) \tag{A.53}$$

$$\frac{d}{dt}\left(\frac{\partial \bar{T}}{\partial \dot{\theta}_4}\right) = I_{RL}\ddot{\theta}_4 + \frac{1}{4}I_E G_R^2(\ddot{\theta}_3 + \ddot{\theta}_4) \tag{A.54}$$

As a result, we can now form the special Lagrange equations to give:

$$m\dot{u} - rmv = P_1(Q_\xi) \tag{A.55}$$

$$m\dot{v} + rmu = P_2(Q_\eta) \tag{A.56}$$

$$I_{ZZ}\dot{r} + umv - vmu = Q_3(Q_\varphi)$$

$$I_{ZZ}\dot{r} = Q_3(Q_\varphi) \tag{A.57}$$

$$I_{FL}\ddot{\theta}_1 = Q_4 \tag{A.58}$$

$$I_{FR}\ddot{\theta}_2 = Q_5 \tag{A.59}$$

$$I_{RL}\ddot{\theta}_3 + \frac{1}{4}I_E G_R^2(\ddot{\theta}_3 + \ddot{\theta}_4) = Q_6 \tag{A.60}$$

$$I_{RR}\ddot{\theta}_4 + \frac{1}{4}I_E G_R^2(\ddot{\theta}_3 + \ddot{\theta}_4) = Q_7 \tag{A.61}$$

The last thing required is an evaluation of the external forces produced by a virtual displacement of the generalised coordinates, δp_j. P_1, P_2, and Q_φ represent the external forces acting in the ξ and η directions and the moment acting about the ζ axis respectively.

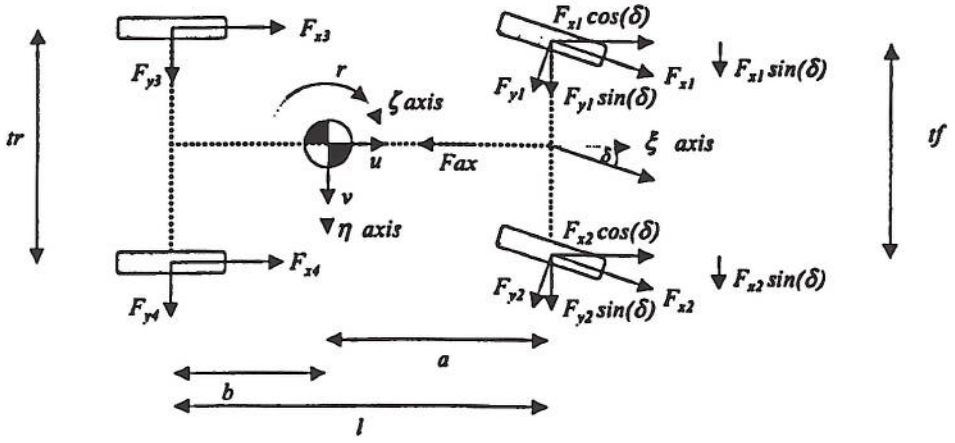

Figure A.2: External Forces acting on the Vehicle.

The external forces producing work from a virtual displacement $\delta\xi$:

$$\delta W_{P1} = \delta\xi[Fx_1\cos(\delta) + Fx_2\cos(\delta) + Fx_3 + Fx_4 - Fy_1\sin(\delta) - Fy_2\sin(\delta) - Fax] \tag{A.62}$$

The external forces producing work from a virtual displacement $\delta\eta$ are

$$\delta W_{P2} = \delta\eta[Fy_1\cos(\delta) + Fy_2\cos(\delta) + Fy_3 + Fy_4 + Fx_1\sin(\delta) + Fx_2\sin(\delta)] \tag{A.63}$$

In a virtual rotation about the ζ axis the external forces producing moments from a virtual rotation $\delta\zeta$ are

$$\begin{aligned}\delta W_{Q3} = \delta\varsigma\Big[&\frac{tf}{2}\{Fx_1\cos(\delta) - Fx_2\cos(\delta) - Fy_1\sin(\delta) + Fy_2\sin(\delta)\} \\ &+\frac{tr}{2}\{Fx_3 - Fx_4\} + a\{Fy_1\cos(\delta) + Fy_2\cos(\delta) + Fx_1\sin(\delta) + Fx_2\sin(\delta)\} \\ &-b\{Fy_3 + Fy_4\}\Big] \end{aligned} \tag{A.64}$$

The external forces contributing to virtual work for the wheels are described here following the SAE sign conventions [36]. Therefore, a positive rotation about the wheel axis (centre of the hub) is counter clockwise i.e clockwise is a negative rotation.

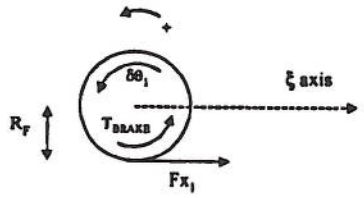

Figure A.3: Left Front Wheel.

$$\delta W_{Q4} = \delta\theta_1\,[TB_{FL} + Fx_1 R_F] \qquad \text{(Figure A.3)} \tag{A.65}$$

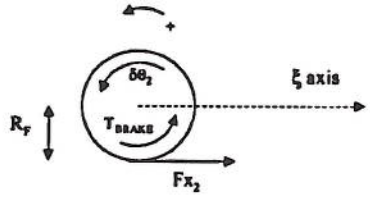

Figure A.4: Right Front Wheel.

$$\delta W_{Q5} = \delta\theta_2\,[TB_{FR} + Fx_2 R_F] \qquad \text{(Figure A.4)} \tag{A.66}$$

$$\delta W_{Q6} = \delta\theta_3\,[TB_{RL} - T_{ENG_{RL}} + Fx_3 R_R] \qquad \text{(Figure A.5)} \tag{A.67}$$

$$\delta W_{Q7} = \delta\theta_4\,[TB_{RR} - T_{ENG_{RR}} + Fx_4 R_R] \qquad \text{(Figure A.6)} \tag{A.68}$$

Before finalising Q_j we need to express some of these new terms in more useful forms:

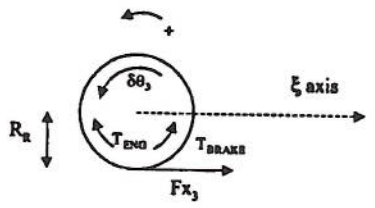

Figure A.5: Left Rear Wheel.

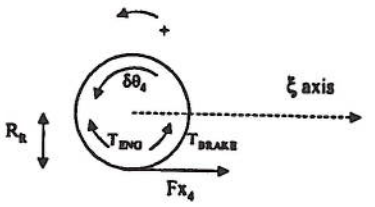

Figure A.6: Right Rear Wheel.

$$T_{ENG_{RL}} = \frac{1}{2}E\_trqG_R + tt \tag{A.69}$$

$$T_{ENG_{RR}} = \frac{1}{2}E\_trqG_R - tt \tag{A.70}$$

So now our generalised external forces can be summarised as follows:

$$P_1 = (Fx_1 + Fx_2)\cos(\delta) + Fx_3 + Fx_4 - (Fy_1 + Fy_2)\sin(\delta) - Fax \tag{A.71}$$

$$P_2 = (Fy_1 + Fy_2)\cos(\delta) + Fy_3 + Fy_4 + (Fx_1 + Fx_2)\sin(\delta) \tag{A.72}$$

$$\begin{aligned} Q_3 \;=\; & \frac{tf}{2}\Big[Fx_1\cos(\delta) - Fx_2\cos(\delta) - Fy_1\sin(\delta) + Fy_2\sin(\delta)\Big] \\ & + \frac{tr}{2}\Big[Fx_3 - Fx_4\Big] + a\Big[Fy_1\cos(\delta) + Fy_2\cos(\delta) + Fx_1\sin(\delta) + Fx_2\sin(\delta)\Big] \\ & - b\Big[Fy_3 + Fy_4\Big] \end{aligned} \tag{A.73}$$

$$Q_4 = TB_{FL} + Fx_1R_F \tag{A.74}$$

$$Q_5 = TB_{FR} + Fx_2R_F \tag{A.75}$$

$$Q_6 = TB_{RL} - \frac{1}{2}E\_trqG_R - tt + Fx_3R_R \tag{A.76}$$

$$Q_7 = TB_{RR} - \frac{1}{2}E\_trqG_R + tt + Fx_4R_R \tag{A.77}$$

Regrouping to find the equations of motion gives

$$m(\dot{u} - rv) = (Fx_1 + Fx_2)\cos(\delta) + Fx_3 + Fx_4 - (Fy_1 + Fy_2)\sin(\delta) - Fax \tag{A.78}$$

$$m(\dot{v} + ru) = (Fy_1 + Fy_2)\cos(\delta) + Fy_3 + Fy_4 + (Fx_1 + Fx_2)\sin(\delta) \tag{A.79}$$

$$\begin{aligned} I_{ZZ}\dot{r} \;=\; & \frac{tf}{2}\Big[Fx_1\cos(\delta) - Fx_2\cos(\delta) - Fy_1\sin(\delta) + Fy_2\sin(\delta)\Big] \\ & + \frac{tr}{2}\Big[Fx_3 - Fx_4\Big] + a\Big[Fy_1\cos(\delta) + Fy_2\cos(\delta) + Fx_1\sin(\delta) + Fx_2\sin(\delta)\Big] \\ & - b\Big[Fy_3 + Fy_4\Big] \end{aligned} \tag{A.80}$$

$$I_{FL}\ddot{\theta}_1 = TB_{FL} + Fx_1R_F \tag{A.81}$$

$$I_{FR}\ddot{\theta}_2 = TB_{FR} + Fx_2R_F \tag{A.82}$$

$$I_{RL}\ddot{\theta}_3 + \frac{1}{4}I_EG_R^2(\ddot{\theta}_3 + \ddot{\theta}_4) = TB_{RL} - \frac{1}{2}E\_trqG_R - tt + Fx_3R_R \tag{A.83}$$

$$I_{RR}\ddot{\theta}_4 + \frac{1}{4}I_EG_R^2(\ddot{\theta}_3 + \ddot{\theta}_4) = TB_{RR} - \frac{1}{2}E\_trqG_R + tt + Fx_4R_R \tag{A.84}$$

Obviously, the equations of motion for A.83 and A.84 have $\ddot{\theta}_3$ and $\ddot{\theta}_4$ in each equation. We need to rectify this to make two independent equations each specified by only one generalised coordinate.

Initially lets rearrange the $\ddot{\theta}_3$ expression in terms of $\ddot{\theta}_4$. We note that $I_{RL} = I_{RR} = I_R$.

$$\ddot{\theta}_3(\frac{1}{4}I_EG_R^2 + I_R) = T_{BRL} - \frac{1}{2}E\_trqG_R - tt + Fx_3R_R - \frac{1}{4}I_EG_R^2\ddot{\theta}_4 \tag{A.85}$$

$$\ddot{\theta}_3 = \frac{T_{BRL} - \frac{1}{2}E\_trqG_R - tt + Fx_3R_R - \frac{1}{4}I_E G_R^2 \ddot{\theta}_4}{\frac{1}{4}I_E G_R^2 + I_R} \tag{A.86}$$

We then substitute $\ddot{\theta}_3$ into the expression for $\ddot{\theta}_4$. We abbreviate a common group for neatness:

$$\lambda = T_{BRL} - \frac{1}{2}E\_trqG_R - tt + Fx_3R_R$$

So we end up with:

$$\ddot{\theta}_3 = \frac{\lambda - \frac{1}{4}I_E G_R^2 \ddot{\theta}_4}{\frac{1}{4}I_E G_R^2 + I_R} \tag{A.87}$$

We also abbreviate the right hand side of A.84 with χ, giving the substituted form of $\ddot{\theta}_3$ into A.84:

$$\ddot{\theta}_4 \left(\frac{1}{4}I_E G_R^2 + I_R\right) + \frac{1}{4}I_E G_R^2 \frac{(\lambda - \frac{1}{4}I_E G_R^2 \ddot{\theta}_4)}{\frac{1}{4}I_E G_R^2 + I_R} = \chi \tag{A.88}$$

Separate $\ddot{\theta}_4$:

$$\ddot{\theta}_4 \left(\frac{1}{4}I_E G_R^2 + I_R\right) - \frac{1}{4}I_E G_R^2 \frac{(\frac{1}{4}I_E G_R^2 \ddot{\theta}_4)}{\frac{1}{4}I_E G_R^2 + I_R} + \frac{1}{4}I_E G_R^2 \frac{\lambda}{\frac{1}{4}I_E G_R^2 + I_R} = \chi \tag{A.89}$$

multiplying through by $\frac{1}{4}I_E G_R^2 + I_R$:

$$\ddot{\theta}_4 \left(\frac{1}{4}I_E G_R^2 + I_R\right)^2 - \ddot{\theta}_4 \left(\frac{1}{4}I_E G_R^2\right)^2 + \frac{1}{4}I_E G_R^2 \lambda = \chi \left(\frac{1}{4}I_E G_R^2 + I_R\right) \tag{A.90}$$

$$\ddot{\theta}_4 \left[\left(\frac{1}{4}I_E G_R^2 + I_R\right)^2 - \left(\frac{1}{4}I_E G_R^2\right)^2\right] = \chi \left(\frac{1}{4}I_E G_R^2 + I_R\right) - \frac{1}{4}I_E G_R^2 \lambda \tag{A.91}$$

$$\ddot{\theta}_4 = \frac{\chi \left(\frac{1}{4}I_E G_R^2 + I_R\right) - \frac{1}{4}I_E G_R^2 \lambda}{\left(\frac{1}{4}I_E G_R^2 + I_R\right)^2 - \left(\frac{1}{4}I_E G_R^2\right)^2} \tag{A.92}$$

Next we need to write out the expression in full to see if we have any opportunities to simplify the expression.

$$\ddot{\theta}_4 = \frac{\left[TB_{RR} - \frac{1}{2}E\_trqG_R + tt + Fx_4R_R\right]\left(\frac{1}{4}I_E G_R^2 + I_R\right) - \frac{1}{4}I_E G_R^2 \left[TB_{LR} - \frac{1}{2}E\_trqG_R - tt + Fx_3R_R\right]}{\left(\frac{1}{4}I_E G_R^2 + I_R\right)^2 - \left(\frac{1}{4}I_E G_R^2\right)^2} \tag{A.93}$$

This is a large expression, it is best to look at the numerator and denominator separately.

In the numerator, We note that $\frac{1}{4}I_E G_R^2$ is a common multiplier either side of the negative sign. We realise that we can use this to inspect the variables in the square brackets and cancel some terms. We see that E_trq can be eliminated. Our only other option is to collect terms to make the appearance better.

$$I_R\left[TB_{RR}-\frac{1}{2}E\_trqG_R+tt+Fx_4R_R\right]+\frac{1}{4}I_E G_R^2\left[TB_{RR}-TB_{LR}+2tt+Fx_4R_R-Fx_3R_R\right]$$

Next, look at the denominator

$$\left(\frac{1}{4}I_E G_R^2+I_R\right)^2-\left(\frac{1}{4}I_E G_R^2\right)^2$$

expanding this gives

$$I_R^2+\left(\frac{1}{4}I_E G_R^2\right)^2+\frac{1}{2}I_E G_R^2-\left(\frac{1}{4}I_E G_R^2\right)^2$$

leaving

$$I_R^2+\frac{1}{2}I_E G_R^2$$

so collecting both terms and reassembling gives:

$$\ddot{\theta}_4=\frac{I_R\left[TB_{RR}-\frac{1}{2}E\_trqG_R+tt+Fx_4R_R\right]+\frac{1}{4}I_E G_R^2\left[TB_{RR}-TB_{LR}+2tt+Fx_4R_R-Fx_3R_R\right]}{I_R^2+\frac{1}{2}I_E G_R^2} \tag{A.94}$$

Using this result allows a simpler calculation for $\ddot{\theta}_3$

$$\ddot{\theta}_3=\frac{TB_{RR}-\frac{1}{2}E\_trqG_R-tt+Fx_3R_R-\frac{1}{4}I_E G_R^2\ddot{\theta}_4}{I_R+\frac{1}{4}I_E G_R^2} \tag{A.95}$$

Appendix B

B.1 Suspension model derivation

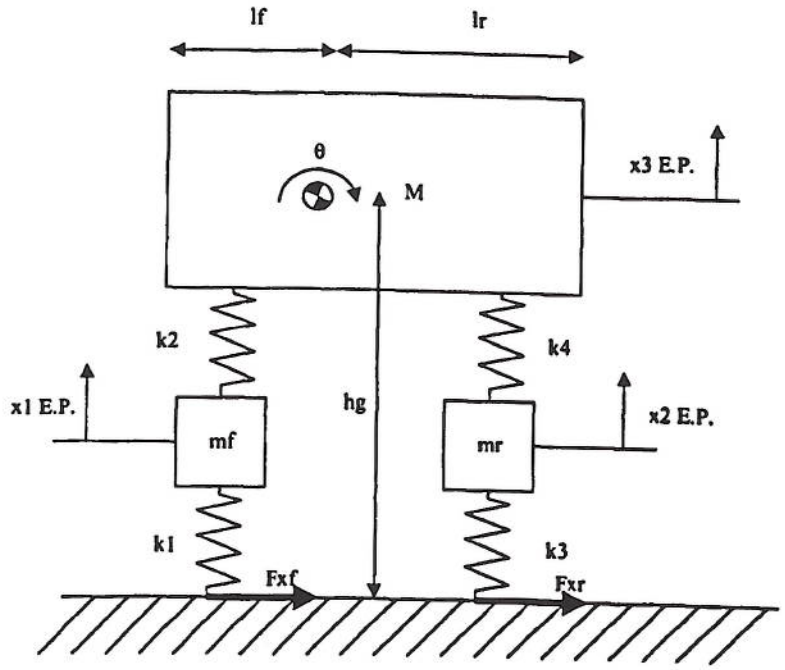

Figure B.1: Four degree of freedom pitch model

E.P	Equilibrium position	
x_1	Displacement of front unsprung mass from the E.P	m
x_2	Displacement of rear unsprung mass from the E.P	m
x_3	Displacement of sprung mass from the E.P	m
θ	Pitch angle from the E.P	rad
m_f	Half of the front unsprung mass	kg
m_r	Half of the rear unsprung mass	kg
M	Half of the sprung mass	kg
I	Chassis mass moment of inertia in pitch mode about centre of gravity	kg/m^2
k_1	spring constant of a front tyre	N/m
k_2	spring constant of one side of the front suspension	N/m
k_3	spring constant of a rear tyre	N/m
k_4	spring constant of one side of the rear suspension	N/m
lf	distance from centre of gravity to front wheel axis of rotation	m
lr	distance from centre of gravity to rear wheel axis of rotation	m
h_g	distance from centre of gravity to ground	m
Fx_f	Front tyre longitudinal force	N
Fx_r	Rear tyre longitudinal force	N

The equations of motion can be obtained by applying the equations of Lagrange:

$$\frac{d}{dt}\left(\frac{\partial T}{\partial \dot{q}_i}\right) - \frac{\partial T}{\partial q_i} + \frac{\partial U}{\partial q_i} = Q_i \tag{B.1}$$

Where q represents the generalised coordinates, Q represents the appropriate externally applied "generalised force", T represents the kinetic energy of the system and U represents the potential energy of the system.

In this system, the generalised coordinates, q_i, are defined as follows:

$q_1 = x_1$

$q_2 = x_2$

$q_3 = x_3$

$q_4 = \theta$

The kinetic energy of the vehicle in terms of these coordinates is required.

Kinetic energy can be produced through a translation, in x_1, x_2, x_3 or a rotation about θ. The kinetic energy, T is:

$$T = \frac{1}{2}m\dot{x_1}^2 + \frac{1}{2}m\dot{x_2}^2 + \frac{1}{2}m\dot{x_3}^2 + \frac{1}{2}I\dot{\theta}^2 \tag{B.2}$$

The potential energy, U assuming the small angle approximation applies is:

$$U = \frac{1}{2}k_2(x_3 + lf\theta - x_1)^2 + \frac{1}{2}k_1x_1^2 + \frac{1}{2}k_4(x_3 - lr\theta - x_2)^2 + \frac{1}{2}k_3x_2^2 \tag{B.3}$$

So firstly, we need to evaluate the necessary partial derivatives of the special Lagrange equations. The following are required:

$$\frac{\partial T}{\partial x_1}, \frac{\partial T}{\partial \dot{x}_1}, \frac{\partial T}{\partial x_2}, \frac{\partial T}{\partial \dot{x}_2}, \frac{\partial T}{\partial x_3}, \frac{\partial T}{\partial \dot{x}_3}, \frac{\partial T}{\partial \theta}, \frac{\partial T}{\partial \dot{\theta}}, \frac{\partial U}{\partial x_1}, \frac{\partial U}{\partial \dot{x}_1}, \frac{\partial U}{\partial x_2}, \frac{\partial U}{\partial \dot{x}_2}, \frac{\partial U}{\partial x_3}, \frac{\partial U}{\partial \dot{x}_3}, \frac{\partial U}{\partial \theta}, \frac{\partial U}{\partial \dot{\theta}}.$$

Inspection of T shows that x_1, x_2, x_3, θ do not feature in B.2 and therefore:

$$\frac{\partial T}{\partial x_1}, \frac{\partial T}{\partial x_2}, \frac{\partial T}{\partial x_3}, \frac{\partial T}{\partial \theta} = 0$$

Also, it can be seen that $\dot{x}_1, \dot{x}_2, \dot{x}_3, \dot{\theta}$ do not feature in equation B.3 and therefore:

$$\frac{\partial U}{\partial \dot{x}_1}, \frac{\partial U}{\partial \dot{x}_2}, \frac{\partial U}{\partial \dot{x}_3}, \frac{\partial U}{\partial \dot{\theta}} = 0$$

For the kinetic energy terms we find:

$$\frac{\partial T}{\partial \dot{x}_1} = m_f\dot{x}_1 \tag{B.4}$$

$$\frac{\partial T}{\partial \dot{x}_2} = m_r\dot{x}_2 \tag{B.5}$$

$$\frac{\partial T}{\partial \dot{x}_3} = M\dot{x}_3 \tag{B.6}$$

$$\frac{\partial T}{\partial \dot{\theta}} = I\dot{\theta} \tag{B.7}$$

and for the potential energy terms we find:

$$\frac{\partial U}{\partial x_1} = k_1x_1 + k_2(x_1 - x_3 - lf\theta) \tag{B.8}$$

$$\frac{\partial U}{\partial x_2} = k_3x_2 + k_4(x_2 - x_3 + lr\theta) \tag{B.9}$$

$$\begin{aligned}\frac{\partial U}{\partial x_3} &= k_4(x_3 - x_2 - lr\theta) \\ &+ k_2(x_3 - x_1 + lf\theta)\end{aligned} \tag{B.10}$$

$$\begin{aligned}\frac{\partial U}{\partial \theta} &= k_4(-x_3 lr + x_2 lr + lr^2\theta) \\ &+ k_2(lf^2\theta + x_3 lf - x_1 lf)\end{aligned} \tag{B.11}$$

To complete the left hand side of the special equations we need to find:

$$\frac{d}{dt}\left(\frac{\partial T}{\partial \dot{x}_1}\right), \frac{d}{dt}\left(\frac{\partial T}{\partial \dot{x}_2}\right), \frac{d}{dt}\left(\frac{\partial T}{\partial \dot{x}_3}\right), \frac{d}{dt}\left(\frac{\partial T}{\partial \dot{\theta}}\right).$$

Again, these are quite simple:

$$\frac{d}{dt}\left(\frac{\partial T}{\partial \dot{x}_1}\right) = m_f \ddot{x}_1 \tag{B.12}$$

$$\frac{d}{dt}\left(\frac{\partial T}{\partial \dot{x}_2}\right) = m_r \ddot{x}_2 \tag{B.13}$$

$$\frac{d}{dt}\left(\frac{\partial T}{\partial \dot{x}_3}\right) = M \ddot{x}_3 \tag{B.14}$$

$$\frac{d}{dt}\left(\frac{\partial T}{\partial \dot{\theta}}\right) = I \ddot{\theta} \tag{B.15}$$

The last thing required is an evaluation of the external forces produced by a virtual displacement of the generalised coordinates. As can be seen in Figure B.1 there are only two external forces acting on the system, Fx_f and Fx_r. As the coordinates x_1, x_2 and x_3 displace in the vertical direction about an equilibrium point the displacements are very small when compared with the centre of gravity height, h_g. To keep the equations simple the assumption that $h_g \gg x_1, x_2, x_3, \theta$ is used and therefore the external forces for $Q_{x_1}, Q_{x_2}, Q_{x_3} = 0$.

However, the external forces produce work from a positive virtual rotation $\delta\theta$. If it is still assumed that $hg \gg x_1, x_2, x_3, \theta$, then :

$$\delta\theta Q_\theta = \delta\theta[Fx_f h_g + Fx_r h_g] \tag{B.16}$$

As $\delta\theta$ tends towards 0, the external force due to a rotation about θ gives:

$$Q_\theta = Fx_f h_g + Fx_r h_g \tag{B.17}$$

Regrouping to find the final equations of motion gives

$$m_f\ddot{x}_1 + x_1(k_1 + k_2) - k_2x_3 - k_2lf\theta = 0 \tag{B.18}$$

$$m_r\ddot{x}_2 + x_2(k_3 + k_4) - k_4x_3 + k_4lr\theta = 0 \tag{B.19}$$

$$\begin{aligned} &M\ddot{x}_3 - k_2x_1 - k_4x_2 + (k_2 + k_4)x_3 \\ &+(k_2lf - k_4lr)\theta = 0 \end{aligned} \tag{B.20}$$

$$\begin{aligned} &I\ddot{\theta} - k_2lfx_1 + k_4lrx_2 + (k_2lf - k_4lr)x_3 \\ &+(k_2lf^2 + k_4lr^2)\theta - (Fx_f h_g + Fx_r h_g) = 0 \end{aligned} \tag{B.21}$$

Appendix C

C.1 Straight line stability

The solution of the equations of motion with the steer input set to zero represents the situation of the vehicle travelling in a straight line. Under these conditions the vehicle is subjected to small perturbations arising from wind gusts, road camber, road irregularities etc and therefore the nonlinear equations of vehicle motion can be realistically be replaced with linear equations. The roots of the set of linear equations of motion yield the frequency and damping for the natural modes of vibration for the vehicle. These roots are called *eigenvalues*. In general the eigenvalues are evaluated at a range of vehicle speeds as the stability of vehicles (stability denoted by negative real parts) generally decreases with increasing speed [1].

Linearisation about a trimmed steady state point can be achieved with a nonlinear model using AutoSIM [4]. AutoSIM is a symbolic multi-body code generator that employs the virtual power principle in the form of Kane's equations to generate equations of motion [109]. AutoSIM symbolically linearises the nonlinear dynamical equations to obtain the Matrix form:

$$\delta\dot{x} = A\delta x + B\delta u \tag{C.1}$$

$$\delta y = C\delta x + D\delta u \tag{C.2}$$

where δx and δu are arrays of linear perturbations of the system state variables and inputs, respectively, about a trimmed steady state point defined by x and u.

The model has seven DOF and therefore has seven eigenvalues.

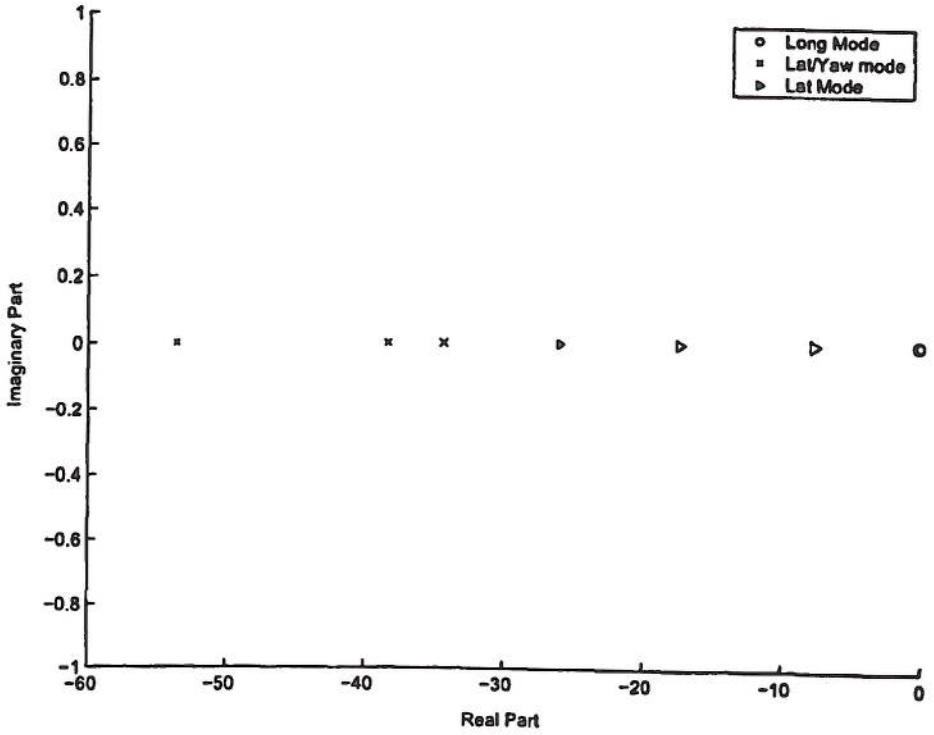

Figure C.1: Root Locus plot - Linear 7DOF model

A set of transient vehicle simulations with the base vehicle configuration set up were conducted with the seven DOF vehicle model in straight line running at constant speed. The values of the steady state vehicle states were then transferred to the linear matrices and the speed dependent eigenvalues were evaluated. Figure C.1 is a root locus plot showing the three eigenvalues of the system that most strongly involve the vehicle states of longitudinal velocity, yaw rate, and lateral velocity. The eigenvalues predominantly related to the four wheel modes are omitted. *Eigenvectors* show which vehicle states are involved with the modes of vibration associated with each eigenvalue. Figure C.1 shows that at vehicle speeds of 30, 50 and 70 m/s (increasing speed is characterised by increasing marker size), the eigenvalues are all real and negative, indicating stable modes. Because the eigenvalues for a particular speed are not coincident or complex conjugate pairs, the vehicle system is seen to be overdamped [110]. This suggests that the vehicle is in a state of oversteer [44]. Whether a system is oscillatory or not is a function of the *damping* of the system. A system is damped if a force inherent in it acts to restrict the oscillatory behaviour of the system [110]. The limit point of oscillation in a system requires critical damping and the damping of the

system is normally compared to this value to form the *damping ratio.*

A set of transient vehicle simulations with the largest CG rearward shift investigated in this research, (37/63% static weight distribution for the front and rear axles respectively) were conducted with the seven DOF vehicle model in the straight line running condition at constant speed. Figure C.2 is a plot of the eigenvalues for speeds 20 to 80 m/s in increments of 20 m/s, with the increasing size of markers representing increasing speed.

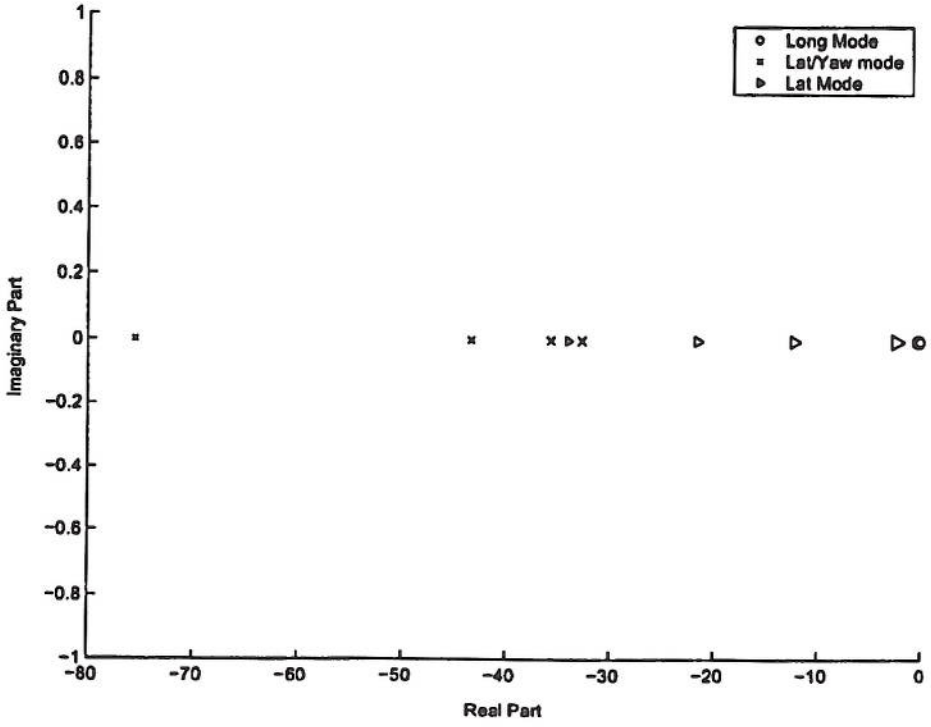

Figure C.2: Root Locus plot - Eigenvalues 7DOF Model CG split 37/63% (Front/Rear)

Figure C.2 shows that the three eigenvalues that strongly involve longitudinal velocity, lateral velocity and yaw rate are all stable with negative real roots. As the speed increases the lateral velocity / yaw rate eigenvalues are moving closer to zero indicating that they are less stable with increasing speed. It appears plausible that the critical speed of the lateral velocity mode is not much higher than 80m/s. The mostly lateral velocity / yaw rate dependent mode is considerably more stable than the mostly lateral

velocity dependent mode, and the mostly longitudinal velocity dependent mode actually becomes more stable with increasing speed. Figure C.2 is for the vehicle with a CG location of 63% of the vehicle static weight on the rear axle. This plot is representative of all the CG locations tested in Chapter 5 as their was no discernable difference between the linear results with respect to the evaluated eigenvalues for all of the CG relocation trials using a constant speed vehicle with no steer input.

C.2 Steady state cornering

Since the nonlinear equations of motion have been linearised about a generalised trimmed steady state point [4], it is also possible to investigate the free vibration response of the vehicle in steady state cornering.

The QSS method generates the solution to the equations of motion that satisfy steady state cornering by requiring that the longitudinal acceleration of the vehicle at the solution must be zero. Therefore all GG speed diagrams generated by the QSS method have a steady state cornering solution for the speed range of the vehicle, and these solutions are on-limit with respect to maximising lateral acceleration.

Figures C.3 and C.4 show the root locus plots for on-limit steady state cornering for both the base vehicle set up and the rearward CG setting of 37/63% front to rear, with increasing marker size corresponding to increasing vehicle longitudinal speed. These two figures label the two lateral velocity / yaw rate modes as 1 and 2 because the lateral velocity was not as distinct in one of the two dependent modes as found in the straight line stability results.

The lowest speed is 20m/s, and at this speed the base setup of the vehicle is unstable. However, at all other speeds the vehicle is stable, and with the exception of the 80m/s result, the results show a stable but oscillatory (under damped) response. This implies that the vehicle is in a state of understeer in the 30-70m/s speed range at the steady state cornering limit. Table C.1 shows the damping ratios at each vehicle speed for the underdamped results. The general trend is that as vehicle speed increases, the vehicle becomes less damped for the base set up vehicle.

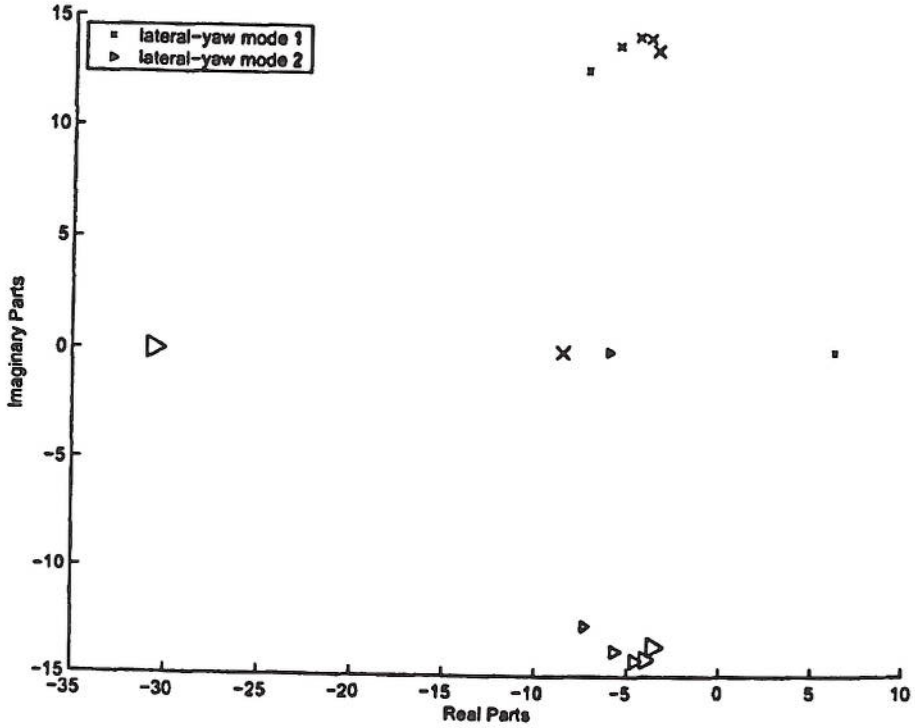

Figure C.3: Root Locus plot - Steady state cornering, Base setup

Conversely, the CG root locus plot (Figure C.4) shows for the speed range 20-70 m/s, at least one of the two lateral-yaw dependent modes is unstable at the steady state solution. This suggests that the difficulties found in populating the GG speed diagram with the rearward CG settings, is likely to be affected by these vehicle instabilities. The zero steer angle input results show that this instability is a function of vehicle cornering behaviour, and will be seen in the high lateral acceleration sections of the GG speed diagram.

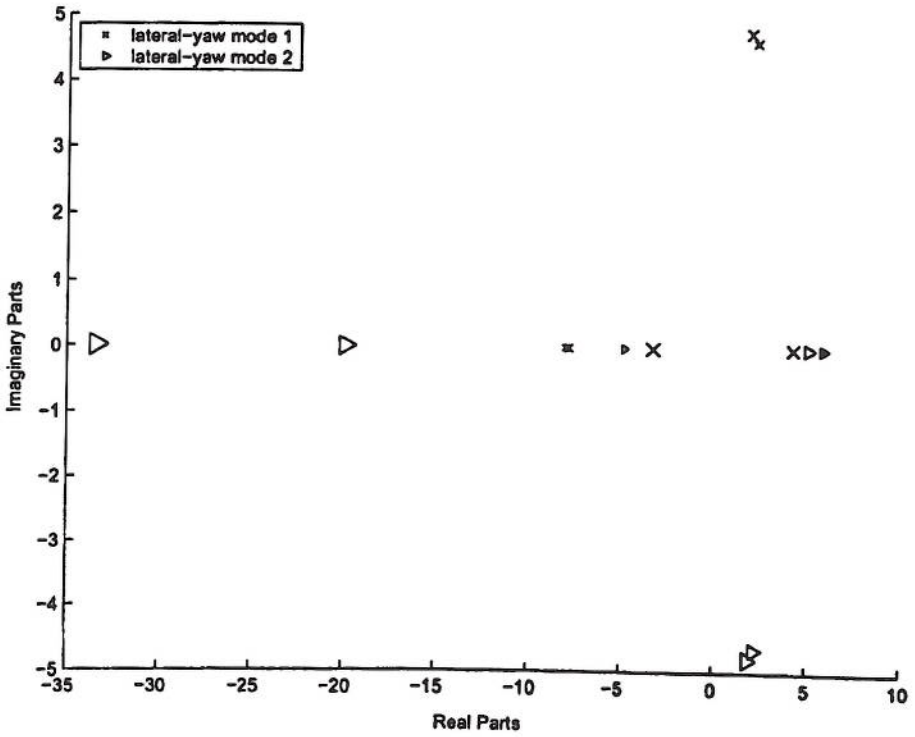

Figure C.4: Root Locus plot - Steady state cornering, CG 37/63% setup

Vehicle Speed [m/s]	Base setup	CG setup
20	-	-
30	0.49	-
40	0.38	-
50	0.31	-0.43
60	0.27	-0.37
70	0.26	-
80	-	-

Table C.1: Damping Ratio found from Root Locus plots

Appendix D

Transient path following

This chapter uses the seven DOF published vehicle model. This choice allowed the inclusion of transient optimal information from published results [3] that used this version of the vehicle model.

D.1 The need for transient information

The QSS method in conjunction with the laptime simulation program has been shown to reproduce the results of a full transient optimisation method over the Grand Prix circuit at Barcelona. The benefits of improved computational times are achieved at the expense of omitting transient information and the path finding calculation. For laptime determination, and for the majority of vehicle manoeuvres, the QSS method seems to be a sufficiently accurate tool for understanding vehicle performance. The downside is that the very definition of the QSS method eliminates the exploration of transient dependent technologies. One such example is traction control. The QSS method is not capable of simulating broken traction, and for the majority of the time, the tyres are at or are very close to operating at optimum slip angles and slip ratios. The use of technologies that aid the drivers ability to reduce wheel spin and loss of vehicle control are impossible to examine with the QSS method. These technologies augment normal driver control and limit unwanted transient behaviour.

Additionally, the results from the QSS method indicate that, due to the sensitive nature of the contemporary race car in certain manoeuvres, i.e. hard braking, the transient aspects could be quite influential on the behaviour of the vehicle.

Chapter 4 showed that the determination of the optimal line for each particular vehicle setup was not necessary for a vehicle CG set up change, which as Section 5.8 showed, creates a complicated change in vehicle performance. This finding suggests that as long as the racing line is accurate to within ± 1m of the fastest racing line for a given vehicle configuration, this will be sufficient for the determination of the minimum laptime problem in line with the current state of the art. Additionally the solution of the minimum time problem becomes significantly easier to solve, as the number of optimisation variables required are reduced by the number of nodes required to optimise the track position of the vehicle.

The achievement of the solution of the minimum laptime optimisation method of Casanova [3] was dependent on judicious choice of the track description and vehicle control discretisation grids, the correct location of the track segmentation points and the minimisation of the number of track constraint equations required to ensure the vehicle remained on the racing circuit. This level of user intervention, combined with the significant computational time, needs to be minimised as much as possible to help generate a more general and therefore transferable method for other circuits and vehicle configurations. Based on these considerations, a transient path following method seems a sensible choice.

D.2 Path following methodology

Early development work with an optimisation program, based on path following, showed that a high level of user intervention was going to be necessary if both the steer and throttle inputs were going to be determined by the optimisation routine for a given manoeuvre. Investigations showed that careful scaling of the steer angle position was going to be required by the optimiser for the vehicle to run in straight line. Alternatively, the approach of Casanova [3] could have been adopted, which locks the steer control to zero angle at points on the circuit where the vehicle would be expected to be running in a straight line. It would also be prudent to allow the steer angle discretisation grid to be modified depending on circuit location. This is based on simple observations of driving behaviour. The decision processing and actual steer input requirements are significantly higher during cornering than those when the driver is required to drive in a straight line. This line of inquiry was developing into a circuit specific solution rather than a general one and would more than likely converge on the

method described by Casanova [3]. Therefore, a different approach is proposed in the interest of producing a more practical method. This approach is illustrated in Figure D.1.

The steer input is decoupled from the optimiser. This step halves the number of variables the optimiser has to solve for, and allows the steer routine to be a function of path tracking error rather than manoeuvre time. This is acceptable because the path is prescribed and the only requirement of the steer control, other than path following, is that the controller be robust to changes in throttle control, which is being optimised for a minimum time solution.

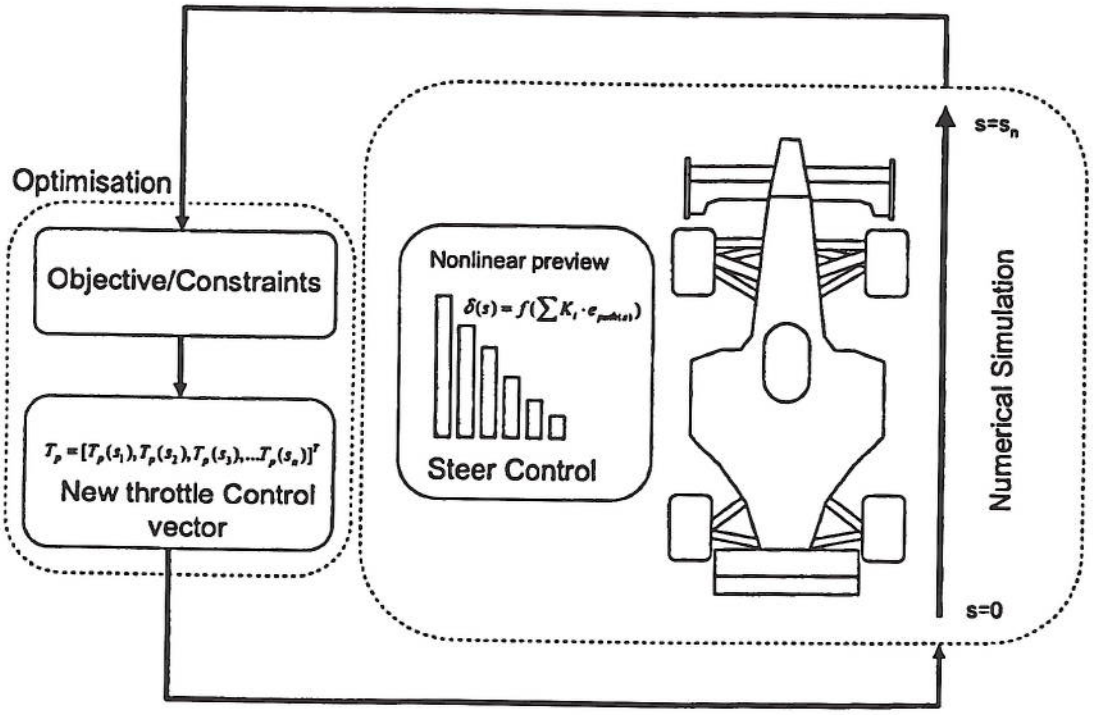

Figure D.1: Transient path following optimisation.

D.2.1 Preview steer control

A brief summary of the nonlinear preview steer model will be given here. For full details, please refer to Sharp et al. [85].

The structure of the steering control is derived from observations made from active suspension results formed from the application of linear optimal discrete time preview control theory. Both discrete time and continuous time approaches have been investigated, and it is reported that the discrete representations are much simpler [85]. Both in Sharp et al. [85] and Tomizuka and Whitney [83] it was found that the amount of preview information required to be 'optimal' is finite, and beyond that finite preview distance/time the controller does not significantly alter its response.

The discrete time linear optimal controller produces the required control using a summation of weighted preview error samples combined with a corresponding summation of the weighted state feedback terms as shown in Figure D.2.

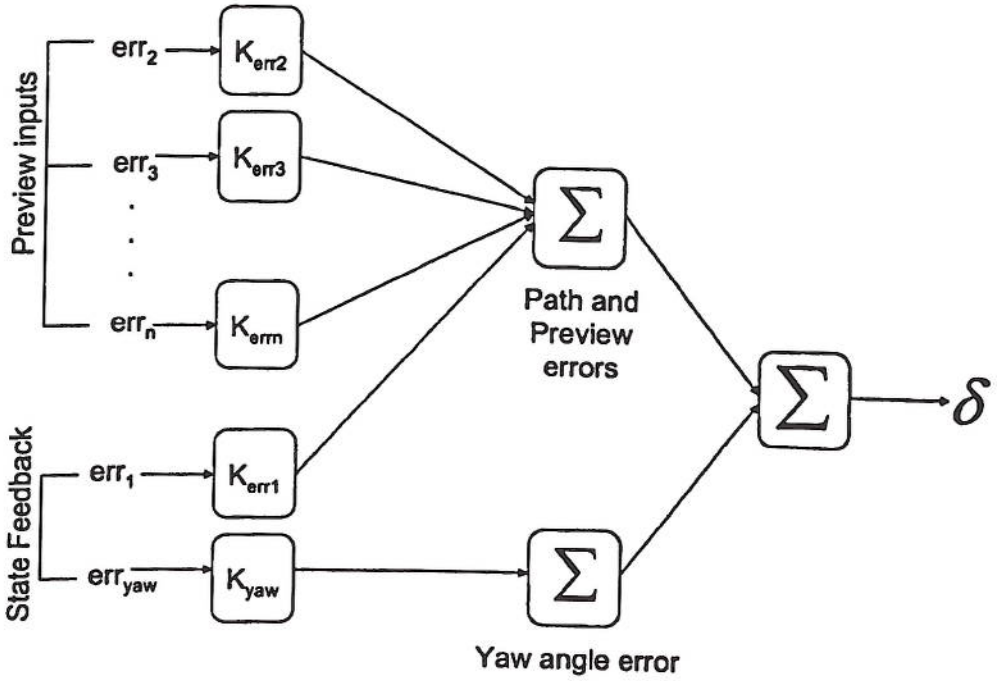

Figure D.2: Linear driver model structure.

To transfer this understanding to a nonlinear (tyre saturating) plant, the underlying linear gain sequence is moderated by the inclusion of saturation functions after each linear gain term. Therefore the control is still a linear function of the preview and state feedback terms, but the effect of the gain is controlled to a maximum response. This situation is illustrated in Figure D.3.

The gains represented by $K_{err_{1:n},yaw}$ were chosen in two ways: The gain terms for the

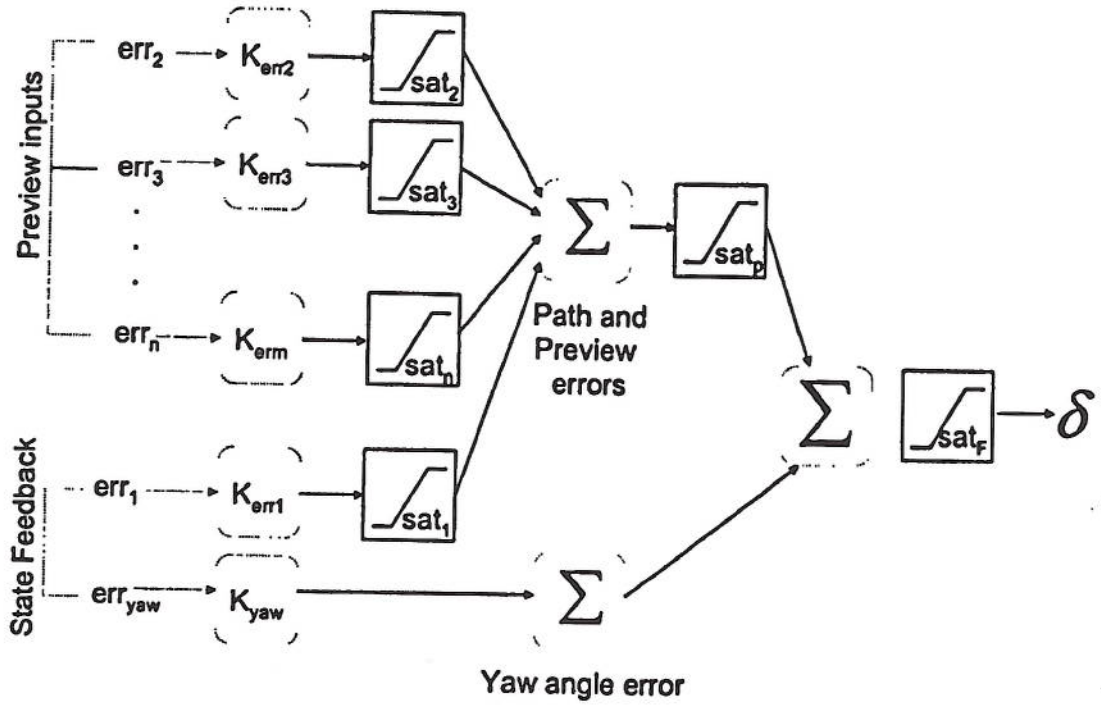

Figure D.3: Nonlinear driver model structure.

preview mirrored the system dynamics; which in this case, was one of a highly damped system. Therefore the gain sequence was chosen to be exponentially convergent to zero for increasingly distant preview samples. The state feedback terms were found from trial and error with a set chosen to reflect both good path tracking performance and vehicle stability. It was emphasised that the value of the attitude control gain was influential in stabilising their vehicle model via steer control if the vehicle was unstable due to strong oversteer [85].

The driver model has been translated as a MATLAB script, and apart from a slight modification to the preview distance, it is as described in Sharp et al. [85] and is referred to as nonlinear preview steer control in Figure D.1.

D.2.2 Optimisation implementation

As shown in Figure D.1, a numerical optimiser is used to find the throttle history required to follow the path in minimum time.

The independent variable of time space has been converted in accordance with the equations developed by Allen [16] and generalised by Casanova [3] to distance space. This is done to remove the free final time constraint which makes the minimum time optimisation problem more difficult to solve.

Because the steering model is operating from preview information and is only called by the numerical integration routine, only one discretised control grid is necessary. This is the control grid for the throttle history, which is defined as a function of distance. This grid is more coarse than the numerical integration one, to reduce the computational time. The throttle positions required by the numerical integrator are found from interpolation routines. The entire throttle history is determined outside of the numerical integration routine and can only be changed by the optimisation routine. Once the optimisation routine has changed the throttle history, a further numerical simulation is run. This process continues until the convergence criteria of the optimiser is reached.

Since the aim of the optimisation is to follow a prescribed racing line in minimum time, the optimiser must be instructed to ensure the vehicle remains on the racing line. This is normally done by adding constraints to the problem. This is commonly done, as shown in Figure D.4.
The first part of Figure D.4 is a graphical representation of an inequality constraint where W is the nominal race track width. Unfortunately for a SQP method which uses derivative information from both the objective and the constraint functions, the first derivative of C_{ineq} is discontinuous at the point $|d| = \frac{W}{2}$. To remove this difficulty, Casanova [3] implemented a quadratic of the form shown in the second part of Figure D.4, which gives smooth, continuous first and second derivative information for the optimiser.

The act of following the racing line is equivalent to 'ring fencing' the racing line with a minimum allowable deviation from that line. This is equivalent to setting $\frac{W}{2}$ to this allowable deviation. However, it was felt that this was a very constrictive method of implementing the path following criterium because it would force the optimiser to focus on areas of the simulation where the path being taken is on or very close to the 'fence'. If a change in the control history resulted in a constraint being violated, then depending on the optimisation methods' way of handling constraint violations, the optimisation could be prematurely halted or it may allow the optimisation to continue if

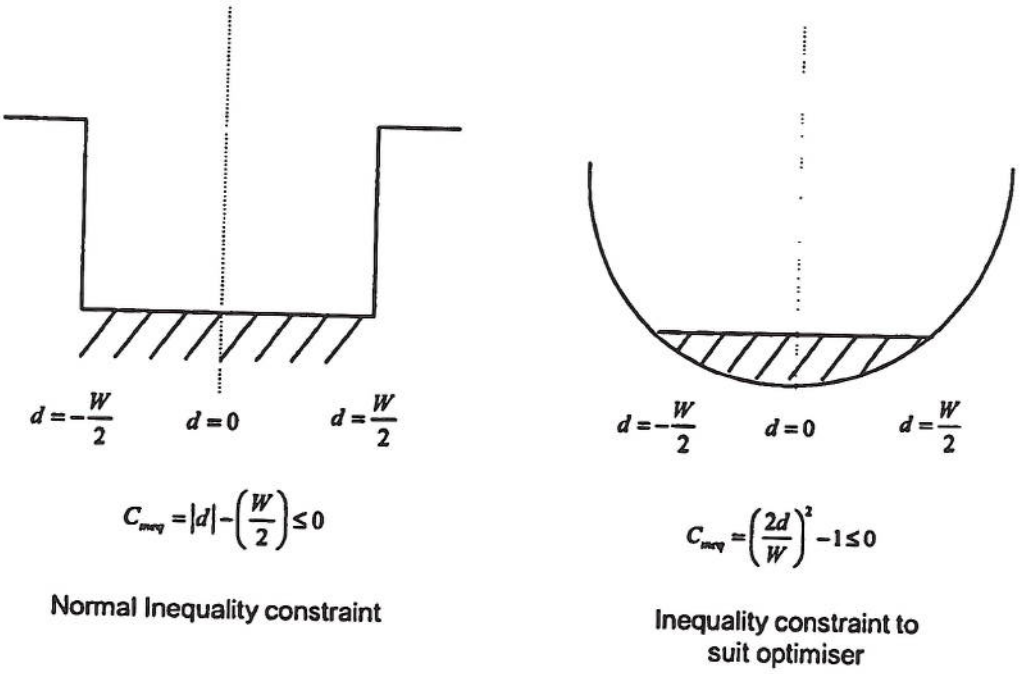

Figure D.4: Inequality constraint implementation methods.

the violation is relatively minor. Instead it was decided to remove these constrictive or 'hard' constraints and replace them with a 'softer' implementation. Instead of devising an optimisation routine with both a constraint and objective function, the constraints were manually assimilated into the objective as a penalty function [17]. Penalty functions are an older method of introducing constraints into a problem description while still being able to use an unconstrained optimisation algorithm.
Penalty functions for inequality constraints are generally defined as [17]:

$$P(x) = \sum_i k_i [g_i(x)]^{2M}, \; k_i > 0 \text{ for all } i, \text{ M a positive integer} \qquad \text{(D.1)}$$

In this instance the same SQP MATLAB constrained optimisation algorithm is still used because the control inputs are bound by upper and lower values, but the program only runs with an objective function. The objective uses a variation of the penalty function described in Walsh [17] and is in fact very similar to the second part of Figure D.4. This function is illustrated in Figure D.5. The fundamental difference is that when the path of the vehicle is following the racing line perfectly, $C_{ineq} = 0$.
The problem which was stated as:

$$\text{minimise } z = f(x) \qquad \text{(D.2)}$$

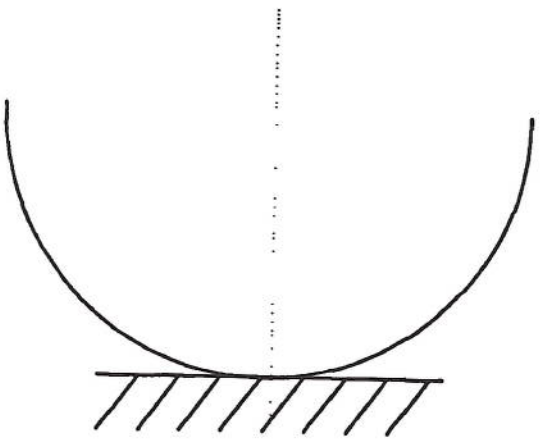

Figure D.5: Inequality constraint for path following.

can now be stated as:

$$\text{minimise } Z = f(x) + P(x) \tag{D.3}$$

where

$$f(x) = t_F \tag{D.4}$$

and

$$P(x) = \sum_i \left[\frac{2 \cdot d_i(x)}{W}\right]^2 \tag{D.5}$$

So when the vehicle is perfectly tracking the prescribed path, Equation D.3 simplifies to Equation D.2, the minimum time objective. Additionally the optimisation is not halted by racing path deviations but the objective is severely penalised when the path location moves beyond the allowable region defined by $\frac{W}{2}$.

There is an additional benefit of reduced computational effort when using the MATLAB *fmincon* SQP routine with a penalised objective because it normally requires that

the constraint function to be specified separately from the objective function. To evaluate the constraint function would require the numerical simulation to be run again just to update the constraint function values, and if finite differencing is used, then to update the Jacobian matrix would require further simulations to be run at significant computational cost.

D.3 Results

To demonstrate this new method, a double lane change is used. The double lane change was run over 280 metres, and took 4.3 hours on a 1000MHz Intel PC. The value of W, the limit of the penalty function was chosen to be 0.2 metres. The optimisation routine runs much faster if there are less variables to solve for. Therefore, to improve the speed of the program, the manoeuvre is broken down into consecutive segments of 40 metres, giving seven optimisations to complete the manoeuvre.

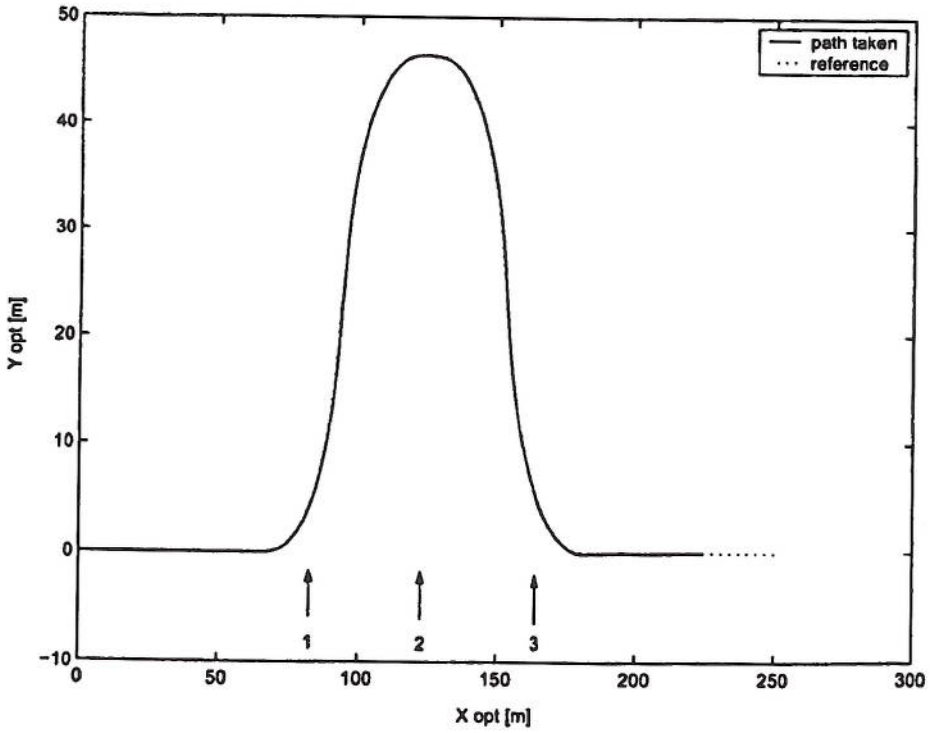

Figure D.6: Double lane change - path following result.

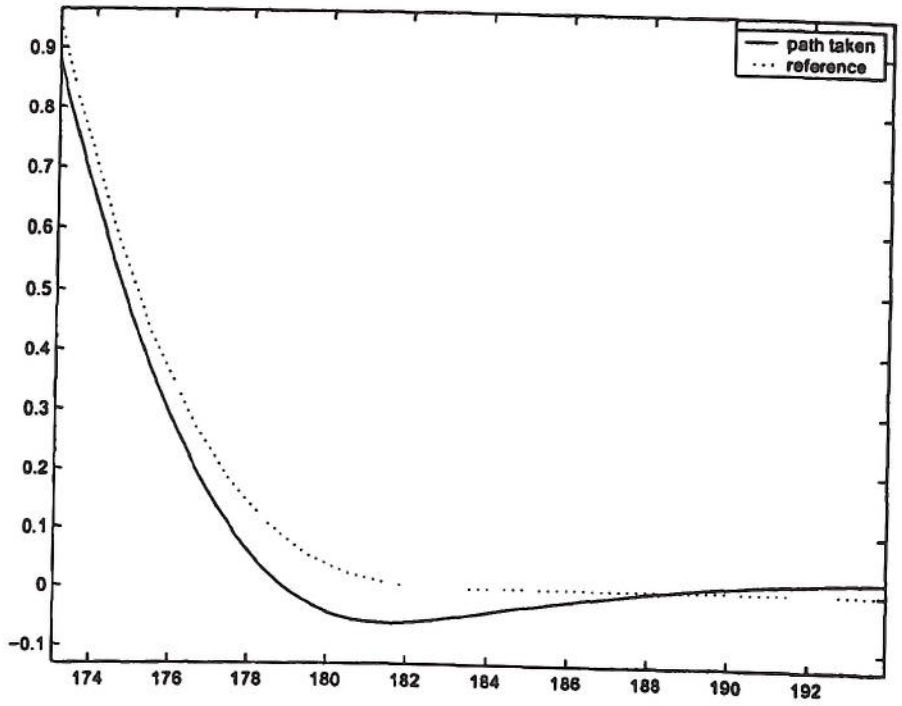

Figure D.7: Double lane change - path following errors.

The path following results of the method as shown in Figure D.6 are positive. The difference between the path taken and the reference path is very difficult to see. Figure D.7 is a magnified picture of the last part of the manoeuvre, where the largest path deviations of the vehicle from the reference path were seen. The largest deviation of the vehicle from the path can be seen to be 0.1 metres, which is well within the value of W.

Figure D.8 and Figure D.9 show the control inputs used throughout the manoeuvre. In conjunction with Figure D.6, the nonlinear path following routine appears to be working effectively. The deviation from the reference path is very low and the steer inputs are smooth and continuous. Given that the maximum steer angle, as defined by the overall saturation value, is $\pm 16°$ the car is controlled well within its limit steer capability. Inspection of the throttle input shows that in contrast to the steer input, the control is quite oscillatory. The throttle input is initially 100% open but the brakes

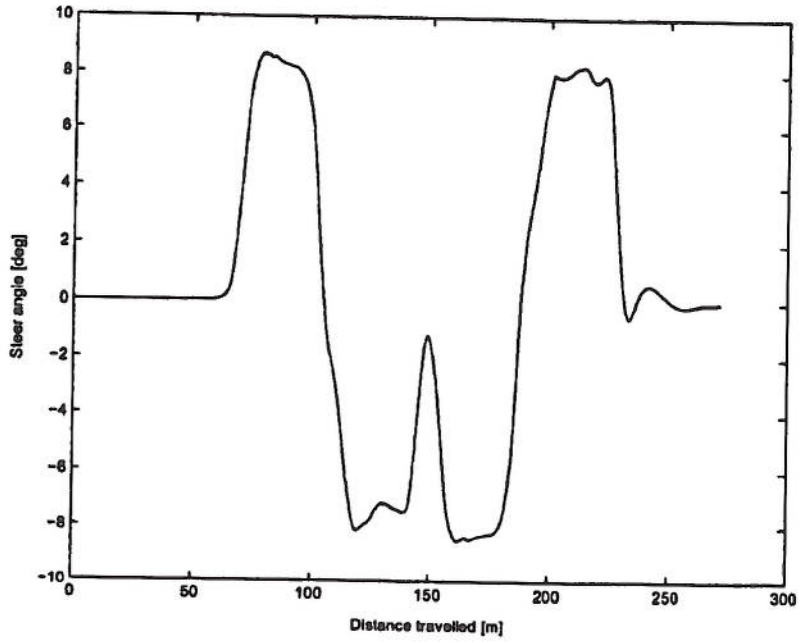

Figure D.8: Double lane change - steer angle.

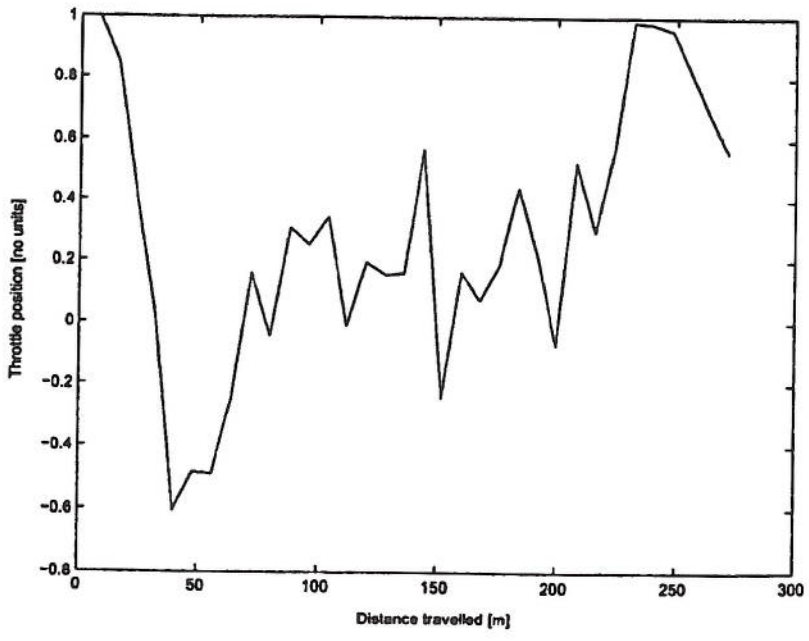

Figure D.9: Double lane change - Throttle position.

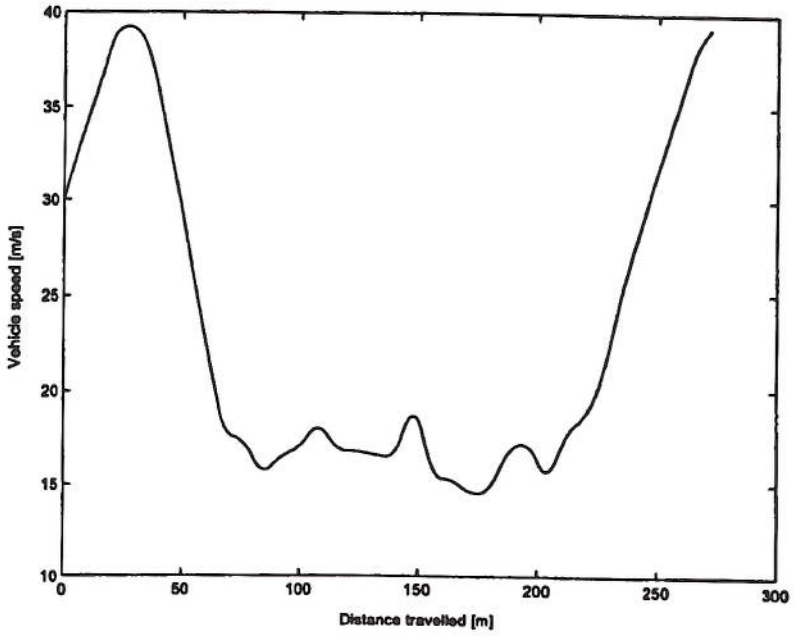

Figure D.10: Double lane change - vehicle speed.

are applied (throttle input less than zero) very early. In the middle of the manoeuvre, the control is oscillatory about zero which is less than ideal. Out of the third corner the throttle input then climbs towards 100% to complete the manoeuvre. The vehicle speed history is much smoother than the throttle history, but still reflecting the oscillatory behaviour seen in the throttle history in the middle of the manoeuvre (Figure D.10). The vehicle speed throughout the manoeuvre also appears quite low considering the performance potential of the vehicle. This can be checked by running the QSS program through the same manoeuvre to provide a reference. The vehicle speed profile for the same base vehicle for the same manoeuvre, starting at 30 m/s, is given in Figure D.11. This comparison shows that the result compares quite well, considering that the GG speed diagram was only calculated down to 20 m/s. The vehicle speed and accelerations are interpolated between 0 and 20 m/s for the QSS simulation, and therefore may be incorrect due to the 20 m/s gap. The vehicle configuration and setup are identical, which implies that the transient path following optimiser is effectively controlling the vehicle, even though the throttle control does appear overly oscillatory. This has been traced to the shape of the radius of curvature information, which is particularly sharp and changes abruptly in the middle of the manoeuvre, and explains why there is a similar trend in the speed history of the QSS simulation result.

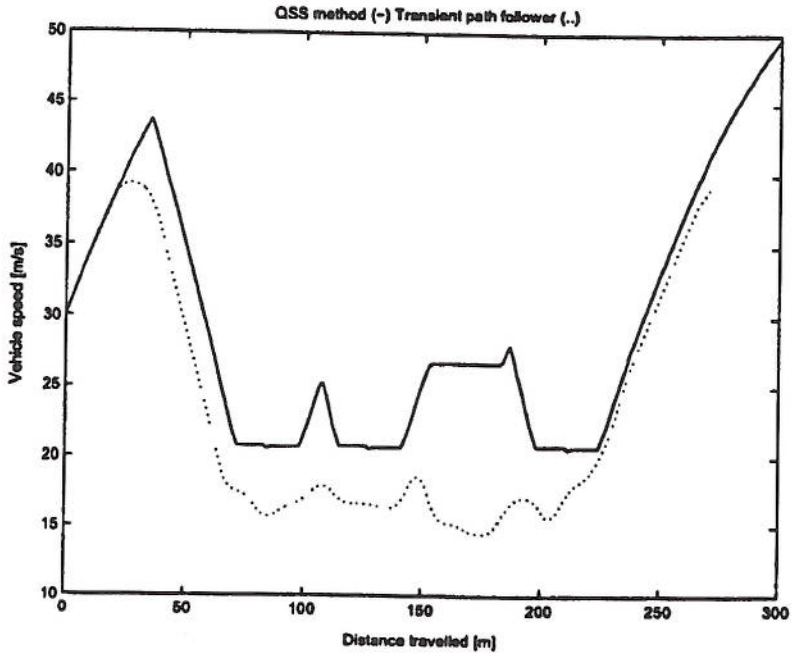

Figure D.11: Double lane change - vehicle speed - QSS check.

To determine whether or not this new transient method can be considered an improvement over Casanova [3]'s method, a comparison of the two methods, with the same vehicle on the same trajectory, is needed. This is achievable using a result found in Casanova et al. [21] for another double lane change.

D.3.1 Transient optimisation

The current method uses finite differencing (FD) for evaluating the derivatives for the SQP method. This was chosen because FD in early trials of the path following optimisation program was found to be significantly faster. To evaluate the derivatives, using FD for one set of derivatives, took 124.2 seconds, while the corresponding AD call took 363.6 seconds. This shows that using FD only takes 33% of the time for the AD result to be determined. FD has been used so far with reasonable results as shown in the previous section.

The path following optimisation method (PF), as described earlier, has been applied to an optimised trajectory to allow direct comparison with the TO method of Casanova [3] to determine its effectiveness.

The PF method result is compared with the TO results in Figures D.12, D.13, and D.14, and took 4.9 hours to run.

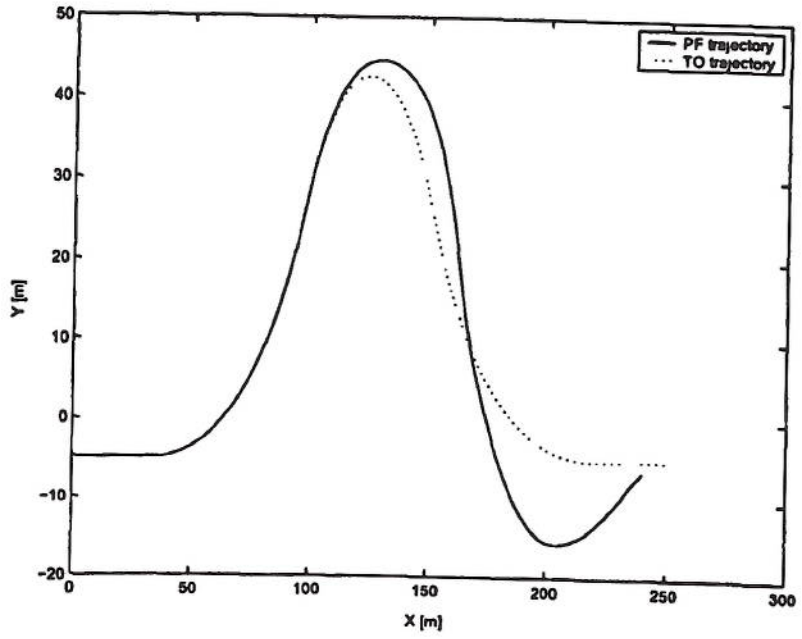

Figure D.12: Double lane change comparison - Path taken.

Clearly, the PF method has not been able to follow the TO trajectory very well (Figure D.12) and the speed of the vehicle in the PF method is very poor compared with the TO result. The steer angle result, while much smoother than the corresponding TO result, clearly saturates at the last corner of the manoeuvre, resulting in significant path deviation. The optimiser did terminate with a converged result, which suggests that either the penalised objective is poorly specified for the aim of minimum time manoeuvring, or the derivative information is not as accurate as it needs to be for the SQP method to produce the correct solution.

Considering that the initial validation exercise on another double lane change appeared to work well, the focus switched to the derivative information. The AD method, which was documented in Section 2.3.3, albeit quite slow for this method implementation, was used. The results of the PF program, under AD calculation of derivative information, is shown compared with the TO results in Figures D.15, D.16, and D.17. The optimisation took on the same reference Intel 1000MHz PC, 10.6 hours, which was nearly twice as long as the FD version.

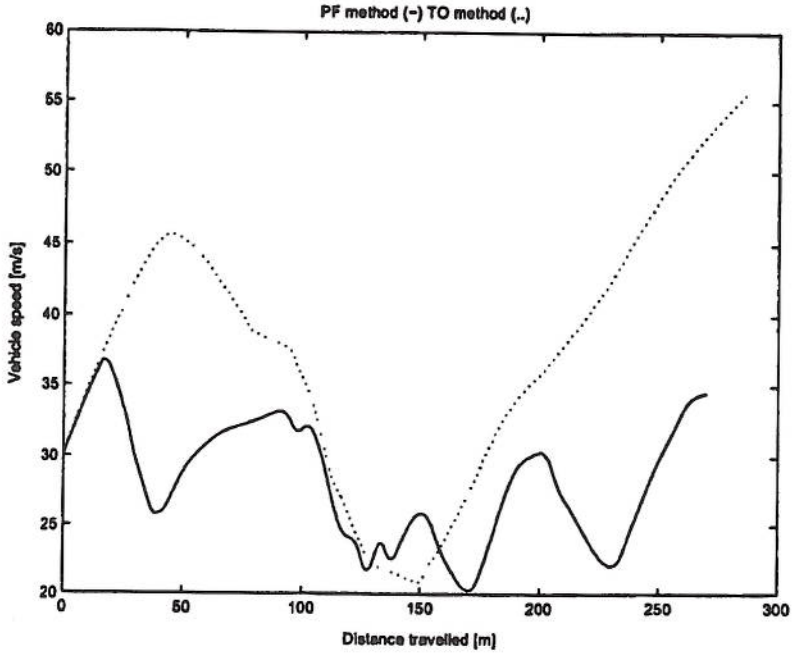

Figure D.13: Double lane change comparison - vehicle speed.

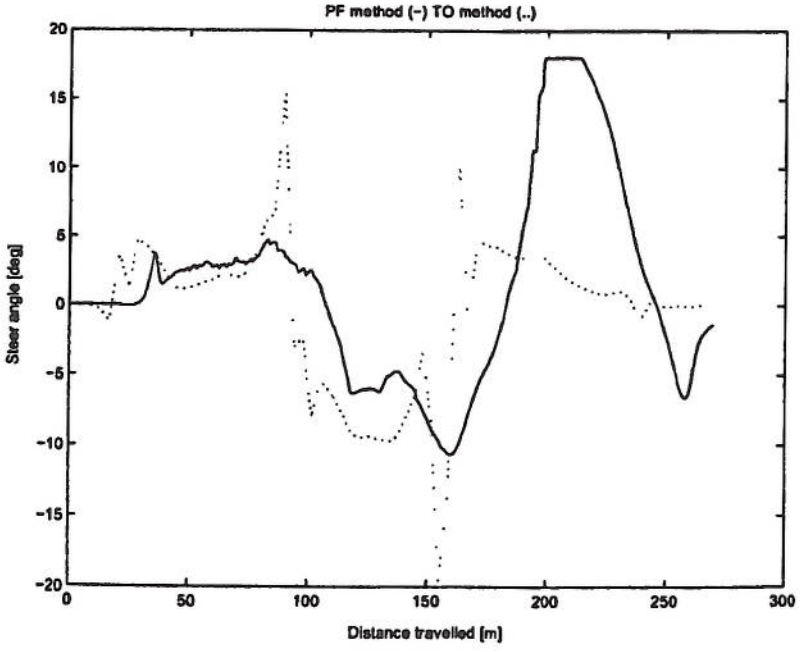

Figure D.14: Double lane change comparison - Steer angle.

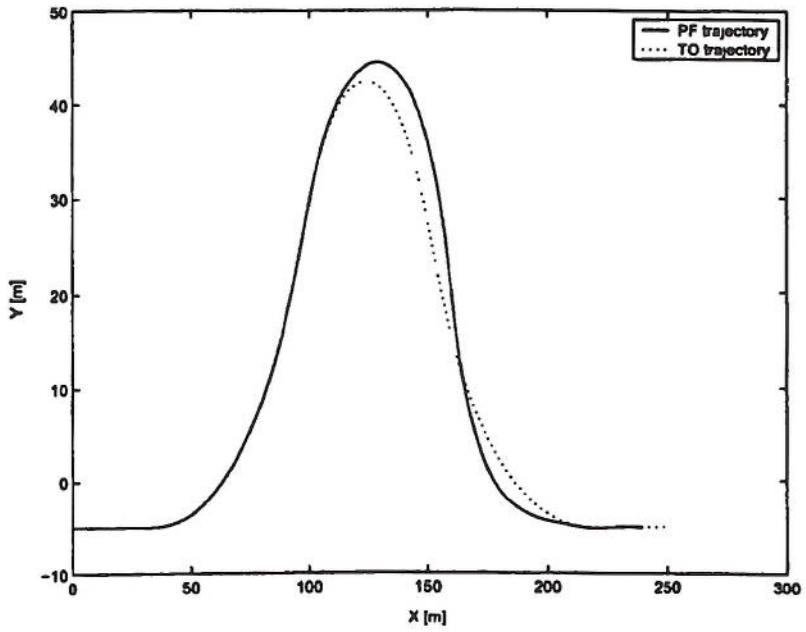

Figure D.15: Double lane change comparison - Path taken AD version.

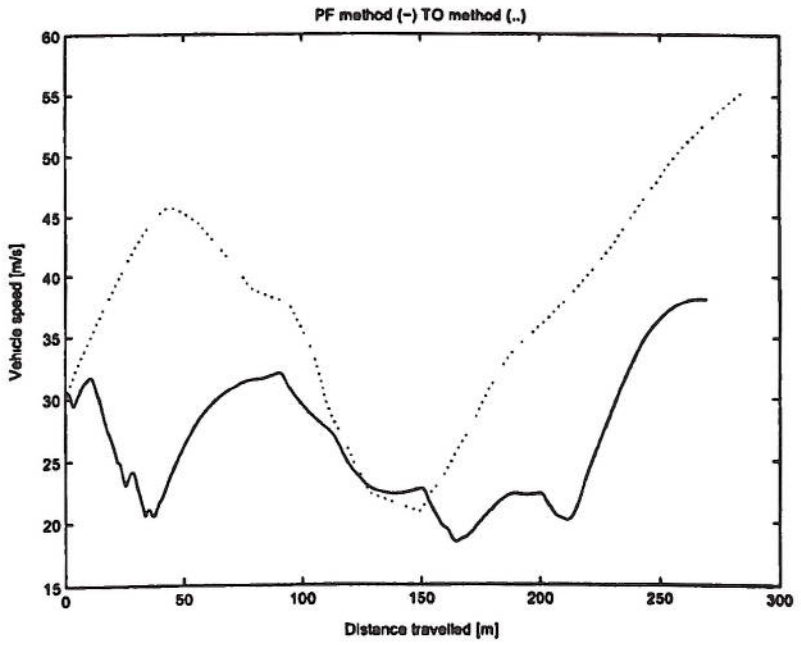

Figure D.16: Double lane change comparison - vehicle speed AD version.

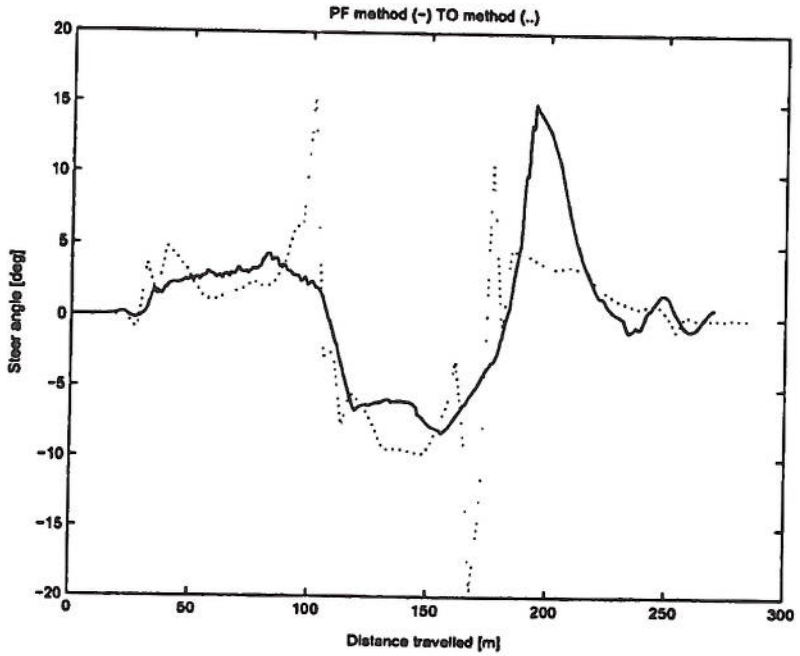

Figure D.17: Double lane change comparison - Steer angle AD version.

The implementation of AD has helped remedy the path tracking problem seen in Figure D.12. The path followed by the vehicle using AD in Figure D.15 is a significant improvement and while not as effective as the tracking achieved in Figure D.6, is sufficient to look beyond the path following and examine other parts of the simulation result. The vehicle speed of the PF result is again quite poor when compared with the TO result. At the beginning of the simulation, the speed of the vehicle is only increased by 3 m/s and then drops off to 20 m/s, whereas the TO result continues to accelerate to 46 m/s before braking into the first turn of the manoeuvre. Beyond this phase the TO result finds the apex at 150 metres, much earlier than the PF result, and then is able to accelerate beyond the apex of turn two and through turn three. The apex of corner two is found to be near 165 metres for the PF result. The PF method vehicle then has a small acceleration up to the final corner, then a further speed reduction followed by hard acceleration afterwards.

The disparity between the results from the two methods is unexpected. Closer inspection of the TO results highlights some very unusual control decisions, which seem contradictory to conventional wisdom on driving techniques. Approaching the first corner, the optimised steer input is found to be low until 100 metres distance travelled

where the steer input rises rapidly to 15° which is equivalent to a very sharp movement from nearly zero steer angle to full lock. This steer angle control occurs under braking. Further, after the apex at the middle of the double lane change, the vehicle is simultaneously accelerated and subjected to a very sharp sinusoidal steer input from full right lock to nearly two thirds left lock. Both of these two aspects of the vehicle control by the TO method through corners one and three would appear to be conducive to destabilising the vehicle. There are two plausible explanations for this:

- The optimiser in the TO method is using the control inputs to generate much higher changes of direction through exciting the yaw mode of the vehicle sprung mass instead of that achievable from utilising the steer input to generate trimmed steady state cornering. As a result the optimiser has found a non-conventional control scheme that while destabilising in nature, ultimately improves the manoeuvre time significantly.

- There is an aspect of the TO method implementation that allows this control situation to occur without the loss of vehicle directional control that would occur normally in a simulation.

To investigate this, the double lane change is run with the optimised control inputs from the TO method to see if the results are reproducible. However, the steer control and throttle control can only be implemented by redefining the results. The TO method is referenced to the centre line of the track, not the current racing line, so the distance travelled must be determined from the cartesian coordinates of the final path, and then the steer and throttle inputs are re-spaced using interpolation methods to give the true distance travelled.

A distance space simulation was then run using the optimal steer and throttle positions found from the TO method, but the simulation crashed after 72 metres where the vehicle spun out after the first corner. The reasons for this could not be determined beyond the possibility that the control inputs are, by definition very close to the limit, and the sharp transients seen in the steer control under braking in the first corner cause the vehicle to spin out under this simulation program which has been written in another programming language and uses a higher order Runge Kutta integrator than Casanova [3].

The QSS method was employed here to determine the vehicle speed history using the same vehicle to determine a sensible reference point to make a value judgement on the PF and TO results. Figure D.18 shows the three results. As can be seen the PF result, which is the better performing AD result, is considerably slower than the capability suggested by the QSS method. A surprisingly result is that the TO method result is actually faster than the QSS method result. This does suggest that the transient behaviour has been exploited by the TO optimiser to control the vehicle beyond that possible in quasi steady state.

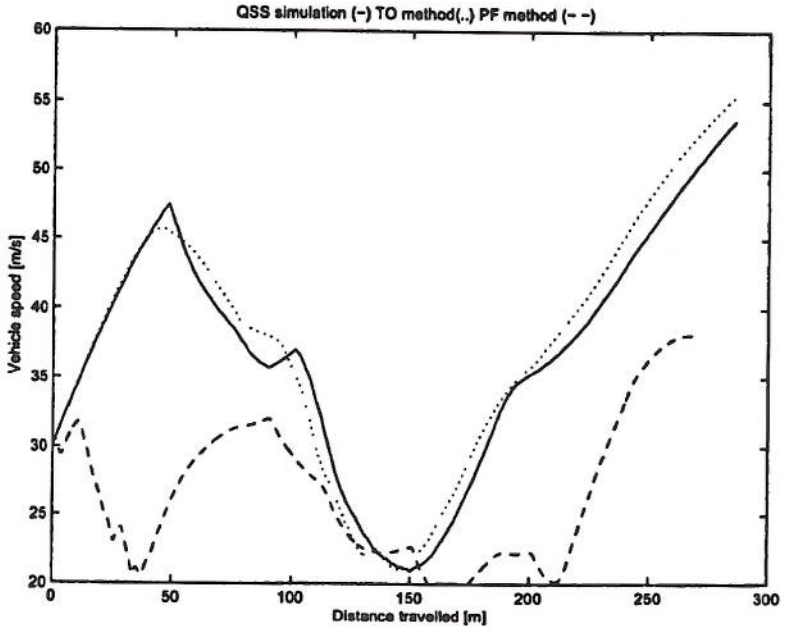

Figure D.18: Double lane change comparison - Vehicle speeds.

There is further work to be done in this area of transient path following optimisation, as can be seen in the disparity between the vehicle speeds shown in Figures D.13 and D.16 of the PF and TO results. While the TO result could not be replicated it is clear that the current PF method is not solving the minimum time problem adequately on this difficult trajectory. The suggested next step to further this development is to separate the path constraint penalty function from the objective to make the minimum time solution clearer for the optimiser to deal with. It is believed that the program could be sped up significantly if the program was translated into a precompiled language, and a SQP algorithm, which can exploit sparsity of the Jacobian, is used. However, this strategy is

heading towards the final form of the TO method research, with separate objective and constraint functions, user defined path segmentation, and differing grid discretisation depending on track geometry to speed up the program computational time. At present the solution time for the current double lane change varies between 4 and 11 hours in MATLAB, whereas the TO C++ program produced by Casanova [3] solved the full circuit problem in an average of 39.8 hours. It is clear to the author that the current program computational time will converge or slightly improve on that achievable using the TO method. It is believed that the research conducted by Casanova [3] represents an efficient means of implementing optimal control methods for the task of solving the minimum time problem and does not need to be re-researched here. The basis that both the PF and TO methods require multiple simulations to find the solution cannot be side stepped using optimal control, and as a consequence will always be a time consuming process. Instead a different approach, which is the subject of the following section, will be described.

D.4 Nonlinear preview Proportional-Integral (PI) control

The essentials of a basic control arrangement are [111]:

- a controlled condition eg vehicle spatial position.
- a device for measuring the value of this condition i.e. a measuring unit.
- an apparatus capable of effecting a change in the controlled condition i.e. a regulating unit.
- a means for operating the regulating unit in response to the measuring unit, i.e. a controlling unit.

For the current PF method the vehicle is controlled to minimise the time for the vehicle to complete a manoeuvre. The apparatus capable of changing the final time is the engine and braking torques applied to the vehicle, which is controlled by the throttle control history of the vehicle throughout the manoeuvre. This problem definition is not a simple one because there are many factors that affect the final time that are non-linear, such as the tyre force response to the wheel slip and the effect of aerodynamics due to vehicle speed change. While the use of the throttle to control the vehicle is a

very powerful method of influencing the final manoeuvre time, the link between the two is clearly complicated, and because the relationship is far from linear an iterative nonlinear method is required to solve the problem.

However, the other significant means of control of the vehicle, the steer input, is controlled in another manner. The PF method uses a nonlinear preview driver model to make the vehicle follow a prescribed vehicle path. It was identified that there was a strong link between the steer input and the vehicles ability to follow a path, if provided with information of the track immediately ahead [85]. Additionally that path could be prescribed exactly before trying to implement the control, allowing measurement of the error in the vehicles current path and the reference path to be made. As a result a modified form of linear feedback control was found to be capable of effecting satisfactory trajectory control, even though the vehicle model itself is nonlinear.

To reduce the computational effort that is associated with running multiple simulations to meet an objective, a control approach similar to the steering control is suggested. As mentioned above, the key requirements are a very strong relationship between the controlled variable and the measured, reference variable, and the ability to prescribe the reference variable exactly before implementing the control. The difficult aspect here is finding the reference variable for the vehicle to be controlled to. In the early stages of this research [112] the use of PI (Proportional plus Integral) control was effective in controlling the vehicle model to meet a constant acceleration target. This was achieved by directly controlling the engine torque and brake torques. Here it is proposed that the minimum time vehicle speed history will serve as the reference to be controlled directly by the throttle.

The only remaining task is finding the minimum time vehicle speed history. In reality this can only be found from a program such as the TO or PF method which has, as an objective, the minimisation of the vehicle lap time. However, there is an alternative which is sub-optimal but very close to the minimum time solution. It is shown in Figure D.18 that the QSS vehicle speed history is very close to that of the TO method. The TO method result could not be replicated in this research with a full numerical simulation that time/distance marched through the entire manoeuvre, but it is plausible that the QSS result could be scaled until the simulation will solve without the vehicle spinning out of control. If the QSS vehicle speed history is used then the result will be sub-optimal but could be very close to the minimum time solution, depending on

the scaling required. In addition the computational savings are significantly reduced because only one numerical simulation is required to complete the problem. The total solution time is a summation of the computational times of the GG speed diagram, the numerical simulation using the GG speed diagram, and the transient numerical simulation. Depending on the vehicle model used, this process could be less than 30 minutes on a 1000MHz Intel PC.

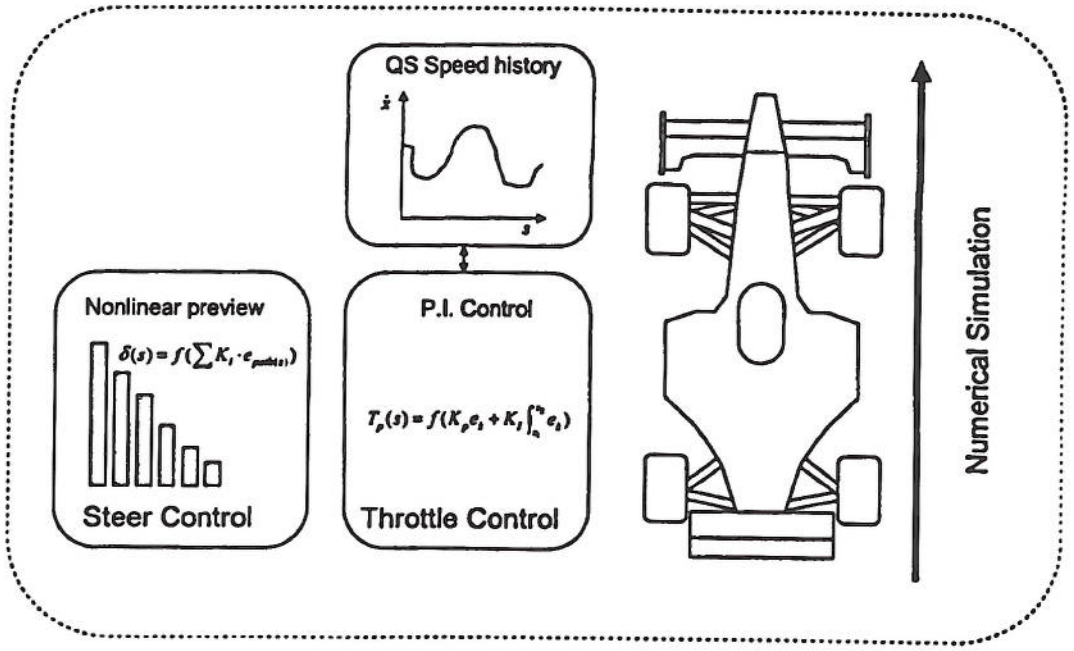

Figure D.19: Transient path following with PI throttle control.

The new nonlinear path following program with PI control is shown diagrammatically in Figure D.19. In the following section the use of PI control will be formalised and the implementation in the seven DOF published vehicle model will be described.

D.4.1 Throttle control

The use of proportional plus integral control has been well documented.

> Proportional action is a mode of controller action in which there is a continuous linear relation between values of the deviation and manipulated variable [113] (p61).

Proportional control follows the following law:

$$m = K_P \cdot e + C \tag{D.6}$$

where

m = manipulated variable.

K_P = proportional gain.

e = deviation.

C = a constant.

The proportional gain is the change of the manipulated variable caused by a unit change in e and is equivalent to an amplifier with an adjustable gain.

> Integral action is a mode of control action in which the value of the manipulated variable m is changed at a rate proportional to the deviation. Thus if the deviation is doubled over a previous value, the final control element is moved twice as fast [113] (p64).

Integral control follows the following law

$$\dot{m} = \frac{1}{T_i} \cdot e \tag{D.7}$$

where

m = manipulated variable.

T_i = integral time.

e = deviation.

The integral time T_i is defined as the time of change of manipulated variable caused by a unit change of deviation [113]. Integral control is normally used in combination with proportional control. Its primary effect on a system is to act on long-term (or steady state) errors in order to reduce them to zero [114].
According to Eckman [113], PI control action is defined by the following integrated form:

$$m = \frac{K_P}{T_i} \int e \cdot dt + K_P \cdot e + C \tag{D.8}$$

where

t = time

C = constant of integration

where the function $\frac{K_P}{T_i}$ defines the integral action and the gain K_P identifies the proportional action. Equation D.8 illustrates that the integral action of the controller is also influenced by the proportional gain. To keep things more distinct, the PI controller on the seven DOF published vehicle model uses a slightly modified form of Equation D.8. Equation D.9 shows that the integral control is defined simply as K_I:

$$m = K_I \int e \cdot dt + K_P \cdot e + C \tag{D.9}$$

where K_I is equivalent to the function $\frac{K_P}{T_i}$.

The numerical simulation program is updated with the PI expression in Equation D.9 where the deviation e is equivalent to the difference in the vehicle speed and the reference speed history at that particular point on the racing line, and m is the resulting throttle position, T_P.

This method relies on the fact that the throttle position can affect a direct change on the vehicle speed, which is believed to be a reasonable assumption. Additionally, it relies on the decoupled steer controller to be sufficiently robust to maintain the vehicle on the correct path, otherwise the value of the current distance in a numerical simulation will not correspond to the same position on the reference trajectory to which the QSS vehicle speed is aligned. This could have dire consequences for the validity of the simulation result. Both the PI throttle controller and the preview steering controller must be robust if the vehicle is to be controlled on the QSS limit of the vehicle performance.

D.4.2 Results

From this point forward the method which uses the QSS vehicle speed history and PI control to administer the throttle control, coupled with the nonlinear preview control for the steer input, will be referred to as the PI method.

The first aspect of setting up the PI method to work properly was to tune the PI controller to provide satisfactory control performance. This was done in the conventional

manner of tuning the proportional gain initially (K_I set to zero) so that the controller responded quickly to changes in vehicle speed. This was found to be achievable with K_P set to 5. Integral control was then introduced until the steady state error was reduced to undetectable levels. This was found to be at a relatively small value of K_I of 0.1. The constant of integration was set to 0.2. In a similar manner to the preview steer controller, a saturation function was applied to the final throttle position. If the throttle position exceeded 1 or was found to be lower than -1 then the throttle was moderated to these maximum values.

Given these settings, the TO double lane trajectory, used in the previous section, was used as a test case. The QSS vehicle speed history for the same manoeuvre was used as the reference for the PI controller (Figure D.18). Initially the entire QSS speed history was scaled to 80% of its original value to determine whether the method was suitable for transient path following. This was successful, and subsequent research showed that the method, without any further adjustments, was capable of following the desired trajectory at the full QSS vehicle speed. The speed tracking result is shown in Figure D.20.

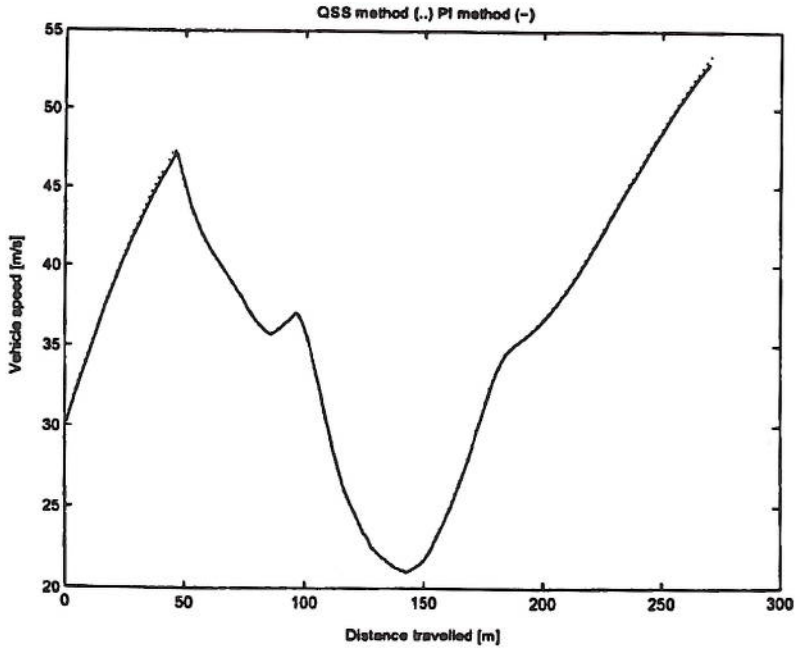

Figure D.20: Double lane change comparison - Vehicle speed PI method.

The vehicle speed tracking control is acceptable. The two vehicle speed histories are virtually indistinguishable. This result shows how close the QSS result is to the corresponding transient result. The time to run the simulation is only 296 seconds and the result is clearly very close to the minimum time solution found by the TO method (Figure D.18).

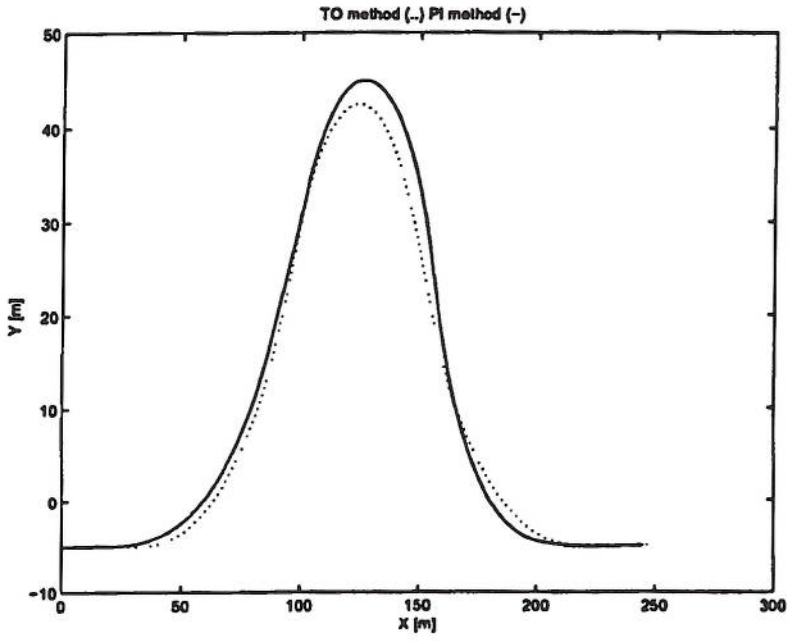

Figure D.21: Double lane change comparison - Path PI method.

The path tracking ability of the steer control shown in Figure D.21 is sufficiently reliable to be a major improvement over the results from both the PF method variants. The maximum deviation from the path was found to be 3 metres, at the middle of the double lane change.

The steering response of the nonlinear preview controller is compared with the corresponding control produced by the TO method (Figure D.22). The trends are very similar, but show that the steer control of the preview controller is significantly smoother than the TO result, and does not contain the same large transients noted in the previous section in the first and third corners.

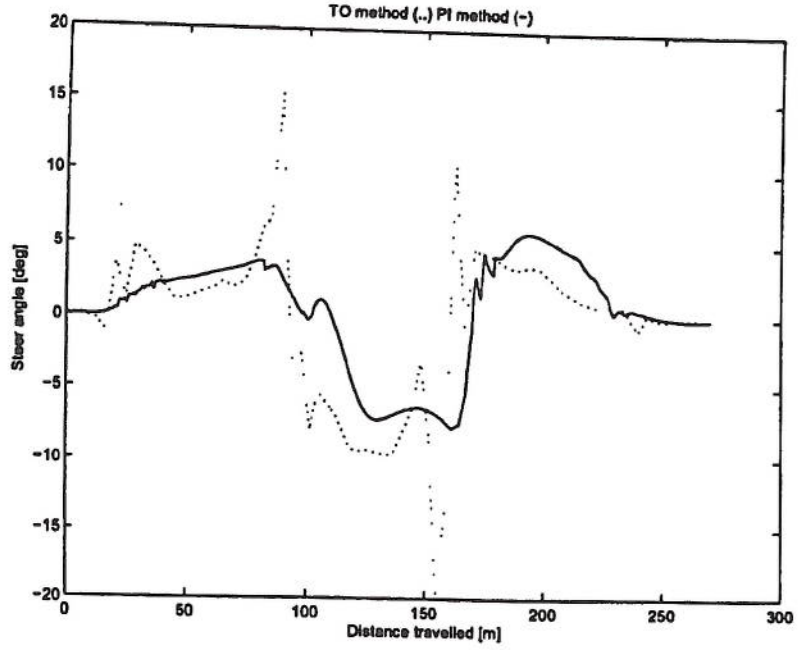

Figure D.22: Double lane change comparison - Steer angle PI method.

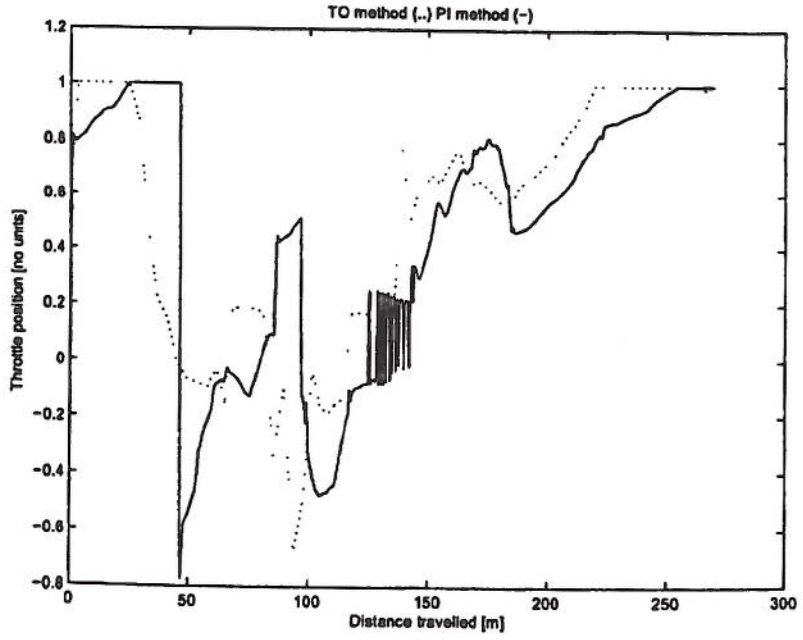

Figure D.23: Double lane change comparison - Throttle position PI method.

The throttle control produced by the PI controller is shown in Figure D.23. Interestingly, the PI throttle is held at 100% for much longer, and the vehicle is braked, more severely than the TO throttle history, into the first corner. Considering that the vehicle cornering speed at the second corner is virtually identical at 21 m/s it seems possible that the vehicle could be made faster than that suggested by the TO and PI methods, if the two speed profiles were combined in some manner. While an interesting prospect, modifying speed histories has not been pursued. The throttle controller appears to find the low speed second corner of the manoeuvre difficult, which is indicated by significant oscillation (Figure D.23). To determine the cause of this, the QSS speed history is interrogated in this region. This region is shown in Figure D.24.

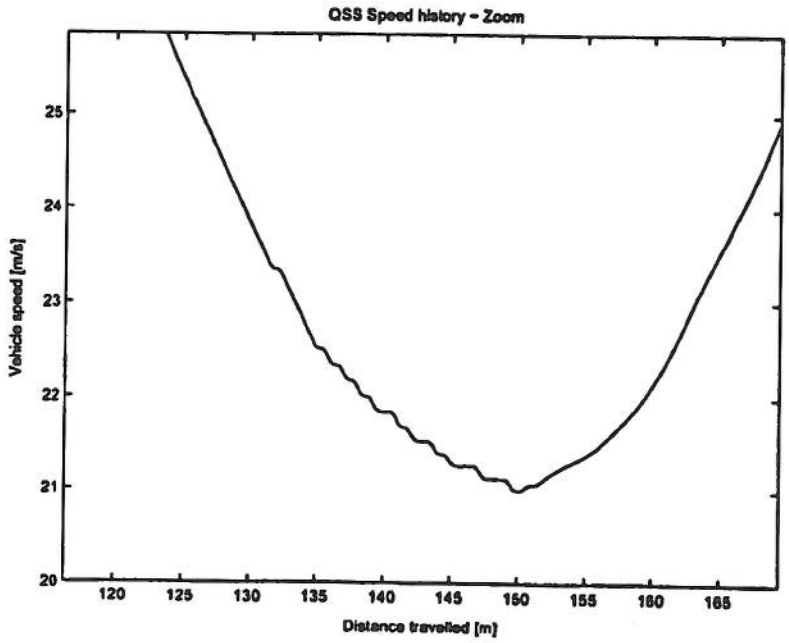

Figure D.24: Double lane change comparison - Vehicle speed PI method (Zoom).

The cause of the controller oscillatory behaviour is now clear. The controller is trying to follow an oscillation in the reference QSS vehicle speed history. This can easily be rectified by smoothing the reference speed history, or by performing the QSS simulation with a better choice of distance step.

As a final validation step, the PI method is provided with the vehicle speed history found by the TO method. This simulation was performed to finally provide an answer

to the question raised in section D.3.1; why the optimiser, used in the TO method, required sharp steer angle transients to complete the manoeuvre.

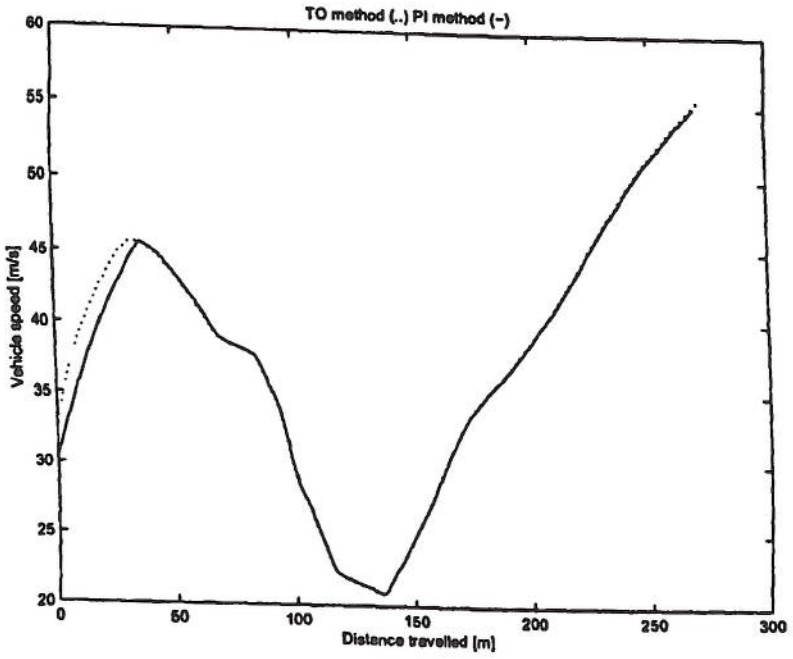

Figure D.25: PI method using Transient speed history - Speed comparison (PI controller performance).

Under the influence of the nonlinear preview steer controller the vehicle has not spun out, and the manoeuvre was negotiated successfully, as seen in Figures D.25 and D.26. The only significant deviation from the prescribed speed history is in the approach to the first corner. This is due to the transients resulting from the initial wheel speeds being incorrect. The initial conditions are approximated by dividing the vehicle speed by the wheel radiuses, in the PI method. More interestingly, the throttle control provided by the PI controller is virtually identical to the TO result in Figure D.27.

Therefore, the trajectory followed by the two PI method controlled simulations suggests that there is an error in the path description, most likely in the radius of curvature estimation for the manoeuvre. This is concluded because the steer controller is not being pushed to the limit of its steering capabilities (Figure D.28), as was seen in Figures D.12 and D.14, and the path following capabilities have been shown to be within 0.1 metres in Figure D.6, where the radius of curvature information was of good quality.

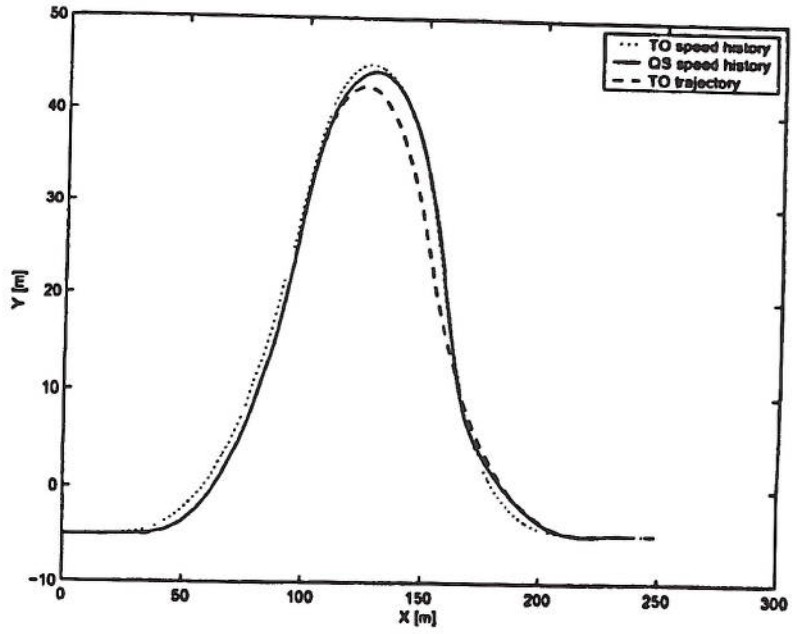

Figure D.26: Path taken by PI method using QSS and TO speed histories.

Bearing this in mind, it can be concluded from this series of results that the steer control of the TO method was the cause of the simulation crash, when the simulation was attempted with the TO control histories. Consequently, the preview steering controller used here appears satisfactory in producing reasonable path following at on-limit or very near the limit capability of the vehicle. Similarly the PI control has been shown to be adequate in following an on-limit or near limit speed history, by being able to reproduce a near optimal throttle history (Figure D.27).

The PI method has a computational time of approximately 25 minutes using the published vehicle model. This is a significant improvement to the four hours of the PF method in its current state and the TO method which is approximately four hours for the double lane change manoeuvre. It is felt that the PF method could be improved further if an optimised transient path follower was required, but the ability of the PI method to provide a near optimal on-limit vehicle transient simulation quickly is attractive as an alternative. Additionally, as a by product of the process, a GG speed diagram is produced, which can be applied to all manner of manoeuvres and circuit geometries for the same vehicle set up and configuration.

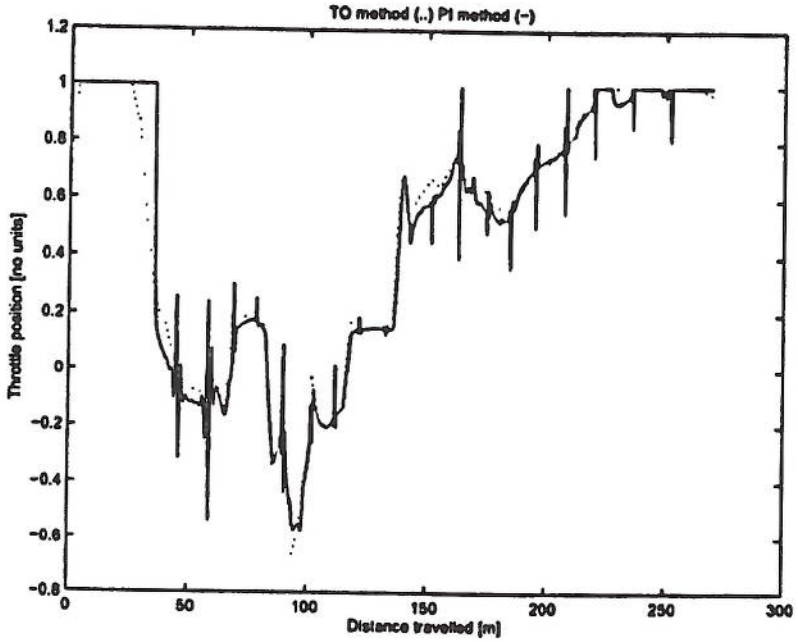

Figure D.27: Throttle history derived by PI controller using TO method speed history.

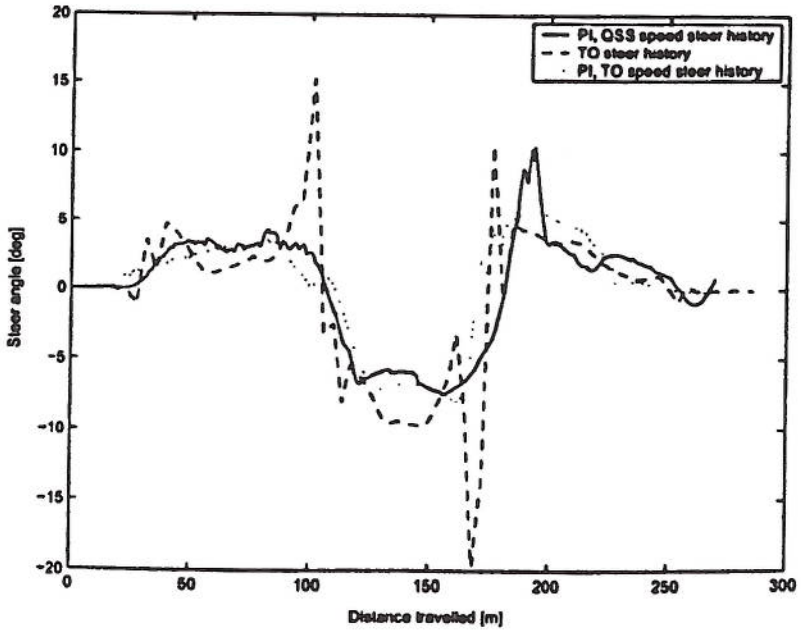

Figure D.28: Steer angle history comparison using the PI method, compared to the TO method steer history.

Appendix E

PI method case study: stability control

E.1 Forms of β control

The niche area of motorsport raises interesting possibilities and challenges for vehicle stability control (VSC). A large proportion of passenger car research focusses on cost effective means of measuring β and $\dot{\varphi}$, [73–76] whereas cost is not a huge issue within the motorsport industry. However, it has been identified that the control of torque distribution between left and right wheels of axles is far more influential than control of torque to an axle *[115]*, but this method is not allowed within the technical regulations of Formula One [45].

The vehicle stability research in this chapter is exploratory and does not address the issues of implementation of sensors. This is assumed to be technically feasible, and the body of literature suggests this to be correct. The question to be answered here is; would a form of VSC be of value in improving the performance of the Formula One vehicle on the limit?

There are two lines of enquiry that have been identified for study that could realistically be applied within the regulations of Formula One:

- Intervention when the value of β reaches a predetermined critical limit.
- The use of $\dot{\beta}$ as a control variable to be minimised.

The reason for investigating $\dot{\beta}$ minimisation is linked to the success of the QSS program. The approximation of quasi steady state for a Formula One car simulation has

been shown in previous chapters to be accurate when compared with a corresponding optimised TO result. Chapter 5 showed that $\dot{\beta}$ must be zero if the vehicle is cornering in steady state and under this assumption the QSS method was capable of producing a lap time in close agreement with a transient minimum time optimised control result. Therefore, if the value of $\dot{\beta}$ can be minimised during a simulation it appears plausible that the vehicle could be stabilised at the QSS limit, during a difficult manoeuvre, by the control.

Based on the Formula One vehicle that has been used throughout this thesis, one practical method offering the potential range of control required is engine torque control.

In practice, engine torque can be reduced by the throttle position, ignition retard, or a switching off of ignition or injection for a defined number of cylinders, as it is done for a traction control system [67]. The torque reduction via the throttle is not favoured in Formula One due to the response time being too slow [67]. It is understood that other means would normally be used to implement engine torque control, but for the purposes of this case study the throttle will be used because it is fast acting in the simulation environment, and adequate for exploratory VSC studies.

E.2 β limit VSC via engine torque control

It was decided to investigate the magnitude of lateral motion change that can be imparted through control of the engine torque. The approach taken here to achieve this is a practical one. A transient simulation, using the base vehicle model, is run at high speed (50 m/s) in a steady state cornering manoeuvre, with a fixed steer angle. The steer angle is then varied using a golden section search method and the simulation re-run to find the steady state steer angle that generates the maximum lateral acceleration. The PI method is used with a fixed longitudinal velocity target to produce the simulation results.

To ascertain the usefulness of engine torque control for VSC, the engine torque must be controlled in response to a signal of some description. Therefore a simple β limit controller, using logic statements, was designed to cut the engine torque completely in response to a $|\beta|$ limit being breached. This method worked, but the speed of the

vehicle consistently dropped down to 20 m/s from the 50 m/s target. The next step taken was to implement a continuous controller using automatic control methods. A proportional controller was implemented to work on the error between the current value of β and the limit value, when the limit had been breached. The β angle response was found to be stable but oscillatory. The following results represent the steady state manoeuvre using a PI controller, with the integral control tuned to dampen much of the oscillation in the vehicle β angle response. Derivative control was also implemented but showed no discernable improvement. Its use was not continued.

The on-limit fixed steer angle of the limited slip differential (LSD) base vehicle was originally found to be 4° (Table 7.1), and this coincided with a limiting value of $\beta = 1.73°$. To show the effect of the β controller a β limit of 1.5° was set and three fixed steer angles were simulated. Steer angles of 2°, 4° and 6° were used, to create three situations: one where the controller action would not be required, one where a reasonable amount of controller action would be required, due to an optimistic steer angle, and finally a situation where significant controller action would be required, due to a high steer angle, for the given vehicle target speed.

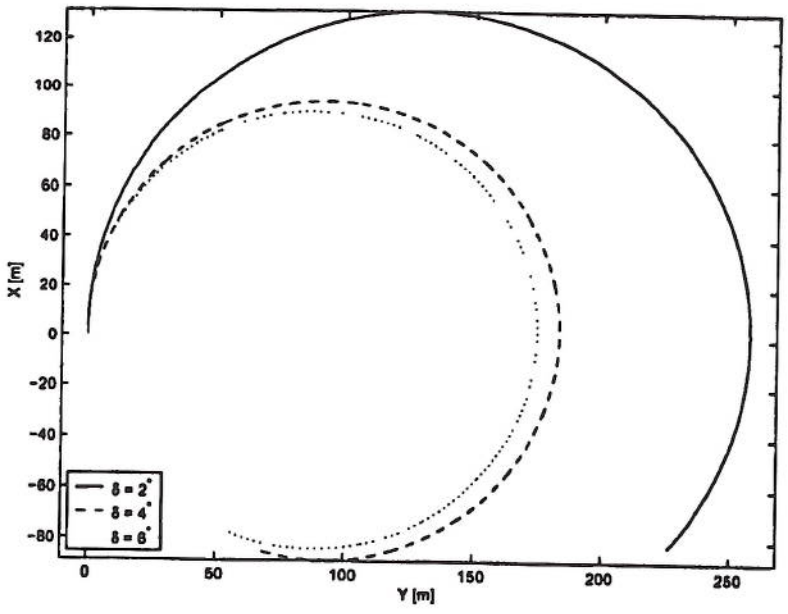

Figure E.1: Path taken with sideslip angle limit $\beta = 1.5°$, for three steer angles.

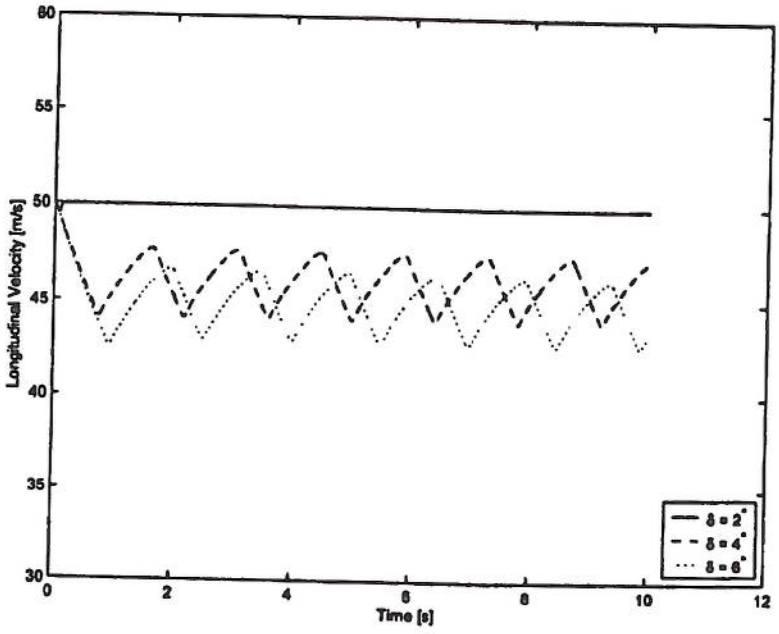

Figure E.2: Vehicle speed with sideslip angle limit $\beta = 1.5°$, for three steer angles.

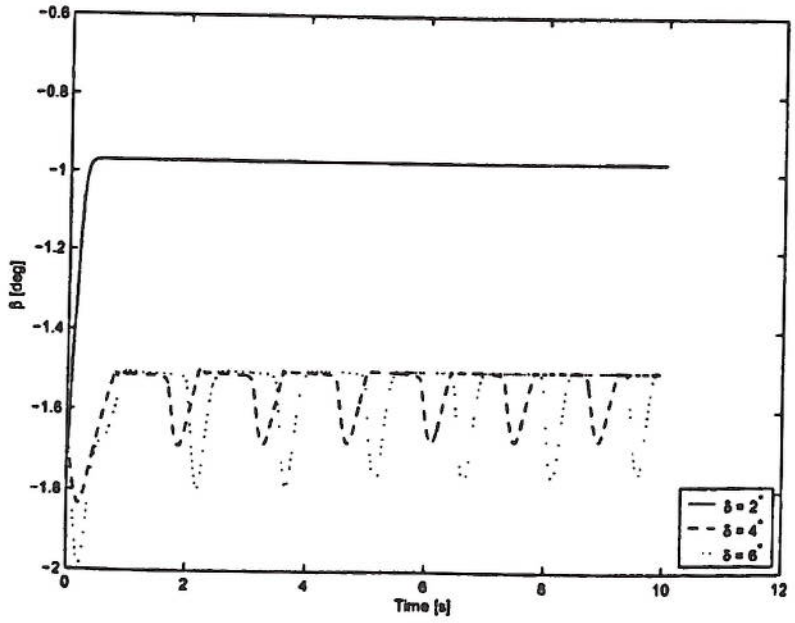

Figure E.3: Sideslip angle with limit $\beta = 1.5°$, for three steer angles.

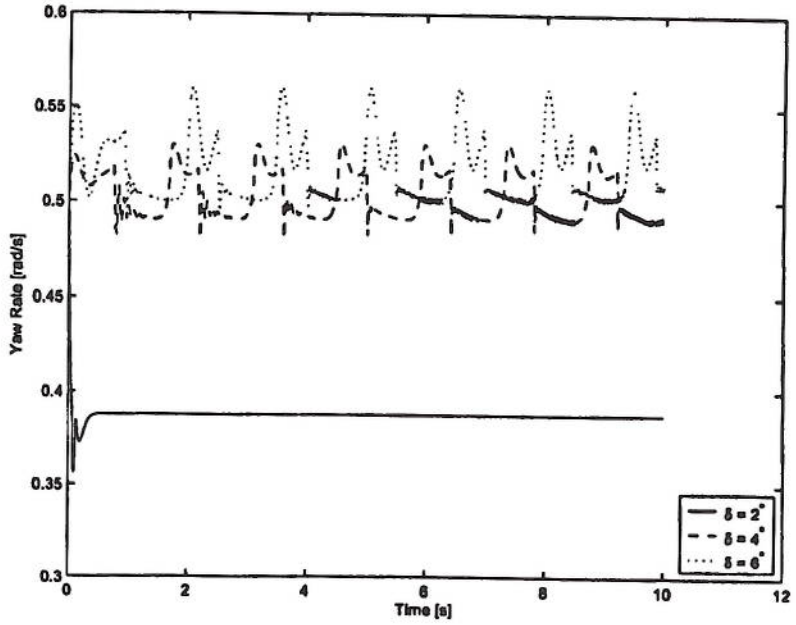

Figure E.4: Yaw rate with sideslip angle limit $\beta = 1.5°$, for three steer angles.

The path taken by the three vehicle simulations is shown in Figure E.1. The widest radius of turn of the three results was produced by the 2° result. The 4° and 6° results were much closer to each other. This is partly because the vehicle speed is now varying as a result of the β limit control. At 2° the limit on β was not reached and the simulation stabilised at $\beta = 0.97°$ (Figure E.3). Figure E.2 shows the respective vehicle speeds for the three simulations. The 4° and the 6° result show significant oscillation. This is due to the action of two competing controllers. The β limit controller closes the throttle if the β limit is reached. This has the effect of reducing the vehicle speed. Once the vehicle sideslip angle stabilises at 1.5° the stability control is stopped, and the PI controller, used by the PI method, opens the throttle to try and achieve its vehicle speed target of 50 m/s. This creates the oscillation seen in the vehicle speeds for the 4° and the 6° results in Figure E.2.

The control of β to a limit using automatic control has been reasonably successful. Figure E.3 shows the vehicle sideslip angle being controlled to 1.5° for both 4 and 6° of steer angle. Since the stability controller only activates on the β limit being breached, there is an inevitable oscillatory component in the control during this manoeuvre.

As a consequence of the β control, the yaw rate is also limited, but for each increase in fixed steer angle, the mean yaw rate increases (Figure E.4). This reinforces the notion that both sideslip angle and yaw rate can increase or decrease independently of each other.

The use of Proportional Integral control appears satisfactory for controlling the vehicle stability and therefore this method will be retained for the β limit strategy and employed for the $\dot{\beta}$ minimisation control strategy. The PI method will be used in the following section to generate an on-limit vehicle control history. Following this, the path friction coefficient will be modified to create instability during the manoeuvre. The simulation will then be run again to highlight the effect of implementing the two prospective control strategies for vehicle on-limit stability control. It should be noted that the implementation of VSC will ultimately penalise the progress of the vehicle because engine torque is sacrificed if the VSC is employed. However, what is unknown is whether the vehicle under VSC will be potentially faster through a manoeuvre. This will be investigated in the next section.

E.3 Vehicle on-limit manoeuvring using β limit and $\dot{\beta}$ VSC

To investigate the effect of employing vehicle stability control on the performance limit, a range of sideslip angle limits were tested through the double lane change manoeuvre described in Chapter D. Initially the methods used will be described and then the results presented.

E.3.1 VSC control methodology

A logic statement embedded in the simulation program of the PI method was installed to trigger a control cycle once the critical level of sideslip angle was reached. An example of this statement is given in Equations E.1 to E.4.

$$\text{If} \beta > |\beta_{Limit}| \tag{E.1}$$

$$\Delta T_P = K_{P(\beta)} \cdot (\beta - \beta_{Limit}) + K_{I(\beta)} \cdot \int_{s_1}^{s_2} (\beta - \beta_{Limit}) \tag{E.2}$$

$$T_P = T_P - \Delta T_P \tag{E.3}$$

End (E.4)

The structure of the control sequence always ensures that the throttle position, T_P, is reduced if the β limit is surpassed during the simulation. Since the value of β can be either positive or negative the absolute value is used in the calculation.

The controller constants $K_{P(\beta)}$ and $K_{I(\beta)}$ were chosen to be 20 and 1 respectively. These numbers were found from a golden section search method using the steady state manoeuvre in Section E.2 to refine the values to maximise the sideslip angle response to the controller, whilst minimising the oscillation in the sideslip angle response of the vehicle.

A similar method to the β limit statements was used for the $\dot{\beta}$ minimisation. The Equations used are given in E.5 and E.6.

$$\Delta T_P = K_{P(\dot{\beta})} \cdot (\dot{\beta}) + K_{I(\dot{\beta})} \cdot \int_{s_1}^{s_2} (\dot{\beta}) \tag{E.5}$$

$$T_P = T_P - \Delta T_P \tag{E.6}$$

This method differs from the β limit method in that a conditional statement is not provided to initiate the control cycle. If the value of the sideslip angular velocity is nonzero, the controller comes into operation. The value of $K_{P(\dot{\beta})}$ found by golden section search was 1000 and the integral gain, $K_{I(\dot{\beta})}$ was again found to be 1. The value of $K_{P(\dot{\beta})}$ is very high because the calculation of $\dot{\beta}$ was made in radians and not degrees during the simulation.

E.3.2 Double lane change results

Due to the exploratory nature of this VSC work, a range of β limit values were tested between 1 and 10°. A selection of these are presented here with the $\dot{\beta}$ minimisation result and the non-control result.

This research was conducted with the PI method. This allows the unsteady state response of the vehicle to interruptions in engine torque during on-limit manoeuvring to be seen in the simulation results. The standard method of implementing the PI method was used, with the non-linear preview driver model and the QSS vehicle velocity profile used as a reference for the longitudinal control. The PI method creates a vehicle

control which operates the vehicle model very close to its optimal performance capability. Under this condition, there is no requirement for a vehicle stability controller. To create this requirement, the local value of the track surface friction coefficient μ_{road}, through the acceleration zone out of corner 2, is reduced by 80%. This corresponds to the travelled distance interval between 140 and 180 metres.

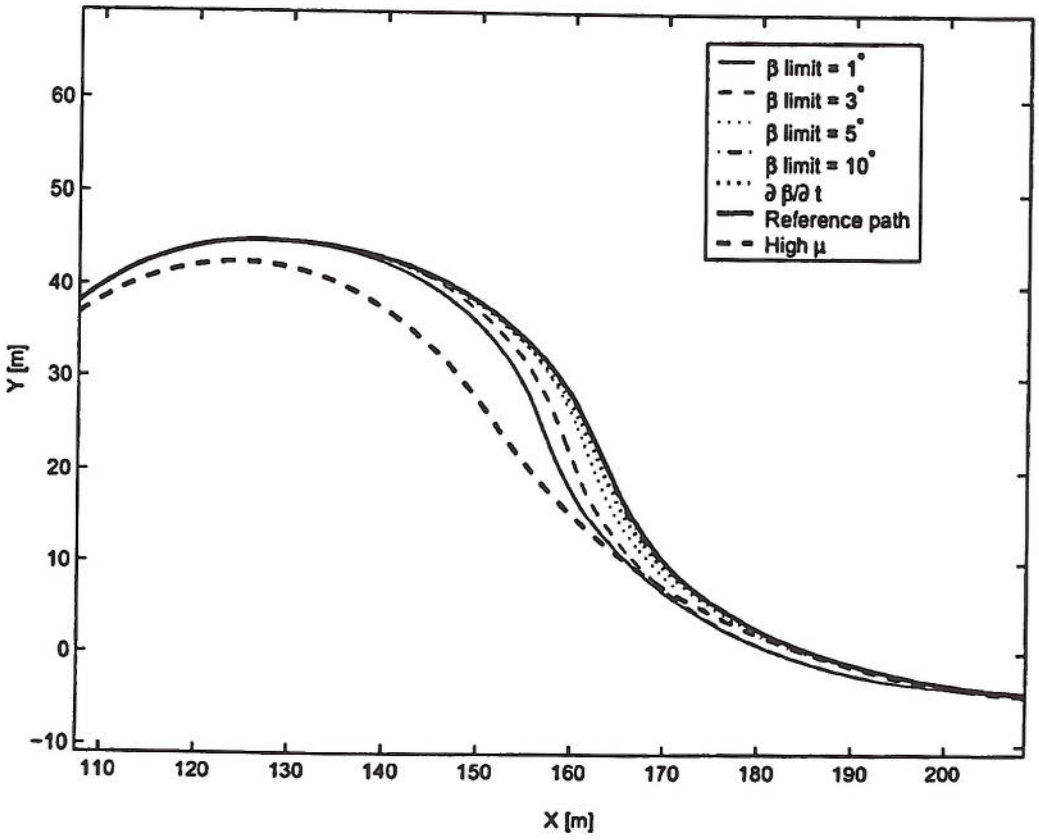

Figure E.5: Path taken, with four sideslip angle limits, and $\dot{\beta}$ minimisation.

The path taken by the vehicle under the various stability control strategies, through this low μ_{road} section of the manoeuvre is shown in Figure E.5. Additionally, the vehicle without any vehicle stability control and the original high friction surface result are also shown. These paths will be referred to as the 'reference path' and 'high μ path' respectively. There is an even spread of paths taken due to controller intervention. The largest deviation from the high μ path taken is produced by the reference path result. As the critical limit of β is reduced from 10 to 1° the path radius taken through the low μ_{road} section is much lower, and follows more closely the high μ path. Sideslip

angular velocity control hardly improves the path following quality but has a vehicle speed penalty (Figure E.6).

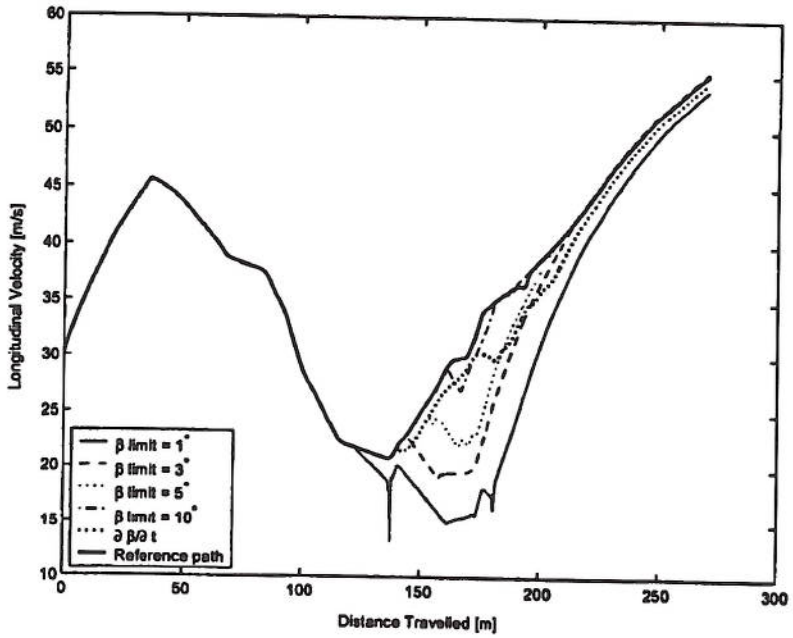

Figure E.6: Vehicle longitudinal velocity, with four sideslip angle limits, and β̇ minimisation.

The improved path following does not come without a penalty. Figure E.6 shows this clearly. As the critical limit of β is reduced towards 1° the vehicle speed is penalised significantly. The result on the overall segment times is shown in Table E.1.

The driver model response is shown in Figure E.7. The largest steer response in corner 2 comes from the 5° limit, which is surprising. The reason for this can be found from inspection of the velocity profile in Figure E.6 and the history of β through the manoeuvre in Figure E.8. In the 1° and 3° results, the β limit is reached during corner 2 or soon after, and the vehicle is decelerated until the sideslip angle is again below the limit and the vehicle begins to accelerate again. For the 5° result the critical value of the sideslip angle is not reached through corner 2 and the vehicle is allowed to accelerate more than the 1° and 3° results. However, as the vehicle is still turning while exiting the corner under acceleration, the critical limit on β is reached and the vehicle is promptly slowed. This generates a yaw moment. The steer controller senses the

Control	Segment time [s]
β limit = 1	9.768
β limit = 3	8.884
β limit = 6	8.566
β limit = 10	8.267
$\dot{\beta} = 0$	8.450
Reference path	8.218

Table E.1: Double lane change manoeuvre segment times.

sudden yaw rate change and compensates (Figure E.10) by increasing the steer angle. Chapter D shows how the steer controller responds to yaw angle path errors, and this is believed to be the reason for the high steer angle response. The 10°β limit controller does not enter a significant control cycle since the critical limit on the sideslip angle is only reached once at 160m, and the car is allowed to accelerate through the corner relatively unaffected.

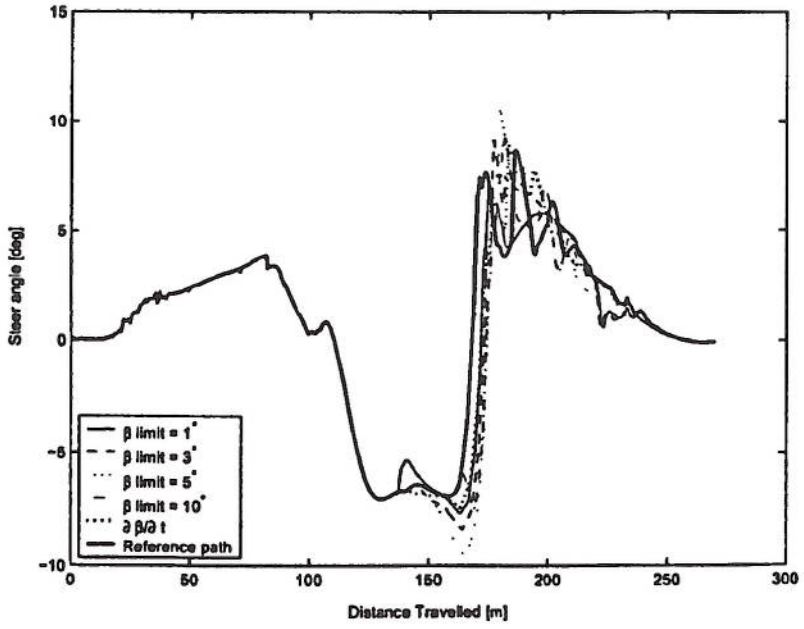

Figure E.7: Steer angle, with four sideslip angle limits, and $\dot{\beta}$ minimisation.

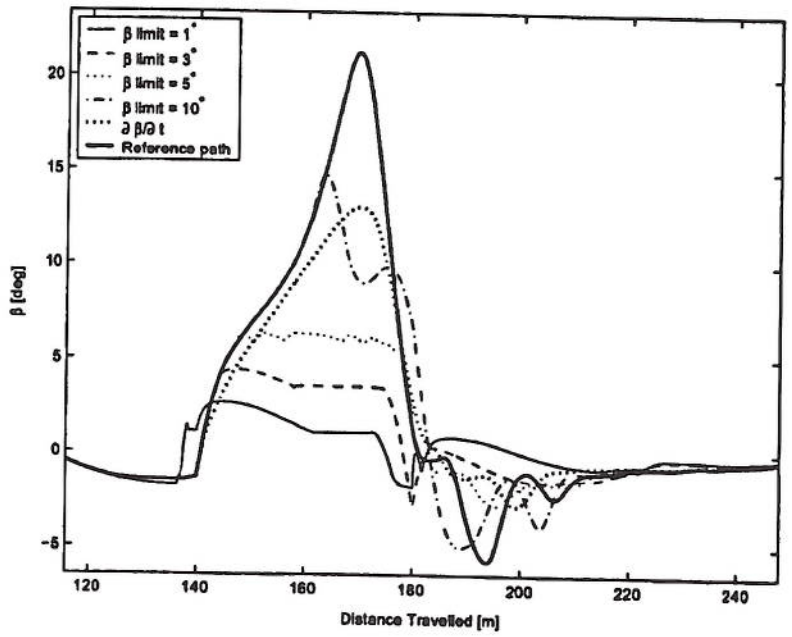

Figure E.8: Sideslip angle, with four sideslip angle limits, and β̇ minimisation.

The simulation histories of the sideslip angle and its time derivative are shown in Figures E.8 and E.9. From these histories of β and β̇ a direct determination of the success of the controllers at completing their tasks can be made.

Two broad conclusions can be made from the five controller responses. The first is that while the β limit controllers did limit the value of β it was not possible for the controllers to act sufficiently fast enough during the first 20 metres of the reduced μ section (140-160m, approximately one second in simulation time), to meet the limit targets. After 160-170 metres distance travelled, the values of β of the vehicles under β limit control converged on their target values. The second is that the aim of minimising β̇ was more satisfactorily accomplished by the β limit controllers set to 1,3 and 5° than the β̇ controller itself.

Through the third corner, the β limit controllers set to 1 and 3° show a damped β response, whereas the higher limit cases show less damping and significant oscillation as the vehicle accelerates. The β̇ minimiser is the least oscillatory controller on exit of corner three (Figure E.8), even though it is not the slowest vehicle through that corner.

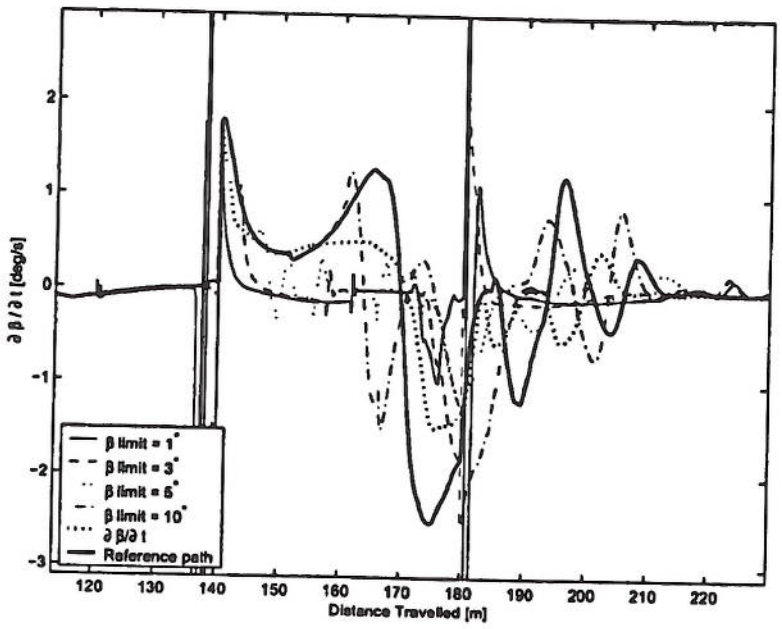

Figure E.9: Sideslip angular velocity, with four sideslip angle limits, and $\dot{\beta}$ minimisation.

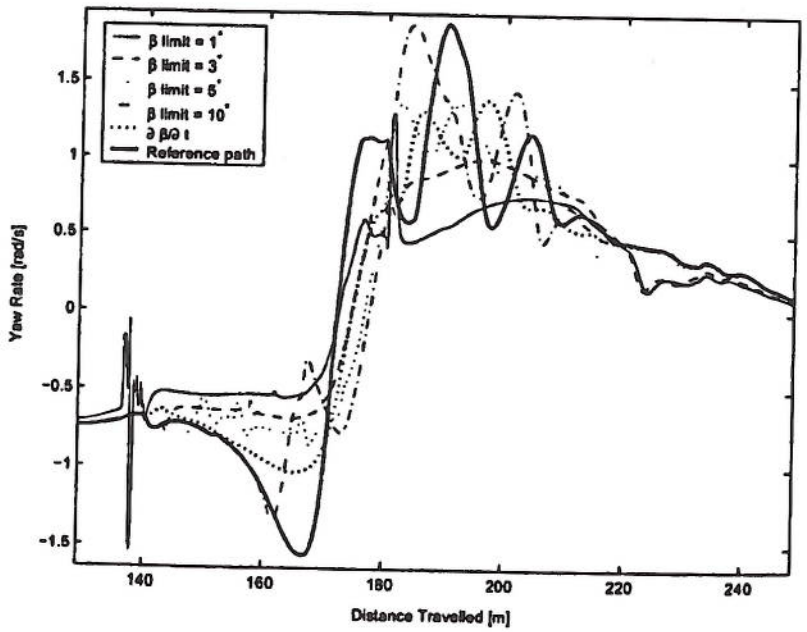

Figure E.10: Yaw rate, with four sideslip angle limits, and $\dot{\beta}$ minimisation.

Comparing the yaw rate response trends of the VSC controlled vehicles to the trends in the vehicle sideslip angle responses, a pattern emerges. Through the low speed second corner, the responses are smooth with the largest yaw rates being generated by the least restrictive stability controllers, and through corner three, the fast, high acceleration corner, the yaw response is quite oscillatory except for the 1 and 3° β limited simulations. The simulation histories of all the controlled vehicles suggests that both sideslip angle and yaw rate are being restricted when compared with the uncontrolled case. The uncontrolled vehicle responses are being damped in direct correlation to the critical value of β, imposed by the stability controllers. The $\dot{\beta}$ result most closely coincided with the β limit setting controlled to 10°.

E.4 Summary

Control of the engine torque is a viable method of regulating vehicle on-limit stability.

Vehicle on-limit stability was explored using the PI method through a challenging double lane change manoeuvre. The use of β limitation and $\dot{\beta}$ minimisation as forms of vehicle stability control were investigated using automatic control methods. Both controllers were found to reduce the sideslip angle and yaw rate vehicle response when compared with a non-VSC enabled vehicle, but at a significant vehicle speed penalty.

The use of VSC-type technology in Formula One does not appear to be particularly useful, based on the results shown here. This is because the control is slow acting and the penalty in vehicle speed is too severe.